Transformation of spatial representations along the mouse hippocampal circuits

Bérénice Gandit

THÈSE DE DOCTORAT

Sorbonne Université
École doctorale Cerveau Cognition Comportement (ed3C)

Réalisée au sein de l'équipe:
« Circuits Neuronaux de la Mémoire et de la Navigation Spatiales »
à l'Institut Pasteur

Sous la supervision de Christoph Schmidt-Hieber

Transformation of spatial representations along the mouse hippocampal circuits

Présentée par

Bérénice Gandit

Présentée et soutenue publiquement le 25 novembre 2021
devant le jury composé de:

Prof. David Dupret	Rapporteur
Prof. Jan Gründemann	Rapporteur
Dr Lisa Roux	Examinatrice
Dr Fekrije Selimi	Examinatrice
Dr Christelle Rochefort	Examinatrice
Dr Christoph Schmidt-Hieber	Directeur de thèse

Abstract

Forming a precise memory of our spatial environment is essential for our survival, as we depend on our ability to store and recall important locations. The hippocampus is thought to provide the brain with a cognitive map of the external world by processing various types of spatial information along its circuits. How essential spatial variables such as direction and position are transformed along hippocampal subregions to construct this global map is unclear. To address this question, we perform single-photon widefield microendoscope calcium imaging of the dentate gyrus, CA3 and CA1 hippocampal subregions in mice freely navigating along a linear track. We find that neurons throughout the hippocampus show directionality in their spatial responses, with particularly strong selectivity for the running direction in the dentate gyrus and in CA3. In addition, spatial activity maps in the dentate gyrus are correlated after aligning them to the running directions, suggesting that they represent the distance covered along the track in egocentric coordinates. Our data suggest that along the hippocampal circuits, spatial representations develop from contextually selective, egocentric distance coding to segmented allocentric representations of the environment.

Résumé

La formation d'une mémoire précise de notre environnement spatial est essentielle à notre survie, car nous dépendons de notre capacité à mémoriser et à nous souvenir des lieux importants. L'hippocampe est censé fournir au cerveau une carte cognitive du monde extérieur en traitant divers types d'informations spatiales le long de ses circuits. La façon dont les variables spatiales essentielles, telles que la direction et la position, sont transformées le long des régions de l'hippocampe pour construire cette carte globale n'est pas claire. Pour répondre à cette question, nous réalisons de l'imagerie calcique par microendoscope à large champ à photon unique du gyrus denté et des régions hippocampiques CA3 et CA1 chez des souris naviguant librement le long d'une piste linéaire. Nous constatons que les neurones de l'hippocampe présentent une directionnalité dans leurs réponses spatiales, avec une sélectivité particulièrement forte pour la direction de la trajectoire dans le gyrus denté et dans CA3. En outre, les cartes d'activité spatiale dans le gyrus denté sont corrélées après alignement sur les directions de course, ce qui suggère qu'elles représentent la distance parcourue le long de la piste en coordonnées égocentriques. Nos données suggèrent que le long des circuits hippocampiques, les représentations spatiales évoluent d'un codage de la distance égocentrique et contextuellement sélectif vers des représentations allocentriques segmentées de l'environnement.

Table of Contents

Abbreviations

DG - Dentate gyrus

EC - Entorhinal cortex

GECI - Genetically encoded calcium indicator

LEC - Lateral entorhinal cortex

LTD - Long-term depression

LTP - Long-term potentiation

MEC - Medial entorhinal cortex

I. Introduction

1. Neuroanatomy and basic physiology of the hippocampus

Ever since the discovery of a link between the medial temporal lobe and declarative memory (Scoville and Milner, 1957), the neuroanatomical organisation of this brain region and its complex connectivity patterns with the parahippocampal region have been intensely studied (van Strien et al., 2009). The hippocampal region is a bilateral brain structure that lies between the septal nucleus rostrally and the temporal cortex caudally, and is part of the cluster of anatomically and functionally related brain structures that form the medial temporal lobe. It derives its name from the resemblance of the human hippocampus to a seahorse and has been widely used as a model system for neurobiology as a result of its unique neuroanatomical organisation (Per et al., 2007). The hippocampal region comprises the dentate gyrus, the *Cornu Ammonis* (CA) fields and the subicular complex and it is strongly connected to the adjacent perirhinal, entorhinal and parahippocampal cortices (Squire et al., 2004). In the framework of this thesis project, we will focus on the dentate gyrus, CA3 and CA1 subregions, which collectively form the hippocampus, as well as its input from the entorhinal cortex.

The hippocampus displays a simple organisation of its principal cell layers and a laminar distribution of its inputs (Per et al., 2007) and is broadly composed of 3 cortical layers, by contrast to the characteristic 6-layered organisation of the neocortex. The deepest layer comprises afferent and efferent fibres as well as interneurons. In the dentate gyrus it corresponds to the inner polymorphic layer or hilus; in the CA region to stratum oriens. The middle layer located superficially to the deeper layer is the principal cell layer, and comprises principal excitatory cells and inhibitory interneurons. In the dentate gyrus it is known as the

granule cell layer and in the CA fields as pyramidal cell layer or *stratum pyramidale*. Most superficially lies the molecular layer in the subiculum and the dentate gyrus, where it contains the dendritic arborisations of the principal cells. In CA3, the molecular layer is divided into sublayers: the *stratum lucidum*, the *stratum radiatum* and the *stratum lacunosum-moleculare* (van Strien et al., 2009).

Inputs from the entorhinal cortex to the hippocampus

The entorhinal cortex processes multiple types of sensory information and provides the hippocampal formation with most of the cortical sensory information necessary to perform its functions (Amaral et al., 2007; Rolls, 2018). The main excitatory input to the hippocampus is conveyed monosynaptically from the entorhinal cortex layer II to the dentate gyrus via the perforant path (PP) fibers. A structural and functional segregation divides the entorhinal cortex into a medial and lateral component: the medial entorhinal cortex (MEC) contains spatially tuned cells while the lateral entorhinal cortex (LEC) contains neurons that preferentially represent non-spatial information (Hargreaves et al., 2005). The perforant path fibers are segregated into a medial and a lateral component according to their region of origin in the entorhinal cortex. Lateral PP fibers terminate in the outer third of the molecular layer while medial PP fibers terminate in the middle third of the molecular layer; both form asymmetric synapses mostly on dendrites of granule cells (Nafstad, 1967) but sometimes also on dendrites of GABA- positive interneurons. Some minor projections to the dentate gyrus also originate in the presubiculum and parasubiculum (Köhler, 1985); their terminals intercalate between lateral PP and medial PP terminals in the molecular layer. The classical model of the hippocampus is that of a unidirectional circuit where principal cells in the dentate gyrus, CA3 and CA1 form synaptic contacts with each other, giving the hippocampus its name of 'trisynaptic circuit'. However, the patterns of connectivity within the hippocampal formation are more complex and backprojections between hippocampal subregions have been observed, as well as direct projections from entorhinal cortex layer III to CA1 (Li et al., 2017; van Strien et al., 2009).

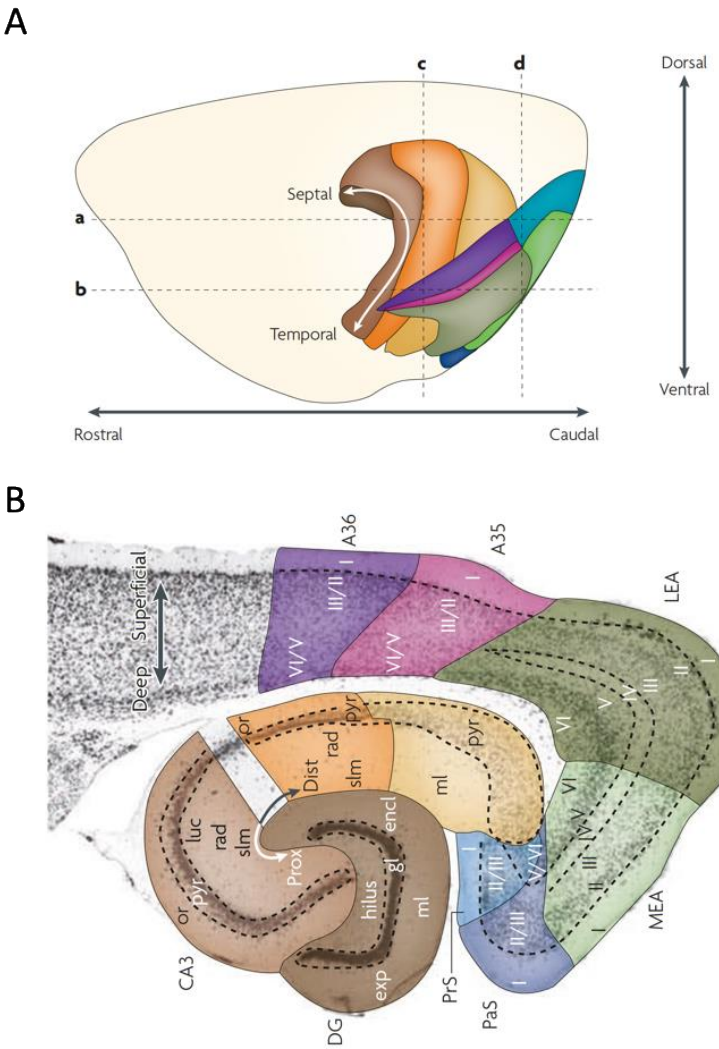

Figure 1.1. Representations of the hippocampal formation and the parahippocampal region in the rat brain. Adapted from (van Strien et al., 2009). (**A**) Lateral view of the hippocampal formation: dentate gyrus (DG; dark brown), CA1 (orange) and the subiculum (yellow), two axes are indicated: the long or septotemporal axis (also referred to as the dorsoventral axis); and the rostrocaudal axis. In the parahippocampal region (green, blue, pink and purple shaded areas), a similar superficial-to-deep axis is used. Additionally, the presubiculum (PrS; medium blue) and parasubiculum (PaS; dark blue) are described by a septotemporal and proximodistal axis. The entorhinal cortex, which has a lateral (LEA; dark green) and a medial (MEA; light green) aspect, is described by a dorsolateral-to-ventromedial gradient and a rostrocaudal axis. The perirhinal cortex (consisting of Brodmann areas (A) 35 (pink) and 36 (purple) and the postrhinal cortex (POR; blue-green) share the latter axis with the entorhinal cortex and are additionally defined by a dorsoventral orientation. The dashed lines in the left panel indicate the levels of two horizontal sections (a,b) and two coronal sections (c,d), which are shown in the original publication. (**B**) A Nissl-stained horizontal cross section in which the cortical layers and three-dimensional axes are marked. The Roman numerals indicate cortical layers. CA, cornu ammonis; dist, distal; dl, dorsolateral part of the entorhinal cortex; encl, enclosed blade of the DG; exp, exposed blade of the DG; gl, granule cell layer; luc, stratum lucidum; ml, molecular layer; or, stratum oriens; prox, proximal; pyr, pyramidal cell layer; rad, stratum radiatum; slm, stratum lacunosum-moleculare; vm, ventromedial part of the entorhinal cortex.

1.1. The dentate gyrus

Neuroanatomical organisation of the dentate gyrus

The dentate gyrus displays a trilaminar structure. The most superficial layer is the molecular layer: it is relatively devoid of cells and is approximately 250 µm thick. It is mostly filled with granule cell dendrites but also includes the perforant path fibers, interneurons and other input terminals. The second layer is the granule cell layer, which is densely packed with the somas of the principal cells of the dentate gyrus – the granule cells. It is V-shaped, the upper part is named suprapyramidal (upper) blade, the lower part, infrapyramidal (lower) blade, and the part where they meet, the crest. The third layer is the polymorphic layer – or hilus (Amaral et al., 2007).

Granule cells are the principal cells of the dentate gyrus, they are numerous and amount to ~1 million in the rat in each hemisphere (Basu and Siegelbaum, 2015). They are tightly packed but not directly recurrently connected. They show unique biophysical, cellular and structural features such as an elliptical cell body of relatively small size (10um-wide; 18um-high (Amaral et al., 1990)), a cytoplasmic ring and a cone-shaped apical dendritic tree that extends through the molecular layer (Amaral et al., 2007). The dentate gyrus also comprises excitatory interneurons named 'mossy cells', which feature large triangular/multipolar cell bodies located in the hilus (Amaral et al., 2007). Mossy cells feature multiple dendrites that branch and extend into the hilus. Proximal dendrites are covered with thorny excrescences, giving mossy cells a unique aspect. Mossy cells receive projections from granule cells, CA3 pyramidal neurons, other mossy cells, hilar interneurons as well as the septum (Scharfman, 2016). They contact granule cell dendrites in the inner third of the molecular layer ipsi- and contralaterally in the rat along the septotemporal axis through the commissural fibers (Scharfman et al., 2003). The reciprocal connection between mossy cells and granule cells forms a loop that enables granule cells to contact one another (Buckmaster, 2012; Laurberg and Sørensen, 1981). The dentate gyrus is also one of the few regions in the brain where neurogenesis takes place throughout the adult life of most mammals. There is a steady-state granule cell turnover and newborn neurons get progressively integrated in the hippocampal circuit.

The dentate gyrus also comprises inhibitory interneurons, which have been classified according to their axonal distribution, their input organisation as well as their electrophysiological properties. Parvalbumin expressing (PV+) interneurons include basket

cells, inhibitory interneurons located in between the granule cell layer and the hilus that form synaptic contacts with the perisomatic domain of granule cells and interneurons, and fast-spiking axo-axonic cells, which send projections to the granule cell axon initial segment (Amaral et al., 2007). In addition, somatostatin expressing (SOM+) interneurons send projections to distal dendrites of granule cells in the outer two thirds of the molecular layer, near the perforant path inputs, and long-range projections to CA1, CA3, the subiculum, medial septum and contralateral hippocampus. Other less well-characterized inhibitory interneurons can also be found in the dentate gyrus (Amaral et al., 2007; Savanthrapadian et al., 2014).

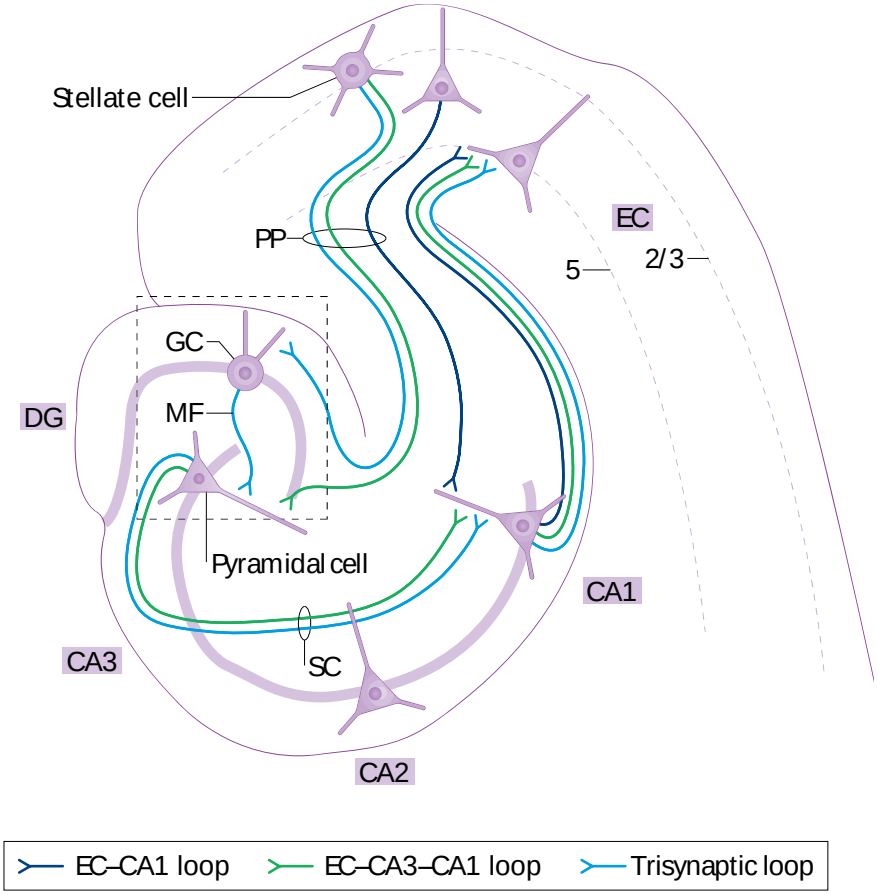

Figure 1.2. Schematic representation of the mouse hippocampal formation and its main synaptic connections. Adapted from (Hainmueller and Bartos, 2020). Dentate gyrus (DG) granule cells (GCs) send mossy- fibre (MF) axons to CA3. CA3 pyramidal cells send Schaffer- collateral (SC) projections to CA1, which then projects back to the entorhinal cortex (EC). All of these areas receive perforant- path (PP) input from the EC, creating multiple parallel loops through which information can flow through the hippocampus.

Dentate gyrus neurophysiology

As the input region of the hippocampus, the dentate gyrus receives most of the excitatory inputs to the hippocampus from the entorhinal cortex and can be seen as the first stage of hippocampal processing. The entorhinal cortex layer II sends the main excitatory inputs to granule cells (Deller et al., 1996), which then send unmyelinated axonal projections to proximal dendrites of CA3 pyramidal cells through the mossy fiber pathway. Mossy fibers form large synaptic boutons with CA3 pyramidal neurons in the *stratum lucidum*, establishing a sparse but powerful synaptic connection. Granule cells also make synaptic connections with mossy cells and inhibitory interneurons through en passant boutons (Amaral et al., 2007).

Early *in vitro* and *in vivo* electrophysiological recordings revealed the propensity of dentate gyrus granule cells to fire in bursts (Scharfman, 2012) during short-term memory tasks in the centre of a place field (Jung and McNaughton, 1993; Leutgeb et al., 2007). More recent experimental work using *in vivo* calcium imaging and immediate early gene (IEG) expression showed that granule cell activity is sparse and that a major portion of the granule cell population is silent in a given environment (Danielson et al., 2016a; Diamantaki et al., 2016; GoodSmith, 2017; Neunuebel and Knierim, 2014; Pilz et al., 2016; Senzai and Buzsáki, 2017). The discrepancy between early and more recent work might arise from the inability of extracellular recordings to identify cellular populations, which may take into account the activity of non-granule cell neurons such as adult-born granule cells and mossy cells (Chawla et al., 2005; Leutgeb et al., 2007; Neunuebel and Knierim, 2012; Senzai and Buzsáki, 2017). On the other hand, calcium imaging and IEG methods lack sufficient temporal resolution to distinguish bursts from single spikes (Danielson et al., 2016b; GoodSmith, 2017; Hainmueller and Bartos, 2018). Recent intracellular recordings reconciled these two contradictory streams of evidence by showing that mature granule cell activity is sparse and heterogeneous, with firing rates comprised between silent and 3Hz, possibly resulting from differences in intrinsic excitability (Vandael et al., 2020; Zhang et al., 2020). Coherently with these results, a subpopulation of granule cells located in the suprapyramidal blade was recently shown to display distinct spatial, morphological, physiological and developmental properties and is ten times more likely to be activated by novel experiences (Erwin et al., 2020).

GABAergic interneurons play an important role in the dentate gyrus local circuit: *in vivo* whole cell patch-clamp recordings have revealed that granule cells inhibit neighbouring granule cells via PV+ interneurons in a process named ‘lateral inhibition’, which may enable a winner-takes-all strategy, thereby maintaining the majority of granule cells in a silent state (Espinoza et al., 2018). Interneuron signalling is distance-dependent in the dentate gyrus and

synaptic strength decreases and inhibitory signal duration increases with increasing distance, allowing the generation of highly synchronous focal gamma bursts enabling the network to process multiple complex inputs in parallel (Strüber et al., 2017). Mossy cells also contribute to implementing inhibition by contacting granule cells and inhibitory interneurons and generating both weak selective activation and disynaptic inhibition (Amaral et al., 2007; Bernstein et al., 2020). Perforant path stimulation might also reduce granule cell excitability and promote sparse firing through long-lasting hyperpolarisation of dentate gyrus granule cells, which requires gamma bursts and local inhibition, and is mediated by both GABA receptors and glutamate receptors (Mircheva et al., 2019). Thus, the integrative action of multiple cell types within the dentate gyrus complex local circuit promotes sparse neuronal firing in the dentate gyrus.

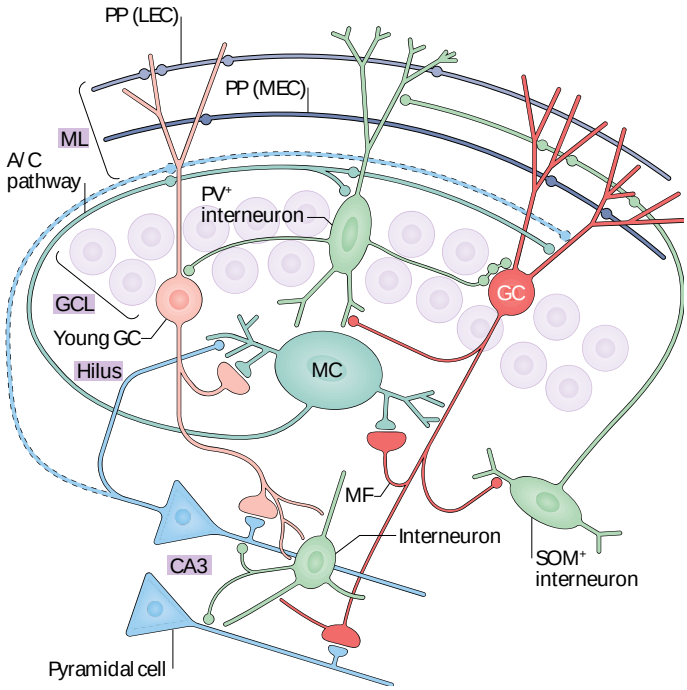

Figure 1.3. Magnified view of the DG microcircuitry, its intrinsic connections and outputs to the CA3. Adapted from (Hainmueller and Bartos, 2020). GCs form the densely packed GC layer (GCL), which also houses parvalbumin-expressing (PV+) basket cells and axo- axonic cells. Wrapped by the GC layer are the CA3 area and the DG hilus, which contains glutamatergic mossy cells (MCs) and other types of GABAergic interneurons, such as those expressing somatostatin (SOM+ interneurons). GCs make synaptic contacts on all of the aforementioned cell types (except other GCs) via their MF axons. A/C, associational–commissural; LEC, lateral entorhinal cortex; MEC, medial entorhinal cortex; ML, molecular layer.

1.2. CA3

CA3 neuroanatomical organisation

The next subdivision of the hippocampal circuit is the hippocampal subregion CA3. It is composed of a principal cell layer made of pyramidal neurons as well as inhibitory interneurons. The morphology of pyramidal neurons is more similar to that of CA1 pyramidal cells than that of granule cells, albeit with a larger cell body. The cell bodies are located in *the stratum pyramidale* and the apical dendrites cross through the *stratum lucidum, radiatum* and *lacunosum moleculare*. There are an estimated 300000 pyramidal cells in the rat (Basu and Siegelbaum, 2015). CA3 pyramidal cells are contacted by dentate gyrus granule cells via mossy fibers which form 'giant' synaptic boutons onto complex postsynaptic elements called 'thorny excrescences'. One CA3 pyramidal cell receives approximately 46 mossy fibers inputs, resulting in a sparseness of connectivity for this synapse of approximately 0.005% (Rolls, 2018). CA3 pyramidal neurons also send axonal projections to CA1 neurons through Schaffer collaterals (Rolls, 2018). The anatomical architecture of CA3 is unique in that CA3 pyramidal neurons are recurrently connected bilaterally through associational and commissural fibers, which provide the largest number of synapses onto CA3 neurons ($1.2x10^4$) (Amaral et al., 1990). CA3 also sends projections to the hilus and to the dentate gyrus molecular layer, in contradiction to the classical unidirectional model of the hippocampus (van Strien et al., 2009)**.** Inhibitory interneurons can be found in multiple CA3 layers and include ivy cells, regular spiking basket cells, fast-spiking basket cells and spiny lucidum cells. They are contacted by mossy fibers and implement feed-forward inhibition onto CA3 pyramidal cells by establishing synaptic contacts mostly onto CA3 pyramidal cell somas (Szabadics and Soltesz, 2009).

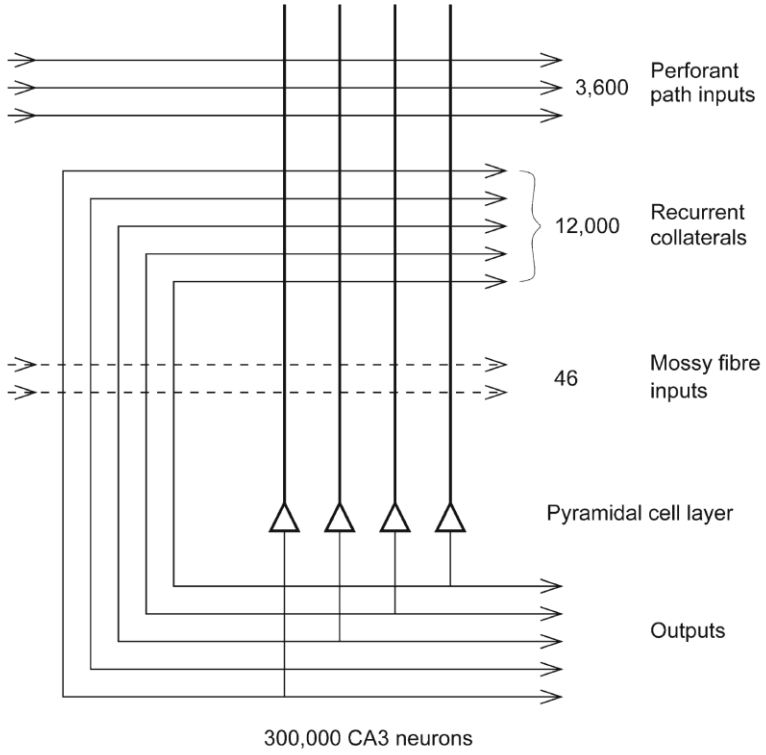

Figure 1.4. Connections from multiple sources onto CA3 pyramidal cells. Adapted from (Rolls, 2018). A diagrammatic representation of the estimated number of connections from three different sources onto each CA3 cell in the rat brain.

CA3 neurophysiology

CA3 neurons have been largely characterized using electrophysiological recordings, revealing firing rates that are lower than those of CA1 neurons but higher than those of dentate gyrus granule cells (Fox and Ranck, 1975; Mizuseki et al., 2012; Oliva et al., 2016), ranging from 0.3 to 5Hz *in* vivo (Henze et al., 2002; Mizuseki et al., 2012; Oliva et al., 2016). About 67% of CA3 pyramidal neurons are silent cells at a given time (Leutgeb et al., 2007). This might result from a preferred mossy fiber innervation of interneurons compared to CA3 pyramidal cells. A characteristic feature of CA3 activity patterns is their ability to fire bursts of action potentials (Fox and Ranck, 1975; Frerking et al., 2005; Mizuseki et al., 2012; Oliva et al., 2016). Complex bursts involve regenerative dendritic mechanisms that play a role in activity-dependent plasticity (Diamantaki et al., 2018; Grienberger et al., 2014; Lee et al., 2012a). CA3 also shows network synchronisation events (Menendez de la Prida et al., 2006; Miles and Wong, 1983; Wittner and Miles, 2007) such as sharp-wave ripples (Buzsáki, 1986; Csicsvari et al., 2000; Hunt et al., 2018). Furthermore, CA3 pyramidal cells show a coordinated hyperpolarisation and a lower membrane potential variance during theta oscillations (Malezieux et al., 2020). Recent *in vivo* imaging of CA3 showed that co-activity

of neuronal pairs can be maintained over days and that spatiotemporal activity patterns are modulated by brain states (Schoenfeld et al., 2021).

1.3. CA2

The hippocampal subregion CA2 was first observed and described by Lorente de Nó (De Nó, 1934) as featuring characteristically large pyramidal neurons and small dendritic branching and was originally characterized based on unique patterns of protein expression (De Nó, 1934; Zhao et al., 2001). CA2 pyramidal neurons receive direct inputs from the entorhinal cortex (Bartesaghi and Gessi, 2004; Kohara et al., 2014), dentate gyrus mossy cells (Kohara et al., 2014) as well as a feedforward inhibitory connections from CA3 (Chevaleyre and Siegelbaum, 2010; Cui et al., 2013). CA2 pyramidal neurons in turn project to hippocampal subregions CA1, CA2 and CA3 and are thereby in a powerful position to influence the hippocampal network (Cui et al., 2013). CA2 is also contacted by extra-hippocampal regions such as the paraventricular nucleus of the hypothalamus and median raphe and is reciprocally connected to the supramammilary nucleus, the diagonal band of Broca and the medial septum (Cui et al., 2013).

CA2 pyramidal neurons show unique intrinsic properties such as a lower membrane potential (Zhao et al., 2007) and a lower membrane resistance as well as a slower action potential firing frequency (Chevaleyre and Siegelbaum, 2010). CA2 plays a role in social aspects of memory formation and social aggression behaviours (Wersinger et al., 2002), and is implicated in multiple brain disorders such as schizophrenia, bipolar disorders and Alzheimer's disease (Benes et al., 1998, 2007; Dickson et al., 1991; Knable et al., 2004). By contrast to other hippocampal subregions, CA2 only shows little involvement in spatial coding (Mankin et al., 2015). In the framework of this thesis project, we will leave CA2 aside and focus on the role of the dentate gyrus and hippocampal subregions CA3 and CA1 in spatial information processing.

1.4. CA1

CA1 neuroanatomical organisation

CA1 is the last station of the hippocampal circuit. It receives its main excitatory input from downstream subregions CA3/CA2 but also receives inputs from entorhinal cortex layer III and sends outward projections to the neocortex (Li et al., 2017). CA1 is composed of pyramidal cells, and is in fact a continuation of CA2 and CA3 since they form a continuous layer of neurons as opposed to the principal cell layer of the dentate gyrus, which is not physically connected to neurons of the *cornu ammonis*. As in CA3, principal cells in CA1 are pyramidal cells. There are about 300000 pyramidal cells in the rat CA1, making it similar in size to CA3 (Basu and Siegelbaum, 2015). While they are connected to each other, CA1 neurons are not as heavily recurrently connected as CA3 neurons. Inhibitory interneurons can also be found in the CA1 principal cell layer.

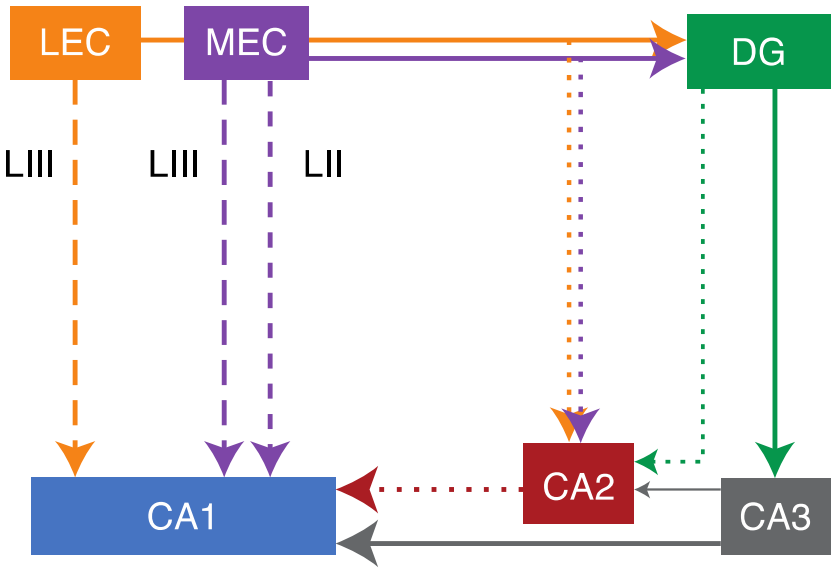

Figure 1.5. Circuit diagram of the cortico-hippocampal circuit. Adapted from (Basu and Siegelbaum, 2015). The cortico-hippocampal circuit with recently discovered glutamatergic inputs from the entorhinal cortex (EC) to the hippocampus as well as connections within the hippocampus. In addition to the classical tri-synaptic (EC layer II [LII] → dentate gyrus [DG] → CA3 → CA1, solid line) and monosynaptic (EC layer III (LIII) → CA1, large-dashed lines) pathways of information flow, CA1 also receives monosynaptic projections from LII of the medial entorhinal cortex (MEC) (small dashed line) and CA2 receives direct inputs from LII of both MEC and lateral entorhinal cortex (LEC) (dotted lines). Within the hippocampus, CA2 sends prominent inputs to CA1, targeting dendritic domains (stratum oriens [SO]/stratum radiatum [SR]) (red) that overlap with the CA3 → CA1 inputs. CA2 also receives weak inputs from DG and CA3. The thickness of the arrowed lines emphasizes the strength of the input connection.

CA1 pyramidal cells receive axonal projections from CA3 neurons through the Schaffer collateral pathway: distal CA3 sends projections to proximal CA1 while proximal CA3

projects to distal CA1. CA1 also receives backprojections from the entorhinal cortex, which are organized in a topographical manner: the septotemporal hippocampal axis is topographically mapped onto the dorsolateral-ventromedial axis of the entorhinal cortex. As the source of the primary output of the hippocampal circuit, CA1 sends out projections back to the subiculum, the entorhinal cortex and parahippocampal structures (Cenquizca and Swanson, 2007; Naber et al., 2001; Swanson et al., 1978). These projections are thought to support recall of information in the hippocampus and transfer to the neocortex (Frankland and Bontempi, 2005; Kesner and Rolls, 2015). CA1 also shows recurrent loops along one septotemporal level (Amaral et al., 1991; Cenquizca and Swanson, 2007; Hjorth-Simonsen, 1973) and sends a backprojection to CA3, probably originating from inhibitory interneurons in the molecular layer, which contrasts with the classical unidirectional model of the trisynaptic circuit (Amaral et al., 1991; Cenquizca and Swanson, 2007; Swanson et al., 1981).

CA1 neurophysiology

CA1 pyramidal neurons differ from CA3 pyramidal cells in terms of firing rates and spike dynamics. Notably, CA1 pyramidal cells exhibit a substantially higher firing rate compared to CA3 neurons as well as a lower burst occurrence and length (Mizuseki et al., 2012). Burst firing is facilitated by dendritic Ca^{2+} currents, which are enhanced by somatodendritic back-propagation of the action potential. These are regulated by the availability of fast inactivating Na^{+} channels which can take up to several hundreds of milliseconds to recover following each spike (Jung et al., 1997; Spruston et al., 1995). Furthermore, CA1 pyramidal neurons are under control of a powerful inhibition exerted by local inhibitory interneurons by means of synaptic contacts formed onto proximal or distal dendrites (Klausberger and Somogyi, 2008; Somogyi and Klausberger, 2005). The inhibition exerted by local inhibitory interneurons outweighs the relatively sparse inputs from CA3 and the entorhinal cortex to CA1 (Ahmed and Mehta, 2009). Overall, the integration of multiple sources of excitation and inhibition result in neuronal firing characteristics in CA1 neurons that are distinct from that of upstream CA3 pyramidal cells.

2. Memory encoding and storage in the hippocampus

The hippocampal circuit can be described as a processing loop, which receives highly processed sensory information from the neocortex via the entorhinal cortex, generates neuronal ensembles to represent memories and sends this information back to the neocortex. By virtue of its input connectivity patterns, the hippocampus is ideally located to associate representations of events and objects with their spatiotemporal context. The anchoring of episodes in their context might be achieved by the integration of external sensory information from the LEC and self-motion based spatial information from the MEC (Knierim et al., 2006).

2.1. Episodic memory

Experimental work in humans, non-human primates and rodents has shed light on the crucial role of the medial temporal lobe in declarative memories - the conscious memory for facts and events. Episodic memory is a type of declarative memory relative to facts and concepts from one's personal experience, which are anchored in a given spatiotemporal context. The medial temporal lobe is thought to work jointly with the neocortex to encode memories, store them in the long run and retrieve them (Frankland and Bontempi, 2005; Rolls, 2018). Early theories about hippocampal function stemmed from instrumental clinical case studies, such as the description and post-mortem study of brains of amnesic patient brains with a thinning of hippocampal tissue by Vladimir Bekhterev in 1900 and the seminal clinical psychological case study of patient Henry Molaison (H.M) by William Scoville and Brenda Milner in 1957 (Scoville and Milner, 1957). Henry Molaison underwent a bilateral medial temporal lobe resection that comprised his two hippocampi in order to relieve him from incapacitating epileptic seizures. As a result of the surgery, HM developed a temporally graded retrograde amnesia as well as an anterograde amnesia rendering him unable to form new long-term memories of recent events. This unexpected outcome of the surgery revealed the crucial role of the medial temporal lobe, and by extension of the hippocampus, in the process of formation of episodic memories. It also showed that memory processing in the brain takes place somewhat independently from other intellectual and perceptual processing, as evidenced by H.M.'s intact procedural memory.

Since these early studies, the role of the hippocampus in episodic memory and the mechanisms underlying memory processing have been studied extensively in humans using

non-invasive imaging, electrode-based- and intracranial recordings and at the cellular level in animal models (Vargha-Khadem, 1997) and particularly in rodents, who are thought to possess a primitive version of the episodic memory system (Allen and Fortin, 2013; Dere et al., 2005). Experimental work in rodents has revealed a crucial role of the hippocampal formation for spatial, contextual and episodic memory processing as well as for behavioural discrimination between learned memories (Amaral et al., 2007; Eichenbaum, 2004; Gilbert et al., 1998; O'Keefe and Nadel, 1978). The rodent hippocampus is required for tasks involving object-location associations (Kesner and Rolls, 2015; Morris and Frey, 1997; Per et al., 2007) and hippocampal-dependent replay of long-term memories to recall an ordered sequence of episodes (Kesner and Rolls, 2015; Panoz-Brown et al., 2018). Episodic memory encoding and retrieval are supported by distinct neural circuits: the pathway connecting CA1 to dorsal subiculum to layer 5 of the MEC cortex supports episodic memory retrieval while the pathway linking CA1 to layer 5 of the entorhinal cortex is required for memory encoding (Roy et al., 2017). In summary, while early clinical studies first identified the role of the hippocampus in episodic memory processing, a large body of recent experimental work has contributed to characterize the neural mechanisms underlying episodic memory encoding and retrieval.

2.2. Cellular basis of memory encoding and storage

Memory Engrams

Episodic memories for events and places need to be created, stored and retrieved upon request. How are memories stored in the brain? Early theoretical predictions stated that learning activates small groups of neurons and induces physical and chemical changes in them (Semon, 1921). They also postulated that the neural substrate of perceptual memory is the strengthening of connections between neurons based on correlated activities during memory acquisition resulting in 'cell assemblies' (Hebb, 1949). As such, if two cells are connected together by an excitatory synapse, their connection is strengthened when the first cell activates the second one (Bliss and Lomo, 1973; Markram et al., 1997; Morris, 1999; Poo et al., 2016). Connections across cortical regions specialized for different memory components are strengthened through synaptic and systems reconfiguration so that the resulting memory trace or 'engram' can subsequently be reactivated independently from the hippocampus (Frankland and Bontempi, 2005; McClelland and O'Reilly, 1995; Squire and Alvarez, 1995; Squire et al., 1975). The activation of specific ensembles of hippocampal

neurons contributing to an engram is sufficient to elicit context-specific memory representations during retrieval (Liu et al., 2012; Tanaka et al., 2014).

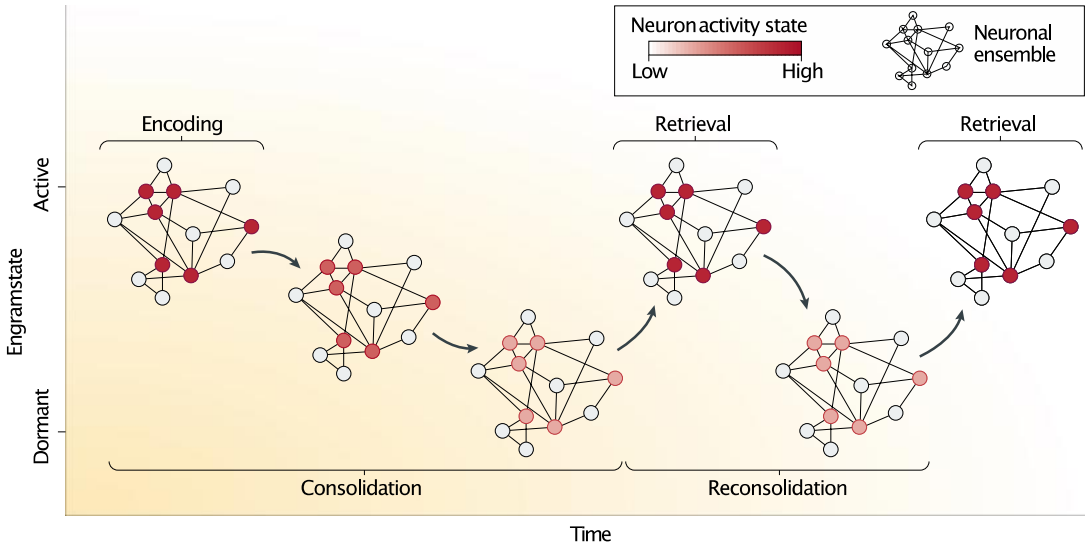

Figure 1.6. Schematic representation of the lifetime of an engram. Adapted from (Josselyn et al., 2015). The formation of an engram (encoding) involves strengthening of connections between collections of neurons (neuronal ensemble) that are active (red) during an event. Consolidation further strengthens the connections between these neurons, which increases the likelihood that the same activity pattern can be recreated at a later time, allowing for successful memory retrieval. During consolidation, the engram enters a mostly dormant state. Memory retrieval returns the engram back to an active state and transiently destabilizes this pattern of connections. The engram may be restabilized through a process of reconsolidation and re-enter a more dormant state. Therefore, an engram may exist in a dormant state between the active processes of encoding and retrieval required to form and recover the memory. In this way, an engram is not yet a memory, but provides the necessary conditions for a memory to emerge.

Cellular basis of engrams

Long-term information storage in the brain depends on structural and functional changes in synapses within the circuits that support the storage of activity patterns in neural ensembles (Morris, 1999). What is the cellular basis of these structural and functional synaptic changes?

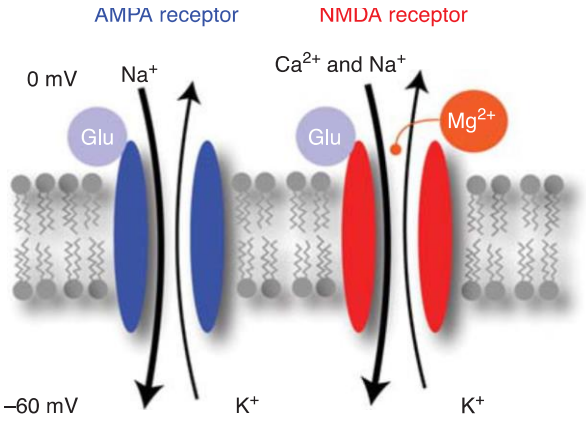

Figure 1.7. Major ionotropic glutamate receptors involved in LTD and LTP. Adapted from (Lüscher and Malenka, 2012). When glutamate binds to AMPA receptors, many sodium ions flow into the cell while only some potassium ions leave the neuron, causing a net depolarization of the membrane. NMDA receptors are also permeable for calcium but only if the magnesium ion is expelled by a slight depolarization of the neuron.

NMDA and AMPA receptors

Neurons communicate by sending each other chemical neurotransmitters through a thin space named the synapse. They can also communicate via electrical synapses made of a gap junction that provides a direct electrical connection, but this type of neuronal communication is beyond the scope of this project. Neurotransmitters are either excitatory, e.g. glutamate, and trigger neuronal activation, or inhibitory, eg. gamma-Aminobutyric acid (GABA) and cause the reduction of activity in adjacent neurons. Chemical synapses require a complex presynaptic molecular machinery to regulate neurotransmitter release. They also require neurotransmitter receptors embedded in the postsynaptic membrane that detect the release of a neurotransmitter from an adjacent neuron and convert the signal back into an electrical signal through biochemical cascades (Frankland and Bontempi, 2005; Rolls, 2018). Neurotransmitter receptors belong to two broad categories: ionotropic ligand gated ion channels and metabotropic G-protein coupled receptors. Ionotropic ion channels respond to the brief pulse of neurotransmitter release, of which two examples are NMDA receptors (NMDARs) and AMPA-type glutamate receptors (AMPARs). NMDARs and AMPARs are present in excitatory synapses and are permeable to Na+ and K+ (Born et al., 2014; Dingledine et al., 1999; Smart and Paoletti, 2012). Ionotropic glutamate receptor activation leads to strong Na+ influx and small K+ outflux, which depolarizes the postsynaptic neuron. AMPARs trigger large and rapid synaptic signalling. When the neuronal membrane potential is negative and close to resting membrane potential, magnesium ions enter the pore of the NMDAR and prevent other ions from passing through. Neuronal depolarisation dislodges the magnesium ion and allows passage of sodium, potassium and calcium ions.

Long-term potentiation / Long-term depression

The ability of a neuron to influence postsynaptic output upon presynaptic activity is called synaptic efficacy and the ability of a synapse to change its synaptic efficacy is called synaptic plasticity. A reduction of synaptic efficacy of postsynaptic terminals in time windows ranging from a few milliseconds to minutes is called short-term depression while a brief increase of synaptic efficacy is called short-term facilitation (Catterall et al., 2013). A seminal discovery was that high-frequency electrical stimulation of hippocampal inputs increases the strength of stimulated synapses for days - a process termed long-term potentiation (LTP). Coordinated activation of synapses that successfully activate a postsynaptic neuron will result in strengthening of these synapses (Collingridge et al., 2004). Long-term plasticity refers to long-lasting changes in synaptic efficacy dependent on presynaptic activity, whether it is enhanced (LTP) or reduced (long-term depression (LTD).

LTP is triggered by specific activity patterns and comprises two phases (Mayford et al., 2012). First, both the pre- and postsynaptic neurons must be active simultaneously and the post-synaptic neuron depolarized such that the magnesium ion blocking its pore is removed upon pre-synaptic release of glutamate. The resulting intracellular Ca2+ influx mediated by the post-synaptic NMDAR is maximal and activates intracellular signalling cascades that ultimately trigger a change in synaptic weight by increasing insertion of AMPA receptors and their conductance in a process named early-LTP (Shi et al., 1999). The second phase (late LTP (L-LTP)) entails the increase of synaptic weight maintained by a process named ‘cellular consolidation’, which is protein-synthesis dependent and results in the increased synthesis of AMPA receptors (Govindarajan et al., 2006; Mayford et al., 2012). In summary, modifications in synaptic strength are thought to support the formation and storage of memories in neuronal ensembles (Malinow et al., 2000). Cellular engrams were shown to exhibit changes in synaptic weight consistent with LTP such as high current amplitude, high excitatory post-synaptic current frequency and amplitude, AMPAR insertion and increased dendritic spine density.

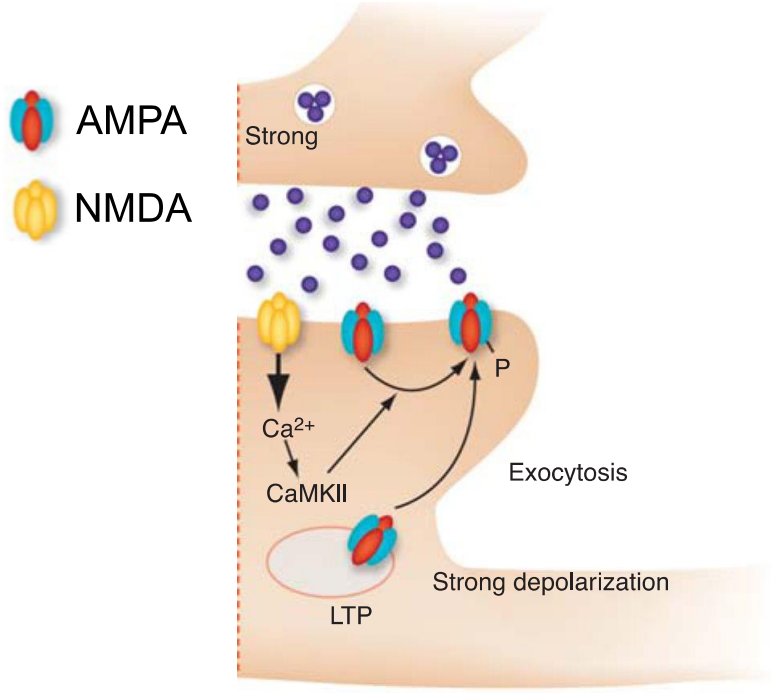

Figure 1.8. Schematic of the postsynaptic expression mechanism of LTP. Adapted from from (Lüscher and Malenka, 2012). Strong activity paired with strong depolarization triggers LTP in part via CaMKII, receptor phosphorylation, and exocytosis.

Causal role of engrams in memory encoding

Experimental work has revealed a causal link between modification of synaptic strength and memory encoding (Nabavi et al., 2014). Using fear conditioning (a type of associative memory) (Markram et al., 1997; Semon, 1921), the authors artificially inactivated and reactivated a fear memory by inducing LTD and LTP, establishing a causal link between changes in synaptic strength and memory encoding. Recent experimental work has also looked at the causal role played by engram neurons during memory encoding and recall by specifically tagging cells that were activated during learning. The authors expressed Channelrhodopsin in these engram cells and optogenetic reactivation of these cells triggered recall of a learned behaviour (Liu et al., 2012). Furthermore, it has been possible to artificially generate a memory trace through neuronal labelling during exposure to a neutral context and subsequent reactivation in a fear-conditioning context. The authors showed that re-exposure to the first neutral context elicited recall of the fear memory in the first neutral context, indicating context-specificity of this fear memory recall (Ramirez et al., 2013). Overall, this body of work has yielded compelling evidence for the crucial role played by cellular engrams during memory encoding and recall.

3. Spatial representations in the hippocampus

A major obstacle in the study of declarative memory in animal models is that they lack the ability to use language, and thus to express what they have learnt in a human understandable form. As a result of the inability of animals to articulate their experiences, certain animal behaviours are used as a substitute for reading out memories. One such behaviour is spatial navigation, since spatial memory is considered to be a subset of declarative memory and since the hippocampus and related structures were shown to be important for it (Eichenbaum and Cohen, 2004; Squire, 1992). Technological improvements in the recording of neuronal activity, in particular microelectrode recordings, have enabled the study of cellular and circuit mechanisms of memory encoding by measuring neuronal population dynamics in the hippocampus in relation to the navigational behaviour of the animal. The study of patterns of neuronal activity in relation to the position of the animal has led to the discovery of hippocampal neurons that represent the location of the animal in a given environment (O'Keefe and Dostrovsky, 1971). Collectively, these neurons are thought to form a cognitive map that guides the animal's navigation in space (Moser et al., 2008; O'Keefe and Nadel, 1978; Tolman, 1948). Whether the functional role of the cognitive maps goes beyond navigation the physical in space remains a matter of debate (Buzsáki and Moser, 2013; O'Keefe and Krupic, 2021). A body of experimental work has suggested that the spatial component of contextual information is not central to the cognitive map but rather, that the neural algorithms underlying spatial processing can process multiple types of information relevant to an episode, whether spatial or non-spatial, to ultimately support the formation of memories related to a given spatial context (Aronov et al., 2017; Buzsáki and Moser, 2013; Wood et al., 1999).

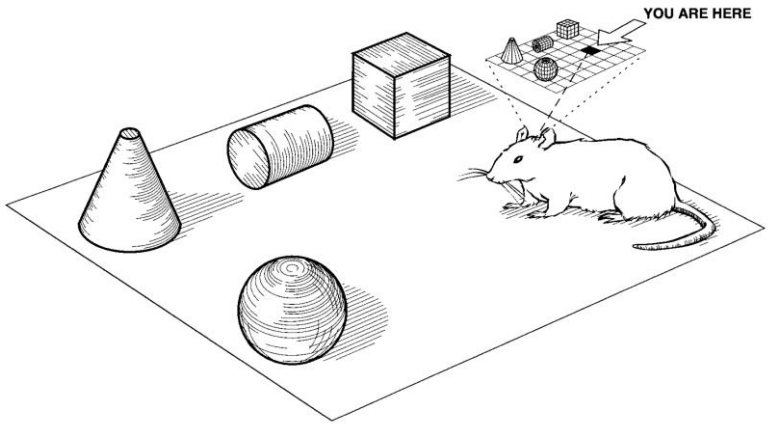

Figure 1.9. Conceptual model of the hippocampal representation of a spatial environment according to the cognitive mapping hypothesis. Adapted from (Eichenbaum et al., 1999).

3.1. Relationship between of spatial coding in the hippocampus and memory

Whether the hippocampus functions to support episodic memory or navigation behaviour, or both, is a difficult one to solve since a representation of the physical environment is nearly always an integral component of episodic memories. It is thought that the mechanisms underlying navigation in the physical space have evolved to form the basis of navigation in mental space, such that the same neural algorithms underlie two seemingly unrelated functions of the hippocampus: memory and navigation. In this scenario, egocentric navigation is necessary for subjective experiences to be encoded by the episodic memory system, which then become context-independent and allow the creation of semantic memory (Buzsáki and Moser, 2013; Kunz et al., 2021). In other words, spatial navigation in the hippocampus would act as an index of experiences necessary for memory organisation (Benna and Fusi, 2019; Eichenbaum, 2017; Tanaka and McHugh, 2018). The discretization of memories, spaces and events takes place along multiple axes and follows stereotyped principles of organisation, allowing continuous insertion and interaction of new memories within a network of prior knowledge in the hippocampus (Gava et al., 2021). Coherent with the idea of a common algorithm supporting navigation and memory, neuronal populations supporting spatial navigation are functional prior to the start of the animal's exploration of its environment, suggesting that the brain system allowing representation and storage of self-location in the environment is at least partly preconfigured and matures with experience (Tan et al., 2017; Wills and Cacucci, 2014; Wills et al., 2014).

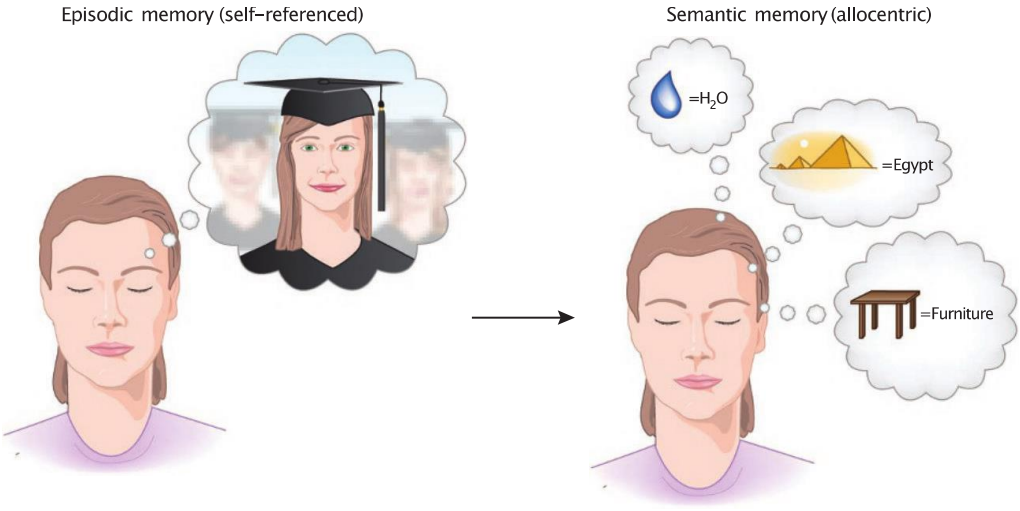

Figure 1.10. Schematic representation of episodic and semantic memory. Adapted from (Buzsáki and Moser, 2013). Episodic memory is 'mental travel' in time and space referenced to self while semantic memory is explicit representation of living things, objects, places and events without temporal or contextual references. Semantic knowledge can be acquired through multiple episodes with common elements.

3.2. CA1 place cells

In 1971, CA1 hippocampal neurons were found to represent the location of freely moving rats in space. This seminal discovery revealed the existence of 'place cells': hippocampal neurons that are active when the animal passes through a specific location of the physical environment (O'Keefe and Dostrovsky, 1971). The locations in the environment where place cells are active are named 'place fields' and are largely statistically independent from each other such that place cell populations collectively represent the entirety of the environment (O'Keefe and Conway, 1978; Wilson and McNaughton, 1993). Place cells were originally discovered in CA1, but the existence of a place code that generates a representation of space and of the animal's position has since then been established in other hippocampal subregions (Jung and McNaughton, 1993; Leutgeb et al., 2007; Lu et al., 2015), in other brain regions such as the visual cortex (Fiser et al., 2016; Pakan et al., 2018; Saleem et al., 2018) and in many mammalian as well as bird species (Ekstrom et al., 2003; Payne et al., 2021; Rolls and Treves, 1997; Ulanovsky and Moss, 2007) including humans (Julian and Doeller, 2021). The rodent remains nevertheless the animal model of choice to investigate spatial representations given the similarity of its neuroanatomy and functionality of its nervous system to that of humans and its accessibility to genetic manipulations, which are a crucial tool to probe the circuit and molecular basis of neuronal computations. Studies using the rodent hippocampus were instrumental to characterize cellular and circuit mechanisms underlying spatial coding and memory in the hippocampus, of which specific features will be discussed in details in the following subchapters.

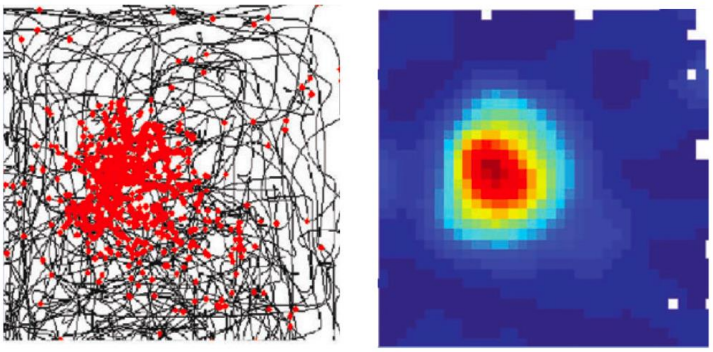

Figure 1.11: Firing field for a representative place cell. Adapted from (Moser et al., 2015). (**left**) Place cell spikes superimposed onto the mouse trajectory; (**right**) corresponding color-coded rate map. The color scale is from blue (silent) to red (peak rate), with pixels not visited shown in white. The rate maps were scaled to the maximum firing rate within the entire testing sequence.

Heterogeneous spatial responses

CA1 neurons represent the physical space heterogeneously and are differentially modulated by changes in contextual information. For instance, some but not all CA1 place cells with a place field in a given environment remap upon exposure to a novel odor (Anderson and Jeffery, 2003). Similarly, subpopulations of CA1 pyramidal neurons respond to taste in addition to spatial information (Herzog et al., 2019) and show variable levels of cell propensity (Lee et al., 2019). The heterogeneity of activity profiles in CA1 might be explained by connectivity patterns: proximal CA1 preferentially receives projections from MEC while distal CA1 receives projections from LEC (Naber et al., 2001; Steward, 1976). By contrast, input segregation along the transverse axis of the hippocampus is not observed in the dentate gyrus and CA3. The differential connectivity patterns of distal and proximal CA1 are related to functional differences within the CA1 population, whereby when exposed to conflicting local and global cues, proximal CA1 shows a conflicted spatial representation coherent with the conflicting inputs received, while distal CA1 shows a stable representation related to the global cues (Deshmukh, 2020). Proximal CA1, which receives stronger inputs from the MEC, is more strongly spatially modulated than distal CA1 (Henriksen et al., 2010). In addition to variations in CA1 activity patterns along the hippocampal transverse axis, layer-specific differences were observed in the CA1 region during spatial navigation: superficial pyramidal cells in the CA1 region form a stable representation of space while their counterparts in deep CA1 layers generate a more flexible representation that is modulated by learning and contextual features (Danielson et al., 2016a). Superficial CA1 pyramidal neurons are also more active in cue-poor environments and are driven by intra-hippocampal inputs whereas deep-layer CA1 neurons are more active in cue-rich environments and use a phase code driven by entorhinal inputs. The interaction between excitatory gamma inputs and local inhibition enables the switch between the two types of coding (Sharif et al., 2021). Thus, subpopulations of CA1 neurons display distinct patterns of connectivity, which might shape distinct profiles of spatial activity.

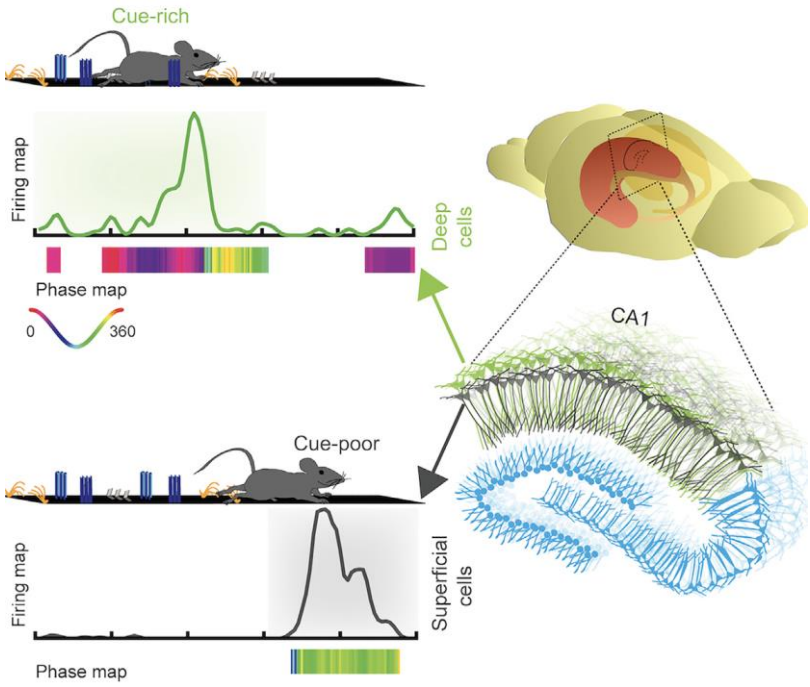

Figure 1.12. Differential role of deep and superficial CA1 place cells during spatial coding across heterogeneous environments. Adapted from (Sharif et al., 2021) (graphical abstract). The existence of segregated hippocampal circuits for spatial coding across heterogeneous environments. Deep and superficial CA1 place cells used different codes for space depending on the availability of cues. A rapid switch between these two spatial coding modes was supported by the interaction between gamma inputs.

CA1 representation of space is dynamic

The hippocampal place code contains both dynamic and stable features. When recorded chronically during a behavioural task, CA1 place cells show a large turnover and a heterogeneous re-organisation, but also maintain a stable and robust representation of the environment (Levy et al., 2019; Ziv et al., 2013). In fact, multiple stable maps of the same environment can co-exist as hippocampal neurons switch between distinct and stable maps across lap crossings in a linear track (Sheintuch et al., 2020). Long-term changes in firing properties of CA1 populations named ‘representational drift’ (Ziv et al., 2013) were shown to arise orthogonally to contextual representations in network space, suggesting that stable and robust contextual representations across weeks and drift in representations can coexist as distinct neural codes within the same population of neurons (Keinath et al., 2020). The orthogonal storage of robust spatial representations and representational drift is consistent with the observation that information stored in networks of synchronously active neurons is resistant to time and hippocampal damage while information stored in individual neurons is labile (Gonzalez et al., 2019). These results suggest that representation of space does not

solely consist in the tuning of hippocampal neurons to a single location in space but rather, consists in a complex interaction of multiple stable maps that co-exist within the hippocampus.

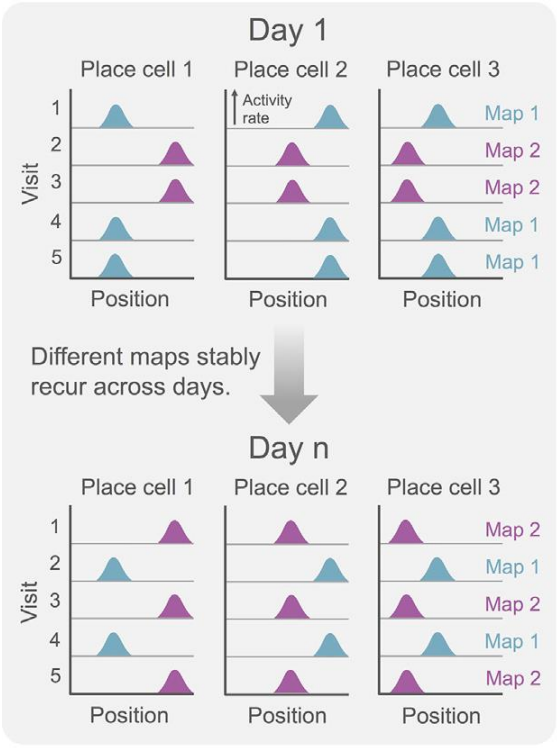

Figure 1.13. Multiple maps of the same spatial context can coexist in the hippocampus. Adapted from (Sheintuch et al., 2020). Hippocampal neurons can switch between distinct spatial representations (maps) across separate visits to the same environment, without any apparent changes in sensory input or behavior. The distinct maps are spatially informative and stable over weeks.

Directionally selective spatial representations

Place cells do not respond exclusively to the position of the animal in space, they also respond to the direction of motion of the animal in the environment. While some studies failed to find directional selectivity in hippocampal firing during navigation in a 2D environment, other work reported that the direction of motion of the animal in space modulates place coding in CA1 and CA3 hippocampal sub-regions as well as the dentate gyrus (Jung and McNaughton, 1993; Markus et al., 1995; Muller et al., 1987; Per et al., 2007). Directional firing is thought not to be an intrinsic firing property but rather, to result from the difference in time spent by the animal in different portions of the place cell firing-field in different head direction sectors (Muller and Kubie, 1987).

Directional selectivity of hippocampal firing develops through experience-dependent plasticity (Navratilova et al., 2012) and can be modulated by multiple factors. For instance, the type of physical environment an animal is exposed to modulates spatial representations such that both grid and place cells increase their spatial tuning and directional selectivity during navigation in a linear corridor or a radial arm maze but not when the animal's path is unrestrained in an open arena (Markus et al., 1995; Muller et al., 1987; Pröll et al., 2018). Directional representations in CA1 are also more pronounced during behavioural tasks anchored in the physical world than in virtual reality, suggesting that the multisensory nature of the physical environment plays an important role in the construction of spatiotemporally selective representations (Ravassard et al., 2013). The behavioural demand of the task also modulates the directionality of representations and directional selectivity of spatial representations is more pronounced when the animal needs to plan a route between different locations (Brunel and Trullier, 1998; Markus et al., 1995). The availability of local sensory cues also affects directional selectivity by inducing bi-directionality in CA1 place cells (Battaglia, 2004), a process that might be mediated by head-direction signals (Acharya et al., 2016), consistently with recent work showing that neurons in the dysgranular retrosplenial cortex encode environmental symmetry by generating directional tuning curves (Zhang et al., 2020). Overall, hippocampal neurons show directionally selective representations, the extent of which varies depending on a range of environmental factors as well as the behavioural demand of the task.

Place cell formation

Some neuronal populations supporting spatial navigation are functional prior to the start of the animal's exploration of its environment, suggesting that the brain system that allows representation and storage of self-location in the environment is at least partly pre-configured and matures with experience (Tan et al., 2017; Wills and Cacucci, 2014; Wills et al., 2014). A number of factors come into play to determine why some neurons become place cells and not others. In a novel environment, place cells have different intrinsic cellular properties and baseline membrane potential compared to silent cells (Epsztein et al., 2011). Activity-dependent synaptic plasticity seems to underlie place field formation (Sheffield et al., 2017). In CA1, conjunctive inputs from entorhinal cortex and CA3 were shown to produce dendritic plateau potentials that modulate place field firing and induce the formation of new place fields (Bittner et al., 2015). Place fields can develop in the absence of theta rhythm and grid cell activity (Brandon et al., 2014). In the dentate gyrus, granule cells are thought to develop a spatial representation of the environment via competitive learning (Kim et al., 2020). This

Winner-takes-all strategy is thought to be implemented by competition between granule cell firing and feedback inhibition from basket cells (Kim and Lim, 2021). Spatial learning engages a reconfiguration of the hippocampal interneuron circuitry, which is thought to assist separation of competing cell assembly patterns (Dupret et al., 2013). Importantly, place cell formation is not sequential along the hippocampal circuit, since the dentate gyrus is not required for place cell formation in CA3 and CA1; and similarly, CA3 is not required for the formation of the CA1 place cells (Brun, 2002; McNaughton et al., 1989; Mizumori et al., 1989).

Selection of 'spatially modulated cells'

To understand how neural correlates of external variables guide behaviour, current research seeks to understand how information relative to the position of the animal in space is encoded in the brain by selecting neurons whose activity is associated with the physical location of the animal and examining their spatial tuning (Hainmueller and Bartos, 2018; Ziv et al., 2013). The selection of these 'spatially modulated cells' is made by setting an arbitrary threshold that is at least in part guided by arbitrary criteria. The arbitrary nature of the selection criteria and the disregard for the contribution of non-spatially modulated cells that are inherent to this selection process are problematic. In fact, neurons that fail to pass typical criteria for place cells provide an important contribution to spatial coding, as the coactive firing of ensembles can represent position or the global environment at the population level even in the absence of apparent spatial modulation at the single-cell level (Levy et al., 2021; Posani et al., 2017; Sheintuch et al., 2020; Stefanini et al., 2018). Non-spatially modulated neurons can also be selective for a given spatial environment based on changes in firing rates (Allegra et al., 2020). The exclusive use of the first order feature firing rate is also changing as millisecond-timescale co-activity of the CA1 neuronal population can also contribute to encoding behaviourally relevant variables (El-Gaby et al., 2021). Thus, recent experimental work has revealed the ability of non-spatially modulated neurons to build representations of an environment, suggesting that spatial representations should not solely be understood in terms of first order feature firing rate of place cells but rather, should consider different population coding mechanisms such as ensemble co-activity and include non-spatially modulated neurons.

Allocentric vs egocentric coordinate systems

Two types of representation of the environment enable flexible navigation. On the one hand, allocentric navigation provides the individual with fixed positional information using a landmark-based reference map anchored in the outside world, while egocentric navigation calculates spatial coordinates using self-motion information (speed, time, head direction) and previous positions (Buzsáki and Moser, 2013; O'Keefe and Burgess, 2005). Conjunctive spatial coding based on navigational signals both in the egocentric reference frame and allocentric head direction signals were observed in many brain regions such as the parietal, retrosplenial, postrhinal cortices, parasubiculum and postsubiculum, suggesting that reference frames are coordinated upstream of the hippocampus (Alexander et al., 2020; Gofman et al., 2019; LaChance et al., 2019; Laurens et al., 2019; Wilber et al., 2014). The combination of these signals is thought to transform spatial representations into an allocentric spatial map and to give rise to 'landmark vector cells' in CA1, which represent distance to landmarks to allow flexible navigation. Although the hippocampus is an essential component of allocentric navigation, it is thought to interact with other brain regions to generate allocentric representations (Burgess et al., 2001; Byrne et al., 2007; Chrastil, 2013; Galati et al., 2010).

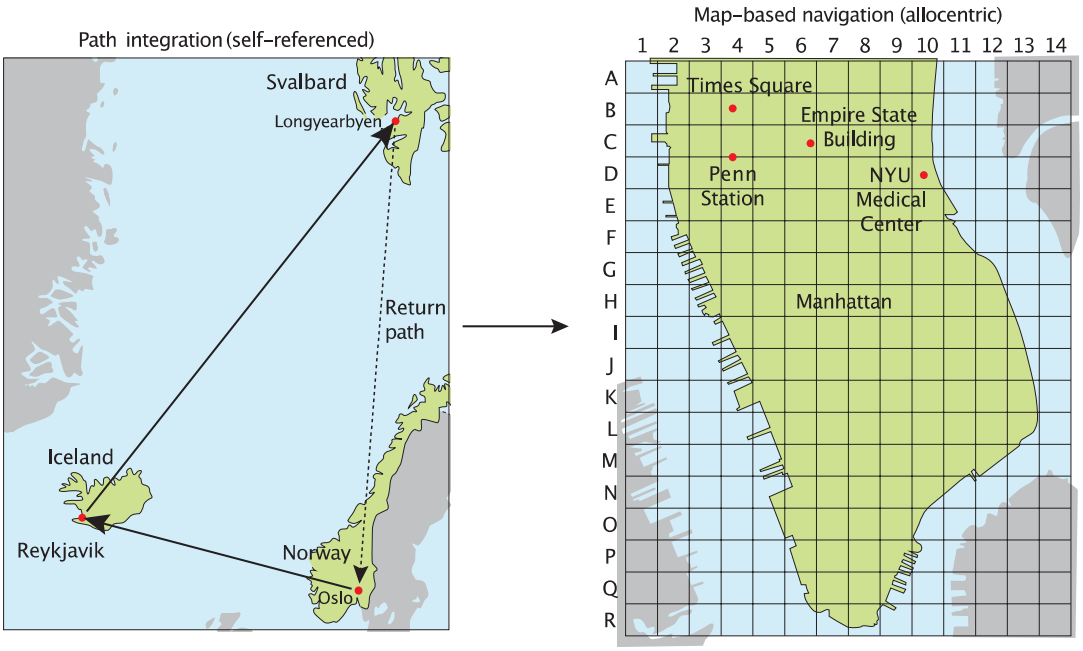

Figure 1.14. Schematic representation of path integration and map-based navigation. Adapted from (Buzsáki and Moser, 2013). Path integration (also known as dead reckoning) is based on self-referenced information by keeping track of travel distances (time elapsed multiplied by speed) and direction of turns. Calculating translocation relative to the start location allows the animal to return to the start along the shortest (homing) path. Map-based navigation is supported by the relationships among visible or otherwise detectable landmarks. A map is constructed by exploration (path integration).

Egocentric representations were recently discovered in the hippocampus and the LEC (Jercog et al., 2019; Laurens et al., 2019). What are the sources of egocentric information for the hippocampus? On the one hand, LEC neurons represent egocentric directional information relative to boundaries or objects, consistently with studies of rodent behaviour suggesting egocentric coding in LEC (Lisman, 2007; Wang et al., 2018). The LEC might receive this egocentric information from perirhinal, postrhinal and parietal cortices, from which it receives strong innervation (Olsen et al., 2017; Wilson and McNaughton, 1993). On the other hand, MEC exhibits allocentric head direction signals and might provide an allocentric representation of self-location through path integration. These could in turn support the formation of allocentric object vector cells in CA1 and MEC (Deshmukh and Knierim, 2011; Høydal et al., 2019) by means of transformation of spatial representations (Bicanski and Burgess, 2018; Byrne et al., 2007; Knierim and McNaughton, 2001). Egocentric coding in the hippocampus would be coherent with its role in processing memories relative to one's personal experience. To represent an episode, the hippocampus integrates egocentric inputs from the LEC to provide information about the content of a memory, while MEC inputs provide a consistent framework across environments (Fyhn et al., 2007). The use of egocentric versus allocentric navigation depends on the availability of spatial landmarks (Gothard et al., 1996).

CA1 binds spatial information into a global context

CA1 is the last outpost of the mostly unidirectional hippocampal circuit and is thought to drive the transfer of information that has been processed in the hippocampus back to neocortical regions. When an animal is exposed to resembling environments, CA1 is less contextually selective than CA3 and the dentate gyrus, responds to common environmental features and builds representations that overlap across environments (Allegra et al., 2020; Leutgeb, 2004). The observation that CA1 neuronal firing is variable during repeated passes through firing fields led to the hypothesis that CA1 might be encoding variables other than spatial information (Fenton and Muller, 1998). Consistently with this hypothesis, it was proposed that CA1 represents abstract spatial variables rather than raw sensory information (Muller and Kubie, 1987) such as the future path of the animal during goal-directed behaviour (Ito et al., 2015), the memory of recent behaviour or experiences (Keinath et al., 2020) and to use previous experience to build an ideal estimate of the environment (Plitt and Giocomo, 2021). Consistently with the idea of a coherent and abstract representation of space, CA1 pyramidal cells are the only hippocampal neurons whose activity is correlated with the animal's behaviour (Allegra et al., 2020). In fact, selective activation of place cells encoding behaviourally relevant locations in a virtual environment biases the animal's behaviour during

a spatial memory task, showing that place cells play an essential role during navigation behaviour (Robinson et al., 2020). In summary, this body of work suggests that CA1 might integrate multiple types of spatial variables to construct a global, coherent and behaviourally relevant representation of the physical environment to then transfer to the neocortical areas.

3.2. Multiple types of neurons contribute to representing the environment

Cells that represent elements of an animal's location and orientation in the physical space were identified in regions other than CA1, such as in the entorhinal cortex. This brain region is located one synapse upstream from the hippocampus and is its main source of excitatory inputs through the perforant path fibers, but it also provides a direct input to other hippocampal subregions. The entorhinal cortex shows structural and functional subdivisions between its medial and lateral components (Hargreaves et al., 2005). The LEC contains neurons that represent non-spatial information such as objects and object-related spatial information, and they were also shown to encode time (Tsao et al., 2013; Wang et al., 2018). By contrast, the MEC contains many types of spatially modulated neurons such as head-direction cells, boundary vector or border cells, object vector cells and grid cells. Single MEC neurons show conjunctive coding of positional, directional and translational information (Sargolini, 2006). In addition to spatial coding, the entorhinal cortex was shown to be sensitive to temporal sequence of events, as well as the content of events. By generating an intrinsic time code, it constructs a temporal sequence of past events, thereby supporting episodic memory (Bright et al., 2020; Heys and Dombeck, 2018; Tsao et al., 2018).

Grid cells

Grid cells were originally discovered in the MEC and form a topographical map of the environment by tiling the entirety of the environment with a geometrically regular pattern made of multiple firing fields to provide a distance metric, by contrast to hippocampal place cells, which display individual place fields (Hafting et al., 2005). They exhibit a stable and preserved representation of the environment, suggesting that they produce a metric that can be applied across multiple environments; the position of the animal can be accurately established from the activity of a few grid cells (Buzsáki and Moser, 2013; Hafting et al., 2005; McNaughton et al., 2006). They are displaced relative to one another, and show a gradient of grid field size along the MEC dorsolateral-ventromedial axis, resulting in a re-scaling and re-orientation of the spatial representation (Brun et al., 2008; Fyhn, 2004). The MEC projects to the hippocampus (Dolorfo and Amaral, 1998; van Groen et al., 2003; Kerr et al., 2007;

Steward, 1976) and grid cells with small field scale in dorsolateral MEC might connect with place cells with small field scale in septal hippocampus while grid cells with large field scales in ventromedial MEC connect with place cells in temporal hippocampus with large place field scale (van Strien et al., 2009).

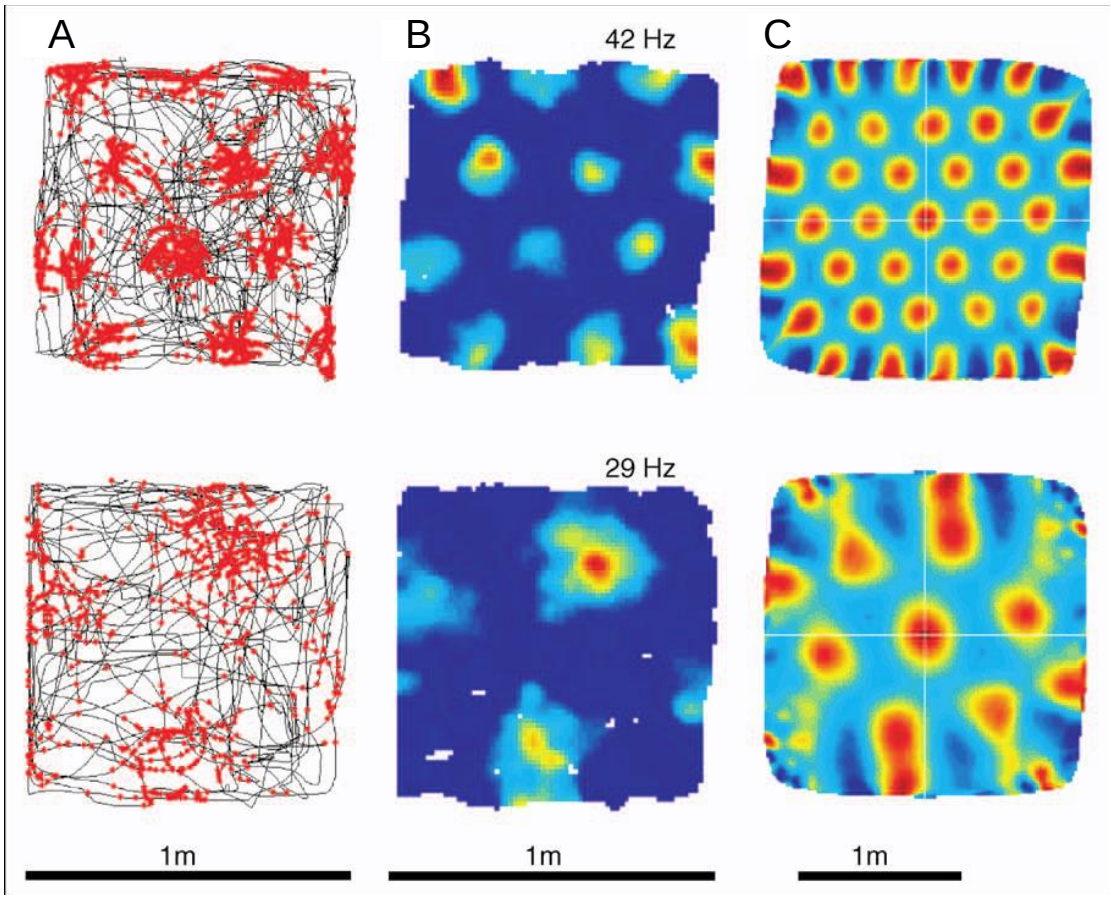

Figure 1.15. Representation of tessellating firing fields of grid cells in the medial entorhinal cortex. Adapted from (Leutgeb et al., 2005). Firing rate distributions are shown for two cells (top and bottom rows, respectively) that were recorded during running in a square enclosure. (**A**) Trajectory of the rat (black line) with superimposed spike locations (red dots); (**B**) rate map; (**C**) spatial autocorrelation for the rate map in B. Maps in B and C are color-coded. In B, blue is 0 Hz, red is peak rate. In C, the scale is from blue (r=_1) through green (r=0) to red (r=1.0). Scale bar indicates size of recording enclosure. Note that the distance scale in the autocorrelation diagrams is half of that of the original maps, with points along the perimeter showing correlations between positions spaced by a distance similar to the width of the enclosure. The distributions were recorded from cells located at different distances from the dorsal border of the medial entorhinal cortex; the top cell was most dorsal.

Similarly to the place code, the grid code for space is highly dynamic, adaptive and displays mixed selectivity (Fyhn, 2004; Hardcastle et al., 2017). Grid cell activity contains information about position (grid vertices), direction (grid orientation), distance (grid cycle number) and displays local directionality, whereby grid-cell firing is modulated by the direction of motion of the animal in a location-dependent manner (Gerlei et al., 2019). Directional modulation of grid cell function is consistent with their receiving inputs from upstream head-direction-dependent conjunctive coding cells (Sargolini, 2006). Path integration, a process that allows

animals to keep track of their position within an environment by integrating linear and angular self-motion information (Etienne and Jeffery, 2004; Sharp et al., 1996) is thought to be implemented in grid cells. This information, which might be conveyed to the hippocampus by MEC grid cells, is an important determinant of place cell activity and might support idiothetic navigation and update of the spatial representation in the hippocampal system (Fuhs, 2006; Moser et al., 2008; O'Keefe and Burgess, 2005; O'Keefe and Conway, 1978).

Transformation from grid to place code

The discovery of grid cells in the MEC has provided a new framework to elucidate the mechanism underlying the emergence of spatial representations in the hippocampus and how they support episodic memory (Fyhn, 2004; Hafting et al., 2005). The transformation of the grid code into the place code has sparked a lot of interest (Cheng and Frank, 2011; Kanter et al., 2017). The place code uses environmental sensory information while the grid code integrates information based on self-motion; this is done through complementary attractor representations (Laptev and Burgess, 2019). CA1 receives inputs from MECIII, which comprises grid cells, although they are more abundant in the entorhinal cortex layer II. Depolarization of MECIII neurons causes a positional shift in downstream CA1 place fields and impairs spatial memory. By contrast, MECIII neurons showed a change in firing rate thus reconfiguring spatial inputs to CA1, but the location of their place fields remained unaltered (Kanter et al., 2017) Contrary to these findings, pharmacological reduction of theta oscillations blocked grid-cell firing patterns while place field firing remained intact. Thus, the diversity of functional projections to CA1 place cells suggests that place cell signals might result from the integration of information from multiple functional cell types in the entorhinal cortex, in addition to CA3 neurons (Zhang et al., 2013) although their precise functional contributions remain to be elucidated.

Other types of spatially modulated neurons

Neurons in the dentate gyrus and hippocampal subregion CA3 also represent the environment; their contributions will be discussed in detail in the following chapters. Other cell types outside the hippocampus construct a representation of space and include head-direction cells, whose activity encodes the direction of movement of the animal (Taube et al., 1990) and boundary vector cells, which are active when the animal approaches obstacles to its movement (Lever et al., 2009; Solstad et al., 2008). Directionally-tuned cells are also observed in the entorhinal cortex, retrosplenial cortex, lateral mammillary nucleus, striatum and anterior and lateral dorsal thalamic nuclei, suggesting that directional signals probably

stem from brain regions outside the hippocampus (Chen et al., 1994; Mizumori and Williams, 1993; Sargolini, 2006; Stackman and Taube, 1997). However, although spatial representations and navigational signals have been observed in other cortical areas such as the parietal and posterior cortex, intact hippocampal activity is required for a cortical spatial representation to be maintained (Esteves et al., 2021; Krumin et al., 2019). Collectively, these cell types build a neural representation of an animal's physical environment and the animal's location within it, which is thought to form the basis of the cognitive map that is the internal representation of the environment that the animal uses to consciously navigate in space (O'Keefe and Nadel, 1978). These discoveries led to the notion that in addition to topographical 'maps' representing sensory information, the hippocampus can integrate highly processed information in order to generate complex cognitive maps.

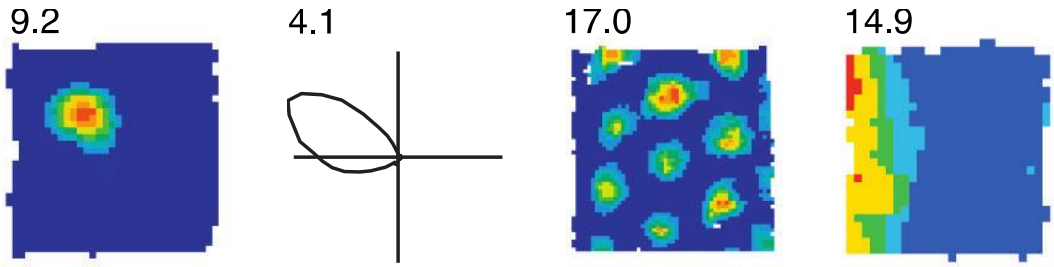

Figure 1.16. Examples of spatially tuned neurons. Adapted from (Wills and Cacucci, 2014). (**Left**) A place cell. (**Middle left**) A head direction cell. (**Middle right**) A grid cell. (**Right**) A boundary vector/border cell. For head-direction cells, the polar plot represents the firing rate (action potentials/seconds of dwell time) for each directional heading. For all other cell types, the false-color firing map represents an overhead view of the recording arena. When the animal visited the positions shown in hot colors, the firing rate was high.

3.3. Representations of non-spatial variables in the hippocampus

The functional role of neurons whose activity is modulated by the location of an animal in space is more complex than merely generating a cartography of a given environment (Eichenbaum et al., 1999; McNamara and Shelton). In addition to representing physical environment and changes associated to it, hippocampal neurons have also been shown to represent non-spatial variables such as non-spatial sensory inputs (Hampson et al., 1993; Leutgeb, 2005; Wood et al., 1999; Young et al., 1994). In fact, the very same neurons that encode the spatial position of the animal can also encode non-spatial variables such as reward or auditory frequencies and can construct representations based on value the same way place cells represent position (Aronov et al., 2017; Gauthier and Tank, 2018; Knudsen and Wallis, 2021). Hippocampal neurons are also sensitive to time and were shown to encode the temporal dimension and sequence of distinct events in addition to space and behaviour (MacDonald et al., 2011; Reddy et al., 2020). Representation of time is also crucial to build

episodic memories: temporal information is robustly represented in neuronal populations in the LEC, by contrast to MEC, dentate gyrus and CA3 (Tsao et al., 2018). Temporal associative memory is dependent on layer III of the entorhinal cortex (Suh et al., 2011) but temporal associative learning does not require persistent neuronal activity (Ahmed et al., 2019). The hippocampus also represents hypothetical experiences and possible scenarios, which might be relevant for imagination and planning cognitive processes (Kay et al., 2020). Coherently with this idea, hippocampal neurons represent events as units of experience using rate remapping and lap crossings as a fundamental unit, and these units can be transferred across experiences (Sun et al., 2020). Hippocampal neurons were also shown to have sequence-like activity spanning up to minutes, which is thought to reflect spatiotemporal context (Liu et al., 2021). The capacity of neurons to represent multiple variables could be explained by their capacity to represent multiple dimensions of variables, as was shown in a study using *C. elegans* (França and Monserrat, 2018). Considering that in an experimental setting the experimenter has little control over variables other than space, such as goal, attention of the animal, the difficulty lies in the disambiguation of the experience from time and space.

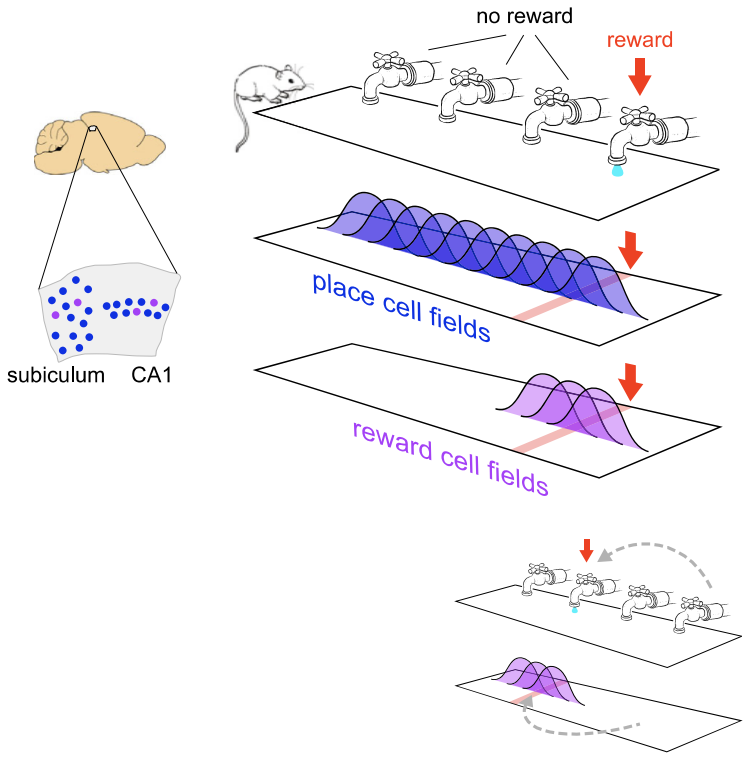

Figure 1.17. A dedicated population of hippocampal neurons code for reward. Adapted from (Gauthier and Tank, 2018). In vivo imaging was used to identify a small population of CA1 and subiculum neurons specialized for encoding reward location. The same cells are active near multiple reward sites in one environment and even across environments during global remapping. Hippocampal maps contain a cell population dedicated to encoding the location of a hidden reward. When the reward location shifts, reward cell fields also shift.

Spatially modulated neurons were also shown to alternate between multiple spatial representations of the same environment and to reflect physical features of the environment and events associated to it (Fyhn et al., 2002; Muller and Kubie, 1987; Shapiro et al., 1997). For instance, CA1 cell ensembles were shown to encode the reward location or lap number in addition to the spatial representation using dedicated pools of cells (Gauthier and Tank, 2018; Sun et al., 2015). In the dentate gyrus, external cues (sensory stimuli or small changes in the environment) are encoded by a subset of neurons that are distinct from that which build a stable representation of the environment (GoodSmith et al., 2021; Tuncdemir et al., 2020). Hippocampal neurons also encode information about external stimuli and their temporal relationships using context-specific sequences. Information about the sensory stimuli was represented using stable cell ensembles while time cell ensembles were represented using sparse and dynamic population activity that remapped readily (Taxidis et al., 2020). Similarly, it was shown that hippocampal ensemble dynamics produce temporal coding whereby experienced events are time-stamped and can be associated or dissociated based on their temporal value (Rubin et al., 2015). This body of experimental work suggests that hippocampal neurons can encode context-specific memories where the spatial component is necessary but non-exclusive. How the spatial and non-spatial components of events are integrated into episodic memories remains to be elucidated.

Hippocampal neurons also change their spatial activity when the animal is exposed to a novel environment. For instance, some CA1 neurons with a place field in a given environment change their spatial activity upon exposure to a novel olfactory stimulus (Anderson and Jeffery, 2003) and following changes in contextual information (Muller and Kubie, 1987). Upon exposure to a novel environment, CA1 place cells develop rapidly and are prone to remapping when the environment changes by contrast to CA3 fields, which arise progressively but are more stable across trials, suggesting that distinct mechanisms underlie place cell formation across subregions (Dong et al., 2021). Repeated exposures to the same environment improve its representation discriminability while exposure to different contexts enhances generalization and network predictability of new contexts (Liu et al., 2021). Neuromodulation is thought to play an important role in novelty detection. It was shown that mossy cells in the ventral hippocampus gate contextual novelty by sending excitatory projections to granule cells in the dorsal hippocampus (Fredes et al., 2021).

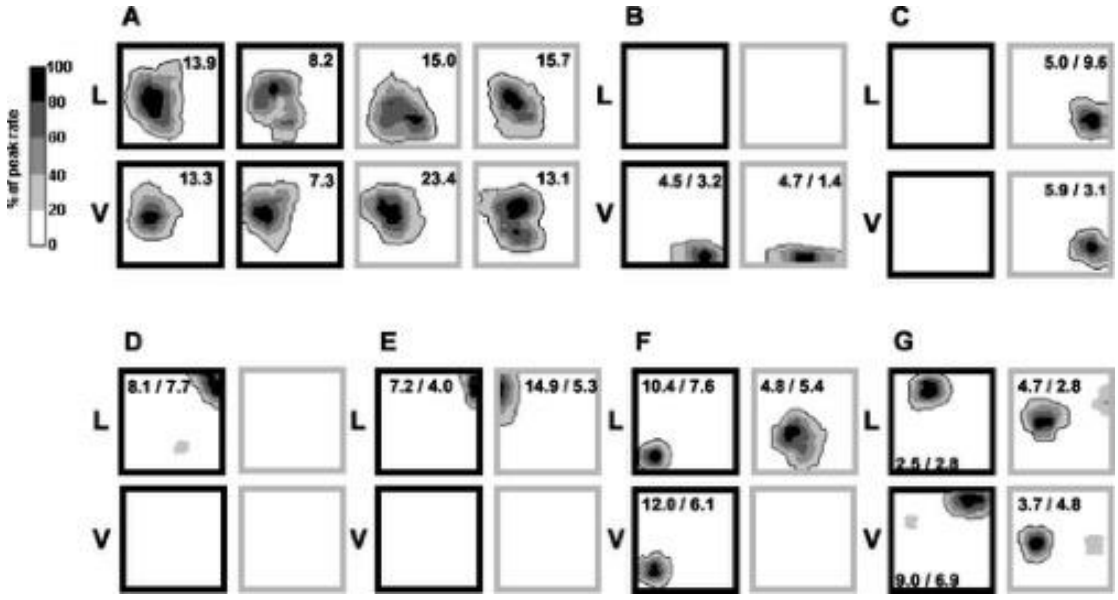

Figure 1.18. Representation of place cell remapping following changes in contextual information. Adapted from (Anderson and Jeffery, 2003) (**A**–**G**) Place cell remapping across contextual configurations (all complete data sets). (**A**) A unit that maintained its place field in all of the contexts (same condition r values: black lemon, 0.89; white lemon, 0.84; black vanilla, 0.91; white vanilla, 0.85; median different condition r values: black lemon and white lemon, 0.72; black lemon and black vanilla, 0.86; black lemon and white vanilla, 0.90; white lemon and black vanilla, 0.57; white lemon and white vanilla, 0.76; black vanilla and white vanilla 0.86). For this unit, all eight trials are displayed. For the units in B–G, only four trials are displayed, one for each context; these units had the same place fields in both trials of each context; the extra trials are omitted to save space. The letter to the left of each figure panel is a description of the context odor (L, lemon; V, vanilla) and refers to each map in that row. The context color is indicated by the dark and light boxes bordering each map (a dark box for the black contexts, a light box for the white contexts). The number inside each box in A indicates the peak firing rate for the corresponding map (in hertz); the two numbers inside each box in B–G indicate the peak firing rates for both trials in the corresponding context, with the rate for the displayed trial given first. Place fields are displayed as contour maps with five levels, each level representing a 20% portion of the peak firing rate for that map (color bar). (**B**) A unit that fired only in the vanilla contexts (black and white), expressing the same place field in both vanilla contexts. (**C**) A unit that fired only in the white contexts (lemon and vanilla). It had the same place field in both white contexts. (**D**) A unit that fired only in the black lemon context. (**E**) A unit that fired only in the lemon contexts (black and white) and remapped between them (compare with the unit in B). (**F**) A unit that had the same place field in the black contexts (lemon and vanilla) but that showed a different place field in the white lemon context and did not fire in the white vanilla context (same condition r values: black lemon, 0.94; white lemon, 0.77; black vanilla, 0.80; median different condition r values: black lemon and white lemon,_0.05; black lemon and black vanilla, 0.74; white lemon and black vanilla,_0.08). (**G**) A unit that fired in all contexts, with the same place field in the white contexts but two new fields in the black lemon and black vanilla contexts.

Within the framework of this project, we will focus on how the CA1, CA3 and the dentate gyrus of the hippocampus represent the physical space, and how these physical representations are modulated by contextual novelty.

4. Contributions of the dentate gyrus to spatial memory function

The neuroanatomical organisation of the dentate gyrus is unique. It is part of a largely unidirectional loop of input/output processing, exhibits large presynaptic terminals (the mossy fiber boutons) and supports the generation of neurons throughout the life of most mammals, suggesting that it plays a unique role in information processing (Amaral et al., 2007). The dentate gyrus is necessary for the formation of distinct representations of mnemonic information (Clelland et al., 2009), spatial memory storage (Lassalle et al., 2000; Pofahl et al., 2021) and acquisition and maintenance of episodic memories (Madroñal et al., 2016) during exploration as well as during immobility and sleep (Pofahl et al., 2021). Until relatively recently, cellular mechanisms underlying dentate gyrus function were unknown owing to the difficulty to identify cell populations and theories of dentate gyrus function were based on lesion studies and theoretical predictions. Now, the combination of electrophysiological recordings with neuronal labelling as well as imaging techniques allow the functional characterisation of identified neuronal populations in the dentate gyrus and their role in spatial memory processing (Preston-Ferrer and Burgalossi, 2018).

4.1. Pattern separation function in the dentate gyrus

One major challenge faced by the brain as individuals evolve in complex environments is to accurately represent information from the environment and prevent confusion between similar landmarks and events. To guide behaviour, it is crucial that the brain detects subtle differences between similar scenarios and generates distinct patterns of neural activity.

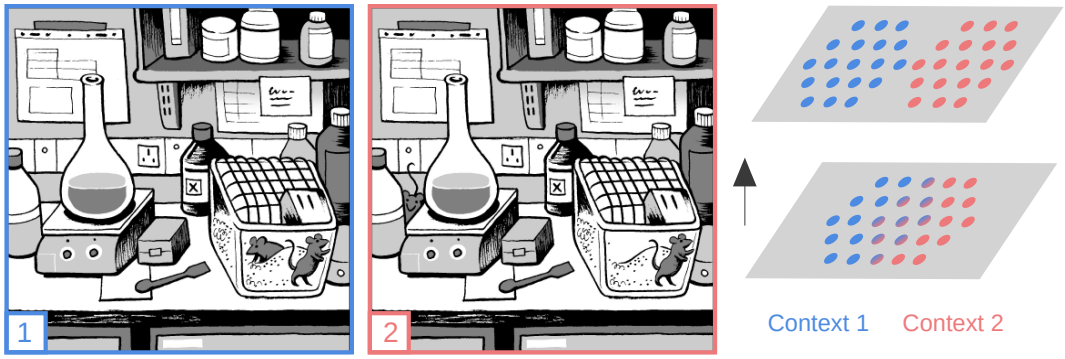

Figure 1.19. Cartoon depicting two near-identical events in a research laboratory. Adapted from (Cayco-Gajic and Silver, 2019). The small difference between the two scenarios is presumed to be behaviorally relevant as the action required in both scenarios is different. Right: Proposed circuit mechanism for disambiguation of similar neural activity patterns ("pattern separation") through activation of non-overlapping neuronal ensembles. Neurons active in context 1 are shown in blue and those active under context 2 are shown in red. Grey represents neurons that are silent in both contexts.

For the behavioural discrimination process to take place in the scene shown in Fig 1.19, the brain must transform similar input patterns into less overlapping output patterns through an orthogonalization process or 'pattern separation'. In other words, it amplifies differences between new representations and already existing memories and reduces the likelihood of interference during storage and errors during recall. The term 'pattern separation' was first defined as a computational operation performed by the cerebellum that describes a computational process taking place in a circuit featuring divergence of inputs onto a more numerous neuronal population with a low neuronal excitability controlled by widespread inhibition. The term is now used with regards to neuronal population activity as well as behavioural processes (Marr, 1969; McNaughton and Morris, 1987; Rolls and Treves, 1997).

As a unidirectional circuit at the entry to the hippocampus, the dentate gyrus is in an ideal position to perform pattern separation. Incoming multisensory inputs from the entorhinal cortex diverge onto a numerous population of granule cells, whose activity is very sparse and whose projections converge onto a smaller population of CA3 neurons (Amaral et al., 2007; Leutgeb, 2005; Rolls et al., 1998). The low probability of granule cells to contact CA3 pyramidal cells and the sparse firing in CA3 contribute to the hypothesis that dentate gyrus input patterns will likely result in non-overlapping activity patterns in CA3. Thus, pattern separation in the dentate gyrus is thought to support discrimination of resembling representations (Cayco-Gajic and Silver, 2019) and to be crucial during learning to store distinct memories of similar events (Rolls and Treves, 1997).

Experimental work based on dentate gyrus lesions and genetic deletions has provided indirect evidence for a role of the dentate gyrus in pattern separation (McHugh et al., 2007) for example during fine discrimination tasks (Gilbert et al., 2001). It is important to keep in mind that in these cases, pattern separation was defined with regards to the behavioural ability of an animal to discriminate similar information so that it can behave accordingly (Clelland et al., 2009). However, while behavioural pattern separation and neuronal pattern separation are distinct mechanisms, it is thought that neuronal pattern separation underlies behavioural pattern separation.

4.2. Spatial representations in the dentate gyrus

Recent experimental work has explored how the dentate gyrus discriminates different environments to better understand neuronal pattern separation. In humans, the first piece of evidence for pattern separation at the neuronal level in dentate gyrus/CA3 was indirect and came from an fMRI study where dentate gyrus/CA3 activity was evoked by closely resembling versions of known images as well as novel images, but not known images (Bakker et al., 2008). Electrophysiological and optical recordings from dentate gyrus granule cells in rodents exploring spatial environments have furthered our understanding of how the dentate gyrus represents the physical environment. Dentate gyrus granule cells exhibit multiple firing fields (Amaral et al., 2007; Leutgeb et al., 2005) and counterintuitively, they are also highly selective for different contexts and more sensitive to subtle changes in the environment than other hippocampal subregions (Allegra et al., 2020; Guo et al., 2021; Leutgeb et al., 2007; Neunuebel and Knierim, 2014). Dentate gyrus spatial representations for the same environment are also more stable across sessions and across days than that of other hippocampal subregions (Hainmueller and Bartos, 2018; Jung and McNaughton, 1993).

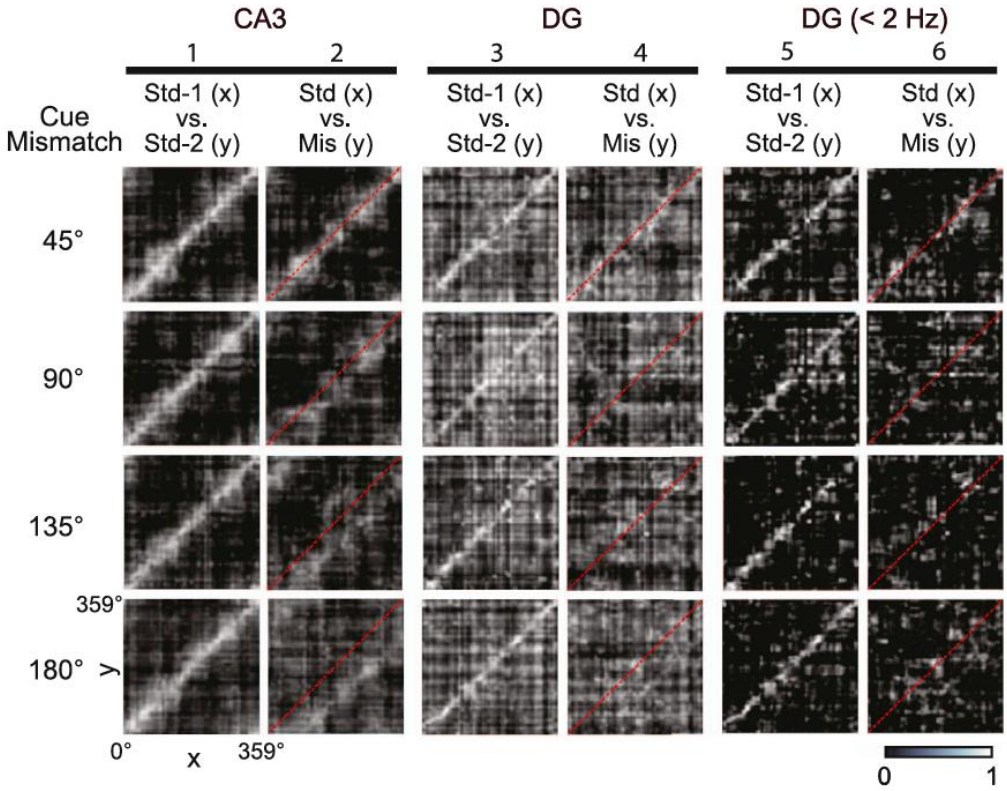

Figure 1.20. Population responses to cue-mismatch manipulations. Adapted from (Neunuebel and Knierim, 2014). Spatial correlation matrices were produced by correlating the normalised firing rate vectors for a standard (Std) session with those of the following Mismatch (Mis) or Std session. CA3 representations maintained coherence in all Mis sessions (column 2), indicated by the bands of high correlation (white) shifting below the identity line (dashed line), despite the decorrelated DG representations found in the input (columns 4 and 6).

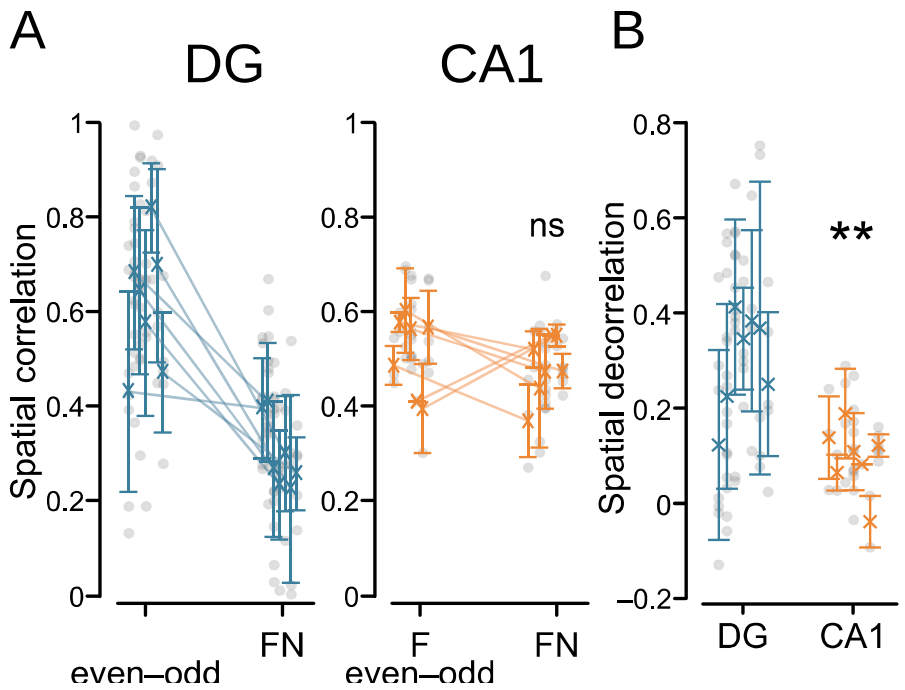

Figure 1.21. Correlations between spatial activity maps in familiar and novel environments. Adapted from (Allegra et al., 2020). (**A**) Correlations between mean spatial activity maps across recording sessions within the F environment (even-odd laps) and between different environments (FN) in the DG (left; spatial correlation: F even-odd, 0.62 ± 0.05; FN, 0.30 ± 0.03, n = 7 mice; Wilcoxon test, t = 0, p = 0.018) and CA1 (right; spatial correlation: F even-odd, 0.51 ± 0.03; FN, 0.48 ± 0.02, n = 7 mice; Wilcoxon test, t = 11, p = 0.61). Symbols with error bars represent mean ± SEM of individual animals. Grey circles represent recording sessions. (**B**) Spatial decorrelation, quantified as the difference between spatial correlations within the F environment (even-odd) and between different environments (FN) in the DG and CA1. Circles indicate single recorded sessions from different animals (spatial decorrelation: DG, 0.32 ± 0.06, n = 7; CA1, 0.03 ± 0.05, n = 7; linear mixed model [LMM], p = 0.002). Same symbols as in A.

Sparsity

Multiple possible mechanisms underlying pattern separation have been proposed (Guzman et al.). One possible mechanism is sparse coding whereby most cells are silent and the minority of active cells form unique activity patterns onto which ambiguous inputs can be mapped (Alme et al., 2010; Danielson et al., 2017; Diamantaki et al., 2016; Hainmueller and Bartos, 2018; Jung and McNaughton, 1993; Neunuebel and Knierim, 2012, 2014; Pilz et al., 2016; Senzai and Buzsáki, 2017). Sparse firing thus allows the dentate gyrus to orthogonalize incoming spatial inputs by mapping spatial environments onto non-overlapping pools of active cells. Individual granule cells active in a single environment are therefore highly selective for context (Allegra et al., 2020; Hainmueller and Bartos, 2018; Neunuebel and Knierim, 2012). Granule cells and mossy cells are thought to represent different environments via distinct neural mechanisms: sparse coding for the dentate gyrus, and neuronal remapping for mossy cells (Danielson et al., 2017; GoodSmith et al., 2017; Neunuebel and Knierim, 2012). Sparse coding in the dentate gyrus is thought to be enabled by inhibitory interneurons that exert an inhibitory influence on granule cells through a process named ‘lateral inhibition’ (Espinoza et al., 2018; Guzman et al.; Morales et al., 2021).

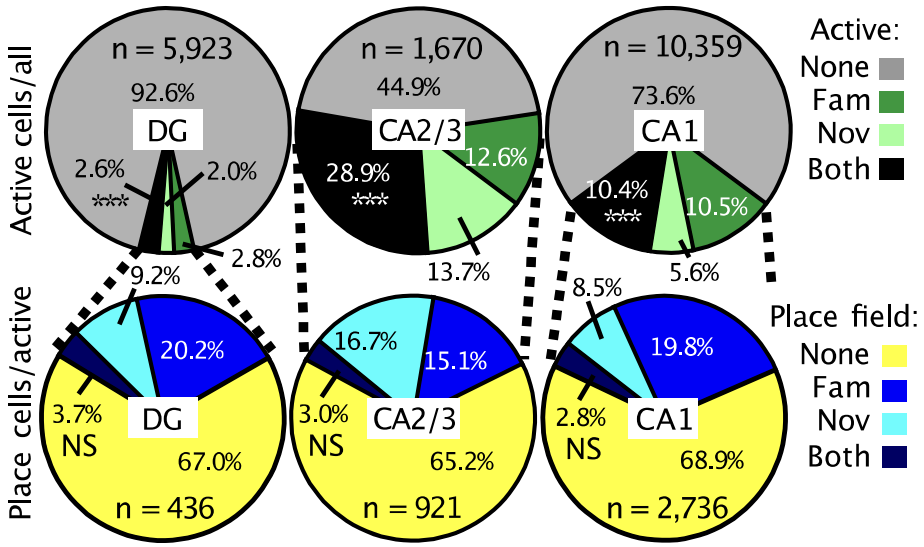

Figure 1.22. Fractions of active, silent cells and place cells in hippocampal regions. Adapted from (Hainmueller and Bartos, 2018). Top, fraction of active (more than 0.05 transients per s) cells among all neurons. Test for population overlap ($\chi 2$ test). Bottom, cells with place fields among active cells.

Rate and global remapping

The dentate gyrus might also represent different environments by implementing changes in the firing patterns of active neurons, which can be achieved by changing the firing rate of active cells while maintaining the location of their firing fields in a process termed 'rate remapping'. This phenomenon takes place in dentate gyrus granule cells when animals discriminate between spatial environments (Leutgeb et al., 2007) and is dependent on NMDA receptor plasticity (McHugh et al., 2007). In fact, sub-second patterns of correlated discharge in granule cells were shown to be sufficient to drive spatial memory discrimination (Chen and Knierim, 2018; van Dijk and Fenton, 2018).

A population of active granule cells can also represent different environments by changing the spatial locations of their firing fields, which is often accompanied by a redistribution of their firing rates. This process is termed 'global remapping' and is thought to both reduce memory interference and provide a read out of pattern separation (Wanjia et al., 2021). The dentate gyrus implements global remapping to discriminate between similar spatial environments (Allegra et al., 2020; Jung and McNaughton, 1993; Neunuebel and Knierim, 2014) although granule cells remap to a lesser extent than mossy cells (Neunuebel and Knierim, 2012; Senzai and Buzsáki, 2017). Overall, this body of experimental evidence suggests that the pattern separation function of the gyrus is supported by multiple distinct neuronal computations.

4.3. Conversion of inputs from the entorhinal cortex to the dentate gyrus

How are inputs converted by the dentate gyrus? Does the dentate gyrus merely function as a pre-processing stage separating input patterns from the entorhinal cortex? Granule cells are driven by both place-like (single) and grid-like (periodic) inputs, which might arise from non-grid MEC neurons or hippocampal place cells, and grid cells or mossy cells, respectively (Zhang et al., 2020). However, only 5% of dentate gyrus granule cells show spatially tuned spiking while 50% granule cells receive spatially tuned input (Zhang et al., 2020). Multiple models of transformation from grid code to place code were proposed. Grid cell to place cell transformation is thought to involve spatial clustering of grid cells on dentate gyrus granule cell dendrites using Hebbian processes during contextual changes (M. Hayman and Jeffery, 2008; Rolls et al., 2006) however recent findings show that both active and silent cells receive spatially modulated input, which is therefore inconsistent with the original model (Zhang et al., 2020). Another model suggesting that the average synaptic input to granule cells is weakly spatially tuned and that place cell tuning emerges through a competitive network mechanism is also disproved by recent evidence that a large amount of granule cells receive spatially tuned input (de Almeida et al., 2009; Zhang et al., 2020). It is thought that the conversion of inputs from the entorhinal cortex to dentate gyrus and CA1 neurons enables fast encoding and efficient recall of spatio-temporal information (Cholvin et al., 2021).

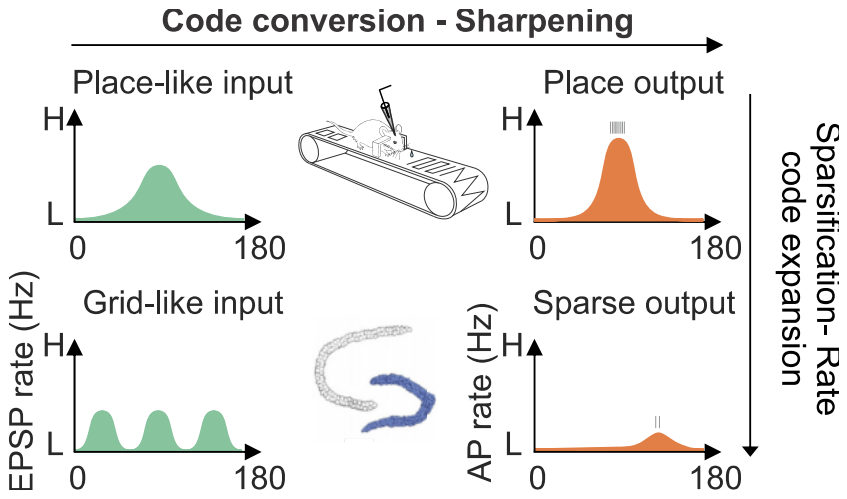

Figure 1.23. Code conversion in dentate gyrus granule cells. Adapted from (Zhang et al., 2020). (**top**) conversion from place inputs into place output (**bottom**) conversion of grid-like input into sparse output.

5. Contributions of CA3 to spatial memory function

5.1. CA3 attractor network

The hippocampus supports the formation of episodic memories, by creating representations of and associating elements of episodic memory (landmarks, events, objects). Episodic memory is a subtype of associative memory, whereby events, landmarks and individuals that share a spatiotemporal context are bound into unique combinations (Howard and Eichenbaum, 2015; Kesner and Rolls, 2015; Markus et al., 1995; McHugh et al., 2007; O'Keefe and Dostrovsky, 1971). It is thought that the attractor dynamics arising from the autoassociative architecture of CA3 supports the formation and recall of episodic memories (Rolls, 2018; Rolls and Treves, 1997). Indeed, the dense recurrent connections of CA3 pyramidal neurons are thought to support the formation of neuronal ensembles that generate rapid and arbitrary combinations of inputs, for instance between landmarks and objects (Rebola et al., 2017; Rolls, 2018; Rolls and Treves, 1997). These associations would lead to an initial and fast encoding of memories (Kesner and Rolls, 2015; Kornblith et al., 2013; Nasr et al., 2011; Piette et al., 2020). The generation of these one-shot associations is supported by the disambiguation of inputs taking place in the dentate gyrus, namely the divergence of overlapping entorhinal inputs that are mapped onto very a large number of sparsely active granule cells, as well as unique activity patterns created in the CA3 population generated by mossy fibres (Cerasti and Treves, 2010; Jung and McNaughton, 1993; Leutgeb et al., 2007; Neunuebel and Knierim, 2012; Rolls, 2013). The unstructured quality of the representations in CA3 allows storage of large amounts of information while minimizing interference (Rolls and Treves, 1997; Treves and Rolls, 1991).

Experimental evidence supports these theoretical predictions. CA3 lesions and region-specific NMDA receptor blockade show that CA3 is necessary for these associations to be formed (Gilbert and Kesner, 2003; Kesner and Rolls, 2015; Rajji, 2006). Similarly, dentate gyrus lesions or NMDA receptor knockout impair the formation of object-place associations (Gilbert and Kesner, 2003; Gilbert et al., 2001; Kesner and Rolls, 2015; McHugh et al., 2007), and mossy fibre damage was shown to prevent memory storage (Daumas et al., 2009; Kesner and Rolls, 2015; Lassalle et al., 2000; Lee and Kesner, 2004), suggesting that pattern separation is required for the associations to be formed in CA3. Thus, CA3 plays a crucial role in supporting the creation of fast and arbitrary associations of elements necessary for

episodic memory encoding, which is enabled by its recurrent architecture as well as the minimization of input interference implemented in the dentate gyrus.

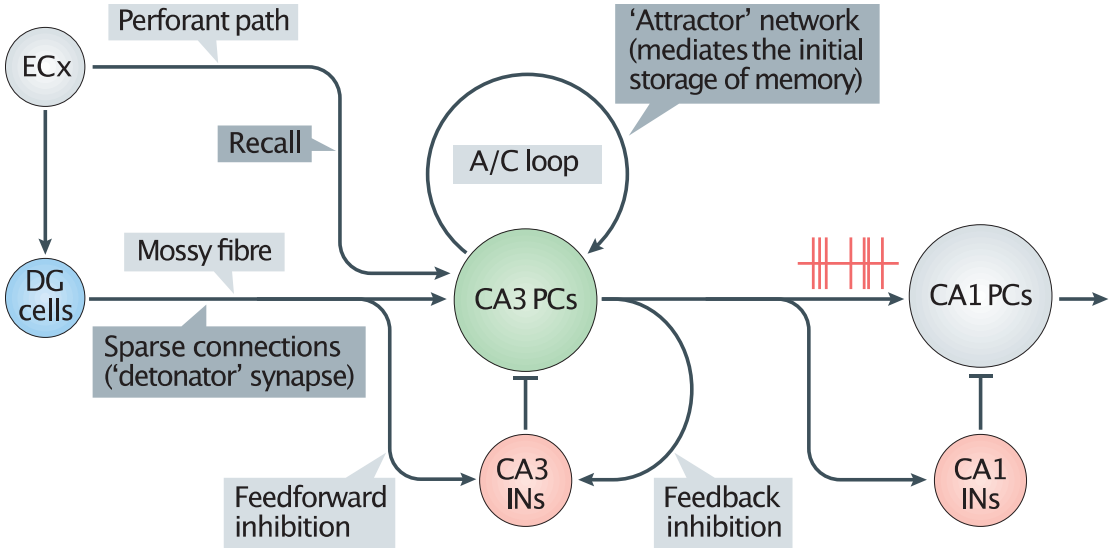

Figure 1.24. CA3 circuits and their proposed role in memory. Adapted from (Rebola et al., 2017). This schematic illustration shows the different elements of CA3 circuits and their hypothesized involvement in memory encoding and recall. The extensive excitatory interconnections between CA3 pyramidal cells (PCs) — known as the associative/commissural (A/C) loop — are proposed to work as an attractor network, in which associative memories are stored and recalled through pattern completion. Mossy fibres originating from the dentate gyrus (DG) provide sparse and powerful excitatory connections (known as 'detonator' synapses) to CA3 PCs; these connections are proposed to assist in the encoding of new patterns of activity (representing new memories) in CA3 through pattern separation. The direct connections from the entorhinal cortex (ECx) to CA3 are thought to provide the cues for retrieval (recall) of information from CA3, especially when incomplete information is provided. Feedforward inhibition via CA3 interneurons (INs) strongly controls information transfer between DG and CA3 depending on the pattern of presynaptic activity, and may be involved in the precision of memory. Inhibitory loops in CA3 control the generation of oscillatory activities and are amenable to substantial structural plasticity upon learning. Within the hippocampus, the main outputs from the CA3 region (illustrated by the red schematic trace) are the axons of CA3 PCs, which make contact with CA1 PCs and CA1 INs.

5.2. Pattern completion / pattern separation

Following the formation of neuronal ensembles during learning, CA3 drives the retrieval of memory representations. Indeed, it can retrieve stored input patterns from incomplete or degraded versions of the initial input by reinstating the activity of previously formed neuronal ensembles in a process termed 'pattern completion' (Guzman et al., 2016; Knierim and Neunuebel, 2016; Leutgeb, 2005; Rolls, 2018). Pattern completion can be performed by CA3 pyramidal neurons thanks to their extensive network of recurrent collaterals that can implement Hebbian learning. When presented with an incomplete or degraded set of inputs (eg. during a cued recall), activation of a subset of CA3 neurons can trigger activity of the rest of the CA3 population involved in encoding the original information (Treves and Rolls,

1991). This process is complementary to the pattern separation process implemented by the dentate gyrus where input patterns are decorrelated (Marr, 1971; McNaughton and Morris, 1987). Experimental work in rodents has also provided evidence that CA3 implements pattern completion. Indeed, when the animal is exposed to a local-global conflict of spatial cues, CA3 displays population activity that is more coherent with the original representation than the degraded inputs, by contrast to the dentate gyrus and CA1 (Lee et al., 2004; Neunuebel and Knierim, 2014). Experimental evidence also shows that lesions to the perforant path input to CA3 impairs memory retrieval, suggesting that this source of input is required for CA3 to perform retrieval of stored memory patterns (Lee and Kesner, 2004). CA3 was also shown to play a crucial role for the recollection of mnemonic information in humans (Grande et al., 2019).

In addition to pattern completion, CA3 is able to perform pattern separation and to switch between pattern completion and pattern separation: it is the final arbiter of which process should be implemented. Thus, by virtue of its network of recurrent connections, CA3 can produce attractor dynamics resulting in pattern completion (generalization) when input patterns resemble stored memories or else perform pattern separation when input patterns are distinct (Rolls and Treves, 1997). How is the switch between pattern completion and pattern separation implemented? It is thought that CA3 function should be considered in terms of its proximal and distal parts rather than as a whole, where proximal CA3 and the dentate gyrus act as a single functional unit that performs pattern separation while distal CA3 functions as an autoassociative network performing pattern completion (GoodSmith, 2017; Lee et al., 2015). Thus, multiple neuronal populations such as the dentate gyrus and CA3 may contribute to perform pattern separation through the implementation of distinct computations.

5.3. How does CA3 represent spatial environments?

Studies that recorded CA3 neural activity in rodents navigating in the physical environment have provided instrumental evidence regarding the representation of space in the hippocampal subregion CA3. They revealed that CA3 discriminates spatial environments by implementing distinct neural mechanisms. First, active CA3 neurons change their firing rates in response to subtle or substantial changes in environmental features (Leutgeb, 2005). CA3 also implements changes in firing rates to build directionally selective representations of the environment (Schwindel et al., 2016). Rate remapping is thought to enable the generation of

unique episodes while maintaining the integrity of the spatial code for locations (Leutgeb, 2005).

Another mechanism through which CA3 represents changes in the environments is the change in the location of firing fields. CA3 shows place cell activity (Kjelstrup et al., 2008) and upon induction of substantial contextual changes, CA3 recruits non-overlapping neuronal populations with distinct spatial rate maps to represent different environments (Leutgeb, 2004; Leutgeb et al., 2007). Multiple studies have revealed a stronger spatial selectivity in CA3 than CA1 by following changes in environmental information, despite the similarity of the CA3 and CA1 population properties (Bostock et al., 1991; Cressant et al., 2002; Hainmueller and Bartos, 2018). CA3 neurons display more compact and stable spatial activity with richer spatial information per spike than CA1, suggesting that CA1 and CA3 perform distinct computations (Mizuseki et al., 2012). It is thought that the dentate gyrus allows CA3 attractor dynamics to perform global remapping in similar environments by performing expansion recoding on overlapping inputs from the entorhinal cortex (Knierim and Neunuebel, 2016) and enables the coordination of CA3 neuronal activity patterns to support goal-directed behaviour and memory (Sasaki et al., 2018).

The quick implementation of changes in both firing rates and spatial field locations as a result of changes in the environment is coherent with a role of CA3 as an auto-associative circuit. It is also consistent with the dual role of CA3 in pattern completion by using rate remapping and integration of information, and pattern separation by using global remapping and representations of distinct environments (Leutgeb et al., 2006). In the framework of global remapping, the recruitment of non-overlapping CA3 neuronal ensembles may be driven by a shift in entorhinal inputs to CA3 (Fyhn et al., 2007). By contrast to CA1, which can be bound to multiple sensory modalities and can switch between different spatial maps (see CA1 section), CA3 is constrained to a single spatial map and bound to a fixed coordinate system (Leutgeb, 2005). It is thought that the dichotomy between the rate and spatial code allows the creation of a spatial matrix in CA3 to which additional non-spatial information can be integrated (Leutgeb and Leutgeb, 2007).

II. Aims and hypotheses

1. Theoretical background

Hippocampal neurons represent the physical environment by reflecting the location of the animal in space in their patterns of activity. Several classes of spatially tuned neurons contribute to this map and collectively represent the physical environment (Hafting et al., 2005; O'Keefe and Dostrovsky, 1971; Taube et al., 1990). Spatially modulated neurons have been found in all hippocampal subregions, including the dentate gyrus and CA3. Neuronal activity in the hippocampus is thought to provide the brain with a "cognitive map" of its spatial surroundings (O'Keefe and Nadel, 1978).

Various types of spatial information are processed and contribute to spatial representations. The location of the animal in allocentric coordinates of the external world was first identified as a determinant of place cell activity. The specific position of the animal in the environment where place cells fire spikes is termed 'place field' of the place cell (O'Keefe and Dostrovsky, 1971). The direction of running also modulates hippocampal firing and contributes to building a representation of the environment. When the environment is narrowed to a linear track, place cell representations in CA1 become increasingly directional such that the presence of place fields depends on the direction of running (McNaughton et al., 1983).

The dentate gyrus, CA3 and CA1 also differ in terms of spatial place cell properties. Place cells in the dentate gyrus show multi-peaked firing fields, low spatial information content, and high stability across recording sessions in the same environment (Hainmueller and Bartos, 2018; Jung and McNaughton, 1993; Leutgeb et al., 2007). Dentate gyrus neurons are sensitive to small differences across environments and most active granule cells only fire in one of two environments (Hainmueller and Bartos, 2018; Leutgeb et al., 2007; Neunuebel and Knierim, 2012; Wanjia et al., 2021). Dentate gyrus and CA3 neurons exhibit extreme changes

of firing rates between environments that can reach an order of magnitude (Leutgeb, 2005; Leutgeb et al., 2007) and show high selectivity for context (Allegra et al., 2020; Hainmueller and Bartos, 2018; Jung and McNaughton, 1993; Neunuebel and Knierim, 2012; Schwindel et al., 2016). CA1 on the other hand might bind spatial information into a global context by building spatial representations that overlap across contexts (Allegra et al., 2020; Leutgeb, 2004) and by representing abstract spatial variables rather than raw sensory information (Ito et al., 2015; Keinath et al., 2020; Muller and Kubie, 1987).

2. Questions

How positional and directional information is processed and transformed in the major hippocampal subregions has not systematically been examined yet in a single comparative study. Consequently, this project was driven by the following questions:

1. How are different types of spatial information processed in hippocampal subregions?
2. How do spatial representations evolve along the hippocampal circuit?
3. How are spatial representations modulated by novelty?

3. Hypotheses

We hypothesize that directional and positional information are differentially processed in hippocampal subregions. This hypothesis is based on theoretical predictions that CA1 relies on positional cues while the dentate gyrus uses navigation-relevant landmarks (Jacobs and Schenk, 2003). It has also been proposed that information relative to the content ('what') and the location ('where') of an event are differentially processed within hippocampal subregions (Mishkin et al., 1983; Chawla et al., 2005) based on anatomical and functional distinctions between the 'what' and 'where' pathway in the dentate gyrus, CA3 and CA1 subregions (Amaral and Witter, 1989; Burke and Barnes, 2011; Chawla et al., 2005; Henriksen et al., 2010; Ishizuka et al., 1990; Ito et al., 2015; Sauvage et al., 2013). Consistent with this hypothesis, immediate early genes (IEG) expression indicates that distal CA1 and proximal CA3, but not the dentate gyrus, may respond to positional cues while the dentate gyrus and proximal CA3 respond to directional cues (Hoang et al., 2018).

Given the projection patterns of the sources of this information to different hippocampal subregions (Nafstad, 1967), we further hypothesize that these information streams are

processed differently along the hippocampal circuit. Hierarchical processing of spatial representations along the hippocampal circuit would be consistent with recent evidence that orientation selectivity, one of the principles underlying representations of distinct experiences, promotes generalisation across contexts upon repeated exposed to the same context (Liu et al., 2021). Transformation of spatial representations along the hippocampal circuit would also be coherent with other brain systems such as the cerebral cortex (Felleman and Van Essen, 1991) or the visual system, where hierarchical convergent processing allows the emergence of distinct response properties in complex cells through integration and summation of the receptive fields of input simple cells (Hubel and Wiesel, 1962).

Lastly, we hypothesize that novelty modulates spatial representations in the hippocampus, consistent with previous reports of novelty modulation of the activity of hippocampal neurons (Dong et al., 2021; Fredes et al., 2021).

4. Experimental approach

Addressing these questions requires recording neuronal activity from identified hippocampal subregions during navigation under identical task conditions. To explore how representations of spatial position, running direction, and distance evolve along the hippocampal circuit, we perform single-photon widefield microendoscope calcium imaging from the dentate gyrus, CA3 and CA1 hippocampal subregions in mice navigating back and forth along a linear track. Single-photon microendoscope imaging is particularly well suited to our study as it allows recording of neuronal activity in freely-moving animals from anatomically identified neuronal populations, which has been problematic in the dentate gyrus in the past (Neunuebel and Knierim, 2012).

III. Methods

1. Single-photon calcium imaging in freely moving animals

The development of experimental techniques enabling recordings of neural activity *in vivo* has furthered our understanding of the neural processes underpinning complex behaviors. However, techniques including electrophysiology (Hubel, 1960; Supèr and Roelfsema, 2005), neurochemical measurements (Clark et al., 2010) and optical imaging (Akerboom et al., 2012; Miyawaki et al., 1997) are limited either by the depth of the region they can record, by the type of behaviour they can investigate, or by the anatomical detail they can provide. Microendoscope *in vivo* imaging was developed to surpass these limitations.

1. 1. Imaging neuronal activity using a microendoscope through a GRIN lens

The development of genetically encoded calcium indicators (GECIs) (Akerboom et al., 2012; Ohkura et al., 2012) has allowed neural dynamics to be reported through changes in fluorescence. During periods of high neural activity (Grienberger and Konnerth, 2012; Palmer and Tsien, 2006), intracellular calcium concentration increases as calcium enters dendritic branches (Cichon and Gan, 2015) and neuronal cell bodies. These fluctuations of intracellular Ca^{2+} can be monitored by GECIs expressed in populations of neurons. GECIs such as GCaMP6f emit a fluorescent signal upon calcium binding, whose intensity increases during periods of high neural activity (Grienberger and Konnerth, 2012; Palmer and Tsien, 2006). The visualization of neural signal dynamics is physically constrained by the necessity to deliver a light source of excitation for the Ca^{2+} indicator as well as a light-sensing device to detect the emitted signal from the neuronal populations of interest (Hamel et al., 2015). The high levels of light scattering displayed by neural tissue has precluded *in vivo* imaging of calcium signals in deep brain regions (Hamel et al., 2015).

Gradient-refractive index (GRIN) lens (attached to a relay lens) were developed to mitigate these effects by relaying light to and from deep brain regions, thus rendering deeper brain regions accessible to optical imaging (Akerboom et al., 2012; Ohkura et al., 2012). Here, we used single-photon microendoscope calcium imaging to record the activity of identified principal neurons in the three major hippocampal regions (Fig 3.1).

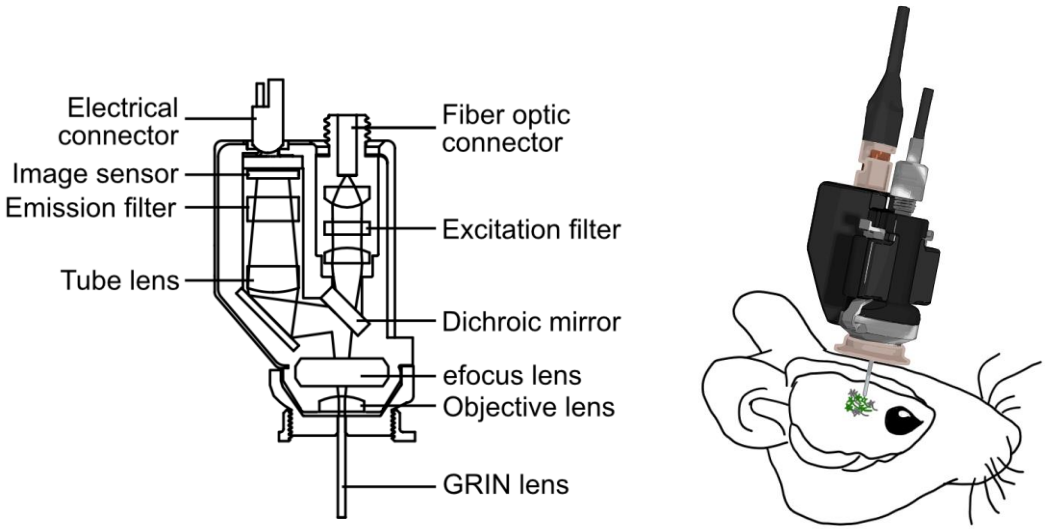

Figure 3.1. *In vivo* calcium imaging through a microendoscope. (**left**) Microendoscope components. (**right**) Schematic of a mouse implanted with a microendoscope to perform in vivo Ca2+ imaging through a GRIN lens.

We performed stereotaxic surgeries to chronically implant a GRIN lens above the principal cell layer in either the dentate gyrus, CA3 or CA1 (Fig 3.2).

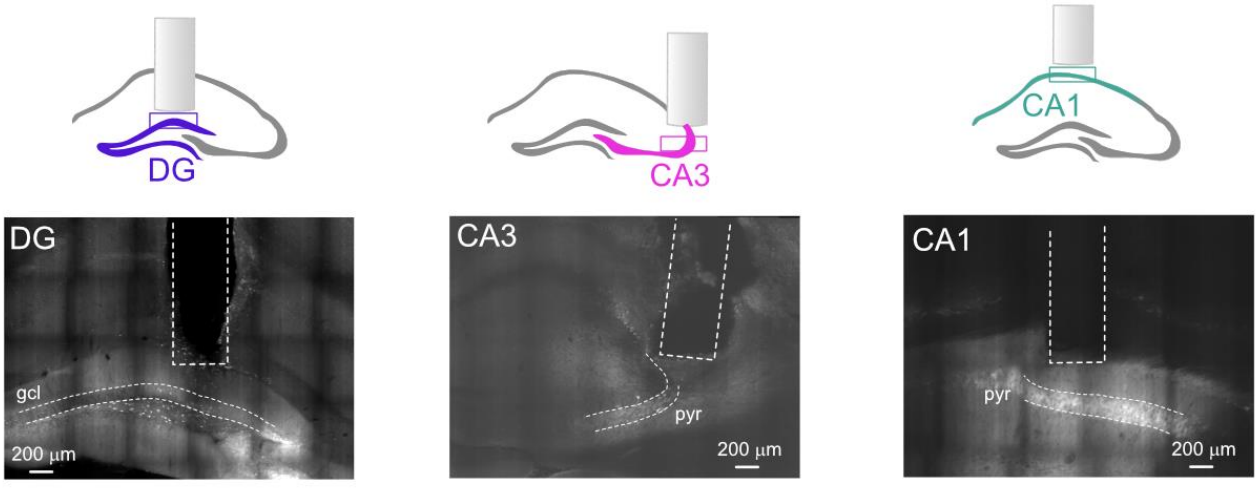

Figure 3.2. Surgical procedure for *in vivo* calcium imaging through a GRIN lens. (**left**) Schematic of a GRIN lens implant in the dentate gyrus and representative confocal image of the GRIN lens position above GCaMP6f-expressing neurons in the dentate gyrus. (**middle**) Same as left but for CA3. (**right**) Same as left but for CA1. The dotted lines highlight the specific imaged region. gcl: granule cell layer; pyr: pyramidal layer.

1. 2. Imaging neuronal activity in freely-moving mice

Microendoscope *in vivo* calcium imaging has greatly expanded the repertoire of complex behaviours that can be investigated (Ghosh et al., 2011). The rigidity and size inherent to traditional imaging technologies restrict the types of behaviours that can be investigated and this limitation has fuelled the development of miniature, integrated microscopes that are light enough to be placed on the animal's head without hindering its motility. Microendoscope single photon imaging allows the investigation of neuronal processes associated with a wide range of naturalistic animal behaviour (Jennings et al., 2015; Resendez and Stuber, 2015).

In this study, we chose to use microendoscope single-photon widefield *in vivo* calcium imaging to record hippocampal population activity while animals were exposed to naturalistic stimuli. We recorded neuronal population activity while the mice navigated spontaneously back and forth along a linear track during 10-minute sessions on multiple days (Fig 3.3). The 60 cm linear track was enriched with visual cues (e.g., playing cards) on the walls as well as Lego bricks at the extremities of the track.

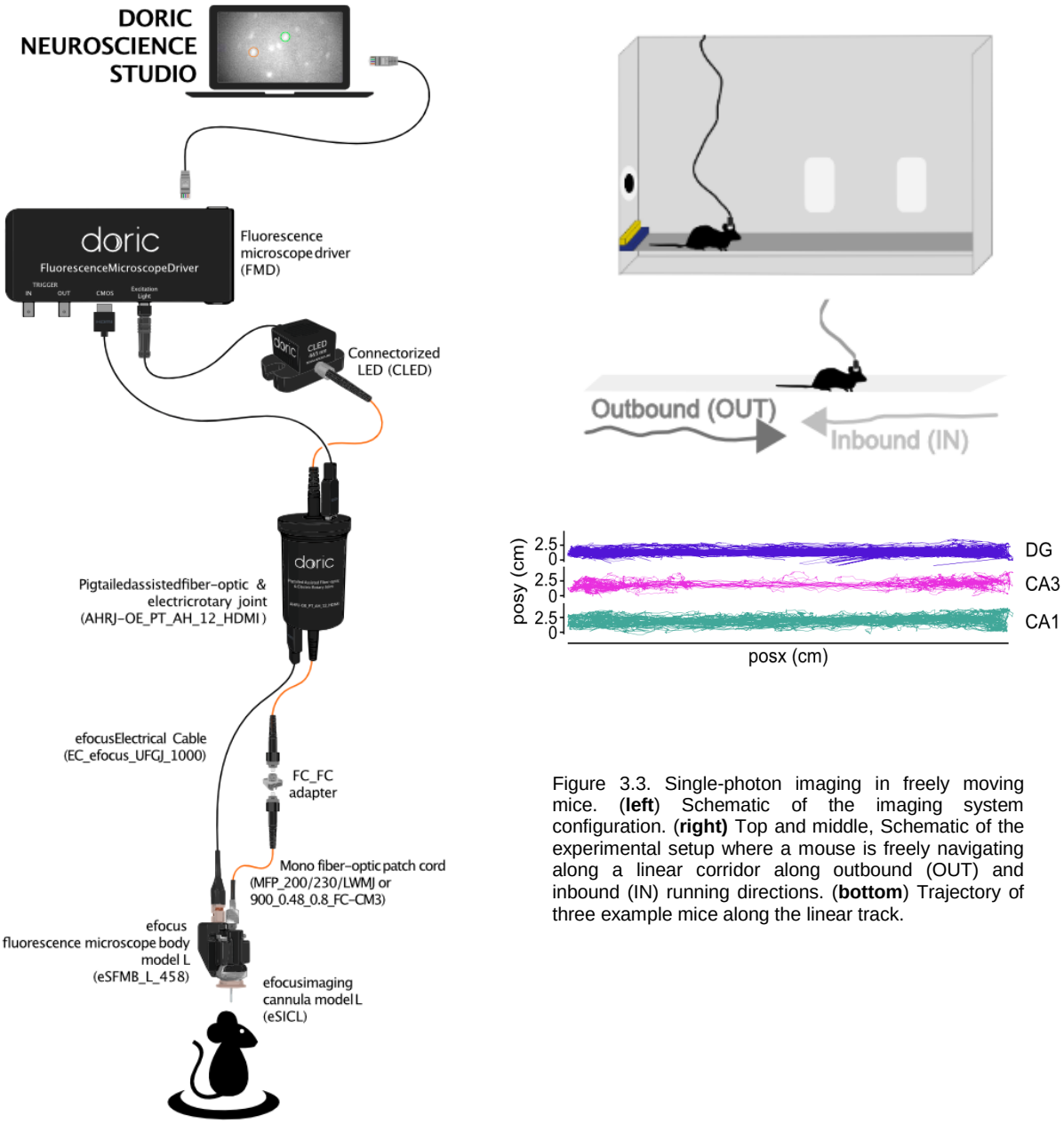

Figure 3.3. Single-photon imaging in freely moving mice. (**left**) Schematic of the imaging system configuration. (**right)** Top and middle, Schematic of the experimental setup where a mouse is freely navigating along a linear corridor along outbound (OUT) and inbound (IN) running directions. (**bottom**) Trajectory of three example mice along the linear track.

This approach allowed us to record neuronal activity from all three identified hippocampal sub-regions in freely navigating animals (Fig 3.4).

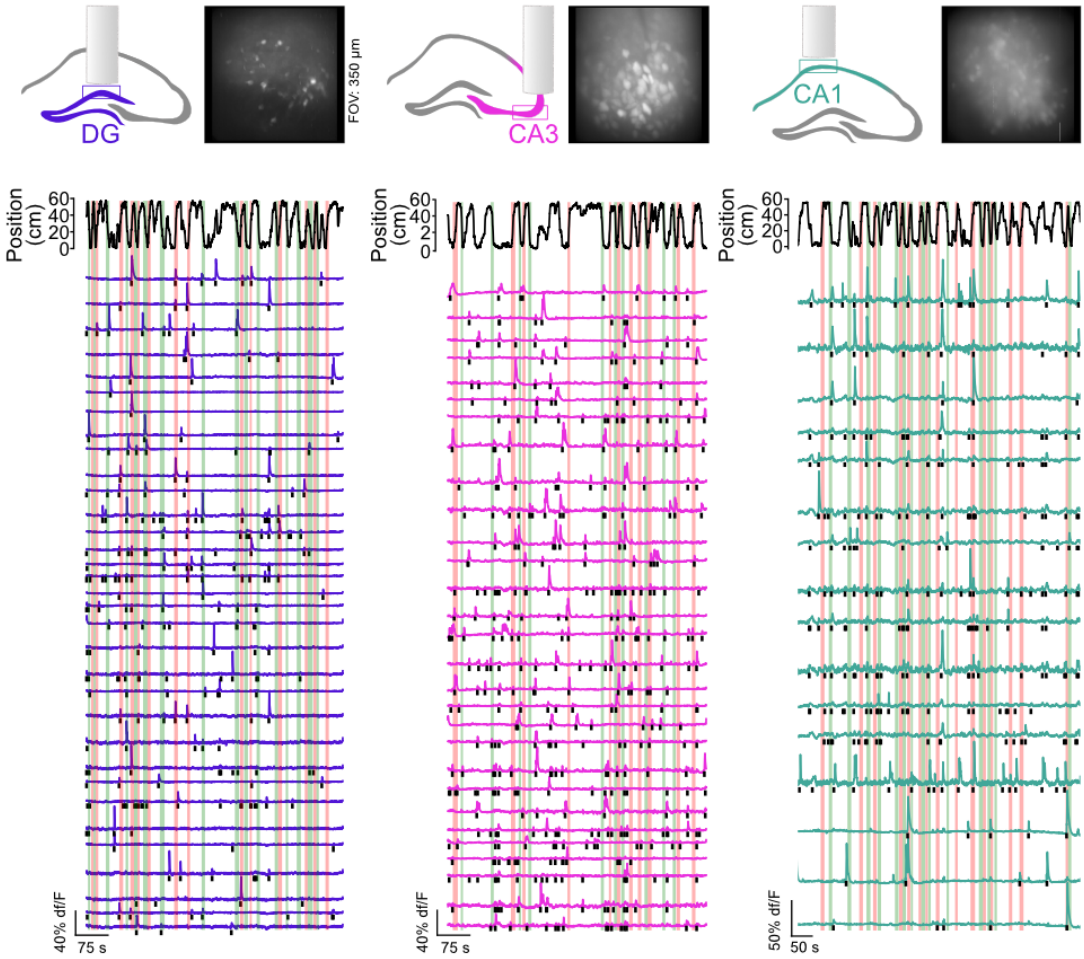

Figure 3.4. Single-photon imaging from hippocampal subregions in freely moving mice (**left**) Top, schematic of the imaging implant in the DG and representative maximum projection of GCaMP6f-expressing granule cells during an in vivo recording session. Bottom: representative imaging session showing animal speed and running direction along the linear track. The bottom traces show fluorescence extracted from regions of interest (ROIs) of an example recording session in the DG. The black tick marks indicate significant calcium transients during running periods. The vertical red and green bars highlight different running directions, inbound or outbound. (**middle**) Same as left but for CA3. (**right**) Same as left but for CA1.

2. Strengths and limitations of *in vivo* single-photon calcium imaging

2. 1. Strengths

Freely navigating animals

Imaging techniques that require head-fixation of the animal greatly reduce the range of behaviours that can be investigated. However, when using microendoscope imaging, the head of the microendoscope is light and portable (Ghosh et al., 2011) and the subject of investigation is connected to the computer by a single flexible cable, which allows the animal to move in a given environment without physical restrictions while exposed to naturalistic stimuli. When investigating neural representations of space, this experimental paradigm is more ethologically sound for rodents that evolved to navigate in the wild. Microendoscope single-photon imaging is therefore well suited to studies that investigate spatial navigation and studies that require unrestrained movement of the animal such as studies exploring adaptive and maladaptive states (Ghosh et al., 2011; Resendez and Stuber, 2015) and has enabled the investigation of different types of associative memory (Grewe et al., 2017).

Access to deep brain regions

Microendoscope imaging coupled with a GRIN lens allows the delivery of light to deep brain tissue and increases the amount of neuronal populations whose activity can be recorded *in vivo*. Deep brain *in vivo* imaging can also be achieved using 2-photon microscopy with additional optical devices, such as GRIN lenses or optical cannulas (Svoboda and Yasuda, 2006) but requires the stable fixation of the animal's head. Implantation of a light weight optics fiber above a region of interest (fiber photometry) also enables recordings from brain neuronal populations combined with a wide range of behaviours (Cui et al., 2014). However, fiber photometry does not allow cellular-level resolution and only enables visualization of aggregate activity in the field of view (Svoboda and Yasuda, 2006). Fiber photometry also requires fixing of the animal to a rigid fiber optic bundle, which might restrict mobility and movement of small mammals (Cui et al., 2014).

Cellular identification

The expression of GECIs in specific neuronal populations allows microendoscope single-photon imaging to record the activity of identified neuronal populations (Jennings et al., 2015; Ohkura et al., 2012). By using combinations of different GECIs, the activity of multiple different identified neuronal populations can be compared and their respective functional role established. Combining a morphological marker and a GECI can also enable the identification of a neuronal subpopulation with a morphological marker while recording the activity of the whole population with a GECI. Although electrophysiological methods do not record from identified neuronal populations (Chawla et al., 2005; GoodSmith et al., 2019; Leutgeb et al., 2007; Senzai and Buzsáki, 2017), the combination of electrophysiological recordings and optogenetic manipulations can in some cases enable identification and manipulation of populations of neurons (Sparta et al., 2011). One limitation, however, is that the location of the monitored cell cannot be determined and that sparsely firing neurons will be detected with more difficulty since detection is based on the shape of the action potential waveform.

Chronic imaging

Furthermore, the same neuronal population can be recorded across sessions and days using single-photon microendoscope imaging, making it suitable to investigate the stability of representations of a given variable or plasticity changes associated with pathological conditions.

2. 2. Limitations

Low temporal resolution

In microendoscope imaging, fluorescence emitted by the GECIs provides temporal information about dynamic changes in neuronal activity (Smetters et al., 1999), and also about the neuron's location within the brain (Ziv and Ghosh, 2015). However, calcium imaging lacks sufficient temporal resolution to distinguish bursts from single spikes under typical *in vivo* recording conditions (Danielson et al., 2016b; GoodSmith, 2017; Hainmueller and Bartos, 2018). Low temporal resolution is a major shortcoming of this experimental technique, since it might bias the interpretation of patterns of population activity. Furthermore, at this time camera frame rates are insufficient to allow imaging of fluorescent voltage sensors, whose temporal resolution is higher than that of GECIs. Thus, developments

in protein engineering and optical imaging devices will be necessary to increase temporal resolution. By contrast, *in vivo* electrophysiological recordings provide a higher temporal resolution and improved spike timing estimations (Cunningham, 2014; Smetters et al., 1999).

Signal-to-noise ratio

Because of scattering of light by brain tissue, signal-to-noise ratio of single-photon imaging is relatively low, and it is therefore under most conditions, including ours, not possible to identify silent cells, as their baseline fluorescence emission is too low. By contrast, 2-photon microscopy provides better signal-to-noise ratio as excitation is more restricted to the focal plane.

Tissue damage

The implant of a 500 µm-diameter GRIN lens causes undeniable tissue damage and might disrupt neural circuits that may support the behaviour or physiological condition being explored. However, the tissue damage induced is limited compared to other types of implants such as imaging cannulas for 2-photon imaging, whose diameter is larger. Furthermore, GRIN lens implants were shown to have less impact on behavioural measurements compared to imaging cannula used for 2-photon recordings (Allegra et al., 2020).

Far red-shifted indicators

Microendoscopes are not compatible with far-red-shifted indicators (Ghosh et al., 2011). Also, further technological developments will be required to allow manipulation of the activity of defined neuronal populations using optogenetic tools, and therefore to establish a causal link between neuronal activity and behaviours.

Data analysis

The rate of data acquisition has increased exponentially, and consequently also the demands on data analysis and storage. Thus, more developments are needed to increase the rate and efficacy at which spatial and temporal information can be obtained from neuronal activity and from environmental and behavioural variables (Cunningham, 2014; Freeman et al., 2014).

Photo bleaching of neurons

Microendoscope single-photon imaging delivers light to the whole field of view while 2-photon microscopy scans the field of view sequentially. Single-photon imaging therefore increases the risk of photo-bleaching of the neurons.

Surgical procedure

Microendoscope single photon imaging in deep brain tissue requires the invasive and chronic implant of a GRIN lens. Most GRIN lenses have a fixed and limited working distance and therefore surgical positioning of the lens into the brain requires extreme precision and yields low success rates (Cunningham, 2014; Smetters et al., 1999).

Not compatible with water-based behaviours

The range of behaviours that can be investigated is also limited, for example microendoscope imaging does not allow water immersed behaviours to be recorded and is therefore not suitable for experiments that require the animal to swim, for example during the Morris water maze (Resendez and Stuber, 2015).

Overall, by enabling the recording of identified populations of neurons in freely navigating animals, single-photon microendoscope calcium imaging offers an unprecedented insight into the neuronal mechanisms underlying naturalistic behaviour and an opportunity to disentangle circuit mechanisms through precise identification of neuronal populations.

3. Methods' details

3. 1. Mice

All procedures were performed in accordance with European and French guidelines on the ethical use of animals for experimentation (EU Directive 2010/63/EU) after approval by the Institut Pasteur Ethics Committee CETEA (protocol number 160066). Wild-type male C57BL/6J mice from Janvier labs aged 6 to 39 weeks were used for all experiments. They were housed collectively or individually in a room maintained at 21C with a 12 hours inverted light cycle, in polycarbonate individually ventilated cages, enriched with running

wheels. Mice used for the GRIN lens experiments had *ad libitum* access to food and water. A total of 12 mice were used in this study.

3. 2. Surgical procedure

The surgical procedures were performed at least 7 days after the arrival of the mice in the animal facility, and were carried out using a stereotaxic apparatus (Kopf instruments). An analgesic solution consisting of buprenorphine (0.05mg/kg, Vetergesic) was administered through intraperitoneal injection at least 30 minutes prior to the surgical intervention. Lidocaine was administered locally (subcutaneous injection) at the start of the procedure. A second analgesic solution consisting of Metacam (10 mg/kg, Metacam) was administered subcutaneously prior to the end of the surgery. Mice were anesthetized with isofluorane throughout the surgery (3/4% during induction and 1/2 % to during the remainder of the surgery**;** 2l/min O2 and 0.2-0.5l/min O2 respectively). The body temperature of the mice was maintained at 36C using a heating pad, and their eyes were protected using a hydrating eye gel (Ocrygel ®). A post-operative analgesic solution (meloxicam 5mg/kg) was administered orally in combination with surgical recovery Dietgel (ClearH2O) for 2 days. The recovery of the mice was monitored for 72h.

Stereotaxic injections of viral vectors

The skin was first covered with Providone-iodine (Betadine) and then cut using a scalpel blade. A small craniotomy was then carried out above the right dorsal hippocampus (1.5mm lateral and 1.9mm posterior to Bregma). An injection of AAV1.Syn.GCaMP6f.WPRE.SV4 (500 nL; $3.4x10^{12}$ TU/mL, Addgene) was made in n=5 animals with DG implants, n=1 animal with a CA3 implant and n=2 animals with CA1 implants and an injection of AAV-CamKII-GCaMP6f-WRPE-SV40 (500 nL; $\geq 1\times10^{12}$ vg/mL, Addgene) was made in n=2 animals with CA3 implants and n=2 animals with CA1 implants. The injection was carried out using an oil injection pump and a glass micropipette at the injection site defined by the following stereotaxic coordinates: DG: 1.9 mm posterior from Bregma, 1.5 mm lateral from the midline and at 1.7 mm depth from the dural surface; CA3: 1.9 mm posterior from Bregma, 2.0 mm lateral from the midline and at 2.1 mm depth from the dural surface; CA1**:** 1.9 mm posterior from Bregma, 1.5 mm lateral from the midline and at 1.25 mm depth from the dural surface. Viral vector injection and GRIN lens implantation were either carried out simultaneously or separately to allow expression of the GECI and implantation under visual control. In instances

where the injection and implant were carried out separately, mice recovered from the injection for at least 1 day before undergoing subsequent procedures.

Chronic GRIN lens implantation

To perform *in vivo* calcium imaging from the dentate gyrus, a Gradient Refractive Index Lens (GRIN lens) was implanted above the granule cell layer of the dentate gyrus or the pyramidal cell layer of CA3 or CA1. GRIN lens implants were performed two to three weeks after viral injection. Mice were anesthetized and the head position and angle was closely monitored to target the region of interest. Following application of Betadine on the skin surface and local analgesic, the skin covering the skull was cut using scissors and removed. Following cleaning of the exposed skull with saline solution, all overlying connective tissue was cleared out by applying a green and a red activator (Super-bond C&B, Sun Medical) onto the exposed skull for one minute and thirty seconds, respectively. A craniotomy was performed (600-900 µm diameter) and the dura mater was removed. First, a stainless steel needle (500 µm diameter, custom-made, Phymep) was lowered down to -1.9 mm for DG, -2.15 mm for CA3, and -1.35 mm for CA1, at a rate of 400 µm/minute. Second, the imaging cannula was slowly lowered at a rate of 100 µm/minute into the implant site at the following target coordinates: DG: 1.9 mm posterior from Bregma, 1.5 mm lateral from the midline and at 1.9 mm depth from the dural surface; CA3: 1.9 mm posterior from Bregma, 2.0 mm lateral from the midline and at 2.15 mm depth from the dural surface; CA1: 1.9 mm posterior from Bregma, 1.5 mm lateral from the midline and at 1.35 mm depth from the dural surface. The procedure was performed blindly in n=1 animal with a DG implant and n=1 animal with a CA1 implant (using 0.5mm diameter SICL_D_500_80 Snap-in Imaging Cannula, Model L-D Depth range: 0mm – 3.46mm from Doric lenses) or under visual control of the microendoscope to increase the success rate of the implant in n=4 animals with DG implants, and n=3 animals with CA3 implants and n=3 animals with CA1 implants (using eSICL_D_500_80 Snap-in Imaging Cannula, eFocus, Model L-D Depth range: 0mm – 3.46mm from Doric lenses). A focussing ring was screwed around the metallic headpost attached to the lens to calibrate the implant depth and increase adhesion to the skull in n=2 animals with DG implants in n=2 animals with CA3 implants and n=4 animals with CA1 implants. Metallic screws were used to stabilize the position of the GRIN lens in n=2 animals with CA3 implants. The lens and protruding metal headpost were then stabilized in all animals using opaque dental cement (Super-bond C&B, Sun Medical).

3. 3. Behavioural Paradigm

Single-photon microendoscope widefield calcium imaging in mice freely navigating in a linear track.

During the imaging sessions, the microscope head was clipped to the metallic ring protruding from the imaging cannula (Snap-in Surface Fluorescence Microscope Body-L, SFMB_L_458, Doric Lenses in n=1 animal with a DG implant and n=1 animal with a CA1 implant or eFocus Snap-In Fluorescence Microscope Body-L, eSFMB_L_458, Doric lenses in n=4 animals with DG implants, n=3 animals with CA3 implants and n=3 animals with CA1 implants). A fiber-optic patchcord transmitting LED light and an HDMI cable collecting the digital signal connected the mouse to the microscope (Fluorescence microscope driver, FMD_L, Doric Lenses). Cable lengths were optimized to allow unrestricted movement of the mouse. In order to obtain high spatial sampling of the physical environment, we chose to expose the animals to a linear track similarly to previous studies (Ziv et al., 2013). The mice were freely navigating in a 60 cm-long, 6 cm-wide and 31 cm-high linear track made of PVC and enriched with visual cues: 3 playing cards placed on one wall and a sheet of paper placed onto the opposing wall, a Lego brick positioned at each end of the linear track and a drawing positioned on each extremity of the linear track made up the visual cues. A plexiglass lid with a linear opening allowing the passage of the microscope cables was placed on top of the linear track.

The imaging recordings were carried out using Doric Neuroscience studio software and the behaviour of the animal was recorded using a camera (Doric, Sony IMX290 sensor) to allow tracking of the animal's trajectory. Doric Neuroscience studio software triggered the behavioural camera by sending a TTL signal for each frame to synchronize the 2 recordings. The exposure time for each frame was set to 50ms (20Hz) and the illumination power setting was optimized for each animal and imaging region, and maintained throughout the experiments.

The imaging field of view (FOV) was first inspected 2-3 weeks following the implant to check for the presence of fluorescent neurons. If fluorescence signals were observed in the FOV, the mice were handled daily the week prior to the start of recordings in order to reduce the animals' stress during the experiments.

Navigation in the linear track

The activity of hippocampal neurons was recorded while the mouse navigated back and forth in opposite directions along a linear track (length: 60cm). The mice were spontaneously exploring the environment without being given any reward. During imaging sessions, mice completed 17.0 ± 2.5 (n = 33 sessions from DG implants), 20.3 ± 2.1 (n = 28 sessions from CA3 implants), or 23.8 ± 4.0 (n = 28 sessions from CA1 implants) continuous runs ("laps" according to the definition given below) across the linear track. Imaging sessions lasted 734 ± 77 s (DG implants), 801 ± 73 s (CA3 implants), or 1034 ± 103 s (CA1 implants).

Odor-cued pattern separation paradigm

We implemented an odor-cued pattern separation paradigm to record the activity of hippocampal neurons of freely navigating mice in two environments that differed only by their olfactory information, to assess whether spatial representations of the hippocampal neurons were modulated by novel contextual information. The mice were first recorded in the linear track described above, devoid of additional odor cues during 10-minute recording sessions over 4 consecutive days to measure baseline activity data. These baseline recordings were carried out in n=1 mouse with a DG implant; n=3 mice with CA3 implants and n=4 mice with CA1 implants. In n=3 mice with DG implants, this set of recordings was skipped to prevent photobleaching of DG granule cells. The mice were then exposed to a first odor (odor A: Benzaldehyde, Sigma Ref: B1334, diluted 1/100 in mineral oil, Sigma Ref: M5904) while freely navigating in the linear track during 10 minute-recording sessions over 4 consecutive days. The odor was homogeneously diffused by placing drops of the odor solution onto a filter paper underneath the metallic floor of the track enabling widespread diffusion of the odor into the linear track. Holes in the metallic floorboard allowed the odor to diffuse through the open field and a plexiglass lid maintained the odors inside the box, thereby creating a non-spatially bound olfactory cue. The odor was allowed to spread for 3 minutes before the start the recordings. On the 5^{th} day, the mice were exposed to the familiar odor for 10 minutes while navigating in the linear track, after which they were allowed a 45min break to rest in a neutral housing cage. They were then re-placed into the linear track where a new odor had been diffused (odor B: Carvone, Sigma Ref: 22060, diluted 1/100 in mineral oil, for n=3 mice with DG implants, n=3 mice with CA3 implants and n=4 mice with CA1 implants or odor C: Isoamyl Acetate, Sigma Ref: W205508, diluted 1/100 in mineral oil for n=1 mouse with a DG implant) and navigated 10 minutes before being granted another 45 minute-break in the resting cage. Finally, the mice were exposed to odor A once again for 10 minutes as a control

measure to rule out temporal drift of neural activity. Sessions without artificial odors, with familiar odor A and familiar odor B were included in the study of hippocampal spatial representations.

3. 4. Post-hoc analysis

Upon completion of the experiments, the animals were perfused with 4% formaldehyde (Sigma) after lethal injection with pentobarbital (150 mg/kg). The brain tissue was collected and sliced into 60-µm thick sections using a vibratome (Leica). The cell bodies were stained using Hoechst 33342, Trihydrochloride, Trihydrate - FluoroPure Grade. Images of the lens position in the tissue and viral injection sites were obtained with confocal microscopy (Bruker, Zeiss).

3. 5. Data analysis

Behavioural analysis

Analysis of behavioural and imaging data was performed using established procedures in the laboratory (Allegra et al., 2020), with some adaptations to account for the specific properties of single-photon widefield imaging.

To track the position of the animal, we filmed the linear track using a camera (Doric, Sony IMX 290 sensor) operating at the same frame rate as the microscope sensor (typically 20Hz). For every frame captured by the microscope sensor, the acquisition software emitted a TTL pulse to trigger a corresponding frame capture with the behavior camera. Animal motion was analyzed with the marker-less pose estimation software DeepLabCut (Mathis et al., 2018). Four labels (snout tip, left and right ear, tail base) were identified across all captured frames. The position of the animal was computed as the mean of the coordinates of the four labels. “Laps”, i.e. continuous runs at a speed of >0.5 cm/s in a single direction along the linear track, were identified after low-pass filtering positional data at f_c=0.5Hz. We were stringent with the lap definition and only included periods of active running to discard large synchronous patterns of population activity observed prior to movement onset in the dentate gyrus, consistently with previous findings (Pofahl et al., 2021). Only continuous runs in one direction that covered at least 70% of the full length of the track were considered a lap. Neuronal activity data were assigned one of two directions (“IN” or “OUT”). Neuronal activity data outside of any laps, including resting periods, were not used for analysis.

Imaging data processing

Recordings of neural activity were first motion corrected in the xy plane to account for artefacts induced by the movement of the animal using an algorithm built into the Doric Neuroscience Studio software. Segmentation into regions of interest (ROIs) was carried out using a singular value decomposition algorithm built into the suite2p software (Pachitariu_Harris16). In order to select DG granule cells, we only selected ROIs corresponding to small and densely packed cell bodies to discard inhibitory interneurons and mossy cells. The fluorescent signal from the neuropil was subtracted from the extracted fluorescence using the suite2p software. The quantification of neuronal activity was based on previously reported methods (Dombeck_Tank10). 'Events' were defined as regions in the normalized fluorescence changes (dF/F) exceeding a threshold of mean +1.0 standard deviations of the overall dF/F signal, a minimum duration above threshold of 300 ms (which corresponds roughly to the GCaMP6f half decay time (Dana_Kim19)), and exceeding an integral of 50 dF/F x 1s. Visual inspection of the event detection result confirmed these parameters (Allegra et al., 2020).

During some recordings of populations of CA1 neurons, we rarely observed large generalised fluorescence transients which saturated the whole field of view, likely caused by motion artefacts as they were typically related to certain movement patterns of the animal, such as exploring the side walls on their hind paws. We discarded these periods manually from further analysis.

Identification of spatially modulated cells

Spatial activity maps were computed based on data from continuous running periods. The linear track was split into 20 spatial bins**.** The sum of events in each spatial bin was divided by the occupancy of the animal in that bin; spatial maps were smoothed with a Gaussian filter (sigma = 4 bins).

Spatially modulated neurons were defined as cells firing consistently at the same location of the linear track across lap crossings in the same running direction. We identified spatially modulated cells by computing the mean pairwise Pearson's R correlation between spatial maps across lap crossings. Outbound and Inbound lap crossings were analysed separately. To

obtain a null model for the mean cross correlation and selectivity, we dissociated firing activity for each neurons and spatial position by shuffling the recorded position in chunks of 300 ms and repeated this bootstrap procedure 10 times. The neurons whose mean cross-correlation value exceeded the bootstrap with a Z-score higher than 1.0 in at least one direction of running were identified as spatially modulated cells. This approach accounts for both coherence and stability of spatially modulated cells, since it will not identify as spatially modulated a cell that fires in a single lap (low stability), or if it fires in different locations across laps (low coherence), or if it fires sparsely yielding a high mean pairwise correlation by chance (low stability, giving low Z score from the bootstrap procedure).

Spatial correlations and decorrelations

To quantify session-wise correlations between spatial activity maps in the running direction (In/In or Out/Out), we split even and odd laps crossings in the same direction of motion. We calculated mean spatial activity maps for each cell for even and odd laps and computed correlations (Pearson's R) between mean spatial activity maps for either all or only neurons that were spatially modulated (see above). We then computed the mean correlation values for each session. To quantify session-wise correlations between spatial activity maps in Inbound and Outbound directions, we computed correlations between spatial activity maps in Inbound and Outbound directions as described above. To quantify distance-coding, we measured correlations between spatial activity maps for lap crossings in the opposite directions after inverting the order ("flipping") of the maps for the outbound direction.

Population vector (PoV) analysis

Population vectors (PoV) were defined as the collection of event rates of the population of all spatially modulated neurons measured in a spatial bin. PoV correlations were obtained by computing Pearson's R between corresponding PoVs of different running directions (OUT vs IN) or of the same running direction split into even and odd lap crossings. PoV correlation matrices depict color-coded PoV .

Rate vector and selectivity

In order to compute contextual selectivity, the event rate for the i-th cell r_i was defined as the number of neural events of a cell divided by the amount of running time in a given direction.

For each recording session, selectivity of the *i*-th neuron was defined as the normalized difference of event rates *r* of that neuron computed during inbound and outbound running: $|r_i^I - r_i^O| / (r_i^I + r_i^O)$. The rate vector was defined as the entirety of event rates of a population of neurons during a lap crossing or a session.

Statistics

Data are presented as Mean ± SEM across animals, unless otherwise stated. Statistical significance was assessed using using Wilcoxon signed-rank tests for paired data and Mann-Whitney U tests for unpaired data. When comparing more than two groups, we first performed an analysis of variance (ANOVA) followed by Bonferroni *post-hoc* correction of the test results.

IV. Results

To explore how different hippocampal subregions construct a representation of space, we recorded neuronal activity from the dentate gyrus, CA3 and CA1 hippocampal subregions using microendoscope single-photon calcium imaging in freely-navigating mice. We first implanted a gradient-index (GRIN) lens above the hippocampal subregion of interest (Figs 3.1 and 3.2). We then proceeded to record neuronal population activity while the mice navigated spontaneously back and forth along a linear track during 10-minute sessions on multiple days (Figs. 3.3 and 3.4). The 60-cm linear track was enriched with visual cues (eg. playing cards) on the walls as well as Lego bricks at the extremities of the track. This approach allowed us to record neuronal activity from all three identified hippocampal subregions in freely navigating animals.

1. Spatial representations are modulated by the running direction in the dentate gyrus, CA3 and CA1

To identify how spatial activity is modulated by the running direction, we split the neuronal activity depending on the direction of motion of the animal (Inbound/Outbound) (Fig 4.1).

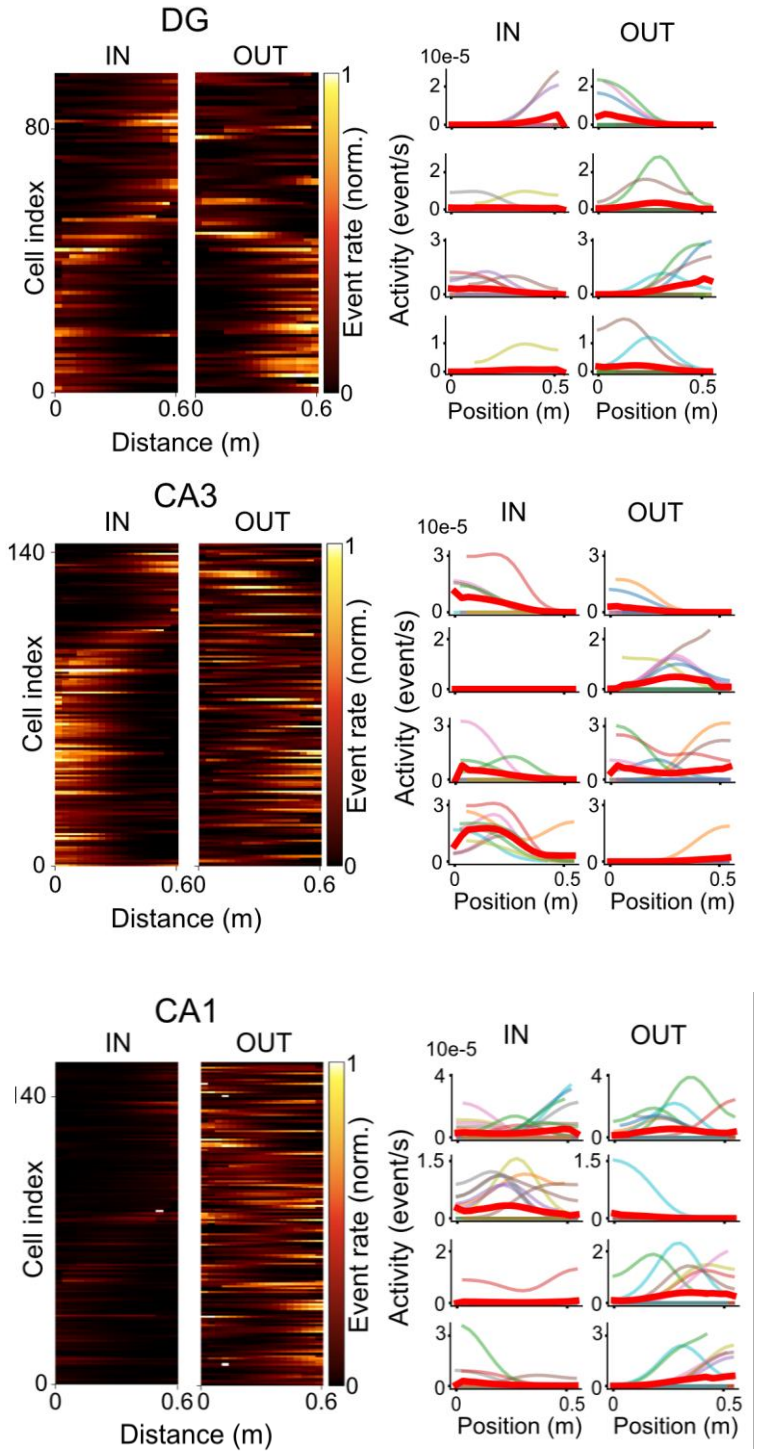

Figure 4.1. Spatial activity maps according to running direction. (**left**) Pairs of spatial activity maps of all spatially modulated neurons in DG, CA3 and CA1 sorted by the position of maximal activity in the left maps (inbound direction). (**right**) spatial activity maps of four sets of example neurons.

We first quantified the fraction of spatially modulated cells, which was similar across the three regions (Fig 4.2).

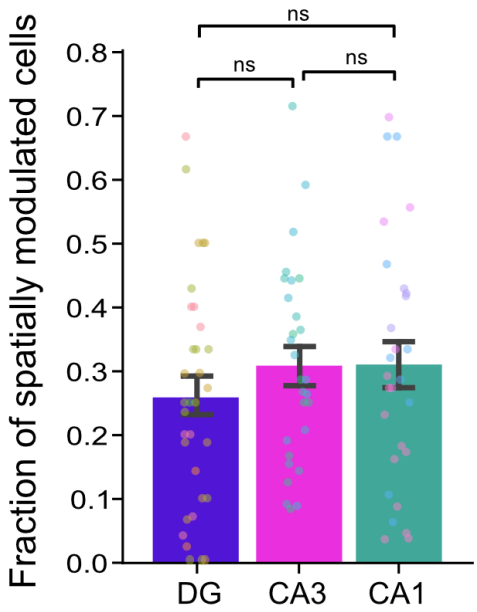

Figure 4.2. Fraction of spatially modulated cells in the DG, CA3 and CA1. (DG, 0.26 ± 0.03; CA3, 0.31 ± 0.03; CA1, 0.31 ± 0.04; DG vs CA3, p = 0.78; DG vs CA1, p = 0.86; CA3 vs CA1, p = 1.00). ns, not significant.

We then compared spatial activity maps in the same running direction by splitting laps into odd and even traversals and comparing map correlations for even laps with correlations for odd laps for a given direction (IN (odd-even) and OUT (odd-even)). The dentate gyrus showed a pronounced correlation for spatial activity maps in the same direction. (Fig 4.3 (top) and (bottom); $p > 0.05$ between IN (odd-even) and OUT (odd-even)). We then compared correlations between spatial activity maps for traversals in the same direction with correlations between spatial activity maps for traversals in opposite directions and found a lower correlation in opposite directions in the dentate gyrus (Fig 4.3 (top) and (bottom); $p < 0.01$)). Comparable results were found for both spatially modulated and unmodulated cells (Fig 4.3 (bottom)).

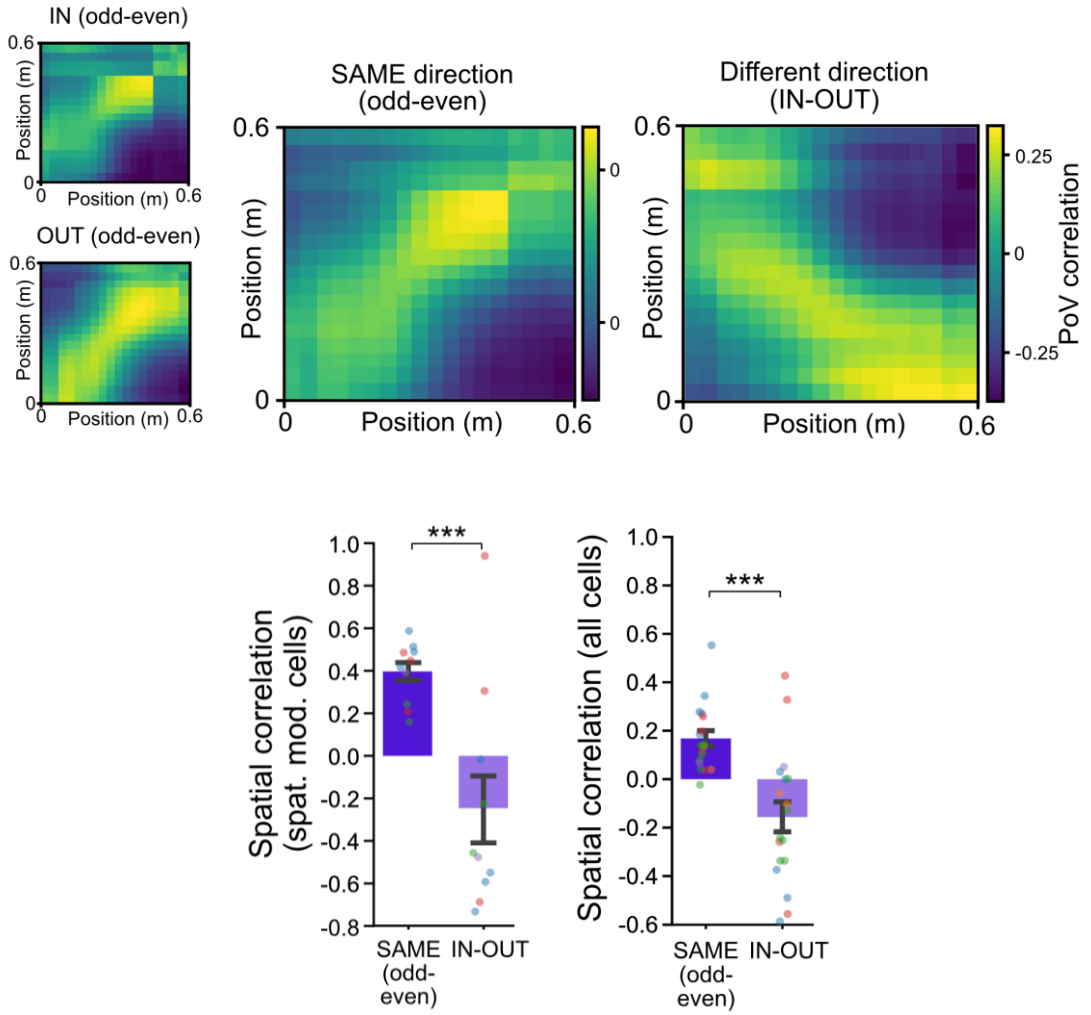

Figure 4.3. Spatial representations are modulated by running direction in the DG. (**top**) Left: Spatial population vector (PoV) correlation matrices for inbound (top) and outbound (bottom) running directions in the DG. PoV correlations were computed for each spatial bin in the even lap crossings (x axis) with each bin in the odd lap crossings (y axis). Right: Spatial PoV correlation matrices for same (left, SAME odd-even) and different (right, IN-OUT) running directions in the DG. (**bottom**) Left: Correlations between mean spatial activity maps across recording sessions within the same direction (SAME even-odd) and between different directions (IN-OUT) in the DG (left, spatial correlation: SAME even-odd, 0.39 ± 0.04; IN-OUT, -0.25 ± 0.17; Wilcoxon test, $p = 7 \times 10^{-7}$). PCs: spatially modulated cells. Right; Same as Left but including both spatially modulated and unmodulated cells in the DG (SAME even-odd, 0.17 ± 0.03; IN-OUT, -0.16 ± 0.06; Wilcoxon test, $p = 2 \times 10^{-6}$). ns, not significant; **, $p < 0.01$; ***, $p < 0.001$.

Similarly to the dentate gyrus, spatial activity maps in CA3 are more correlated in the same running direction than opposite directions, both in spatially and non-spatially modulated neurons (Fig 4.4 (top) and (bottom); $p > 0.05$ between IN (odd-even) and OUT (odd-even); $p < 0.01$ between IN and OUT)).

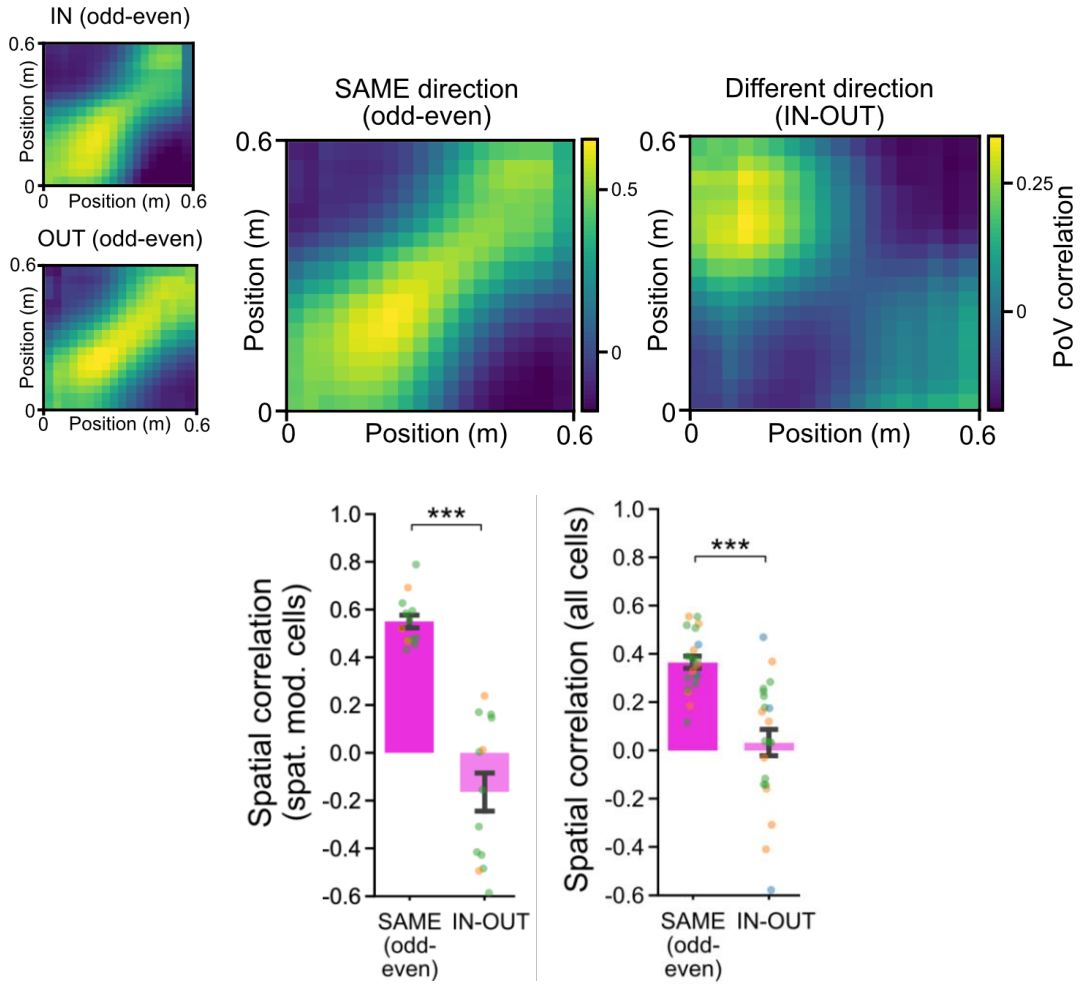

Figure 4.4. Spatial representations are modulated by running direction in CA3. (**top**) Left: Spatial population vector (PoV) correlation matrices for inbound (top) and outbound (bottom) running directions in CA3. PoV correlations were computed for each spatial bin in the even lap crossings (x axis) with each bin in the odd lap crossings (y axis). Right: Spatial PoV correlation matrices for same (left, SAME odd-even) and different (right, IN-OUT) running directions in CA3. (**bottom**) Left: Correlations between mean spatial activity maps across recording sessions within the same direction (SAME even-odd) and between different directions (IN-OUT) in CA3 (middle, spatial correlation: SAME even-odd, 0.549 ± 0.03. IN-OUT, -0.16 ± 0.08; Wilcoxon test, $p = 3 \times 10^{-6}$). PCs: spatially modulated cells. Right; Same as Left but including both spatially modulated and unmodulated cells in CA3 (SAME even-odd, 0.36 ± 0.03; IN-OUT, 0.03 ± 0.06; Wilcoxon test, $p = 4 \times 10^{-6}$). ns, not significant; **, $p < 0.01$; ***, $p < 0.001$.

We also applied this analysis to CA1 and similarly to the dentate gyrus and CA3, spatial activity maps in CA1 are more correlated in the same running direction that in opposite directions, both in spatially and non-spatially modulated neurons (Fig 4.5 (top) and (bottom); $p > 0.05$ between IN (odd-even) and OUT (odd-even); $p < 0.01$ between IN and OUT)).

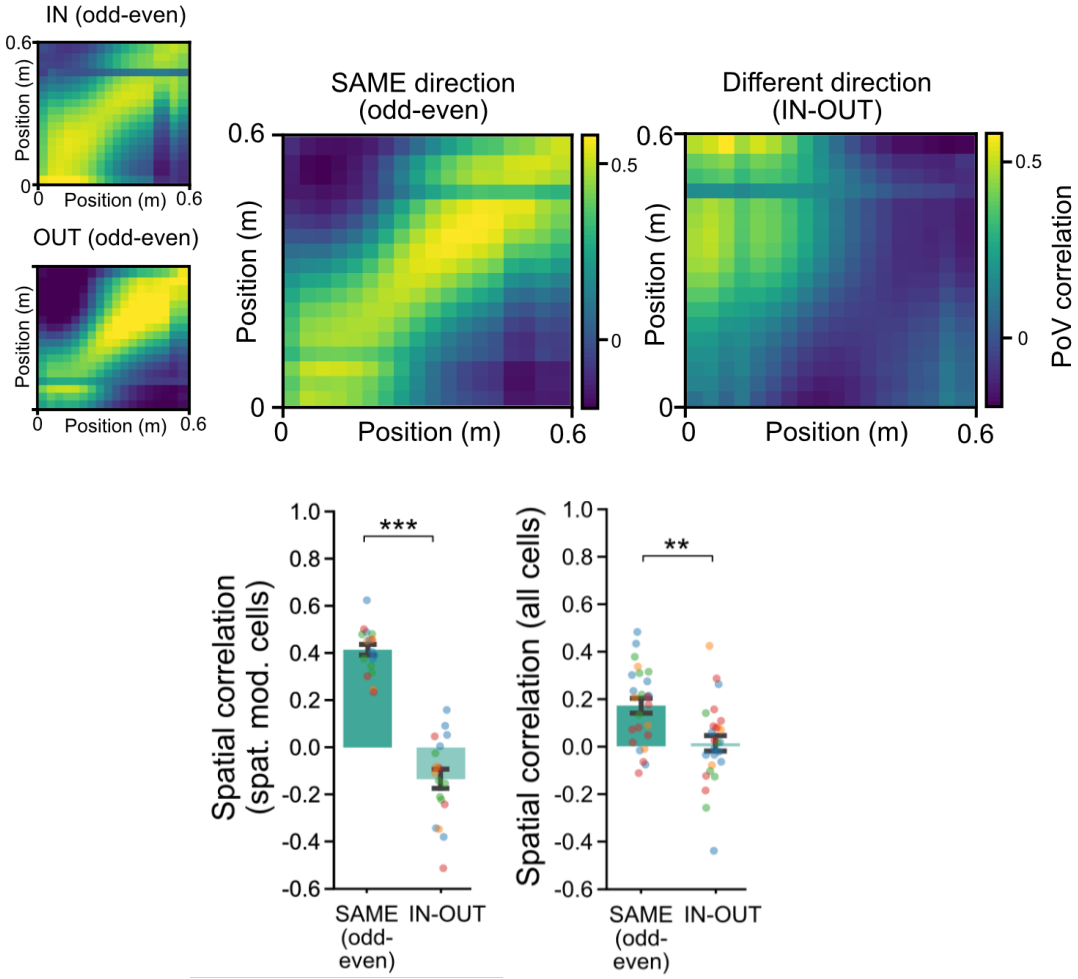

Figure 4.5. Spatial representations are modulated by running direction in CA1. (**top**) Left: Spatial population vector (PoV) correlation matrices for inbound (top) and outbound (bottom) running directions in CA1. PoV correlations were computed for each spatial bin in the even lap crossings (x axis) with each bin in the odd lap crossings (y axis). Right: Spatial PoV correlation matrices for same (left, SAME odd-even) and different (right, IN-OUT) running directions in CA1. (**bottom**) Left: Correlations between mean spatial activity maps across recording sessions within the same direction (SAME even-odd) and between different directions (IN-OUT) in CA1 (right, spatial correlation: SAME even-odd, 0.41 ± 0.02; IN-OUT, -0.13 ± 0.04; Wilcoxon test, $p = 3 \times 10^{-6}$). PCs: spatially modulated cells. Right; Same as Left but including both spatially modulated and unmodulated cells in CA1 (SAME even-odd, 0.17 ± 0.03; IN-OUT, 0.01 ± 0.03; Wilcoxon test, p = 0.002). ns, not significant; **, $p < 0.01$; ***, $p < 0.001$.

To determine how directional spatial representations evolve along the hippocampal circuits, we directly compared the three hippocampal subregions by measuring the spatial decorrelation (e.g. the reduction in correlation). No significant difference was observed between the three hippocampal subregions, regardless of whether only spatially modulated or all cells were included (Fig 4.6). Overall, these results indicate that all three hippocampal subregions show directional spatial representations along the linear track.

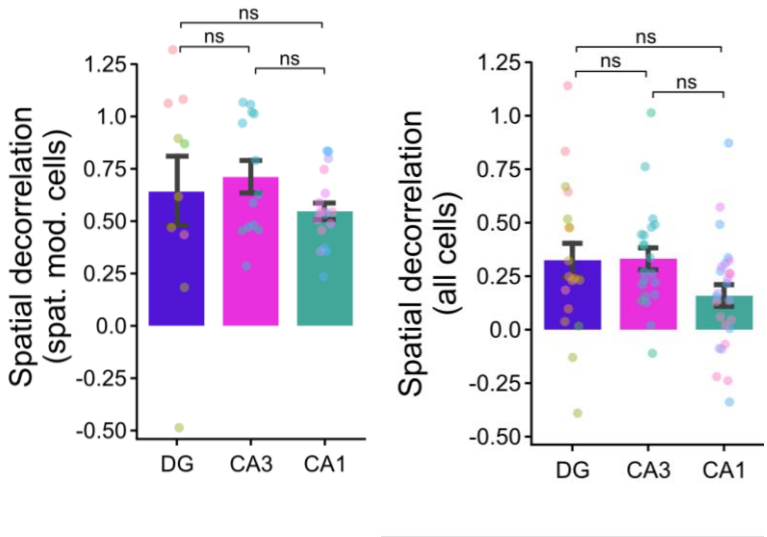

Figure 4.6. Spatial decorrelation in the DG, CA3 and CA1. (**left**) Spatial decorrelation, quantified as the difference between spatial correlations within the same direction (even-odd) and between different directions (inbound and outbound) in spatially modulated neurons in the DG (0.64 ± 0.17), CA3 (0.71 ± 0.08) and CA1 (0.55 ± 0.04). No differences have been found between the three hippocampal subregions (DG vs CA3: ANOVA with Bonferroni correction, p = 0.99; DG vs CA1: ANOVA with Bonferroni correction, p = 0.99; CA3 vs CA1: ANOVA with Bonferroni correction, p = 0.16). (**right**) Same as left but including both spatially modulated and unmodulated cells in the DG (0.35 ± 0.08), CA3 (0.33 ± 0.05) and CA1 (0.16 ± 0.05). No differences have been found between the three hippocampal subregions (DG vs CA3: ANOVA with Bonferroni correction, p = 0.99; DG vs CA1: ANOVA with Bonferroni correction, p = 0.25; CA3 vs CA1: ANOVA with Bonferroni correction, p = 0.08). Bars represent mean ± SEM. Circles represent recording sessions color-coded for each animal (DG, n = 10 sessions from 5 animals; CA3, n = 13 sessions from 3 animals; CA1, n = 18 sessions from 4 animals). ns, not significant; **, p < 0.01; ***, p < 0.001.

2. Selectivity for running direction is higher in the dentate gyrus and CA3 than in CA1

Activity in the dentate gyrus has been reported to be highly selective for the environmental context (Allegra et al., 2020; Neunuebel and Knierim, 2014). We wondered whether such selectivity would also be reflected by overall changes in firing rates across running directions. To assess whether distinct hippocampal subregions show selective activity for different running directions within the same environment, we quantified relative differences in event rates during runs in one *vs* the other direction, without accounting for the spatial modulation of individual neurons. We found that context (directional) selectivity was highest in the dentate gyrus and CA3 (Fig 4.7 (left); DG vs CA3, $p > 0.05$)). Consistent with previous reports of CA1 showing low context selectivity (Allegra et al., 2020; Neunuebel and Knierim, 2014), CA1 selectivity for running direction was lower than in the dentate gyrus ($p < 0.01$) and in CA3 ($p < 0.01$). Sparse firing in the dentate gyrus may contribute to its high selectivity, as we found lower activity in the dentate gyrus compared to CA3 and CA1 (Fig 4.7 (right); DG vs CA3, $p < 0.05$; DG vs CA1, $p > 0.05$; CA3 vs CA1, $p > 0.05$)). In contrast, activity rates in CA3 and CA1 were similarly high.

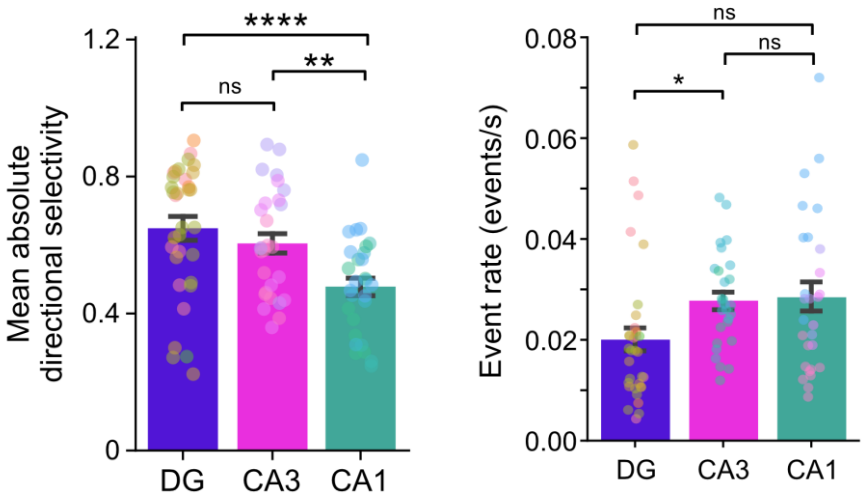

Figure 4.7. Selectivity for running direction is higher in DG and CA3 than CA1. (**left**) Absolute selectivity for running direction in DG (0.65 ± 0.03), CA3 (0.60 ± 0.03) and CA1 (0.48 ± 0.03). Absolute selectivity was higher in both DG and CA3 compared to CA1 (DG vs CA1: ANOVA with Bonferroni correction, p = 0.0008; CA3 vs CA1, ANOVA with Bonferroni correction, p = 0.008), whereas DG and CA3 showed comparable levels (DG vs CA3, ANOVA with Bonferroni correction, p = 0.99). (**right**) Event rate in the three hippocampal subregions (left; DG, 0.020 ± 0.002; CA3, 0.028 ± 0.002; CA1, 0.028 ± 0.003. DG vs CA3, ANOVA with Bonferroni correction, p = 0.04; DG vs CA1, ANOVA with Bonferroni correction, p = 0.08; CA3 vs CA1, ANOVA with Bonferroni correction, p = 0.99).

To verify whether the higher selectivity for running directions in the dentate gyrus arises from its sparse coding, we computed the expected selectivity from a shuffled version of the experimental dataset. We found that selectivity in the dentate gyrus was comparable to the selectivity expected from the shuffled dataset (Fig 4.8; DG vs bootstrap > 0.05). By contrast, selectivity in CA3 was higher than expected from the bootstrap dataset ($p < 0.001$). Together, these results reveal that selectivity for running directions is highest in the dentate gyrus and CA3. Furthermore, sparse firing can explain selectivity in the dentate gyrus but not in CA3, which may inherit selectivity from the upstream dentate gyrus.

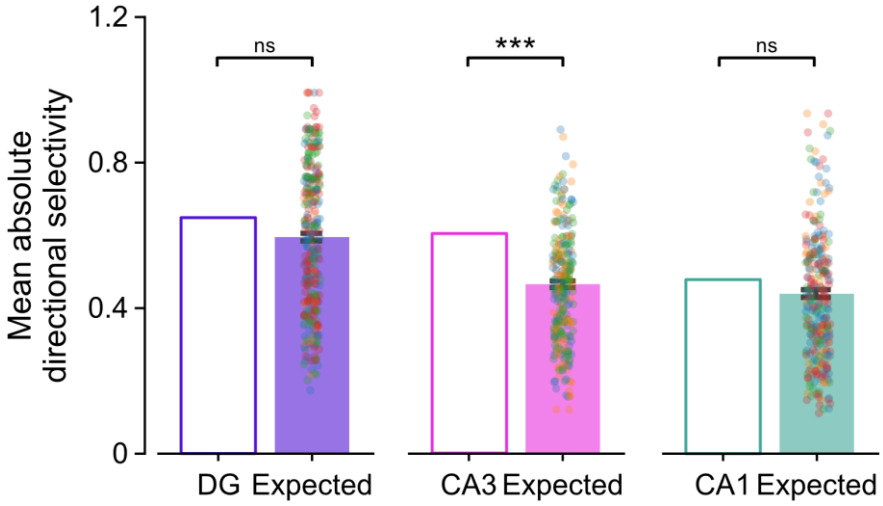

Figure 4.8. Expected selectivity in the DG, CA3 and CA1. Absolute selectivity for running direction compared to a bootstrap dataset (expected selectivity) within each region (**left**) DG, same as fig 4.7(left); expected, 0.59 ± 0.01, p = 0.14; middle: CA3, same as fig 4.7(left); expected, 0.46 ± 0.01, p = 7 x 10^{-6}; right: CA1, same as fig 4.7(left); expected, 0.44 ± 0.01, p = 0.26). Bars represent mean ± SEM. Circles represent recording sessions color-coded for each animal (DG, n = 33 sessions from 5 animals; CA3, n = 28 sessions from 3 animals; CA1, n = 28 sessions from 4 animals). ns, not significant; *, p < 0.05; **, p < 0.01; ***, p < 0.001.

3. The dentate gyrus uses distance-coding to build spatial representations

While spatial representations in all regions were uncorrelated between different running directions, we noticed that population vector correlations in the dentate gyrus were correlated when one of the running directions was reversed (Fig. 4.9). This observation suggests that representations at corresponding distances measured from the starting point of a track traversal are preserved, indicating that spatial firing is tuned to the distance covered by the animal rather than to allocentric positional coordinates.

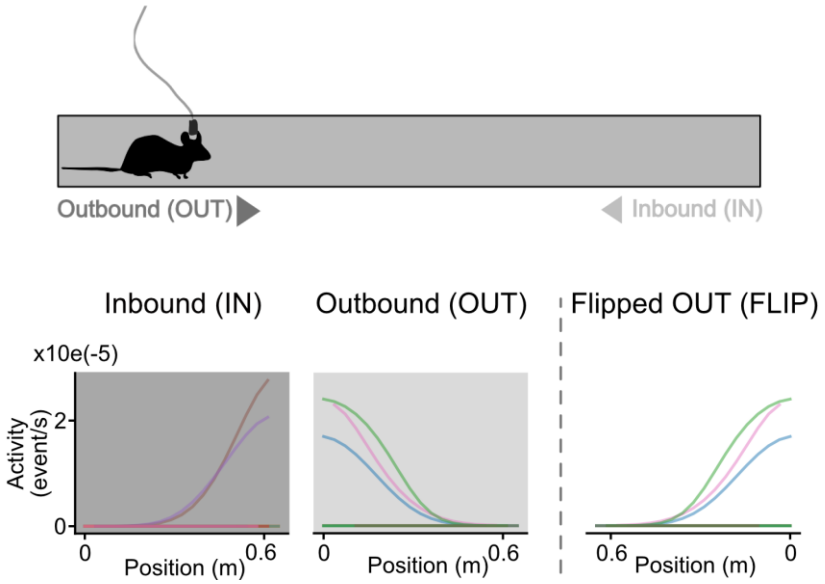

Figure 4.9. Flipping spatial activity maps. (**top**) Schematic of a mouse freely navigating along a linear track in outbound (OUT) and inbound (IN) running directions. (**bottom**) Spatial activity maps for an example cell in inbound (IN, left), outbound (OUT, middle) and flipped outbound running directions (FLIP, right).

To quantify this observation, we measured correlations between spatial activity maps for traversals in opposite directions after reversing the order ("flipping") of the maps for the outbound direction (Fig 4.10). We found that the dentate gyrus showed substantial correlations between flipped maps that were on the order of the correlations observed between maps for the same running direction ($p > 0.05$). The same result was obtained when including all cells, both spatially modulated and unmodulated ($p > 0.05$). This finding is consistent with the notion that neuronal activity in the dentate gyrus encodes covered distance along the track in either running direction.

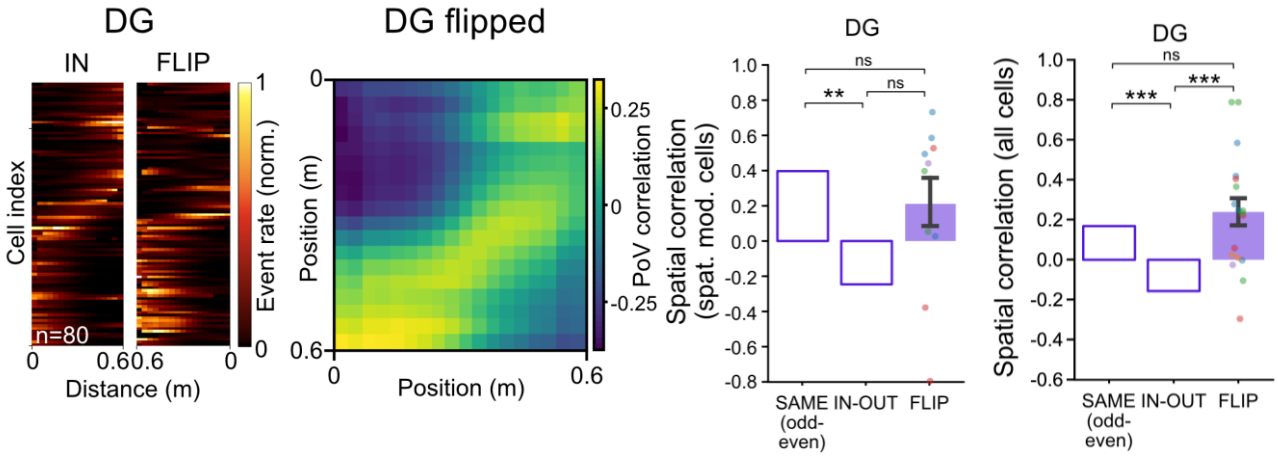

Figure 4.10. Spatial information in DG reflects distance coding in egocentric coordinates. (**left**): pair of spatial activity maps of all spatially modulated neurons in the DG sorted by the position of maximal activity in the left map (inbound direction). (**middle left**) spatial population vector (PoV) correlation matrices for inbound and flipped outbound running direction in the DG. PoV correlations were computed for each spatial bin in the inbound lap crossings (x axis) with each bin in the flipped outbound lap crossings (y axis). (**middle right**) Correlations between mean spatial activity maps across recording sessions within the same direction (SAME even-odd), between different directions (IN-OUT) and between inbound and flipped outbound directions in the DG (left, spatial correlation: same dataset as Fig 4.3 bottom, FLIP, 0.21 ± 0.15; SAME odd-even vs IN-OUT, $p = 0.005$; IN-OUT vs FLIP, $p = 0.17$; SAME odd-even vs FLIP, $p = 0.78$). (**right**) Same as middle right but including both spatially modulated and unmodulated cells in the DG (same data as Fig 4.3 bottom, FLIP, 0.24 ± 0.07; SAME odd-even vs IN-OUT, $p = 0.0003$, IN-OUT vs FLIP, $p = 0.0006$; SAME odd-even vs FLIP, $p = 0.99$. Bars represent mean ± SEM. Circles represent recording sessions color-coded for each animal.

By contrast, no substantial correlations between flipped maps were observed in the downstream region CA3. In this region, the correlation of the flipped maps was lower than correlation in the same direction, independently of whether all cells or only spatially modulated cells were included in the analysis (Fig 4.11; $p < 0.01$ in both cases).

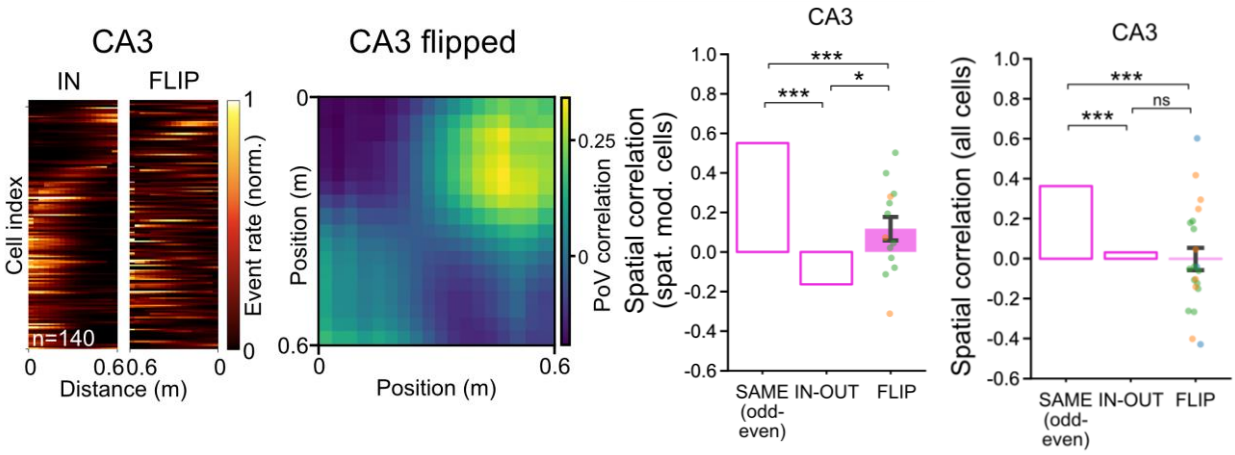

Figure 4.11. Spatial information in CA3 does not reflect distance coding in egocentric coordinates. (**left**) Pair of spatial activity maps of all spatially modulated neurons in CA3 sorted by the position of maximal activity in the left map (inbound direction). (**middle left**): spatial population vector (PoV) correlation matrices for inbound and flipped outbound running direction in CA3. PoV correlations were computed for each spatial bin in the inbound lap crossings (x axis) with each bin in the flipped outbound lap crossings (y axis). (**middle right**) Correlations between mean spatial activity maps across recording sessions within the same direction (SAME even-odd), between different directions (IN-OUT) and between inbound and flipped outbound directions in CA3 (middle, spatial correlation: same data as Fig 4.4 bottom, FLIP, 0.12 ± 0.06; SAME odd-even vs IN-OUT, p = 7 x 10^{-8}; IN-OUT vs FLIP, p = 0.04; SAME odd-even vs FLIP, p = 5 x $10^{}$). (**right**) Same as middle right but including both spatially modulated and unmodulated cells in CA3 (same data as Fig 4.4 bottom, FLIP, -0.001 ± 0.06; SAME odd-even vs IN-OUT, p = 1 x 10^{-5}; IN-OUT vs FLIP, p = 0.99; SAME odd-even vs FLIP, p = 2 x $10^{}$). Bars represent mean ± SEM. Circles represent recording sessions color-coded for each animal.

In CA1, a significant difference was observed between flipped maps and maps of the same direction when including spatially modulated cells only (Figs 4.12; $p<0.01$), but the correlation between flipped maps was not significant when including all cells (Fig 4.12 $p = 0.05$).

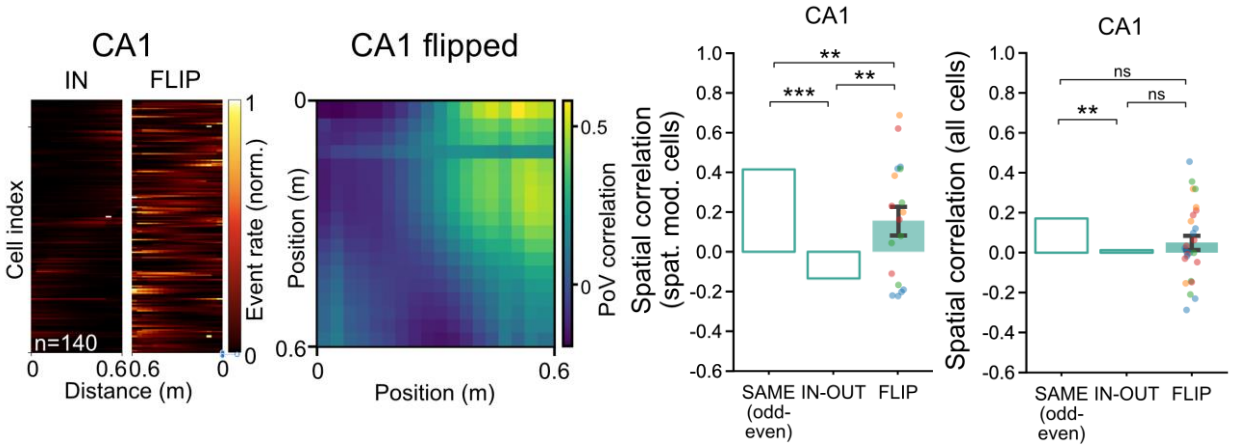

Figure 4.12. Spatial information in CA1 does not reflect distance coding in egocentric coordinates. (**left**) Pair of spatial activity maps of all spatially modulated neurons in CA1 sorted by the position of maximal activity in the left map (inbound direction). (**middle left**): spatial population vector (PoV) correlation matrices for inbound and flipped outbound running direction in CA1. PoV correlations were computed for each spatial bin in the inbound lap crossings (x axis) with each bin in the flipped outbound lap crossings (y axis). (**middle right**) Correlations between mean spatial activity maps across recording sessions within the same direction (SAME even-odd), between different directions (IN-OUT) and between inbound and flipped outbound directions in CA1 (right, spatial correlation: same dataset as Fig 4.5 bottom, FLIP, 0.16 ± 0.07; SAME odd-even vs IN-OUT, p = 1 x 10^{-12}; IN-OUT vs FLIP, p = 0.003; SAME odd-even vs FLIP, p = 0.004). (**right**) same as middle right but including both spatially modulated and unmodulated cells in CA1 (same data as Fig 4.5 bottom, FLIP, 0.05 ± 0.04; SAME odd-even vs IN-OUT, p = 0.004; IN-OUT vs FLIP, p = 0.99; SAME odd-even vs FLIP, p = 0.99). Bars represent mean ± SEM. Circles represent recording sessions color-coded for each animal.

We defined a measure of distance-coding by subtracting the correlation value of the maps in opposite directions from the correlation values of the flipped maps, and found that when selecting spatially modulated cells exclusively, the measure of distance-coding in the dentate gyrus was not significantly different from that of other hippocampal subregions (Fig 4.13; p>0.05). However, when selecting all cells, the measure of distance coding was significantly more pronounced in the dentate gyrus than in other regions (Fig 4.13; p values <0.01). Overall, these results indicate that at the single-cell level, during track crossings in different directions, spatial firing fields appear at equivalent locations in egocentric coordinates, suggesting that they represent the distance that the animal has covered from its starting point rather than position in allocentric coordinates of the external world.

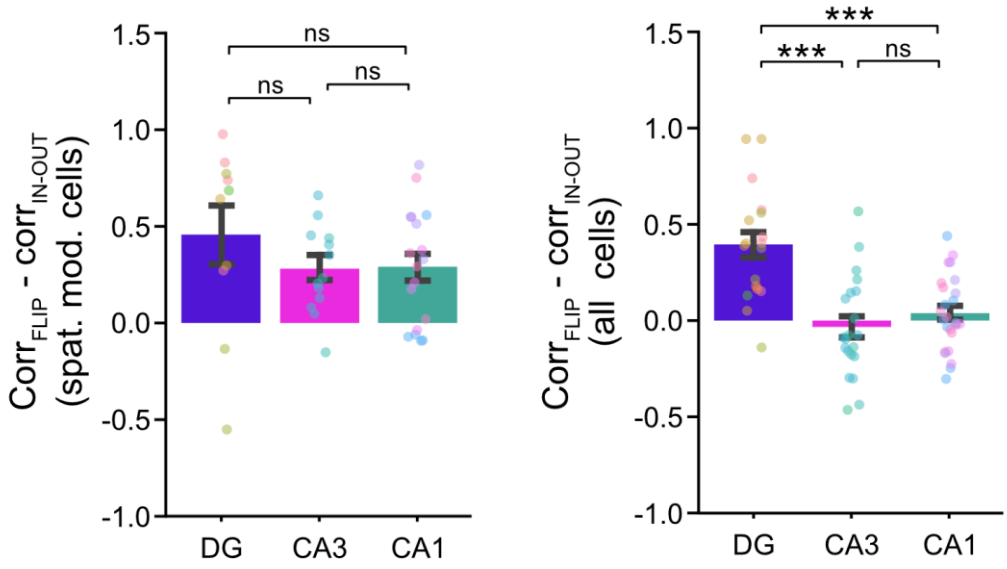

Figure 4.13. The DG uses distance coding but not CA3 and CA1. (**left**) Quantification of the difference between spatial correlations within the flipped (inbound-flipped outbound, FLIP) and different (inbound-outbound, IN-OUT) directions in the DG (0.46 ± 0.15), CA3 (0.28 ± 0.06) and CA1 (0.29 ± 0.07). No statistically significant differences were found between the three hippocampal subregions (DG vs CA3: p = 0.77; DG vs CA1, p = 0.80; CA3 vs CA1, p = 1.00), (**right**) Same as left but including both spatially modulated and unmodulated cells in the DG (0.39 ± 0.07), CA3 (-0.03 ± 0.06) and CA1 (0.04 ± 0.04). The difference between the spatial correlations within flipped (FLIP) and opposite (IN-OUT) directions was significantly higher in DG than in CA3 and CA1 (CA3 vs DG, p = 7 x 10^{-5}; DG vs CA1, p = 4 x 10^{-5}), whereas no difference was found between CA3 and CA1 (p = 0.85). Bars represent mean ± SEM. Circles indicate single recorded sessions color-coded for each animal (DG, n = 10 sessions from 5 animals; CA3, n = 13 sessions from 3 animals; CA1, n = 18 sessions from 4 animals). ANOVA with Bonferroni correction: ns, not significant; *, p < 0.05; **, p ≤ 0.01; ***, p < 0.001.

4. Representations of space are differentially modulated by novelty in hippocampal subregions

We wondered whether the representations of space we observed in hippocampal subregions would be modulated by novelty. We used olfactory stimuli as novel contextual information by homogeneously diffusing odors of neutral valance throughout a linear track. Animals were exposed to an odor (odor A, familiar) during 10 minute-sessions on four consecutive days. On

the fifth day, the neuronal activity of the dentate gyrus, CA3 and CA1 was recorded in this now familiar olfactory environment followed by a novel olfactory environment (odor B, novel) (Fig 4.14).

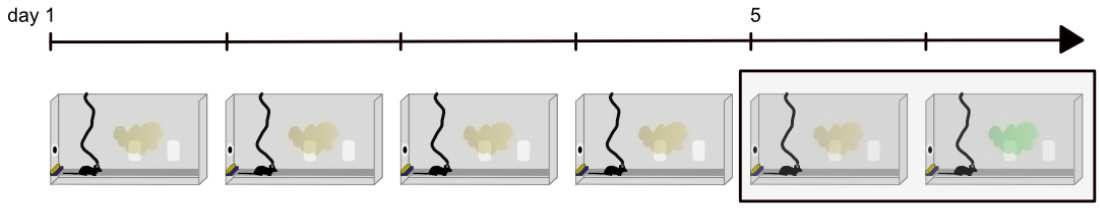

Figure 4.14. Schematic of the experimental paradigm illustrating a mouse freely navigating along a linear track while exposed to changing olfactory stimuli. Animals were habituated to an odor (odor A, familiar, light brown) during 10 minute-recording sessions on four instances in the linear track. The animals were then exposed to the now familiar odor A as well as novel odor (odor B, novel, light green), each during a 10 minute-recording session in the linear track.

We applied the previously introduced measure of selectivity for running direction (Fig 4.7) by quantifying relative differences in event rates during runs in one *vs* the other direction, and compared this selectivity for running direction across olfactory environments. These data are preliminary since the limited number of sessions does not allow statistical significance to be established or firm conclusion to be drawn. In the familiar environment, selectivity for running direction is higher in the dentate gyrus and CA3 than in CA1 (Fig 4.15), consistently with our previous results (Fig 4.7).

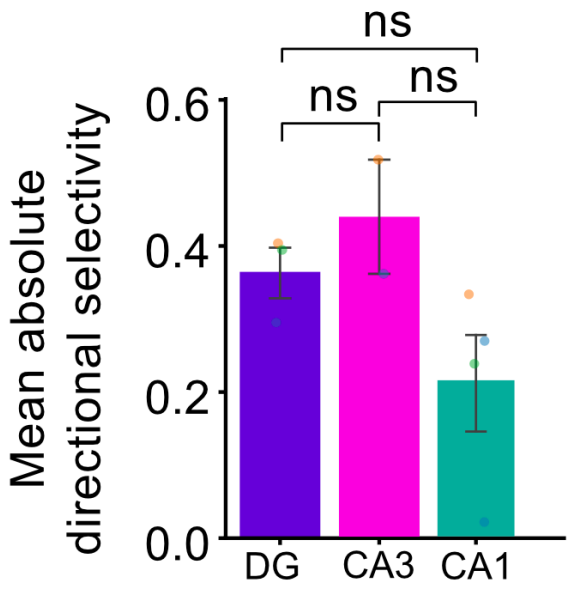

Figure 4.15. Mean absolute selectivity for running direction in the familiar olfactory environment in the DG (0.365 ± 0.035), CA3 (0.438 ± 0.078) and CA1 (0.214 ± 0.068). Absolute selectivity seemed higher in both DG and CA3 compared to CA1 but not significant (DG vs CA1: ANOVA with Bonferroni correction, p = 1.0, CA3 vs CA1, ANOVA with Bonferroni correction, p = 0.35), whereas DG and CA3 showed comparable levels of selectivity (DG vs CA3, ANOVA with Bonferroni correction, p = 0.41).

We then measured selectivity for running direction in a novel contextual environment by homogeneously diffusing the novel odor B into the linear track. Selectivity for running direction remains high upon exposure to the novel odor in the dentate gyrus (Fig 4.16; $p > 0.05$) but shows a pronounced decrease upon exposure to the novel odor in CA3 ($p > 0.05$). Moreover, CA1 selectivity for running direction seems to increase with novelty, consistent with previous reports that activity of CA1 neurons are modulated by olfactory stimuli (Anderson and Jeffery, 2003).

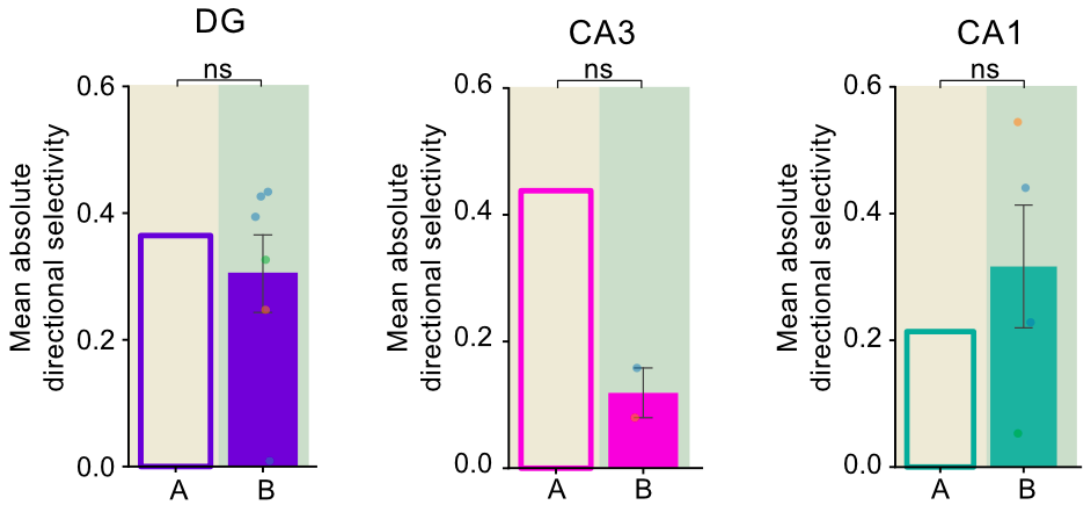

Figure 4.16. Mean absolute selectivity for running direction in DG, CA3 and CA1 in familiar and novel olfactory environments. Absolute selectivity for running direction in DG in odor B (0.306 ± 0.066; $p > 0.05$), CA3 (0.119 ± 0.039, $p > 0.05$) and CA1 (0.317 ± 0.110, $p > 0.05$), light brown: familiar olfactory environment (odor A); light green: novel olfactory environment, odor B.

To verify whether the changes in selectivity for running direction observed upon exposure to contextual novelty resulted from changes in overall firing rates, we quantified firing rates in the dentate gyrus, CA3 and CA1 in both the familiar and novel odor and found that the firing rates remain constant across olfactory environments in the three hippocampal regions.

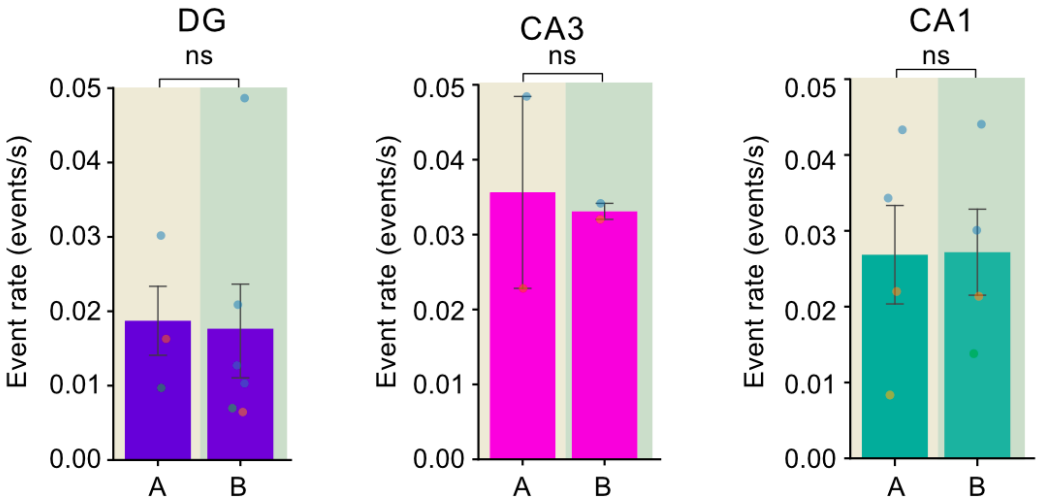

4.17. (right) Event rate in the three hippocampal subregions in familiar and novel olfactory environments (left). Event rate in DG with novel odor, B and familiar odor, A (A, 0.019 ± 0.006; B, 0.018 ± 0.007; A vs B, $p > 0.05$); (middle) Event rate in CA3 with novel odor, B and familiar odor, A (A, 0.036 ± 0.013; B, 0.033 ± 0.001; A vs B, $p > 0.05$); Event rate in CA1 with novel odor, B and familiar odor, A (A, 0.027 ± 0.008; B, 0.027 ± 0.006; A vs B, $p > 0.05$). light brown: familiar olfactory environment (odor A); light green: novel olfactory environment, odor B.

In summary, our results indicate that the direction of running modulates spatial firing patterns in all hippocampal subregions and that the dentate gyrus and CA3 are more selective for running direction than CA1 based on changes in firing rates. Also, we show that in the dentate gyrus, spatial representations reflect distance coding. Preliminary evidence further suggests that the selectivity for the spatial environment is differentially modulated by novelty in hippocampal regions.

V. Discussion

1. Summary and discussion of the main findings

In this study, we explore how representations of spatial position, running direction, and distance evolve along the hippocampal circuit. By performing single-photon calcium imaging from the dentate gyrus, CA3 and CA1, we provide one of the first descriptions of these representations in all major hippocampal subregions under the same task conditions in freely moving animals. In mice spontaneously running back and forth along a linear track, all regions display directionality in their spatial firing patterns, with spatial activity maps for the two opposing running directions being almost completely uncorrelated. We find that neuronal activity in the dentate gyrus and in CA3 is more selective for the direction of running than activity in CA1 based on changes in firing rates. Furthermore, activity in the dentate gyrus shows pronounced correlations of spatial activity maps after aligning them to the running direction, indicating that it encodes covered distance in egocentric coordinates. We also find that selectivity for running direction in the dentate gyrus, CA3 and CA1 is differentially modulated by contextual novelty.

1. 1. Directional modulation of spatial activity in hippocampal subregions

Hippocampal neurons are known to change the location of their spatial fields to represent a novel environment or contextual changes within a given environment (Anderson and Jeffery, 2003; Muller and Kubie, 1987). Here, we measured the ability of neuronal populations to discriminate distinct environments by quantifying the correlations of spatial activity maps across directions. We find that in the dentate gyrus, CA3 and CA1, spatial activity maps are modulated by the direction of running of the animal (Figs 4.3-6) (inbound and outbound), consistently with previous reports (Jung and McNaughton, 1993; Navratilova et al., 2012; Schwindel et al., 2016). These data indicate that the directional modulation of spatial representations is implemented through changes in the location of firing fields in an allocentric coordinate system, in a process called ‘global remapping’. The hippocampus

might therefore construct, at least partially, a spatial representation of the inbound and outbound trajectories as two distinct contexts anchored in an allocentric coordinate system.

1. 2. Directional selectivity of neuronal activity

To assess directional discrimination independently of the spatial modulation of individual neurons, we quantified 'directional selectivity' as the relative difference in firing rates between the two running directions. Our findings show that this directional selectivity varies along the hippocampal circuit and is more pronounced in the dentate gyrus and CA3 than in CA1 (Fig 4.7). This observation is consistent with previous reports of high context selectivity in the dentate gyrus (Allegra et al., 2020; Neunuebel and Knierim, 2012) and selectivity for running direction in the dentate gyrus, CA3 and CA1 (Jung and McNaughton, 1993; Navratilova et al., 2012; Schwindel et al., 2016). We show that in the dentate gyrus, selectivity is not significantly different from that expected from a bootstrap dataset. This result agrees with previous experimental evidence that selectivity in the dentate gyrus is implemented by sparse coding. Sparse coding allows the dentate gyrus to orthogonalize ambiguous spatial inputs by mapping spatial environments onto non-overlapping pools of active cells. Conversely, selectivity in CA3 and CA1 differ significantly from that expected from the bootstrap, suggesting that another neural mechanism is at play in CA3 to generate high selectivity for running direction. It is possible that the high selectivity for running direction observed in CA3 is generated by the dentate gyrus through sparse coding and transferred to CA3.

Our data show that CA1 is less selective for running direction than CA3 and the dentate gyrus but don't rule out that CA1 might represent changes in contextual information by subtle changes in its firing rates (McNaughton et al., 2006; Navratilova et al., 2012). However these firing rate changes might take place to a lesser extent than firing rate changes in CA3 and in the dentate gyrus, which can reach up to an order of magnitude (Leutgeb, 2005; Leutgeb et al., 2007), possibly to limit interference between resembling environments and events (Colgin et al., 2008). It is important to note that fine-grained rate changes are difficult to assess with single-photon *in vivo* calcium imaging, as individual spikes cannot easily be resolved. Also, while such directional selectivity has been previously reported in CA1 (Navratilova et al., 2012), it was shown to decrease upon exposure to multimodal local cues (Battaglia, 2004). Since most recording sessions take place in an environment that is familiar to the mice, experience-dependent directionality might explain why we observe a lower selectivity in CA1. Lower selectivity for running direction in CA1 than in CA3 and dentate gyrus is

consistent with recent work showing that CA1 is less selective for context than the dentate gyrus and responds to environmental features common to both environments (Allegra et al., 2020; Leutgeb, 2004; Leutgeb et al., 2007). Low selectivity for running direction might therefore indicate that CA1 constructs a global representation of the environment, consistent with reports that CA1 represents abstract information relative to the environment such as recent behaviour (Keinath et al., 2020), future path (Ito et al., 2015) and shows activity that is correlated with the animal's behaviour (Allegra et al., 2020). These findings offer a possible interpretation of our results, whereby directionally selective spatial maps in CA1 correspond to fragmented spatial maps of the global environment, consistent with previous work showing that CA1 switches between different stable spatial maps of the same environment (Sheintuch et al., 2020). In this scenario, CA1 would be switching between stable spatial maps for each running direction in order to construct a global representation of the environment.

1. 3. Origin of directional signals

One possible source of directionally tuned inputs to the hippocampus might be head-direction cells that are located in the MEC (Sargolini, 2006). Alternatively, directionally tuned inputs to the hippocampus might be provided by grid cells. Even though grid cells are not tuned to a single direction, they show modulation by head direction in a location-dependent manner (Gerlei et al., 2019). Grid cells are most abundant in layer II of the MEC and while they only represent a minority of MEC neurons (10/20%) that project to the hippocampus (Diehl et al., 2017; Sargolini, 2006; Sun et al., 2015; Zhang et al., 2013), the MECII projects heavily to the dentate gyrus and provides the main source of the entorhinal cortical inputs to CA3 (Deshmukh, 2020; Kerr et al., 2007; Witter and Amaral, 1991; Witter et al., 2000). A second type of grid cells might also provide directionally tuned inputs to the hippocampus: a majority of grid cells located in MEC III and V show conjunctive coding of position and direction (Sargolini, 2006). The MEC III projects to CA1 (Li et al., 2017) and this might provide CA1 with a source of directionally tuned inputs. By contrast to the dentate gyrus and CA1, the source of directionally tuned inputs to CA3 remains to be elucidated since the connectivity patterns between the entorhinal cortex and CA3 vary across species: the rat CA3 receives inputs from layer II of the entorhinal cortex (Deshmukh, 2020; Dolorfo and Amaral, 1998; Kerr et al., 2007; Steward, 1976; Witter et al., 2000), while the mouse CA3 receives inputs from the entorhinal cortex layer III (van Groen et al., 2003). It is possible that hippocampal neurons receive multiple sources of inputs such that the dentate gyrus and CA3 receive directionally tuned inputs from grid cells in MEC II while CA1 receives directionally tuned inputs from conjunctive coding grid cells in MEC III. Such a dual nature of directionally

tuned inputs to the hippocampus might explain why the dentate gyrus and CA3 are selective for running direction based on firing rates but not CA1.

By contrast to head-direction cells in other brain regions, it is thought that directional tuning is not a fundamental firing property of hippocampal neurons and may instead arise from experience-dependent learning. This notion is based on the variability of directional firing in hippocampal neurons (McNaughton et al., 1996; Navratilova et al., 2012; Schwindel et al., 2016) and the modulation of directional firing by different factors such as experience (McNaughton et al., 1983; Navratilova et al., 2012; Schwindel et al., 2016) and the availability of local cues (Battaglia, 2004). Directional tuning of hippocampal neurons may therefore arise from non-homogeneous distributions of head-direction signals caused by differences in the positions visited at different head directions, which may then lead to preferred firing in the running directions that have been encountered most (Muller et al., 1994). Related theoretical work has proposed that directional firing can be interpreted as a predictive code that emerges from repeated visits of the same running direction (Stachenfeld et al., 2017).

1. 4. Distance coding in the dentate gyrus

Our finding that spatial activity maps were decorrelated for different running directions in all three hippocampal subregions indicates that the environment is not represented in a single, allocentric reference frame when it is encountered in different running directions. However, we find that spatial activity maps for the dentate gyrus show substantial correlations after aligning them to the direction of running, which were on the order of the correlations observed between maps for the same running direction (Figs 4.10 and 4.13). This finding indicates that rather than encoding position of the animal in allocentric coordinates, the dentate gyrus encodes distance run along the linear track. Such egocentric distance coding was not observed in other hippocampal regions. Interestingly, this observation is made when including all recorded cells, but not when selecting spatially modulated cells, indicating that neurons that are not apparently spatially modulated play an important role to encode distance run along the track to construct spatial representations. These results are consistent with previous reports of mixed selectivity and multiplexed coding in the dentate gyrus (Morris et al., 2013a, 2013b; Murano et al., 2020; Stefanini et al., 2018). However, at first sight high directional selectivity and distance coding appear contradictory, as distance coding requires neuronal activity at equivalent distances in both directions of running, and would therefore counteract directionally selective firing. We hypothesize that the two observations can be

reconciled by rate changes of the distance coding, "flipped" firing fields - i.e. the firing fields appear at equivalent distances, but with different rates. In addition, a separate population of dentate gyrus neurons shows complete selectivity (selectivity = 1) by only firing during runs in one direction, but not in the other, as has been described by previous reports about context selectivity in dentate gyrus neurons (Allegra et al., 2020; Cholvin et al., 2021). Our results are consistent with a prediction that the dentate gyrus creates a unified representation of space and task. Indeed, the observation that disruption of the dentate gyrus local circuit prevents visual inputs to drive selective and stable spatial firing in CA1 led to the hypothesis that the dentate gyrus builds a representation of physical space by binding an internal representation of space and external landmarks that is required for a stable spatial code in CA1 (Lee et al., 2012b).

1. 5. What is the source of distance information?

While directional signals to the dentate gyrus might be provided by the MEC, where does the information about distance arise? One possible answer is that distance signals arise as a result of spatial signals also conveyed to the hippocampus by the MEC. During exploration of an environment, animals integrate information relative to self-movements to determine their position within the environment through a process named 'path integration' (Knierim et al., 2014), enabling them to find their homes after a convoluted journey devoid of external sensory information (Whishaw and Tomie, 1997). MEC neurons generate a dynamic representation of the animal's position during navigation by integrating information about self-motion (Campbell et al., 2018; Savelli et al., 2008; Solstad et al., 2008). Specifically, some MEC neurons are tuned to the distance travelled and integrate self-motion information to modulate estimates of position (Campbell et al., 2018). MEC neurons are also sensitive to the distance that separates an animal from an object, which led to categorising a subpopulation of MEC neurons as 'object-vector cells' (Høydal et al., 2019). Integration of self-motion information was also reported in grid cells, which constitute a subpopulation of MEC neurons (Hafting et al., 2005; Jacob et al., 2019; Kraus et al., 2015). Grid cells exhibit spatial representations that are highly dynamic and display mixed selectivity (Hardcastle et al., 2017) and it is thought that conjunctive coding of position, direction and distance updates grid coordinates during self-motion-based navigation (Sargolini, 2006). The MEC projects to the dentate gyrus via the medial perforant path that contacts granule cell dendrites (Dolorfo and Amaral, 1998; van Groen et al., 2003; Kerr et al., 2007; Steward, 1976). The conversion of inputs from the entorhinal cortex to dentate gyrus is thought to enable fast encoding and efficient recall of spatio-temporal information (Cholvin et al., 2021). Consistent with the

notion that distance signals are conveyed to the DG by the MEC, the MECII-DG pathway was shown to create a persistent representation of the behavioural task performed by the animal, based on learned visual cues and integration of positional and spatial information suggesting that the MECII-DG pathway plays a crucial role in the representation of non-allocentric information (Cholvin et al., 2021; Qin et al., 2018).

1. 6. Decoding position, direction and distance in the dentate gyrus, CA3 and CA1

Our analysis of spatial correlations of 'flipped' maps indicates that in the dentate gyrus, but not in CA3 and CA1, individual neurons produce spatial representations consistent with an egocentric spatial representation, encoding the distance that the animal has travelled from its starting point rather than its allocentric position along the track. However, a low egocentric map correlation at the single-cell level does not imply that travelled distance is *not* represented in CA3 and CA1 activity, as these neural populations could employ different encoding schemes to jointly represent position and travelled distance. For example, separate coding schemes could be used to encode travelled distance at different running directions, resulting in low spatial "flip" correlations despite a high discriminability of different running distances.

To evaluate the extent to which egocentric and allocentric coordinates are represented along the hippocampal circuit, a collaborator of ours isolated population activity vectors from the first and the last 20% of the track and labelled them according to both position and distance travelled. He then used a linear decoder to predict the value of these labels from population activity in a cross-validated decoding scheme (Stefanini et al., 2018) (Fig 5.1). To ensure that the two variables were independently assessed, the decoder for one variable was performed on a balanced training set that did not favor any of the two values of the second variable. To do so, the decoder for position (0 vs 1) was trained on a balanced mix of distance (*start* and *end*) for each of the two position values: (0-start + 0-end) vs (1-start + 1-end) - and vice versa for the distance decoding analysis. Consistent with the findings on single-cell spatial remapping (Fig. 5), this decoding analysis revealed that information on egocentric distance is more decodable than allocentric position in the dentate gyrus ($p < 0.001$), whereas the opposite is true for CA1 activity ($p < 0.001$). Interestingly, despite the low flipped spatial correlation, he found that neuronal activity in CA3 represents both variables similarly well $p > 0.05$), suggesting that CA3 employs different coding strategies for egocentric and allocentric position in different running directions, while DG and CA1 primarily encode egocentric and allocentric position, respectively.

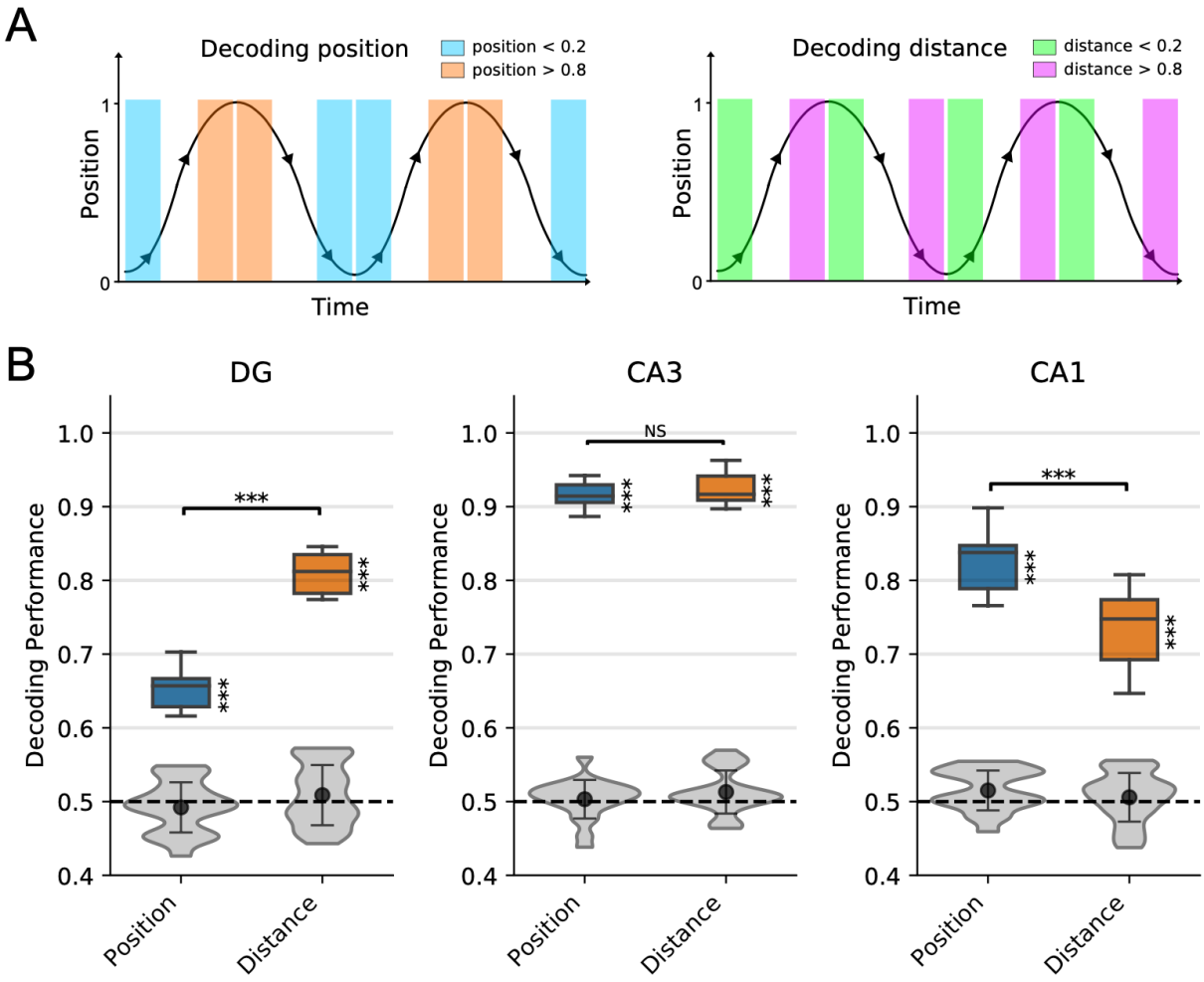

Figure 5.1. Transformation of population codes for position and distance along hippocampal circuits. (**A**) Schematic of the different labeling of the neural data used for the decoding analysis of allocentric position (left) and egocentric traveled distance (right). In the two cases, neural data is the same but the label is changed according to different behavioral correlates. (**B**) Decoding performance obtained by the analysis in A for activity in the DG (mean decoding performance: Position 0.65; Distance: 0.81, $p < 0.001$), CA3 (mean decoding performance: Position 0.915; Distance: 0.925, $P>0.2$) and CA1 (mean decoding performance: Position 0.83; Distance: 0.73, $P<0.001$). Box plots show the distribution for n=25 cross-validation folds using pseudo-simultaneous activity built from all animals combined. Grey violin plots show decoding results for a shuffled dataset (see Methods). Significance levels are computed by a Mann–Whitney U test (NS: $P>0.05$, ***: $P<0.001$).

1. 7. Coherence with theoretical predictions

Our findings provide direct experimental evidence for several theories of how the hippocampus constructs the cognitive map along its circuits. First, they are consistent with the parallel maps theory, which predicts that the dentate gyrus constructs primarily a "bearing map" from self-movement and directional cues, whereas CA1 constructs a "sketch map" from positional cues (Jacobs and Schenk, 2003). In addition, our results are also compatible with the two-stream hypothesis, which describes a separation between the processing of

information relative to the content (‘what’) and the location (‘where’) of an event within hippocampal subregions . These predictions were made based on functional and anatomical distinctions between the ‘what’ and ‘where’ pathway in the dentate gyrus, CA3, and CA1 subregions (Amaral and Witter, 1989; Burke and Barnes, 2011; Chawla et al., 2005; Henriksen et al., 2010). Consistently with this hypothesis, previous reports using immediate early genes (IEG) expression showed that distal CA1 and proximal CA3 respond to positional (discrete cues) but not the dentate gyrus. By contrast, the dentate gyrus and proximal CA3 but not CA1 respond to directional cues (general, obvious cues) (Hoang et al., 2018). Our results provide direct evidence for these predictions for the differential roles of the dentate gyrus, CA3 and CA1 in representing space. In particular, our results for distance coding are coherent with a representation of space based on navigational signals in the dentate gyrus.

1. 8. Cells that are not strongly spatially modulated contribute to represent the environment

The finding that in the dentate gyrus, neurons that are not spatially modulated also contribute to distance coding is relevant to the process of selecting spatially modulated cells, a widespread practice in recent studies of spatial navigation. The definition of spatially modulated cells was developed as a result of the discovery of spatial coding in hippocampal neurons and is based on an arbitrary threshold that is at least in part guided by arbitrary criteria. Recent work revealed that neurons that fail the spatial modulation criteria also contribute to building representations of the physical environment (Liu et al., 2021; Sheintuch et al., 2020; Stefanini et al., 2018). Our finding of distance coding in non-spatially modulated neurons is coherent with these previous studies and with the view that non-spatially modulated neurons contribute to the representation of the spatial environment.

1. 9. Representations of space are differentially modulated by novelty in hippocampal subregions

My work also addresses whether the selectivity we observed for running direction is modulated by novelty. We used olfactory information as a form of contextual novelty and recorded neural activity in hippocampal regions while animals navigated in the linear track and were exposed to changing olfactory stimuli. In the familiar environment, selectivity for running direction was higher in the DG and CA3 than in CA1 (Fig 4.15), confirming our results showing that the dentate gyrus and CA3 are more selective for running direction (Fig 4.7). In the dentate gyrus, selectivity for running direction remains similarly high upon

exposure to the novel odor. Constant levels of selectivity in the dentate gyrus might be explained by sparse firing in the dentate gyrus, whereby the capacity of the circuit to disambiguate contextual information based on firing rates would remain stable regardless of contextual changes (Danielson et al., 2017; GoodSmith et al., 2019; Neunuebel and Knierim, 2012).

Our preliminary data also suggest that in CA3, selectivity for running direction drops upon exposure to novel contextual information, suggesting that CA3 is sensitive to contextual novelty. This is coherent with previous reports indicating that CA3 implements changes in firing rates immediately upon changes in sensory cues (Leutgeb et al., 2006). CA3 pyramidal neurons are thought to support the formation of neuronal ensembles that generate rapid and arbitrary combinations of inputs, for instance between landmarks and objects (Rebola et al., 2017; Rolls et al., 1998), which might lead to an initial and fast encoding of memories (Kesner and Rolls, 2015; Kornblith et al., 2013; Nasr et al., 2011; Piette et al., 2020). This fast encoding of novel contextual information would therefore be consistent with role of CA3 as an autoassociative network (Leutgeb et al., 2006).

Finally, consistently with our previous results, CA1 selectivity was lowest in the hippocampal subregions but seems to increase upon exposure to novel contextual information. This is consistent with previous reports of the modulation of CA1 activity by contextual information (Muller and Kubie, 1987) such as olfactory stimuli (Anderson and Jeffery, 2003). Olfaction is a powerful sensory modality for rodents and olfactory stimuli may signal environmental changes that impact the animal's behaviour. An increase in selectivity for running direction would be consistent with the idea that CA1 produces an abstract representation of the environment (Ito et al., 2015; Keinath et al., 2020) that is relevant to the behaviour of the animal (Allegra et al., 2020). It would also be coherent with recent work showing that repeated exposures to different contexts enhance generalization in CA1 neurons, possibly to enhance the predictability of new contexts (Liu et al., 2021).

Overall, our preliminary results suggest that contextual novelty differentially modulates representations of space in hippocampal regions, suggesting that the dentate gyrus, CA3 and CA1 might play specific functional roles during processing of contextual novelty. Larger sample numbers will be required to draw final, statistically robust conclusions.

1.10. Non-measured variables may impact neuronal firing

The present behavioural paradigm did not include any quantification of the amount or concentration of the odor inhaled by the animal, the animal's breathing rate or behavioural differences across olfactory environments, and therefore fails to take into account possible variability in the amount of olfactory information available to the animal. Similarly, variables that are not being measured might impact the neuronal activity recordings obtained in this study, such as attention of the animal, goal or thirst. Future work will require more precise experimental setups to assess the effect of these variables (Schmidt-Hieber, 2018).

1.11. Variability in neuronal responses

Throughout this study, differences may arise because of functional differences within regions, linked to structural differences that have not been characterized yet. The wide range of selectivity and spatial correlation values obtained within each hippocampal subregion might be caused by different factors. First, variability in the results obtained within hippocampal subregions might be caused by variability in the positioning of the GRIN lens in the neural tissue. The high spatial precision required by GRIN lens implants for microendoscope calcium imaging combined with morphological differences across animals and variability during the experimental procedure generates variability in the position of the GRIN lens in the neural tissue. A second explanation for the variability observed might be the naturally occuring structural and functional heterogeneity. Strong evidence of structure-function relationship in the hippocampus was provided by the characterisation of inhibitory interneuron circuits (Preston-Ferrer and Burgalossi, 2018) but while it is now possible to identify broad cell groups such as granule cells and mossy cells in the dentate gyrus, a more precise neuronal classification is needed. Identified neuronal populations are heterogeneous and can display different connectivity, genetics, morphologies, functional roles (Anderson and Jeffery, 2003; Deshmukh, 2020; Erwin et al., 2020; Henriksen et al., 2010; Hunt et al., 2018; Lee et al., 2015; Li et al., 2017; Schoenfeld et al., 2021; Vandael et al., 2020), as well as differential theta modulation and innervation patterns by the entorhinal cortex (Oliva et al., 2016). Neuronal classification must therefore be refined in order to resolve structure-function relationships and reveal cellular mechanisms underlying hippocampal circuit computations. A third explanation for the variability observed is that neurons within a population may be tuned to different variables and some may respond more strongly to the variables measured by the experimenter than others (Preston-Ferrer and Burgalossi, 2018).

2. Strength and limitations of the study

2.1 Strengths of the study

Single-photon microendoscope calcium imaging allows the recording of neural activity from identified neuronal populations in freely-moving animals. Here, we recorded the activity from identified dentate gyrus granule cells, and pyramidal neurons in CA3 and CA1 while animals navigated freely in a linear track. Compared to many modern techniques where animals are head-fixed or navigating in virtual reality, microendoscope single photon imaging allows the investigation of neuronal processes associated with a wide-range of naturalistic animal behaviour (Jennings et al., 2015; Resendez and Stuber, 2015). Specifically, microendoscopes allow unrestrained navigation of the animals, which is more ethologically sound for rodents that evolved to navigate in the wild (Ghosh et al., 2011; Resendez and Stuber, 2015). Here, we investigated spatial representations in hippocampal neurons in mice that navigated spontaneously back and forth along a linear track. The mice were quick to habituate to the weight of the microscope and already showed good mobility during their first exposure to the linear track. By performing single-photon calcium imaging from the dentate gyrus, CA3, and CA1, we provide one of the first descriptions of representations of spatial position, running direction, and distance in all major hippocampal subregions under the same task conditions in freely moving animals.

2.2. Limitations of the study

Calcium imaging lacks sufficient temporal resolution to distinguish bursts from single spikes under typical *in vivo* recording conditions (Danielson et al., 2016b; GoodSmith, 2017; Hainmueller and Bartos, 2018). Furthermore, because of scattering of light by brain tissue, signal-to-noise ratio of single-photon imaging is relatively low, and it is therefore under most conditions, including ours, not possible to identify silent cells as their baseline fluorescence emission is too low. In addition, while microendoscopes allow unrestrained navigation of the animals, which is more ethologically sound for rodents that evolved to navigate in the wild, microendoscope single photon imaging does not allow precise control of the many stimuli that might modulate neural activity.

Single-photon microendoscope calcium imaging requires the implant of a GRIN lens (500 um diameter in this study). The implant of a 500um GRIN lens causes undeniable tissue damage

and might impact neuronal activity observed when a subregion is lesioned (for example a lesion of the CA1 hippocampal subregion during recordings of the dentate gyrus). It is important to note however that the tissue damage resulting from an implant is smaller compared to other types of implants such as imaging cannulas for 2-photon imaging, whose diameter is larger.

We did not investigate the long-term dynamics in the same populations of identified hippocampal neurons. Previous work has revealed that spatial representations are dynamic and that a stable representation of the environment is maintained despite a substantial turnover in spatially modulated neurons (Ziv et al., 2013). Future experiments should explore long-term stability of representations of spatial position, running direction and distance in hippocampal subregions and investigate whether processing of distinct spatial variables evolves over time.

Lastly, we did not identify the elements of the hippocampal circuits that support processing of spatial position, running direction and distance and their transformation along the hippocampal axis. Future work should manipulate the activity of different elements to disentangle the circuit mechanisms at play. For instance, blockade of MEC neurons located at different depths would enable the identification of the input source giving rise to the selectivity for direction that we observe in the dentate gyrus and CA3 and the directionally selective spatial representations observed in all regions. Similarly, blockade of MEC neurons would indicate whether they are the source of the distance coding that we observed in the dentate gyrus. Furthermore, sequential inactivation of principal cell populations in the hippocampal regions would also provide a valuable insight into the transformations of spatial representations along the hippocampal circuit, and whether they arise as a result of hierarchical processing or rather, by direct inputs from extra-hippocampal regions.

3. Concluding remarks

In this study, we explore how representations of spatial position, running direction, and distance evolve along the hippocampal circuit. By performing single-photon calcium imaging from the dentate gyrus, CA3, and CA1, we find that in mice spontaneously running back and forth along a linear track, all regions display directionality in their spatial firing patterns, neuronal activity in the dentate gyrus and in CA3 is more selective for the direction of running than activity in CA1 and activity in the dentate gyrus encodes covered distance in egocentric coordinates. We also find that selectivity for running direction in the dentate gyrus,

CA3 and CA1 is differentially modulated by novelty. Overall, we provide one of the first descriptions of these representations in all major hippocampal subregions under the same task conditions in freely moving animals. Future work should involve chronic recordings of the same neuronal populations to assess the stability of neuronal representations over time, as well as manipulation of neuronal activity to identify the sources of positional, directional and distance-tuned inputs to the hippocampus and confirm hierarchical processing along the hippocampal circuit.

VI. References

Acharya, L., Aghajan, Z.M., Vuong, C., Moore, J.J., and Mehta, M.R. (2016). Causal Influence of Visual Cues on Hippocampal Directional Selectivity. Cell *164*, 197–207.

Ahmed, O.J., and Mehta, M.R. (2009). The hippocampal rate code: anatomy, physiology and theory. Trends Neurosci. *32*, 329–338.

Ahmed, M.S., Priestley, J.B., Castro, A., Stefanini, F., Balough, E.M., Lavoie, E., Mazzucato, L., Fusi, S., and Losonczy, A. (2019). Hippocampal network reorganization underlies the formation of a temporal association memory (Neuroscience).

Akerboom, J., Chen, T.-W., Wardill, T.J., Tian, L., Marvin, J.S., Mutlu, S., Calderón, N.C., Esposti, F., Borghuis, B.G., Sun, X.R., et al. (2012). Optimization of a GCaMP calcium indicator for neural activity imaging. J. Neurosci. Off. J. Soc. Neurosci. *32*, 13819–13840.

Alexander, A.S., Carstensen, L.C., Hinman, J.R., Raudies, F., Chapman, G.W., and Hasselmo, M.E. (2020). Egocentric boundary vector tuning of the retrosplenial cortex. Sci. Adv. *6*, eaaz2322.

Allegra, M., Posani, L., Gómez-Ocádiz, R., and Schmidt-Hieber, C. (2020). Differential Relation between Neuronal and Behavioral Discrimination during Hippocampal Memory Encoding. Neuron *108*, 1103-1112.e6.

Allen, T.A., and Fortin, N.J. (2013). The evolution of episodic memory. Proc. Natl. Acad. Sci. *110*, 10379–10386.

Alme, C.B., Buzzetti, R.A., Marrone, D.F., Leutgeb, J.K., Chawla, M.K., Schaner, M.J., Bohanick, J.D., Khoboko, T., Leutgeb, S., Moser, E.I., et al. (2010). Hippocampal granule cells opt for early retirement. Hippocampus *20*, 1109–1123.

de Almeida, L., Idiart, M., and Lisman, J.E. (2009). The Input-Output Transformation of the Hippocampal Granule Cells: From Grid Cells to Place Fields. J. Neurosci. *29*, 7504–7512.

Amaral, D.G., and Witter, M.P. (1989). The three-dimensional organization of the hippocampal formation: a review of anatomical data. Neuroscience *31*, 571–591.

Amaral, D.G., Ishizuka, N., and Claiborne, B. (1990). Neurons, numbers and the hippocampal network. Prog. Brain Res. *83*, 1–11.

Amaral, D.G., Dolorfo, C., and Alvarez-Royo, P. (1991). Organization of CA1 projections to the subiculum: A PHA-L analysis in the rat. Hippocampus *1*, 415–435.

Amaral, D.G., Scharfman, H.E., and Lavenex, P. (2007). The dentate gyrus: fundamental neuroanatomical organization (dentate gyrus for dummies). In Progress in Brain Research, (Elsevier), pp. 3–790.

Anderson, M.I., and Jeffery, K.J. (2003). Heterogeneous Modulation of Place Cell Firing by Changes in Context. J. Neurosci. *23*, 8827–8835.

Aronov, D., Nevers, R., and Tank, D.W. (2017). Mapping of a non-spatial dimension by the hippocampal–entorhinal circuit. Nature *543*, 719–722.

Bakker, A., Kirwan, C.B., Miller, M., and Stark, C.E.L. (2008). Pattern Separation in the Human Hippocampal CA3 and Dentate Gyrus. Science *319*, 1640–1642.

Bartesaghi, R., and Gessi, T. (2004). Parallel activation of field CA2 and dentate gyrus by synaptically elicited perforant path volleys. Hippocampus *14*, 948–963.

Basu, J., and Siegelbaum, S.A. (2015). The Corticohippocampal Circuit, Synaptic Plasticity, and Memory. Cold Spring Harb. Perspect. Biol. *7*, a021733.

Battaglia, F.P. (2004). Local Sensory Cues and Place Cell Directionality: Additional Evidence of Prospective Coding in the Hippocampus. J. Neurosci. *24*, 4541–4550.

Benes, F.M., Kwok, E.W., Vincent, S.L., and Todtenkopf, M.S. (1998). A reduction of nonpyramidal cells in sector CA2 of schizophrenics and manic depressives. Biol. Psychiatry *44*, 88–97.

Benes, F.M., Lim, B., Matzilevich, D., Walsh, J.P., Subburaju, S., and Minns, M. (2007). Regulation of the GABA cell phenotype in hippocampus of schizophrenics and bipolars. Proc. Natl. Acad. Sci. *104*, 10164–10169.

Benna, M.K., and Fusi, S. (2019). Are place cells just memory cells? Memory compression leads to spatial tuning and history dependence (Neuroscience).

Bernstein, H.L., Lu, Y.-L., Botterill, J.J., Duffy, Á.M., LaFrancois, J.J., and Scharfman, H.E. (2020). Excitatory effects of dentate gyrus mossy cells and their ability to influence granule cell firing: an optogenetic study in adult mouse hippocampal slices (Neuroscience).

Bicanski, A., and Burgess, N. (2018). A neural-level model of spatial memory and imagery. ELife *7*, e33752.

Bittner, K.C., Grienberger, C., Vaidya, S.P., Milstein, A.D., Macklin, J.J., Suh, J., Tonegawa, S., and Magee, J.C. (2015). Conjunctive input processing drives feature selectivity in hippocampal CA1 neurons. Nat. Neurosci. *18*, 1133–1142.

Bliss, T.V., and Lomo, T. (1973). Long-lasting potentiation of synaptic transmission in the dentate area of the anaesthetized rabbit following stimulation of the perforant path. J. Physiol. *232*, 331–356.

Born, G., Breuer, D., Wang, S., Rohlmann, A., Coulon, P., Vakili, P., Reissner, C., Kiefer, F., Heine, M., Pape, H.-C., et al. (2014). Modulation of synaptic function through the α-neurexin-specific ligand neurexophilin-1. Proc. Natl. Acad. Sci. U. S. A. *111*, E1274-1283.

Bostock, E., Muller, R.U., and Kubie, J.L. (1991). Experience-dependent modifications of hippocampal place cell firing. Hippocampus *1*, 193–205.

Brandon, M.P., Koenig, J., Leutgeb, J.K., and Leutgeb, S. (2014). New and Distinct Hippocampal Place Codes Are Generated in a New Environment during Septal Inactivation. Neuron *82*, 789–796.

Bright, I.M., Meister, M.L.R., Cruzado, N.A., Tiganj, Z., Buffalo, E.A., and Howard, M.W. (2020). A temporal record of the past with a spectrum of time constants in the monkey entorhinal cortex. Proc. Natl. Acad. Sci. *117*, 20274–20283.

Brun, V.H. (2002). Place Cells and Place Recognition Maintained by Direct Entorhinal-Hippocampal Circuitry. Science *296*, 2243–2246.

Brun, V.H., Solstad, T., Kjelstrup, K.B., Fyhn, M., Witter, M.P., Moser, E.I., and Moser, M.-B. (2008). Progressive increase in grid scale from dorsal to ventral medial entorhinal cortex. Hippocampus *18*, 1200–1212.

Brunel, N., and Trullier, O. (1998). Plasticity of Directional Place Fields in a Model of Rodent CA3. 15.

Buckmaster, P.S. (2012). Mossy cell dendritic structure quantified and compared with other hippocampal neurons labeled in rats in vivo: Mossy Cell Dendritic Structure. Epilepsia *53*, 9–17.

Burgess, N., Maguire, E.A., Spiers, H.J., and O'Keefe, J. (2001). A Temporoparietal and Prefrontal Network for Retrieving the Spatial Context of Lifelike Events. NeuroImage *14*, 439–453.

Burke, M.R., and Barnes, G.R. (2011). The neural correlates of inhibiting pursuit to smoothly moving targets. J. Cogn. Neurosci. *23*, 3294–3303.

Buzsáki, G. (1986). Hippocampal sharp waves: their origin and significance. Brain Res. *398*, 242–252.

Buzsáki, G., and Moser, E.I. (2013). Memory, navigation and theta rhythm in the hippocampal-entorhinal system. Nat. Neurosci. *16*, 130–138.

Byrne, P., Becker, S., and Burgess, N. (2007). Remembering the past and imagining the future: A neural model of spatial memory and imagery. Psychol. Rev. *114*, 340–375.

Campbell, M.G., Ocko, S.A., Mallory, C.S., Low, I.I.C., Ganguli, S., and Giocomo, L.M. (2018). Principles governing the integration of landmark and self-motion cues in entorhinal cortical codes for navigation. Nat. Neurosci. *21*, 1096–1106.

Catterall, W.A., Leal, K., and Nanou, E. (2013). Calcium Channels and Short-term Synaptic Plasticity. J. Biol. Chem. *288*, 10742–10749.

Cayco-Gajic, N.A., and Silver, R.A. (2019). Re-evaluating Circuit Mechanisms Underlying Pattern Separation. Neuron *101*, 584–602.

Cenquizca, L.A., and Swanson, L.W. (2007). Spatial organization of direct hippocampal field CA1 axonal projections to the rest of the cerebral cortex. Brain Res. Rev. *56*, 1–26.

Cerasti, E., and Treves, A. (2010). How informative are spatial CA3 representations established by the dentate gyrus? PLoS Comput. Biol. *6*, e1000759.

Chawla, M.K., Guzowski, J.F., Ramirez-Amaya, V., Lipa, P., Hoffman, K.L., Marriott, L.K., Worley, P.F., McNaughton, B.L., and Barnes, C.A. (2005). Sparse, environmentally selective expression ofArc RNA in the upper blade of the rodent fascia dentata by brief spatial experience. Hippocampus *15*, 579–586.

Chen, X., and Knierim, J.J. (2018). It's About Time: Temporal Dynamics of Dentate Gyrus Pattern Separation. Neuron *98*, 681–683.

Chen, J.L., Andermann, M.L., Keck, T., Xu, N.-L., and Ziv, Y. (2013). Imaging neuronal populations in behaving rodents: paradigms for studying neural circuits underlying behavior in the mammalian cortex. J. Neurosci. Off. J. Soc. Neurosci. *33*, 17631–17640.

Chen, L.L., Lin, L.H., Green, E.J., Barnes, C.A., and McNaughton, B.L. (1994). Head-direction cells in the rat posterior cortex. I. Anatomical distribution and behavioral modulation. Exp. Brain Res. *101*, 8–23.

Cheng, S., and Frank, L.M. (2011). The structure of networks that produce the transformation from grid cells to place cells. Neuroscience *197*, 293–306.

Chevaleyre, V., and Siegelbaum, S.A. (2010). Strong CA2 Pyramidal Neuron Synapses Define a Powerful Disynaptic Cortico-Hippocampal Loop. Neuron *66*, 560–572.

Cholvin, T., Hainmueller, T., and Bartos, M. (2021). The Hippocampus Converts Volatile Entorhinal Inputs into Stable Spatial Maps. SSRN Electron. J.

Chrastil, E.R. (2013). Neural evidence supports a novel framework for spatial navigation. Psychon. Bull. Rev. *20*, 208–227.

Cichon, J., and Gan, W.-B. (2015). Branch-specific dendritic Ca(2+) spikes cause persistent synaptic plasticity. Nature *520*, 180–185.

Clark, J.J., Sandberg, S.G., Wanat, M.J., Gan, J.O., Horne, E.A., Hart, A.S., Akers, C.A., Parker, J.G., Willuhn, I., Martinez, V., et al. (2010). Chronic microsensors for longitudinal, subsecond dopamine detection in behaving animals. Nat. Methods *7*, 126–129.

Clelland, C.D., Choi, M., Romberg, C., Clemenson, G.D., Fragniere, A., Tyers, P., Jessberger, S., Saksida, L.M., Barker, R.A., Gage, F.H., et al. (2009). A Functional Role for Adult Hippocampal Neurogenesis in Spatial Pattern Separation. Science *325*, 210–213.

Colgin, L.L., Moser, E.I., and Moser, M.-B. (2008). Understanding memory through hippocampal remapping. Trends Neurosci. *31*, 469–477.

Collingridge, G.L., Isaac, J.T.R., and Wang, Y.T. (2004). Receptor trafficking and synaptic plasticity. Nat. Rev. Neurosci. *5*, 952–962.

Cressant, A., Muller, R.U., and Poucet, B. (2002). Remapping of place cell firing patterns after maze rotations. Exp. Brain Res. *143*, 470–479.

Csicsvari, J., Hirase, H., Mamiya, A., and Buzsáki, G. (2000). Ensemble Patterns of Hippocampal CA3-CA1 Neurons during Sharp Wave–Associated Population Events. Neuron *28*, 585–594.

Cui, G., Jun, S.B., Jin, X., Luo, G., Pham, M.D., Lovinger, D.M., Vogel, S.S., and Costa, R.M. (2014). Deep brain optical measurements of cell type-specific neural activity in behaving mice. Nat. Protoc. *9*, 1213–1228.

Cui, Z., Gerfen, C.R., and Young, W.S. (2013). Hypothalamic and other connections with dorsal CA2 area of the mouse hippocampus: CA2 Connections in Mouse. J. Comp. Neurol. *521*, 1844–1866.

Cunningham, J.P. (2014). Analyzing neural data at huge scale. Nat. Methods *11*, 911–912.

Danielson, N.B., Zaremba, J.D., Kaifosh, P., Bowler, J., Ladow, M., and Losonczy, A. (2016a). Sublayer-Specific Coding Dynamics during Spatial Navigation and Learning in Hippocampal Area CA1. Neuron *91*, 652–665.

Danielson, N.B., Kaifosh, P., Zaremba, J.D., Lovett-Barron, M., Tsai, J., Denny, C.A., Balough, E.M., Goldberg, A.R., Drew, L.J., Hen, R., et al. (2016b). Distinct Contribution of Adult-Born Hippocampal Granule Cells to Context Encoding. Neuron *90*, 101–112.

Danielson, N.B., Turi, G.F., Ladow, M., Chavlis, S., Petrantonakis, P.C., Poirazi, P., and Losonczy, A. (2017). In Vivo Imaging of Dentate Gyrus Mossy Cells in Behaving Mice. Neuron *93*, 552-559.e4.

Daumas, S., Ceccom, J., Halley, H., Frances, B., and Lassalle, J.-M. (2009). Activation of metabotropic glutamate receptor type 2/3 supports the involvement of the hippocampal mossy fiber pathway on contextual fear memory consolidation. Learn. Mem. *16*, 504–507.

De Nó, L. (1934). Studies on the structure of the cerebral cortex. II. Continuation of the study of the ammonic system. Journal für Psychologie und Neurologie *46*, 113-177.

Deller, T., Martinez, A., Nitsch, R., and Frotscher, M. (1996). A Novel Entorhinal Projection to the Rat Dentate Gyrus: Direct Innervation of Proximal Dendrites and Cell Bodies of Granule Cells and GABAergic Neurons. J. Neurosci. *16*, 3322–3333.

Dere, E., Huston, J.P., and De Souza Silva, M.A. (2005). Integrated memory for objects, places, and temporal order: Evidence for episodic-like memory in mice. Neurobiol. Learn. Mem. *84*, 214–221.

Deshmukh, S.S. (2020). Distal CA1 maintains a more coherent spatial representation than proximal CA1 when local and global cues conflict (Neuroscience).

Deshmukh, S.S., and Knierim, J.J. (2011). Representation of Non-Spatial and Spatial Information in the Lateral Entorhinal Cortex. Front. Behav. Neurosci. *5*.

Diamantaki, M., Frey, M., Berens, P., Preston-Ferrer, P., and Burgalossi, A. (2016). Sparse activity of identified dentate granule cells during spatial exploration. ELife *5*, e20252.

Diamantaki, M., Coletta, S., Nasr, K., Zeraati, R., Laturnus, S., Berens, P., Preston-Ferrer, P., and Burgalossi, A. (2018). Manipulating Hippocampal Place Cell Activity by Single-Cell Stimulation in Freely Moving Mice. Cell Rep. *23*, 32–38.

Dickson, D.W., Ruan, D., Crystal, H., Mark, M.H., Davies, P., Kress, Y., and Yen, S.H. (1991). Hippocampal degeneration differentiates diffuse Lewy body disease (DLBD) from Alzheimer's disease: light and electron microscopic immunocytochemistry of CA2-3 neurites specific to DLBD. Neurology *41*, 1402–1409.

Diehl, G.W., Hon, O.J., Leutgeb, S., and Leutgeb, J.K. (2017). Grid and Nongrid Cells in Medial Entorhinal Cortex Represent Spatial Location and Environmental Features with Complementary Coding Schemes. Neuron *94*, 83-92.e6.

van Dijk, M.T., and Fenton, A.A. (2018). On How the Dentate Gyrus Contributes to Memory Discrimination. Neuron *98*, 832-845.e5.

Dingledine, R., Borges, K., Bowie, D., and Traynelis, S.F. (1999). The glutamate receptor ion channels. Pharmacol. Rev. *51*, 7–61.

Dolorfo, C.L., and Amaral, D.G. (1998). Entorhinal cortex of the rat: Topographic organization of the cells of origin of the perforant path projection to the dentate gyrus. 24.

Dong, C., Madar, A.D., and Sheffield, M.E.J. (2021). Distinct place cell dynamics in CA1 and CA3 encode experience in new environments. Nat. Commun. *12*, 2977.

Dupret, D., O'Neill, J., and Csicsvari, J. (2013). Dynamic Reconfiguration of Hippocampal Interneuron Circuits during Spatial Learning. Neuron *78*, 166–180.

Eichenbaum, H. (2004). Hippocampus: cognitive processes and neural representations that underlie declarative memory. Neuron *44*, 109–120.

Eichenbaum, H. (2017). The role of the hippocampus in navigation is memory. J. Neurophysiol. *117*, 1785–1796.

Eichenbaum, H., and Cohen, N.J. (2004). From Conditioning to Conscious Recollection (Oxford University Press).

Eichenbaum, H., Dudchenko, P., Wood, E., Shapiro, M., and Tanila, H. (1999). The hippocampus, memory, and place cells: is it spatial memory or a memory space? Neuron *23*, 209–226.

Ekstrom, A.D., Kahana, M.J., Caplan, J.B., Fields, T.A., Isham, E.A., Newman, E.L., and Fried, I. (2003). Cellular networks underlying human spatial navigation. Nature *425*, 184–188.

El-Gaby, M., Reeve, H.M., Lopes-dos-Santos, V., Campo-Urriza, N., Perestenko, P.V., Morley, A., Strickland, L.A.M., Lukács, I.P., Paulsen, O., and Dupret, D. (2021). An emergent neural coactivity code for dynamic memory. Nat. Neurosci. *24*, 694–704.

Epsztein, J., Brecht, M., and Lee, A.K. (2011). Intracellular determinants of hippocampal CA1 place and silent cell activity in a novel environment. Neuron *70*, 109–120.

Erwin, S.R., Sun, W., Copeland, M., Lindo, S., Spruston, N., and Cembrowski, M.S. (2020). A Sparse, Spatially Biased Subtype of Mature Granule Cell Dominates Recruitment in Hippocampal-Associated Behaviors. Cell Rep. *31*, 107551.

Espinoza, C., Guzman, S.J., Zhang, X., and Jonas, P. (2018). Parvalbumin+ interneurons obey unique connectivity rules and establish a powerful lateral-inhibition microcircuit in dentate gyrus. Nat. Commun. *9*, 4605.

Esteves, I.M., Chang, H., Neumann, A.R., Sun, J., Mohajerani, M.H., and McNaughton, B.L. (2021). Spatial Information Encoding across Multiple Neocortical Regions Depends on an Intact Hippocampus. J. Neurosci. *41*, 307–319.

Etienne, A.S., and Jeffery, K.J. (2004). Path integration in mammals. Hippocampus *14*, 180–192.

Felleman, D.J., and Van Essen, D.C. (1991). Distributed hierarchical processing in the primate cerebral cortex. Cereb. Cortex N. Y. N 1991 *1*, 1–47.

Fenton, A.A., and Muller, R.U. (1998). Place cell discharge is extremely variable during individual passes of the rat through the firing field. Proc. Natl. Acad. Sci. *95*, 3182–3187.

Fiser, A., Mahringer, D., Oyibo, H.K., Petersen, A.V., Leinweber, M., and Keller, G.B. (2016). Experience-dependent spatial expectations in mouse visual cortex. Nat. Neurosci. *19*, 1658–1664.

Fox, S.E., and Ranck, J.B. (1975). Localization and anatomical identification of theta and complex spike cells in dorsal hippocampal formation of rats. Exp. Neurol. *49*, 299–313.

França, T.F.A., and Monserrat, J.M. (2018). How the Hippocampus Represents Memories: Making Sense of Memory Allocation Studies. BioEssays *40*, 800068.

Frankland, P.W., and Bontempi, B. (2005). The organization of recent and remote memories. Nat. Rev. Neurosci. *6*, 119–130.

Fredes, F., Silva, M.A., Koppensteiner, P., Kobayashi, K., Joesch, M., and Shigemoto, R. (2021). Ventro-dorsal Hippocampal Pathway Gates Novelty-Induced Contextual Memory Formation. Curr. Biol. *31*, 25-38.e5.

Freeman, J., Vladimirov, N., Kawashima, T., Mu, Y., Sofroniew, N.J., Bennett, D.V., Rosen, J., Yang, C.-T., Looger, L.L., and Ahrens, M.B. (2014). Mapping brain activity at scale with cluster computing. Nat. Methods *11*, 941–950.

Frerking, M., Schulte, J., Wiebe, S.P., and Stäubli, U. (2005). Spike Timing in CA3 Pyramidal Cells During Behavior: Implications for Synaptic Transmission. J. Neurophysiol. *94*, 1528–1540.

Fuhs, M.C. (2006). A Spin Glass Model of Path Integration in Rat Medial Entorhinal Cortex. J. Neurosci. *26*, 4266–4276.

Fyhn, M. (2004). Spatial Representation in the Entorhinal Cortex. Science *305*, 1258–1264.

Fyhn, M., Molden, S., Hollup, S., Moser, M.-B., and Moser, E.I. (2002). Hippocampal Neurons Responding to First-Time Dislocation of a Target Object. Neuron *35*, 555–566.

Fyhn, M., Hafting, T., Treves, A., Moser, M.-B., and Moser, E.I. (2007). Hippocampal remapping and grid realignment in entorhinal cortex. Nature *446*, 190–194.

Galati, G., Pelle, G., Berthoz, A., and Committeri, G. (2010). Multiple reference frames used by the human brain for spatial perception and memory. Exp. Brain Res. *206*, 109–120.

Gauthier, J.L., and Tank, D.W. (2018). A Dedicated Population for Reward Coding in the Hippocampus. Neuron *99*, 179-193.e7.

Gava, G.P., McHugh, S.B., Lefèvre, L., Lopes-dos-Santos, V., Trouche, S., El-Gaby, M., Schultz, S.R., and Dupret, D. (2021). Integrating new memories into the hippocampal network activity space. Nat. Neurosci. *24*, 326–330.

Gerlei, K., Passlack, J., Hawes, I., Vandrey, B., Stevens, H., Papastathopoulos, I., and Nolan, M.F. (2019). Grid cells encode local head direction (Neuroscience).

Ghosh, K.K., Burns, L.D., Cocker, E.D., Nimmerjahn, A., Ziv, Y., Gamal, A.E., and Schnitzer, M.J. (2011). Miniaturized integration of a fluorescence microscope. Nat. Methods *8*, 871–878.

Gilbert, P.E., and Kesner, R.P. (2003). Localization of Function Within the Dorsal Hippocampus: The Role of the CA3 Subregion in Paired-Associate Learning. Behav. Neurosci. *117*, 1385–1394.

Gilbert, P.E., Kesner, R.P., and DeCoteau, W.E. (1998). Memory for Spatial Location: Role of the Hippocampus in Mediating Spatial Pattern Separation. J. Neurosci. *18*, 804–810.

Gilbert, P.E., Kesner, R.P., and Lee, I. (2001). Dissociating hippocampal subregions: A double dissociation between dentate gyrus and CA1. Hippocampus *11*, 626–636.

Gofman, X., Tocker, G., Weiss, S., Boccara, C.N., Lu, L., Moser, M.-B., Moser, E.I., Morris, G., and Derdikman, D. (2019). Dissociation between Postrhinal Cortex and Downstream Parahippocampal Regions in the Representation of Egocentric Boundaries. Curr. Biol. CB *29*, 2751-2757.e4.

Gonzalez, W.G., Zhang, H., Harutyunyan, A., and Lois, C. (2019). Persistence of neuronal representations through time and damage in the hippocampus. 6.

GoodSmith, D. (2017). Spatial Representations of Granule Cells and Mossy Cells of the Dentate Gyrus. 20.

GoodSmith, D., Chen, X., Wang, C., Kim, S.H., Song, H., Burgalossi, A., Christian, K.M., and Knierim, J.J. (2017). Spatial Representations of Granule Cells and Mossy Cells of the Dentate Gyrus. Neuron *93*, 677-690.e5.

GoodSmith, D., Lee, H., Neunuebel, J.P., Song, H., and Knierim, J.J. (2019). Dentate Gyrus Mossy Cells Share a Role in Pattern Separation with Dentate Granule Cells and Proximal CA3 Pyramidal Cells. J. Neurosci. *39*, 9570–9584.

GoodSmith, D., Kim, S.H., Puliyadi, V., Ming, G., Song, H., Knierim, J.J., and Christian, K.M. (2021). Flexible encoding of objects and space in single cells of the dentate gyrus (Neuroscience).

Gothard, K.M., Skaggs, W.E., and McNaughton, B.L. (1996). Dynamics of Mismatch Correction in the Hippocampal Ensemble Code for Space: Interaction between Path Integration and Environmental Cues. J. Neurosci. *16*, 8027–8040.

Govindarajan, A., Kelleher, R.J., and Tonegawa, S. (2006). A clustered plasticity model of long-term memory engrams. Nat. Rev. Neurosci. *7*, 575–583.

Grande, X., Berron, D., Horner, A.J., Bisby, J.A., Düzel, E., and Burgess, N. (2019). Holistic Recollection via Pattern Completion Involves Hippocampal Subfield CA3. J. Neurosci. *39*, 8100–8111.

Grewe, B.F., Gründemann, J., Kitch, L.J., Lecoq, J.A., Parker, J.G., Marshall, J.D., Larkin, M.C., Jercog, P.E., Grenier, F., Li, J.Z., et al. (2017). Neural ensemble dynamics underlying a long-term associative memory. Nature *543*, 670–675.

Grienberger, C., and Konnerth, A. (2012). Imaging calcium in neurons. Neuron *73*, 862–885.

Grienberger, C., Chen, X., and Konnerth, A. (2014). NMDA Receptor-Dependent Multidendrite Ca 2+ Spikes Required for Hippocampal Burst Firing In Vivo. Neuron *81*, 1274–1281.

van Groen, T., Miettinen, P., and Kadish, I. (2003). The entorhinal cortex of the mouse: Organization of the projection to the hippocampal formation. Hippocampus *13*, 133–149.

Guo, W., Favila, S.E., Kim, G., Molitor, R.J., and Kuhl, B.A. (2021). Abrupt remapping in human CA3/dentate gyrus signals resolution of memory interference. 25.

Guzman, S.J., Schlogl, A., Frotscher, M., and Jonas, P. (2016). Synaptic mechanisms of pattern completion in the hippocampal CA3 network. Science *353*, 1117–1123.

Guzman, S.J., Schlögl, A., Espinoza, C., Zhang, X., Suter, B., and Jonas, P. Fast signaling and focal connectivity of PV+ interneurons ensure efficient pattern separation by lateral inhibition in a full-scale dentate gyrus network model. 55.

Hafting, T., Fyhn, M., Molden, S., Moser, M.-B., and Moser, E.I. (2005). Microstructure of a spatial map in the entorhinal cortex. Nature *436*, 801–806.

Hainmueller, T., and Bartos, M. (2018). Parallel emergence of stable and dynamic memory engrams in the hippocampus. Nature *558*, 292–296.

Hainmueller, T., and Bartos, M. (2020). Dentate gyrus circuits for encoding, retrieval and discrimination of episodic memories. Nat. Rev. Neurosci. *21*, 153–168.

Hamel, E.J.O., Grewe, B.F., Parker, J.G., and Schnitzer, M.J. (2015). Cellular level brain imaging in behaving mammals: an engineering approach. Neuron *86*, 140–159.

Hampson, R.E., Heyser, C.J., and Deadwyler, S.A. (1993). Hippocampal cell firing correlates of delayed-match-to-sample performance in the rat. Behav. Neurosci. *107*, 715–739.

Hardcastle, K., Maheswaranathan, N., Ganguli, S., and Giocomo, L.M. (2017). A Multiplexed, Heterogeneous, and Adaptive Code for Navigation in Medial Entorhinal Cortex. Neuron *94*, 375-387.e7.

Hargreaves, E.L., Rao, G., Lee, I., and Knierim, J.J. (2005). Major dissociation between medial and lateral entorhinal input to dorsal hippocampus. Science *308*, 1792–1794.

Hebb, D.O. (1949). The Organization of Behavior: A Neuropsychological Theory. p.

Henriksen, E.J., Colgin, L.L., Barnes, C.A., Witter, M.P., Moser, M.-B., and Moser, E.I. (2010). Spatial Representation along the Proximodistal Axis of CA1. Neuron *68*, 127–137.

Henze, D.A., Wittner, L., and Buzsáki, G. (2002). Single granule cells reliably discharge targets in the hippocampal CA3 network in vivo. Nat. Neurosci. *5*, 6.

Herzog, L.E., Pascual, L.M., Scott, S.J., Mathieson, E.R., Katz, D.B., and Jadhav, S.P. (2019). Interaction of Taste and Place Coding in the Hippocampus. J. Neurosci. *39*, 3057–3069.

Heys, J.G., and Dombeck, D.A. (2018). Evidence for a subcircuit in medial entorhinal cortex representing elapsed time during immobility. Nat. Neurosci. *21*, 1574–1582.

Hjorth-Simonsen, A. (1973). Some intrinsic connections of the hippocampus in the rat: An experimental analysis. J. Comp. Neurol. *147*, 145–161.

Hoang, T.-H., Aliane, V., and Manahan-Vaughan, D. (2018). Novel encoding and updating of positional, or directional, spatial cues are processed by distinct hippocampal subfields: Evidence for parallel information processing and the "what" stream. Hippocampus *28*, 315–326.

Howard, M.W., and Eichenbaum, H. (2015). Time and space in the hippocampus. Brain Res. *1621*, 345–354.

Høydal, Ø.A., Skytøen, E.R., Andersson, S.O., Moser, M.-B., and Moser, E.I. (2019). Object-vector coding in the medial entorhinal cortex. Nature *568*, 400–404.

Hubel, D.H. (1960). Single unit activity in lateral geniculate body and optic tract of unrestrained cats. J. Physiol. *150*, 91–104.

Hubel, D.H., and Wiesel, T.N. (1962). Receptive fields, binocular interaction and functional architecture in the cat's visual cortex. J. Physiol. *160*, 106–154.

Hunt, D.L., Linaro, D., Si, B., Romani, S., and Spruston, N. (2018). A novel pyramidal cell type promotes sharp-wave synchronization in the hippocampus. Nat. Neurosci. *21*, 985–995.

Ishizuka, N., Weber, J., and Amaral, D.G. (1990). Organization of intrahippocampal projections originating from CA3 pyramidal cells in the rat. J. Comp. Neurol. *295*, 580–623.

Ito, H.T., Zhang, S.-J., Witter, M.P., Moser, E.I., and Moser, M.-B. (2015). A prefrontal–thalamo–hippocampal circuit for goal-directed spatial navigation. Nature *522*, 50–55.

Jacob, P.-Y., Capitano, F., Poucet, B., Save, E., and Sargolini, F. (2019). Path integration maintains spatial periodicity of grid cell firing in a 1D circular track. Nat. Commun. *10*, 840.

Jacobs, L.F., and Schenk, F. (2003). Unpacking the cognitive map: The parallel map theory of hippocampal function. Psychol. Rev. *110*, 285–315.

Jennings, J.H., Ung, R.L., Resendez, S.L., Stamatakis, A.M., Taylor, J.G., Huang, J., Veleta, K., Kantak, P.A., Aita, M., Shilling-Scrivo, K., et al. (2015). Visualizing hypothalamic network dynamics for appetitive and consummatory behaviors. Cell *160*, 516–527.

Jercog, P.E., Ahmadian, Y., Woodruff, C., Deb-Sen, R., Abbott, L.F., and Kandel, E.R. (2019). Heading direction with respect to a reference point modulates place-cell activity. Nat. Commun. *10*, 2333.

Josselyn, S.A., Köhler, S., and Frankland, P.W. (2015). Finding the engram. Nat. Rev. Neurosci. *16*, 521–534.

Julian, J.B., and Doeller, C.F. (2021). Remapping and realignment in the human hippocampal formation predict context-dependent spatial behavior. Nat. Neurosci. *24*, 863–872.

Jung, M.W., and McNaughton, B.L. (1993). Spatial selectivity of unit activity in the hippocampal granular layer. Hippocampus *3*, 165–182.

Jung, H.-Y., Mickus, T., and Spruston, N. (1997). Prolonged Sodium Channel Inactivation Contributes to Dendritic Action Potential Attenuation in Hippocampal Pyramidal Neurons. J. Neurosci. *17*, 6639–6646.

Jung, J.C., Mehta, A.D., Aksay, E., Stepnoski, R., and Schnitzer, M.J. (2004). In vivo mammalian brain imaging using one- and two-photon fluorescence microendoscopy. J. Neurophysiol. *92*, 3121–3133.

Kanter, B.R., Lykken, C.M., Avesar, D., Weible, A., Dickinson, J., Dunn, B., Borgesius, N.Z., Roudi, Y., and Kentros, C.G. (2017). A Novel Mechanism for the Grid-to-Place Cell Transformation Revealed by Transgenic Depolarization of Medial Entorhinal Cortex Layer II. Neuron *93*, 1480-1492.e6.

Kay, K., Chung, J.E., Sosa, M., Schor, J.S., Karlsson, M.P., Larkin, M.C., Liu, D.F., and Frank, L.M. (2020). Constant Sub-second Cycling between Representations of Possible Futures in the Hippocampus. Cell *180*, 552-567.e25.

Keinath, A.T., Nieto-Posadas, A., Robinson, J.C., and Brandon, M.P. (2020). DG–CA3 circuitry mediates hippocampal representations of latent information. Nat. Commun. *11*, 3026.

Kerr, K.M., Agster, K.L., Furtak, S.C., and Burwell, R.D. (2007). Functional neuroanatomy of the parahippocampal region: The lateral and medial entorhinal areas. Hippocampus *17*, 697–708.

Kesner, R.P., and Rolls, E.T. (2015). A computational theory of hippocampal function, and tests of the theory: New developments. Neurosci. Biobehav. Rev. *48*, 92–147.

Kim, S.-Y., and Lim, W. (2021). Dynamical Origin for Winner-Take-All Competition in A Biological Network of The Hippocampal Dentate Gyrus (Neuroscience).

Kim, S., Jung, D., and Royer, S. (2020). Place cell maps slowly develop via competitive learning and conjunctive coding in the dentate gyrus. Nat. Commun. *11*, 4550.

Kjelstrup, K.B., Solstad, T., Brun, V.H., Hafting, T., Leutgeb, S., Witter, M.P., Moser, E.I., and Moser, M.-B. (2008). Finite Scale of Spatial Representation in the Hippocampus. *321*, 5.

Klausberger, T., and Somogyi, P. (2008). Neuronal Diversity and Temporal Dynamics: The Unity of Hippocampal Circuit Operations. Science *321*, 53–57.

Knable, M.B., Barci, B.M., Webster, M.J., Meador-Woodruff, J., and Torrey, E.F. (2004). Molecular abnormalities of the hippocampus in severe psychiatric illness: postmortem findings from the Stanley Neuropathology Consortium. Mol. Psychiatry *9*, 609–620.

Knierim, J.J., and McNaughton, B.L. (2001). Hippocampal place-cell firing during movement in three-dimensional space. J. Neurophysiol. *85*, 105–116.

Knierim, J.J., and Neunuebel, J.P. (2016). Tracking the flow of hippocampal computation: Pattern separation, pattern completion, and attractor dynamics. Neurobiol. Learn. Mem. *129*, 38–49.

Knierim, J.J., Lee, I., and Hargreaves, E.L. (2006). Hippocampal place cells: parallel input streams, subregional processing, and implications for episodic memory. Hippocampus *16*, 755–764.

Knierim, J.J., Neunuebel, J.P., and Deshmukh, S.S. (2014). Functional correlates of the lateral and medial entorhinal cortex: objects, path integration and local–global reference frames. Philos. Trans. R. Soc. B Biol. Sci. *369*, 20130369.

Knudsen, E.B., and Wallis, J.D. (2021). Hippocampal neurons construct a map of an abstract value space. Cell *184*, 4640-4650.e10.

Kohara, K., Pignatelli, M., Rivest, A.J., Jung, H.-Y., Kitamura, T., Suh, J., Frank, D., Kajikawa, K., Mise, N., Obata, Y., et al. (2014). Cell type–specific genetic and optogenetic tools reveal hippocampal CA2 circuits. Nat. Neurosci. *17*, 269–279.

Köhler, C. (1985). Intrinsic projections of the retrohippocampal region in the rat brain. I. The subicular complex: INTRAHIPPOCAMPAL PROJECTIONS OF SUBICULAR COMPLEX. J. Comp. Neurol. *236*, 504–522.

Kornblith, S., Cheng, X., Ohayon, S., and Tsao, D.Y. (2013). A Network for Scene Processing in the Macaque Temporal Lobe. Neuron *79*, 766–781.

Kraus, B.J., Brandon, M.P., Robinson, R.J., Connerney, M.A., Hasselmo, M.E., and Eichenbaum, H. (2015). During Running in Place, Grid Cells Integrate Elapsed Time and Distance Run. Neuron *88*, 578–589.

Krumin, M., Lee, J.J., Harris, K.D., and Carandini, M. (2019). Decision and navigation in mouse parietal cortex. 21.

Kunz, L., Brandt, A., Reinacher, P.C., Staresina, B.P., Reifenstein, E.T., Weidemann, C.T., Herweg, N.A., Patel, A., Tsitsiklis, M., Kempter, R., et al. (2021). A neural code for egocentric spatial maps in the human medial temporal lobe. Neuron *109*, 2781-2796.e10.

LaChance, P.A., Todd, T.P., and Taube, J.S. (2019). A sense of space in postrhinal cortex. Science *365*, eaax4192.

Laptev, D., and Burgess, N. (2019). Neural Dynamics Indicate Parallel Integration of Environmental and Self-Motion Information by Place and Grid Cells. Front. Neural Circuits *13*, 59.

Lassalle, J.-M., Bataille, T., and Halley, H. (2000). Reversible Inactivation of the Hippocampal Mossy Fiber Synapses in Mice Impairs Spatial Learning, but neither Consolidation nor Memory Retrieval, in the Morris Navigation Task. Neurobiol. Learn. Mem. *73*, 243–257.

Laurberg, S., and Sørensen, K.E. (1981). Associational and commissural collaterals of neurons in the hippocampal formation (Hilus fasciae dentatae and subfield CA3). Brain Res. *212*, 287–300.

Laurens, J., Abrego, A., Cham, H., Popeney, B., Yu, Y., Rotem, N., Aarse, J., Asprodini, E.K., Dickman, J.D., and Angelaki, D.E. (2019). Multiplexed code of navigation variables in anterior limbic areas (Neuroscience).

Lee, I., and Kesner, R.P. (2004). Encoding versus retrieval of spatial memory: Double dissociation between the dentate gyrus and the perforant path inputs into CA3 in the dorsal hippocampus. Hippocampus *14*, 66–76.

Lee, D., Lin, B.-J., and Lee, A.K. (2012a). Hippocampal Place Fields Emerge upon Single-Cell Manipulation of Excitability During Behavior. Science *337*, 849–853.

Lee, H., Wang, C., Deshmukh, S.S., and Knierim, J.J. (2015). Neural Population Evidence of Functional Heterogeneity along the CA3 Transverse Axis: Pattern Completion versus Pattern Separation. Neuron *87*, 1093–1105.

Lee, I., Yoganarasimha, D., Rao, G., and Knierim, J.J. (2004). Comparison of population coherence of place cells in hippocampal subfields CA1 and CA3. Nature *430*, 456–459.

Lee, J.S., Briguglio, J., Romani, S., and Lee, A.K. (2019). The statistical structure of the hippocampal code for space as a function of time, context, and value (Neuroscience).

Lee, J.W., Kim, W.R., Sun, W., and Jung, M.W. (2012b). Disruption of Dentate Gyrus Blocks Effect of Visual Input on Spatial Firing of CA1 Neurons. J. Neurosci. *32*, 12999–13003.

Leutgeb, S. (2004). Distinct Ensemble Codes in Hippocampal Areas CA3 and CA1. Science *305*, 1295–1298.

Leutgeb, S. (2005). Independent Codes for Spatial and Episodic Memory in Hippocampal Neuronal Ensembles. Science *309*, 619–623.

Leutgeb, S., and Leutgeb, J.K. (2007). Pattern separation, pattern completion, and new neuronal codes within a continuous CA3 map. Learn. Mem. *14*, 745–757.

Leutgeb, J.K., Leutgeb, S., Moser, M.-B., and Moser, E.I. (2007). Pattern Separation in the Dentate Gyrus and CA3 of the Hippocampus. Science *315*, 961–966.

Leutgeb, S., Leutgeb, J.K., Moser, M.-B., and Moser, E.I. (2005). Place cells, spatial maps and the population code for memory. Curr. Opin. Neurobiol. *15*, 738–746.

Leutgeb, S., Leutgeb, J.K., Moser, E.I., and Moser, M.-B. (2006). Fast rate coding in hippocampal CA3 cell ensembles. Hippocampus *16*, 765–774.

Lever, C., Burton, S., Jeewajee, A., O'Keefe, J., and Burgess, N. (2009). Boundary Vector Cells in the Subiculum of the Hippocampal Formation. J. Neurosci. *29*, 9771–9777.

Levy, E.R.J., Park, E.H., Redman, W.T., and Fenton, A.A. (2021). A neuronal code for space in hippocampal coactivity dynamics independent of place fields (Neuroscience).

Levy, S.J., Kinsky, N.R., Mau, W., Sullivan, D.W., and Hasselmo, M.E. (2019). Hippocampal spatial memory representations in mice are heterogeneously stable (Neuroscience).

Li, Y., Xu, J., Liu, Y., Zhu, J., Liu, N., Zeng, W., Huang, N., Rasch, M.J., Jiang, H., Gu, X., et al. (2017). A distinct entorhinal cortex to hippocampal CA1 direct circuit for olfactory associative learning. Nat. Neurosci. *20*, 559–570.

Lisman, J.E. (2007). Role of the dual entorhinal inputs to hippocampus: a hypothesis based on cue/action (non-self/self) couplets. Prog. Brain Res. *163*, 615–625.

Liu, K., Sibille, J., and Dragoi, G. (2021). Orientation selectivity enhances context generalization and generative predictive coding in the hippocampus. Neuron S0896-6273(21)00610-3.

Liu, X., Ramirez, S., Pang, P.T., Puryear, C.B., Govindarajan, A., Deisseroth, K., and Tonegawa, S. (2012). Optogenetic stimulation of a hippocampal engram activates fear memory recall. Nature *484*, 381–385.

Lu, L., Igarashi, K.M., Witter, M.P., Moser, E.I., and Moser, M.-B. (2015). Topography of Place Maps along the CA3-to-CA2 Axis of the Hippocampus. Neuron *87*, 1078–1092.

Lüscher, C., and Malenka, R.C. (2012). NMDA receptor-dependent long-term potentiation and long-term depression (LTP/LTD). Cold Spring Harb. Perspect. Biol. *4*, a005710.

M. Hayman, R., and Jeffery, K.J. (2008). How heterogeneous place cell responding arises from homogeneous grids-A contextual gating hypothesis. Hippocampus *18*, 1301–1313.

MacDonald, C.J., Lepage, K.Q., Eden, U.T., and Eichenbaum, H. (2011). Hippocampal "Time Cells" Bridge the Gap in Memory for Discontiguous Events. Neuron *71*, 737–749.

Madroñal, N., Delgado-García, J.M., Fernández-Guizán, A., Chatterjee, J., Köhn, M., Mattucci, C., Jain, A., Tsetsenis, T., Illarionova, A., Grinevich, V., et al. (2016). Rapid erasure of hippocampal memory following inhibition of dentate gyrus granule cells. Nat. Commun. *7*, 10923.

Malezieux, M., Kees, A.L., and Mulle, C. (2020). Theta Oscillations Coincide with Sustained Hyperpolarization in CA3 Pyramidal Cells, Underlying Decreased Firing. Cell Rep. *32*, 107868.

Malinow, R., Mainen, Z.F., and Hayashi, Y. (2000). LTP mechanisms: from silence to four-lane traffic. 6.

Mankin, E.A., Diehl, G.W., Sparks, F.T., Leutgeb, S., and Leutgeb, J.K. (2015). Hippocampal CA2 Activity Patterns Change over Time to a Larger Extent than between Spatial Contexts. Neuron *85*, 190–201.

Markram, H., Lübke, J., Frotscher, M., and Sakmann, B. (1997). Regulation of synaptic efficacy by coincidence of postsynaptic APs and EPSPs. Science *275*, 213–215.

Markus, E., Qin, Y., Leonard, B., Skaggs, W., McNaughton, B., and Barnes, C. (1995). Interactions between location and task affect the spatial and directional firing of hippocampal neurons. J. Neurosci. *15*, 7079–7094.

Marr, D. (1969). A theory of cerebellar cortex. J. Physiol. *202*, 437–470.

Marr, D. (1971). Simple memory: a theory for archicortex. Philos. Trans. R. Soc. Lond. B. Biol. Sci. *262*, 23–81.

Mayford, M., Siegelbaum, S.A., and Kandel, E.R. (2012). Synapses and memory storage. Cold Spring Harb. Perspect. Biol. *4*, a005751.

McClelland, J.L., and O'Reilly, R.C. (1995). Why There Are Complementary Learning Systems in the Hippocampus and Neocortex:InsightsFrom the Successesand Failuresof Connectionist Models of Learning and Memory. 39.

McHugh, T.J., Jones, M.W., Quinn, J.J., Balthasar, N., Coppari, R., Elmquist, J.K., Lowell, B.B., Fanselow, M.S., Wilson, M.A., and Tonegawa, S. (2007). Dentate Gyrus NMDA Receptors Mediate Rapid Pattern Separation in the Hippocampal Network. Science *317*, 94–99.

McNamara, T.P., and Shelton, A.L. Cognitive Maps and the Hippocampus. 6.

McNaughton, N., and Morris, R.G. (1987). Chlordiazepoxide, an anxiolytic benzodiazepine, impairs place navigation in rats. Behav. Brain Res. *24*, 39–46.

McNaughton, B.L., Barnes, C.A., and O'Keefe, J. (1983). The contributions of position, direction, and velocity to single unit activity in the hippocampus of freely-moving rats. 9.

McNaughton, B.L., Barnes, C.A., Meltzer, J., and Sutherland, R.J. (1989). Hippocampal granule cells are necessary for normal spatial learning but not for spatially-selective pyramidal cell discharge. Exp. Brain Res. *76*, 485–496.

McNaughton, B.L., Barnes, C.A., Gerrard, J.L., Gothard, K., Jung, M.W., Knierim, J.J., Kudrimoti, H., Qin, Y., Skaggs, W.E., Suster, M., et al. (1996). Deciphering the hippocampal polyglot: the hippocampus as a path integration system. J. Exp. Biol. *199*, 173–185.

McNaughton, B.L., Battaglia, F.P., Jensen, O., Moser, E.I., and Moser, M.-B. (2006). Path integration and the neural basis of the "cognitive map." Nat. Rev. Neurosci. *7*, 663–678.

Menendez de la Prida, L., Huberfeld, G., Cohen, I., and Miles, R. (2006). Threshold Behavior in the Initiation of Hippocampal Population Bursts. Neuron *49*, 131–142.

Miles, R., and Wong, R.K.S. (1983). Single neurones can initiate synchronized population discharge in the hippocampus. Nature *306*, 371–373.

Mircheva, Y., Peralta, M.R., and Tóth, K. (2019). Interplay of Entorhinal Input and Local Inhibitory Network in the Hippocampus at the Origin of Slow Inhibition in Granule Cells. J. Neurosci. *39*, 6399–6413.

Mishkin, M., Ungerleider, L.G., and Macko, K.A. (1983). Object vision and spatial vision: two cortical pathways. Trends Neurosci. *6*, 414–417.

Miyawaki, A., Llopis, J., Heim, R., McCaffery, J.M., Adams, J.A., Ikura, M., and Tsien, R.Y. (1997). Fluorescent indicators for Ca2+ based on green fluorescent proteins and calmodulin. Nature *388*, 882–887.

Mizumori, S.J.Y., and Williams, J.D. (1993). Directionally Selective Mnemonic Properties of Neurons in the Lateral Dorsal Nucleus of the Thalamus of Rats. 14.

Mizumori, S., McNaughton, B., Barnes, C., and Fox, K. (1989). Preserved spatial coding in hippocampal CA1 pyramidal cells during reversible suppression of CA3c output: evidence for pattern completion in hippocampus. J. Neurosci. *9*, 3915–3928.

Mizuseki, K., Royer, S., Diba, K., and Buzsáki, G. (2012). Activity dynamics and behavioral correlates of CA3 and CA1 hippocampal pyramidal neurons. Hippocampus *22*, 1659–1680.

Morales, C., Morici, J.F., Espinosa, N., Sacson, A., Lara-Vasquez, A., García-Pérez, M.A., Bekinschtein, P., Weisstaub, N.V., and Fuentealba, P. (2021). Dentate Gyrus Somatostatin Cells are Required for Contextual Discrimination During Episodic Memory Encoding. Cereb. Cortex *31*, 1046–1059.

Morris, R.G. (1999). D.O. Hebb: The Organization of Behavior, Wiley: New York; 1949. Brain Res. Bull. *50*, 437.

Morris, R.G.M., and Frey, U. (1997). Hippocampal synaptic plasticity: role in spatial learning or the automatic recording of attended experience? Philos. Trans. R. Soc. Lond. B. Biol. Sci. *352*, 1489–1503.

Morris, A.M., Curtis, B.J., Churchwell, J.C., Maasberg, D.W., and Kesner, R.P. (2013a). Temporal associations for spatial events: The role of the dentate gyrus. Behav. Brain Res. *256*, 250–256.

Morris, A.M., Weeden, C.S., Churchwell, J.C., and Kesner, R.P. (2013b). The role of the dentate gyrus in the formation of contextual representations. Hippocampus *23*, 162–168.

Moser, E.I., Kropff, E., and Moser, M.-B. (2008). Place Cells, Grid Cells, and the Brain's Spatial Representation System. Annu. Rev. Neurosci. *31*, 69–89.

Moser, M.-B., Rowland, D.C., and Moser, E.I. (2015). Place Cells, Grid Cells, and Memory. Cold Spring Harb. Perspect. Biol. *7*, a021808.

Muller, R., and Kubie, J. (1987). The effects of changes in the environment on the spatial firing of hippocampal complex-spike cells. J. Neurosci. *7*, 1951–1968.

Muller, R., Kubie, J., and Ranck, J. (1987). Spatial firing patterns of hippocampal complex-spike cells in a fixed environment. J. Neurosci. *7*, 1935–1950.

Muller, R., Bostock, E., Taube, J., and Kubie, J. (1994). On the directional firing properties of hippocampal place cells. J. Neurosci. *14*, 7235–7251.

Murano, T., Nakajima, R., Nakao, A., Hirata, N., Amemori, S., Murakami, A., Kamitani, Y., Yamamoto, J., and Miyakawa, T. (2020). Multiple types of navigational information are independently encoded in the population activities of the dentate gyrus neurons (Neuroscience).

Nabavi, S., Fox, R., Proulx, C.D., Lin, J.Y., Tsien, R.Y., and Malinow, R. (2014). Engineering a memory with LTD and LTP. Nature *511*, 348–352.

Naber, P.A., Lopes da Silva, F.H., and Witter, M.P. (2001). Reciprocal connections between the entorhinal cortex and hippocampal fields CA1 and the subiculum are in register with the projections from CA1 to the subiculum. Hippocampus *11*, 99–104.

Nafstad, P.H.J. (1967). An electron microscope study on the termination of the perforant path fibres in the hippocampus and the fascia dentata. Z. F[illegible] Zellforsch. Mikrosk. Anat. *76*, 532–542.

Nasr, S., Liu, N., Devaney, K.J., Yue, X., Rajimehr, R., Ungerleider, L.G., and Tootell, R.B.H. (2011). Scene-Selective Cortical Regions in Human and Nonhuman Primates. J. Neurosci. *31*, 13771–13785.

Navratilova, Z., Hoang, L.T., Schwindel, C.D., Tatsuno, M., and McNaughton, B.L. (2012). Experience-dependent firing rate remapping generates directional selectivity in hippocampal place cells. Front. Neural Circuits *6*.

Neunuebel, J.P., and Knierim, J.J. (2012). Spatial Firing Correlates of Physiologically Distinct Cell Types of the Rat Dentate Gyrus. J. Neurosci. *32*, 3848–3858.

Neunuebel, J.P., and Knierim, J.J. (2014). CA3 Retrieves Coherent Representations from Degraded Input: Direct Evidence for CA3 Pattern Completion and Dentate Gyrus Pattern Separation. Neuron *81*, 416–427.

Ohkura, M., Sasaki, T., Sadakari, J., Gengyo-Ando, K., Kagawa-Nagamura, Y., Kobayashi, C., Ikegaya, Y., and Nakai, J. (2012). Genetically encoded green fluorescent Ca2+ indicators with improved detectability for neuronal Ca2+ signals. PloS One *7*, e51286.

O'Keefe, J., and Burgess, N. (2005). Dual phase and rate coding in hippocampal place cells: Theoretical significance and relationship to entorhinal grid cells. Hippocampus *15*, 853–866.

O'Keefe, J., and Conway, D.H. (1978). Hippocampal place units in the freely moving rat: Why they fire where they fire. Exp. Brain Res. *31*.

O'Keefe, J., and Dostrovsky, J. (1971). The hippocampus as a spatial map. Preliminary evidence from unit activity in the freely-moving rat. Brain Res. *34*, 171–175.

O'Keefe, J., and Krupic, J. (2021). Do hippocampal pyramidal cells respond to nonspatial stimuli? Physiol. Rev. *101*, 1427–1456.

O'Keefe, J., and Nadel, L. (1978). The hippocampus as a cognitive map (Clarendon Press).

Oliva, A., Fernández-Ruiz, A., Buzsáki, G., and Berényi, A. (2016). Spatial coding and physiological properties of hippocampal neurons in the Cornu Ammonis subregions: SPATIAL CODING AND PHYSIOLOGICAL PROPERTIES OF HIPPOCAMPAL NEURONS. Hippocampus *26*, 1593–1607.

Olsen, G.M., Ohara, S., Iijima, T., and Witter, M.P. (2017). Parahippocampal and retrosplenial connections of rat posterior parietal cortex. Hippocampus *27*, 335–358.

Pakan, J.M.P., Currie, S.P., Fischer, L., and Rochefort, N.L. (2018). The Impact of Visual Cues, Reward, and Motor Feedback on the Representation of Behaviorally Relevant Spatial Locations in Primary Visual Cortex. Cell Rep. *24*, 2521–2528.

Palmer, A.E., and Tsien, R.Y. (2006). Measuring calcium signaling using genetically targetable fluorescent indicators. Nat. Protoc. *1*, 1057–1065.

Panoz-Brown, D., Iyer, V., Carey, L.M., Sluka, C.M., Rajic, G., Kestenman, J., Gentry, M., Brotheridge, S., Somekh, I., Corbin, H.E., et al. (2018). Replay of Episodic Memories in the Rat. Curr. Biol. *28*, 1628-1634.e7.

Payne, H.L., Lynch, G.F., and Aronov, D. (2021). Neural representations of space in the hippocampus of a food-caching bird. Science *373*, 343–348.

Per, A., Morris, R., Amaral, D.G., and O'Keefe, J. (2007). The Hippocampus Book (Oxford University Press).

Piette, C., Touboul, J., and Venance, L. (2020). Engrams of Fast Learning. Front. Cell. Neurosci. *14*, 575915.

Pilz, G.-A., Carta, S., Stauble, A., Ayaz, A., Jessberger, S., and Helmchen, F. (2016). Functional Imaging of Dentate Granule Cells in the Adult Mouse Hippocampus. J. Neurosci. *36*, 7407–7414.

Plitt, M.H., and Giocomo, L.M. (2021). Experience-dependent contextual codes in the hippocampus. Nat. Neurosci. *24*, 705–714.

Pofahl, M., Nikbakht, N., Haubrich, A.N., Nguyen, T.M., Masala, N., Distler, F.J., Braganza, O., Macke, J.H., Ewell, L.A., Golcuk, K., et al. (2021). Synchronous activity patterns in the dentate gyrus during immobility. ELife *10*, e65786.

Poo, M., Pignatelli, M., Ryan, T.J., Tonegawa, S., Bonhoeffer, T., Martin, K.C., Rudenko, A., Tsai, L.-H., Tsien, R.W., Fishell, G., et al. (2016). What is memory? The present state of the engram. BMC Biol. *14*, 40.

Posani, L., Cocco, S., Ježek, K., and Monasson, R. (2017). Functional connectivity models for decoding of spatial representations from hippocampal CA1 recordings. J. Comput. Neurosci. *43*, 17–33.

Preston-Ferrer, P., and Burgalossi, A. (2018). Linking neuronal structure to function in rodent hippocampus: a methodological prospective. Cell Tissue Res. *373*, 605–618.

Pröll, M., Häusler, S., and Herz, A.V.M. (2018). Grid-Cell Activity on Linear Tracks Indicates Purely Translational Remapping of 2D Firing Patterns at Movement Turning Points. J. Neurosci. *38*, 7004–7011.

Qin, H., Fu, L., Hu, B., Liao, X., Lu, J., He, W., Liang, S., Zhang, K., Li, R., Yao, J., et al. (2018). A Visual-Cue-Dependent Memory Circuit for Place Navigation. Neuron *99*, 47-55.e4.

Rajji, T. (2006). The Role of CA3 Hippocampal NMDA Receptors in Paired Associate Learning. J. Neurosci. *26*, 908–915.

Ramirez, S., Liu, X., Lin, P.-A., Suh, J., Pignatelli, M., Redondo, R.L., Ryan, T.J., and Tonegawa, S. (2013). Creating a False Memory in the Hippocampus. *341*, 6.

Ravassard, P., Kees, A., Willers, B., Ho, D., Aharoni, D., Cushman, J., Aghajan, Z.M., and Mehta, M.R. (2013). Multisensory Control of Hippocampal Spatiotemporal Selectivity. Science *340*, 1342–1346.

Rebola, N., Carta, M., and Mulle, C. (2017). Operation and plasticity of hippocampal CA3 circuits: implications for memory encoding. Nat. Rev. Neurosci. *18*, 208–220.

Reddy, L., Zoefel, B., Possel, J.K., Peters, J.C., Dijksterhuis, D., Poncet, M., and Self, M.W. (2020). Human hippocampal neurons track moments in a sequence of events. 22.

Resendez, S.L., and Stuber, G.D. (2015). In vivo calcium imaging to illuminate neurocircuit activity dynamics underlying naturalistic behavior. Neuropsychopharmacol. Off. Publ. Am. Coll. Neuropsychopharmacol. *40*, 238–239.

Resendez, S.L., Jennings, J.H., Ung, R.L., Namboodiri, V.M.K., Zhou, Z.C., Otis, J.M., Nomura, H., McHenry, J.A., Kosyk, O., and Stuber, G.D. (2016). Visualization of cortical, subcortical and deep brain neural circuit dynamics during naturalistic mammalian behavior with head-mounted microscopes and chronically implanted lenses. Nat. Protoc. *11*, 566–597.

Robinson, N.T.M., Descamps, L.A.L., Russell, L.E., Buchholz, M.O., Bicknell, B.A., Antonov, G.K., Lau, J.Y.N., Nutbrown, R., Schmidt-Hieber, C., and Häusser, M.

(2020). Targeted Activation of Hippocampal Place Cells Drives Memory-Guided Spatial Behavior. Cell *183*, 1586-1599.e10.

Rolls, E.T. (2013). The mechanisms for pattern completion and pattern separation in the hippocampus. Front. Syst. Neurosci. *7*.

Rolls, E.T. (2018). The storage and recall of memories in the hippocampo-cortical system. Cell Tissue Res. *373*, 577–604.

Rolls, E., and Treves, A. (1997). Neural Networks and Brain Function (Oxford University Press).

Rolls, E.T., Treves, A., Robertson, R.G., Georges-François, P., and Panzeri, S. (1998). Information about spatial view in an ensemble of primate hippocampal cells. J. Neurophysiol. *79*, 1797–1813.

Rolls, E.T., Stringer, S.M., and Elliot, T. (2006). Entorhinal cortex grid cells can map to hippocampal place cells by competitive learning. Netw. Comput. Neural Syst. *17*, 447–465.

Roy, D.S., Kitamura, T., Okuyama, T., Ogawa, S.K., Sun, C., Obata, Y., Yoshiki, A., and Tonegawa, S. (2017). Distinct Neural Circuits for the Formation and Retrieval of Episodic Memories. Cell *170*, 1000-1012.e19.

Rubin, A., Geva, N., Sheintuch, L., and Ziv, Y. (2015). Hippocampal ensemble dynamics timestamp events in long-term memory. ELife *4*, e12247.

Saleem, A.B., Diamanti, E.M., Fournier, J., Harris, K.D., and Carandini, M. (2018). Coherent encoding of subjective spatial position in visual cortex and hippocampus. Nature *562*, 124–127.

Sargolini, F. (2006). Conjunctive Representation of Position, Direction, and Velocity in Entorhinal Cortex. Science *312*, 758–762.

Sasaki, T., Piatti, V.C., Hwaun, E., Ahmadi, S., Lisman, J.E., Leutgeb, S., and Leutgeb, J.K. (2018). Dentate network activity is necessary for spatial working memory by supporting CA3 sharp-wave ripple generation and prospective firing of CA3 neurons. Nat. Neurosci. *21*, 258–269.

Sauvage, M.M., Nakamura, N.H., and Beer, Z. (2013). Mapping memory function in the medial temporal lobe with the immediate-early gene Arc. Behav. Brain Res. *254*, 22–33.

Savanthrapadian, S., Meyer, T., Elgueta, C., Booker, S.A., Vida, I., and Bartos, M. (2014). Synaptic Properties of SOM- and CCK-Expressing Cells in Dentate Gyrus Interneuron Networks. 13.

Savelli, F., Yoganarasimha, D., and Knierim, J.J. (2008). Influence of boundary removal on the spatial representations of the medial entorhinal cortex. Hippocampus *18*, 1270–1282.

Scharfman, H.E. (2012). Differentiation of rat dentate neurons by morphology and electrophysiology in hippocampal slices: granule cells, spiny hilar cells and aspiny 'fast-spiking' cells. 24.

Scharfman, H.E. (2016). The enigmatic mossy cell of the dentate gyrus. Nat. Rev. Neurosci. *17*, 562–575.

Scharfman, H.E., Sollas, A.L., Berger, R.E., and Goodman, J.H. (2003). Electrophysiological Evidence of Monosynaptic Excitatory Transmission Between Granule Cells After Seizure-Induced Mossy Fiber Sprouting. J. Neurophysiol. *90*, 2536–2547.

Schmidt-Hieber, C. (2018). How Does a Memory Find Its Neurons? BioEssays *40*, 1800189.

Schoenfeld, G., Carta, S., Rupprecht, P., Ayaz, A., and Helmchen, F. (2021). *In Vivo* Calcium Imaging of CA3 Pyramidal Neuron Populations in Adult Mouse Hippocampus. Eneuro *8*, ENEURO.0023-21.2021.

Schwindel, C.D., Navratilova, Z., Ali, K., Tatsuno, M., and McNaughton, B.L. (2016). Reactivation of Rate Remapping in CA3. J. Neurosci. *36*, 9342–9350.

Scoville, W.B., and Milner, B. (1957). Loss of recent memory after bilateral hippocampal lesions. J. Neurol. Neurosurg. Psychiatry *20*, 11–21.

Semon, R. (1921). The nmeme (Leipzig: George Allen & Unwin).

Senzai, Y., and Buzsáki, G. (2017). Physiological Properties and Behavioral Correlates of Hippocampal Granule Cells and Mossy Cells. Neuron *93*, 691-704.e5.

Shapiro, M.L., Tanila, H., and Eichenbaum, H. (1997). Cues that hippocampal place cells encode: dynamic and hierarchical representation of local and distal stimuli. Hippocampus *7*, 624–642.

Sharif, F., Tayebi, B., Buzsáki, G., Royer, S., and Fernandez-Ruiz, A. (2021). Subcircuits of Deep and Superficial CA1 Place Cells Support Efficient Spatial Coding across Heterogeneous Environments. Neuron *109*, 363-376.e6.

Sharp, P.E., Blair, H.T., and Brown, M. (1996). Neural network modeling of the hippocampal formation spatial signals and their possible role in navigation: A modular approach. 15.

Sheffield, M.E.J., Adoff, M.D., and Dombeck, D.A. (2017). Increased Prevalence of Calcium Transients across the Dendritic Arbor during Place Field Formation. Neuron *96*, 490-504.e5.

Sheintuch, L., Geva, N., Baumer, H., Rechavi, Y., Rubin, A., and Ziv, Y. (2020). Multiple Maps of the Same Spatial Context Can Stably Coexist in the Mouse Hippocampus. Curr. Biol. *30*, 1467-1476.e6.

Shi, S.H., Hayashi, Y., Petralia, R.S., Zaman, S.H., Wenthold, R.J., Svoboda, K., and Malinow, R. (1999). Rapid spine delivery and redistribution of AMPA receptors after synaptic NMDA receptor activation. Science *284*, 1811–1816.

Smart, T.G., and Paoletti, P. (2012). Synaptic neurotransmitter-gated receptors. Cold Spring Harb. Perspect. Biol. *4*.

Smetters, D., Majewska, A., and Yuste, R. (1999). Detecting action potentials in neuronal populations with calcium imaging. Methods San Diego Calif *18*, 215–221.

Solstad, T., Boccara, C.N., Kropff, E., Moser, M.-B., and Moser, E.I. (2008). Representation of Geometric Borders in the Entorhinal Cortex. Science *322*, 1865–1868.

Somogyi, P., and Klausberger, T. (2005). Defined types of cortical interneurone structure space and spike timing in the hippocampus: Interneurones structure space and spike timing in the hippocampus. J. Physiol. *562*, 9–26.

Sparta, D.R., Stamatakis, A.M., Phillips, J.L., Hovelsø, N., van Zessen, R., and Stuber, G.D. (2011). Construction of implantable optical fibers for long-term optogenetic manipulation of neural circuits. Nat. Protoc. *7*, 12–23.

Spruston, N., Schiller, Y., Stuart, G., and Sakmann, B. (1995). Activity-dependent action potential invasion and calcium influx into hippocampal CA1 dendrites. Science *268*, 297–300.

Squire, L.R. (1992). Memory and the hippocampus: A synthesis from findings with rats, monkeys, and humans. Psychol. Rev. *99*, 195–231.

Squire, L.R., and Alvarez, P. (1995). Retrograde amnesia and memory consolidation: a neurobiological perspective. Curr. Opin. Neurobiol. *5*, 169–177.

Squire, L., Slater, P., and Chace, P. (1975). Retrograde amnesia: temporal gradient in very long term memory following electroconvulsive therapy. Science *187*, 77–79.

Squire, L.R., Stark, C.E.L., and Clark, R.E. (2004). THE MEDIAL TEMPORAL LOBE. Annu. Rev. Neurosci. *27*, 279–306.

Stachenfeld, K.L., Botvinick, M.M., and Gershman, S.J. (2017). The hippocampus as a predictive map. Nat. Neurosci. *20*, 1643–1653.

Stackman, R.W., and Taube, J.S. (1997). Firing properties of head direction cells in the rat anterior thalamic nucleus: dependence on vestibular input. J. Neurosci. Off. J. Soc. Neurosci. *17*, 4349–4358.

Stefanini, F., Kushnir, L., Jimenez, J.C., Jennings, J.H., Stuber, G.D., Kheirbek, M.A., Hen, R., and Fusi, S. (2018). A Distributed Neural Code in the Dentate Gyrus and in CA1. 38.

Steward, O. (1976). Topographic organization of the projections from the entorhinal area to the hippocampal formation of the rat. J. Comp. Neurol. *167*, 285–314.

van Strien, N.M., Cappaert, N.L.M., and Witter, M.P. (2009). The anatomy of memory: an interactive overview of the parahippocampal–hippocampal network. Nat. Rev. Neurosci. *10*, 272–282.

Strüber, M., Sauer, J.-F., Jonas, P., and Bartos, M. (2017). Distance-dependent inhibition facilitates focality of gamma oscillations in the dentate gyrus. Nat. Commun. *8*, 758.

Suh, J., Rivest, A.J., Nakashiba, T., Tominaga, T., and Tonegawa, S. (2011). Entorhinal Cortex Layer III Input to the Hippocampus Is Crucial for Temporal Association Memory. Science *334*, 1415–1420.

Sun, C., Kitamura, T., Yamamoto, J., Martin, J., Pignatelli, M., Kitch, L.J., Schnitzer, M.J., and Tonegawa, S. (2015). Distinct speed dependence of entorhinal island and ocean cells, including respective grid cells. Proc. Natl. Acad. Sci. *112*, 9466–9471.

Sun, C., Yang, W., Martin, J., and Tonegawa, S. (2020). Hippocampal neurons represent events as transferable units of experience. Nat. Neurosci. *23*, 651–663.

Supèr, H., and Roelfsema, P.R. (2005). Chronic multiunit recordings in behaving animals: advantages and limitations. Prog. Brain Res. *147*, 263–282.

Svoboda, K., and Yasuda, R. (2006). Principles of two-photon excitation microscopy and its applications to neuroscience. Neuron *50*, 823–839.

Swanson, L., Sawchenko, P., and Cowan, W. (1981). Evidence for collateral projections by neurons in Ammon's horn, the dentate gyrus, and the subiculum: a multiple retrograde labeling study in the rat. J. Neurosci. *1*, 548–559.

Swanson, L.W., Wyss, J.M., and Cowan, W.M. (1978). An autoradiographic study of the organization of intrahippocampal association pathways in the rat. J. Comp. Neurol. *181*, 681–715.

Szabadics, J., and Soltesz, I. (2009). Functional Specificity of Mossy Fiber Innervation of GABAergic Cells in the Hippocampus. J. Neurosci. *29*, 4239–4251.

Tan, H.M., Wills, T.J., and Cacucci, F. (2017). The development of spatial and memory circuits in the rat. WIREs Cogn. Sci. *8*.

Tanaka, K.Z., and McHugh, T.J. (2018). The Hippocampal Engram as a Memory Index. J. Exp. Neurosci. *12*, 117906951881594.

Tanaka, K.Z., Pevzner, A., Hamidi, A.B., Nakazawa, Y., Graham, J., and Wiltgen, B.J. (2014). Cortical Representations Are Reinstated by the Hippocampus during Memory Retrieval. Neuron *84*, 347–354.

Taube, J., Muller, R., and Ranck, J. (1990). Head-direction cells recorded from the postsubiculum in freely moving rats. II. Effects of environmental manipulations. J. Neurosci. *10*, 436–447.

Taxidis, J., Pnevmatikakis, E.A., Dorian, C.C., Mylavarapu, A.L., Arora, J.S., Samadian, K.D., Hoffberg, E.A., and Golshani, P. (2020). Differential Emergence and Stability of Sensory and Temporal Representations in Context-Specific Hippocampal Sequences. Neuron *108*, 984-998.e9.

Tolman, E.C. (1948). Cognitive maps in rats and men. Psychol. Rev. *55*, 189–208.

Treves, A., and Rolls, E.T. (1991). What determines the capacity of autoassociative memories in the brain? Netw. Comput. Neural Syst. *2*, 371–397.

Tsao, A., Moser, M.-B., and Moser, E.I. (2013). Traces of Experience in the Lateral Entorhinal Cortex. Curr. Biol. *23*, 399–405.

Tsao, A., Sugar, J., Lu, L., Wang, C., Knierim, J.J., Moser, M.-B., and Moser, E.I. (2018). Integrating time from experience in the lateral entorhinal cortex. Nature *561*, 57–62.

Tuncdemir, S.N., Grosmark, A.D., Turi, G., Shank, A., Bowler, J., Ordek, G., Losonczy, A., Hen, R., and Lacefield, C. (2020). Parallel processing of sensory cue and spatial information in the Dentate Gyrus (Neuroscience).

Ulanovsky, N., and Moss, C.F. (2007). Hippocampal cellular and network activity in freely moving echolocating bats. Nat. Neurosci. *10*, 224–233.

Vandael, D., Borges-Merjane, C., Zhang, X., and Jonas, P. (2020). Short-Term Plasticity at Hippocampal Mossy Fiber Synapses Is Induced by Natural Activity Patterns and Associated with Vesicle Pool Engram Formation. Neuron *107*, 509-521.e7.

Vargha-Khadem, F. (1997). Differential Effects of Early Hippocampal Pathology on Episodic and Semantic Memory. Science *277*, 376–380.

Wang, C., Chen, X., Lee, H., Deshmukh, S.S., Yoganarasimha, D., Savelli, F., and Knierim, J.J. (2018). Egocentric coding of external items in the lateral entorhinal cortex. Science *362*, 945–949.

Wanjia, G., Favila, S.E., Kim, G., Molitor, R.J., and Kuhl, B.A. (2021). Abrupt hippocampal remapping signals resolution of memory interference. Nat. Commun. *12*, 4816.

Wersinger, S.R., Ginns, E.I., O'Carroll, A.-M., Lolait, S.J., and Young III, W.S. (2002). Vasopressin V1b receptor knockout reduces aggressive behavior in male mice. Mol. Psychiatry *7*, 975–984.

Whishaw, I.Q., and Tomie, J.-A. (1997). Piloting and dead reckoning dissociated by fimbria-fornix lesions in a rat food carrying task. Behav. Brain Res. *89*, 87–97.

Wilber, A.A., Clark, B.J., Forster, T.C., Tatsuno, M., and McNaughton, B.L. (2014). Interaction of Egocentric and World-Centered Reference Frames in the Rat Posterior Parietal Cortex. J. Neurosci. *34*, 5431–5446.

Wills, T.J., and Cacucci, F. (2014). The development of the hippocampal neural representation of space. Curr. Opin. Neurobiol. *24*, 111–119.

Wills, T.J., Muessig, L., and Cacucci, F. (2014). The development of spatial behaviour and the hippocampal neural representation of space. Philos. Trans. R. Soc. B Biol. Sci. *369*, 20130409.

Wilson, M., and McNaughton, B. (1993). Dynamics of the hippocampal ensemble code for space. Science *261*, 1055–1058.

Witter, M.P., and Amaral, D.G. (1991). Entorhinal cortex of the monkey: V. Projections to the dentate gyrus, hippocampus, and subicular complex. J. Comp. Neurol. *307*, 437–459.

Witter, M.P., Naber, P.A., van Haeften, T., Machielsen, W.C., Rombouts, S.A., Barkhof, F., Scheltens, P., and Lopes da Silva, F.H. (2000). Cortico-hippocampal communication by way of parallel parahippocampal-subicular pathways. Hippocampus *10*, 398–410.

Wittner, L., and Miles, R. (2007). Factors defining a pacemaker region for synchrony in the hippocampus: CA3a *versus* CA3b in hippocampal synchrony. J. Physiol. *584*, 867–883.

Wood, E.R., Dudchenko, P.A., and Eichenbaum, H. (1999). The global record of memory in hippocampal neuronal activity. Nature *397*, 613–616.

Young, B., Fox, G., and Eichenbaum, H. (1994). Correlates of hippocampal complex-spike cell activity in rats performing a nonspatial radial maze task. J. Neurosci. *14*, 6553–6563.

Zhang, S.-J., Ye, J., Miao, C., Tsao, A., Cerniauskas, I., Ledergerber, D., Moser, M.-B., and Moser, E.I. (2013). Optogenetic Dissection of Entorhinal-Hippocampal Functional Connectivity. Science *340*, 1232627.

Zhang, X., Schlögl, A., and Jonas, P. (2020). Selective Routing of Spatial Information Flow from Input to Output in Hippocampal Granule Cells. Neuron *107*, 1212-1225.e7.

Zhao, M., Choi, Y.-S., Obrietan, K., and Dudek, S.M. (2007). Synaptic Plasticity (and the Lack Thereof) in Hippocampal CA2 Neurons. J. Neurosci. *27*, 12025–12032.

Zhao, X., Lein, E.S., He, A., Smith, S.C., Aston, C., and Gage, F.H. (2001). Transcriptional profiling reveals strict boundaries between hippocampal subregions. J. Comp. Neurol. *441*, 187–196.

Ziv, Y., and Ghosh, K.K. (2015). Miniature microscopes for large-scale imaging of neuronal activity in freely behaving rodents. Curr. Opin. Neurobiol. *32*, 141–147.

Ziv, Y., Burns, L.D., Cocker, E.D., Hamel, E.O., Ghosh, K.K., Kitch, L.J., Gamal, A.E., and Schnitzer, M.J. (2013). Long-term dynamics of CA1 hippocampal place codes. Nat. Neurosci. *16*, 264–266.

VII. Acknowledgements

I would like to thank my colleagues for their contributions to this PhD project, and in particular, my supervisor Christoph for welcoming me to Schlab as a member of the starting crew. This PhD project has taught me tremendous amounts and I am grateful for your support, availability and kindness throughout the past four years. CZ, thank you for the technical training and guidance, for your support especially during the Covid period as well as for the Chinese wisdom. I am now equipped. Manu, thank for your help with this project and for the time spent together, evolving in the lab over the years, whether in surgeries or in the lady's office. Ruy my PhD brother: thank you for your companionship - this PhD journey would not have been the same without you. Je voudrais également remercier Lucile et Claire pour votre aide avec ce projet: et avec Cantin, pour la bouffée d'enthousiasme et de bonne humeur que vous apportez. I would also like to thank Hsin-Lun for and Lorenzo for their contributions and work with the data analysis axis of this project. Merci également aux secrétaries successives de notre laboratoire – Anaïs, Rebecca, Rhizlane et Tara pour votre gentillesse, et votre aide administrative précieuse, en particulier avec les procédures complexes d'envoi de microscopes au Canada.

Soham, thank you for your multi-faceted support and empathy throughout the 4-year marathon – they have been greatly appreciated, and so was your work with the analysis throughout the last leg of the project.

Je voudrais également remercier infiniment Stéphanie pour ton expertise et pour tout le temps que tu as dédié à notre collaboration sur les cellules nouvellement générées. Malgré les difficultés rencontrées pour trouver ces cellules *in vivo*, j'ai beaucoup appris à tes côtés et je t'en suis reconnaissante.

Importantly, I thank those who, in their own way, have contributed to the success of this project by supporting me throughout the last four year (especially the last two). These include, mes parents - mes pilliers, merci pour votre soutien inconditionnel; my other half upside down – thank you for standing strong next to me throughout the impossible; my dear dear friends – Sixtou, Annou, Renée, Linny, Anna, Pim, Coco and the one and only Aunty' and Uncle's club: Marta, Adriana, Emilia, Lukas, Matthias, Umbi and big Lou: you were my guiding lights; mais aussi Dani et le Capitaine pour votre confiance, vos présences toujours à mes côtés et pour les journées merveilleuses sur le lac, Marie-France pour tes pensées de loin et pour me faire rêver d'autres mondes, Samos et Marjokine Pou pour nos fous rires et nos grandes aventures, tatie, tonton, tatie et tonton pour votre soutien permanent mais aussi les anciens du PDG and the Stable hands whom I miss so very dearly; Deb and Bruce and the Gooley clan for the family support like that of my own; Dave for your guidance and mentorship, and for your ferocious respect of the human dimension of science, and Bec, last but not least, for paving the way and eternally inspiring me. I am infinitely grateful to you all.

I would also like to thank my colleagues in the department, whom I like to come across in the couloirs ou bien à la cantine and who always have a helping hand at the ready: Seb (parfois même à vélo!), Charly, Gabi, Mariana, Antoine, Gael, Florian, Zuzanna, Ilana, Sébastien (Le Gal), Ferdinand, Mathilde, Lena, François, Corentin, Mohammed, Karima, Paul, Enzo, Semih, Mathilde, Lena, Assunta et Lorène.

Finally, I would like to thank the Institut Pasteur and the Fondation pour la Recherche Médicale (FRM) for funding my PhD degree and the Pasteur Paris Université (PPU) international doctoral programme for providing me with a welcoming and supportive professional structure as well as a vibrant group of PhD companions.

VIII. Annexe

Gandit, B., Posani, L., Zhang, C.L., Saha, S., Allegra, M., Schmidt-Hieber, C. (2021) Transformation of spatial representations along hippocampal circuits. *In preparation*

Transformation of spatial representations along hippocampal circuits

Bérénice Gandit[1], Lorenzo Posani[2], Chunlei Zhang[1], Soham Saha[1,3], Manuela Allegra[1,4,*], Christoph Schmidt-Hieber[1,*]

[1]Institut Pasteur, Université de Paris, Neural Circuits for Spatial Navigation and Memory, F-75015 Paris, France
[2] Center for Theoretical Neuroscience, Mortimer B. Zuckerman Mind Brain Behavior Institute, Columbia University, New York, NY, USA
[3] Present address: Medinsights, 6, rue de l'eglise 02810 Veuilly la Poterie, France
[4] Present address: Neuroscience Institute, National Research Council (IN-CNR), Viale Giuseppe Colombo 3, 35131 Padua, Italy.

* Correspondence: manuela.allegra@cnr.it and christoph.schmidt-hieber@pasteur.fr

ABSTRACT

Forming a precise memory of our spatial environment is essential for our survival, as we depend on our ability to store and recall important locations. The hippocampus is thought to provide the brain with a cognitive map of the external world by processing various types of spatial information along its circuits. How essential spatial variables such as direction and position are hierarchically transformed along hippocampal subregions to construct this global map is unclear. To address this question, we perform single-photon widefield microendoscope calcium imaging of the dentate gyrus, CA3 and CA1 hippocampal subregions in mice freely navigating along a linear track. We find that neurons throughout the hippocampus show directionality in their spatial responses, with particularly strong selectivity for the running direction in the dentate gyrus and in CA3. In addition, spatial activity maps in the dentate gyrus are correlated after aligning them to the running directions, suggesting that they represent the distance covered along the track in egocentric coordinates. In combination with decoding of population activity, our data suggest that along the hippocampal circuit, spatial representations develop from contextually selective, egocentric distance coding to segmented allocentric representations of the environment.

INTRODUCTION

Neuronal activity in the hippocampus is thought to provide the brain with a cognitive map of its spatial surroundings. This map is constructed from the collective firing of place cells, which fire spikes at one or more specific locations of the environment termed their place fields (O'Keefe and Dostrovsky, 1971). To produce the striking place cell code, anchored in allocentric coordinates of the external world, various sources of spatial information need to be processed in hippocampal circuits, including external cues such as landmarks and boundaries, as well as internal information such as vestibular and proprioceptive stimuli.

How is the cognitive map built from this information along the hippocampal circuit? While best described and studied in area CA1 of the hippocampus, place cells have been found in all hippocampal subregions, including the dentate gyrus and CA3. Different types of spatial variables are processed and contribute to spatial representations. The location of the animal in the environment was first identified as a determinant of place cell activity. The basic properties of place cells differ between hippocampal regions. Compared to CA3 and CA1, place cells in the dentate gyrus more often have multi-peaked firing fields, low spatial information content, and high stability across recording sessions in the same environment (Hainmueller and Bartos, 2018; Jung and McNaughton, 1993; Leutgeb et al., 2007). Place cells in these regions also differ in the way they respond to changes in the spatial environment. When either a new environment is encountered or the context of the present environment changes, some place cells respond with changes in the location of their firing field ("global remapping"), while others retain the location of their firing fields, but change the rate of firing at this location ("rate remapping"). Global and rate remapping are found to different degrees among the place cell populations in the three regions. While a substantial fraction of place cells in the dentate gyrus (Allegra et al., 2020; Hainmueller and Bartos, 2018; Jung and McNaughton, 1993; Leutgeb et al., 2007; Neunuebel and Knierim, 2012, 2014) and in CA3 (Leutgeb et al., 2007, 2004, 2005; Schwindel et al., 2016) show global remapping, rate remapping dominates among CA1 place cells (Anderson and Jeffery, 2003; McNaughton et al., 1983; Navratilova et al., 2012). These differences in both static and dynamic aspects of the place cell code suggest that hippocampal subregions serve different purposes in constructing the cognitive map.

What type of spatial information is required to build the cognitive map? When animals navigate in open 2-dimensional environments, the spatial firing of place cells is anchored in a global, "allocentric" coordinate system that is centered in the outside world and largely independent of an animal's orientation. However, to make use of

e.g. spatial landmarks that have been visually identified, additional information is required about the position relative to a body-centered, egocentric coordinate system so that one's position in world-centered coordinates can be computed. Egocentric information is also required to produce directional representations in place cells, which are increasingly encountered when the environment is narrowed from open 2-dimensional surroundings to a linear track, where the presence and location of place fields depend on the direction of running (McNaughton et al., 1983; Navratilova et al., 2012). Ego- and allocentric information is thought to be conveyed to the hippocampus by distinct input sources (Lisman, 2007). The lateral entorhinal cortex (LEC) represents information relative to external cues in egocentric coordinates, while the medial entorhinal cortex (MEC) processes information about self-motion in an allocentric coordinate system (Hafting et al., 2005; Wang et al., 2018). As the entorhinal cortex shows different projection patterns to hippocampal subregions, these information streams will be differentially available along the hippocampal circuit.

In addition to neurons that are spatially modulated at the single-neuron level, such as place cells, neurons with no apparent spatial tuning may also contribute to spatial coding at the population level. Non-spatial neurons in both the dentate gyrus and CA1 have been shown to contribute to a population code of space that contains information about position, direction, and speed of an animal (Stefanini et al., 2020). Similarly, when exposed to a familiar or a novel environment, a substantial fraction of dentate gyrus neurons selectively only fire in one of the two environments at all, allowing to decode the spatial environment from neuronal activity without accounting for the spatial modulation of the individual neurons (Allegra et al., 2020). Thus, the cognitive map can be built not only from place cells, but also from neurons that individually do not show any apparent spatial modulation.

Previous theoretical work has predicted that the cognitive map is built from distinct contributions from different hippocampal subregions, where CA1 relies on positional cues, while the dentate gyrus uses navigation-relevant landmarks (Hoang et al., 2018; Jacobs and Schenk, 2003; Lee et al., 2012). Furthermore, it has been proposed that the content ('what') and the location ('where') of an event are differentially processed within hippocampal subregions (Chawla et al., 2005; Hoang et al., 2018). These predictions were made based on functional and anatomical distinctions between the 'what' and 'where' pathway in the dentate gyrus, CA3, and CA1 subregions (Amaral and Witter, 1989; Burke et al., 2011; Chawla et al., 2005; Henriksen et al., 2010). Consistent with this hypothesis, immediate early gene (IEG) expression indicates that distal CA1 and proximal CA3, but not the dentate gyrus,

may respond to positional cues. By contrast, the dentate gyrus and proximal CA3, but not CA1, may respond to directional cues (Hoang et al., 2018). However, these predictions have not been directly tested yet by assessing how variables such as contextual selectivity, directional, and positional information are processed and transformed along the hippocampal circuit. Given the projection patterns of the sources of this information to different hippocampal subregions, we hypothesize that these information streams are processed differently along the hippocampal circuit, similarly to other brain systems that show hierarchical processing (Felleman and Van Essen, 1991). Testing this hypothesis requires recording neuronal activity from identified hippocampal subregions during navigation under identical task conditions. To tackle this challenge, we perform single-photon widefield microendoscope calcium imaging from the dentate gyrus, CA3 and CA1 hippocampal subregions in mice freely navigating along a linear track. We find that spatial representations in all areas depend on the direction of travel. Furthermore, representations in DG and CA3 are significantly more selective for directional context than area CA1. In addition to strong selectivity, spatial representations in the dentate gyrus are also highly correlated after aligning them to the direction of travel, indicating that distance covered is represented in egocentric coordinates in this region. Together with decoding of population activity, our results suggest that spatial representations evolve from egocentric representations in the dentate gyrus towards segmented allocentric maps in area CA1. Our findings are consistent with the notion that the dentate gyrus and CA3 regions are highly selective for spatial context. They are also compatible with theories of the cognitive map where the dentate gyrus provides egocentric information, while downstream regions then construct an allocentric positional cognitive map of space.

RESULTS

Single-photon microendoscope calcium imaging in mice freely navigating along a linear track.

To explore how different hippocampal subregions construct a representation of space, we recorded neuronal activity from the dentate gyrus, CA3 and CA1 hippocampal subregions using microendoscope single-photon calcium imaging in freely navigating mice. We first implanted a gradient-index (GRIN) lens above the hippocampal subregion of interest (Fig 1). We then proceeded to record neuronal population activity while the mice navigated spontaneously back and forth along a

linear track during 10-minute sessions on multiple days (Fig. 2). The 60-cm linear track was enriched with visual cues (eg. playing cards) on the walls as well as Lego bricks at the extremities of the track. This approach allowed us to record neuronal activity from all three identified hippocampal subregions in freely navigating animals.

Figure 1

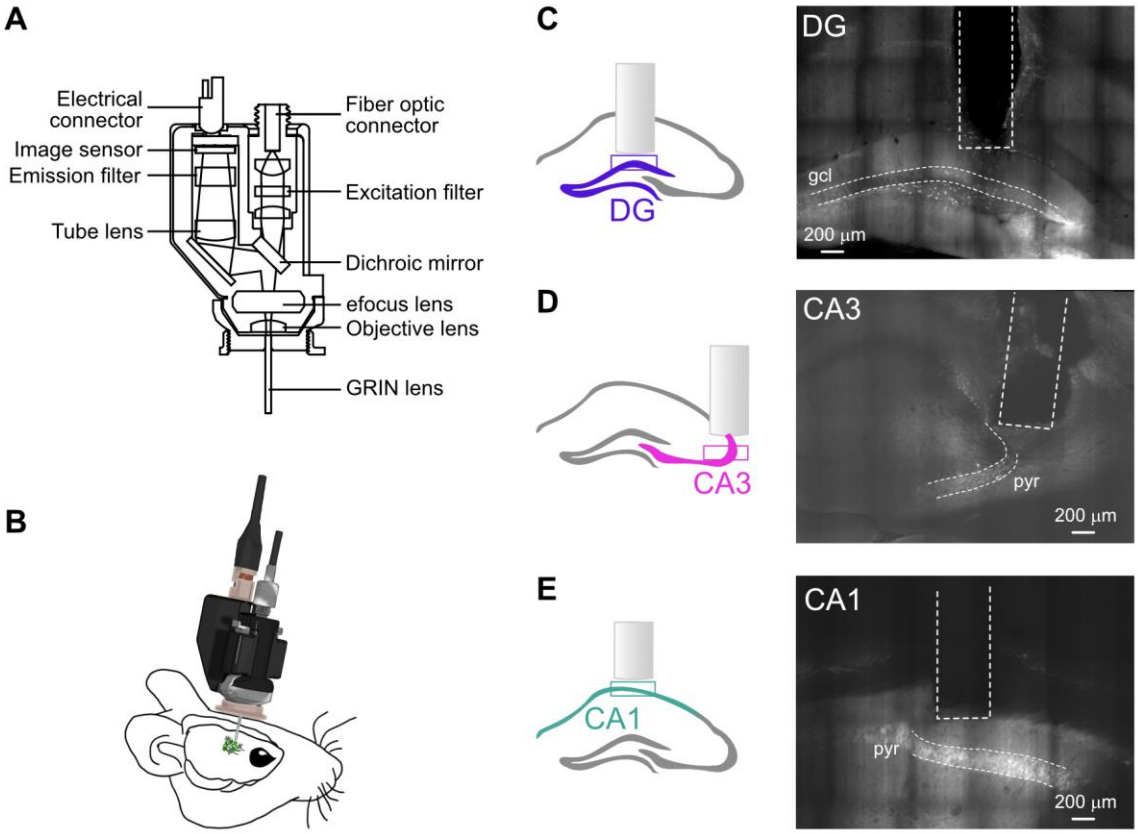

Figure 1. Experimental approach for *in vivo* Ca^{2+} imaging through a microendoscope

(**A**) Schematic of the microendoscope (Doric efocus) allowing electronic focussing. (**B**) Cartoon of a mouse implanted with a microendoscope for performing *in vivo* Ca^{2+} imaging through a GRIN lens. (**C**) Left, schematic of the imaging implant in the dentate gyrus. Right, representative confocal image of the GRIN lens position above GCaMP6f-expressing neurons in the dentate gyrus. (**D**) Left, same as C left but for CA3. Right, same as C right but for CA3. (**E**) Left, same as C left but for CA1. Right, same as C right but for CA1. The dotted lines highlight the specific imaged region. gcl: granule cell layer; pyr: pyramidal layer.

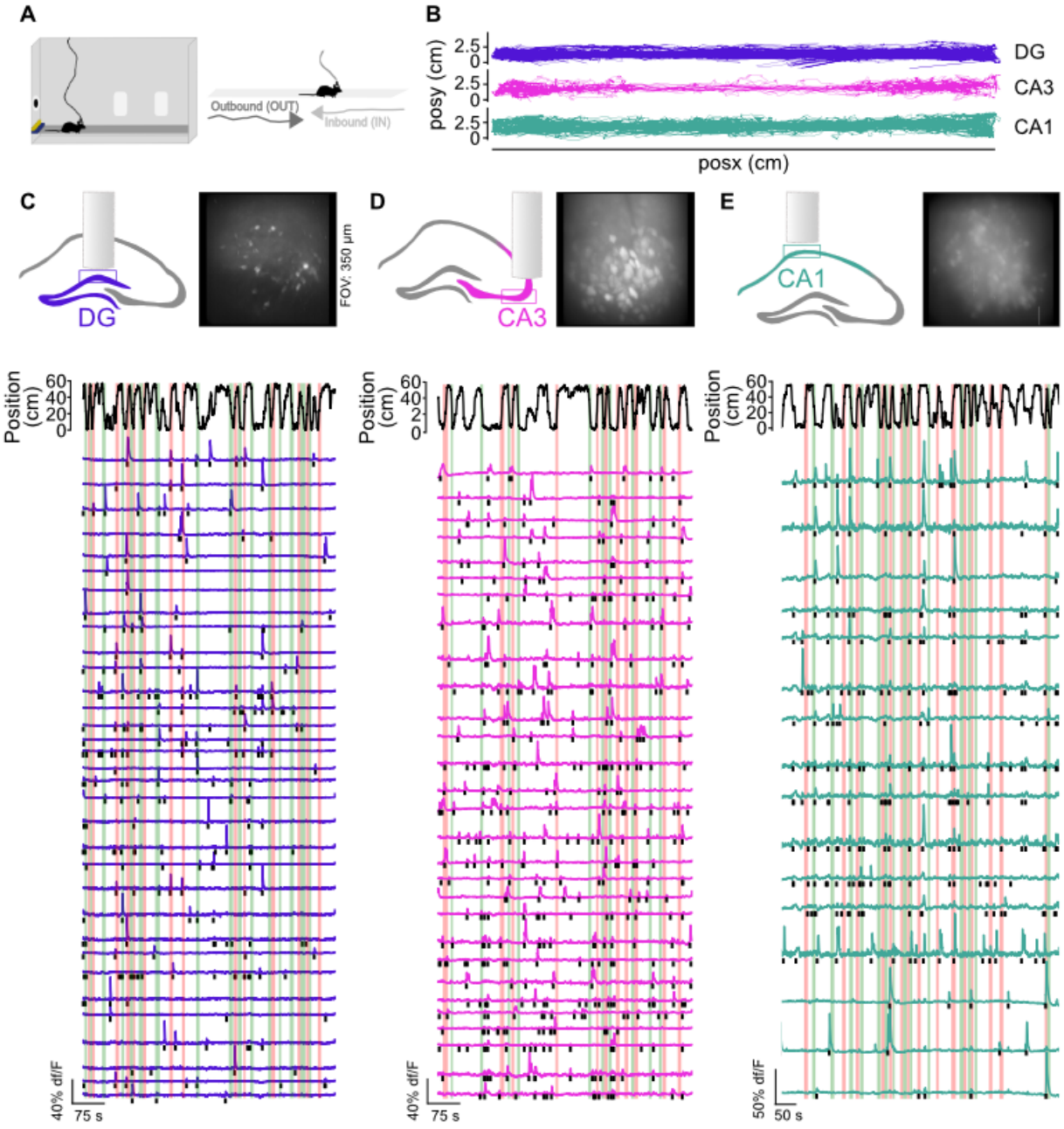

Figure 2. Single-photon imaging from hippocampal subregions in freely moving animals.

(**A**) Schematic of the experimental setup illustrating a mouse freely navigating along a linear corridor (left) in outbound (OUT) and inbound (IN) running directions (right). (**B**) Trajectory of three example mice along the 60-cm linear track. (**C**) Top: schematic of the imaging implant in the dentate gyrus (left) and a representative maximum projection of GCaMP6f-expressing granule cells during an *in vivo* recording session (right). FOV: field of view. Bottom: representative imaging session showing animal speed and motion direction along the linear track. The bottom traces show fluorescence extracted from regions of interest (ROIs) of an example recording session in the DG. The black tick marks indicate detected activity events during running periods. The red and green vertically shaded regions highlight inbound or outbound running directions. (**D**) Same as C but for CA3. (**E**) Same as C but for CA1.

Spatial representations are modulated by the direction of motion in DG, CA3, CA1

To identify how spatial activity is modulated by the running direction, we split the neuronal activity depending on the direction of motion of the animal (Fig 3A, C and E). We first quantified the fraction of spatially modulated cells, which was similar across the three regions (Fig S1). We then compared spatial activity maps for the same running directions by splitting laps into odd and even traversals and comparing map correlations for even laps with correlations for odd laps for a given direction (IN (odd-even) and OUT (odd-even); Fig 3B,D,F left panels). The dentate gyrus, CA3 and CA1 showed a pronounced correlation for spatial activity maps in the same direction (Fig 3B,D,F middle panel and Fig 3G; $p > 0.05$ between IN (odd-even) and OUT (odd-even)). We then compared correlations between spatial activity maps for traversals in the same direction with correlations between spatial activity maps for traversals in opposite directions and found a lower correlation in opposite directions in all three regions (Fig 3B,D,F and G; $p < 0.01$). Comparable results were found for both spatially modulated and unmodulated cells (Fig 3I). To determine how directional spatial representations evolve along the hippocampal circuits, we directly compared the three hippocampal subregions by measuring the spatial decorrelation (e.g. the reduction in correlation). No significant difference was observed between the three hippocampal subregions, regardless of whether only spatially modulated or all cells were included (Fig 3H and 3J). Overall, these results indicate that all three hippocampal subregions show directional spatial representations along the linear track.

Supplementary Figure 1

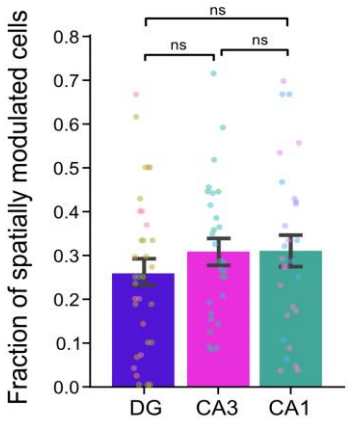

Figure S1. Supplement to Figure 3.

Fraction of spatially modulated cells in DG, CA3 and CA1 (DG, 0.26 ± 0.03; CA3, 0.31 ± 0.03; CA1, 0.31 ± 0.04; DG vs CA3, $p = 0.78$; DG vs CA1, $p = 0.86$; CA3 vs CA1, $p = 1.00$). ns, not significant.

Figure 3

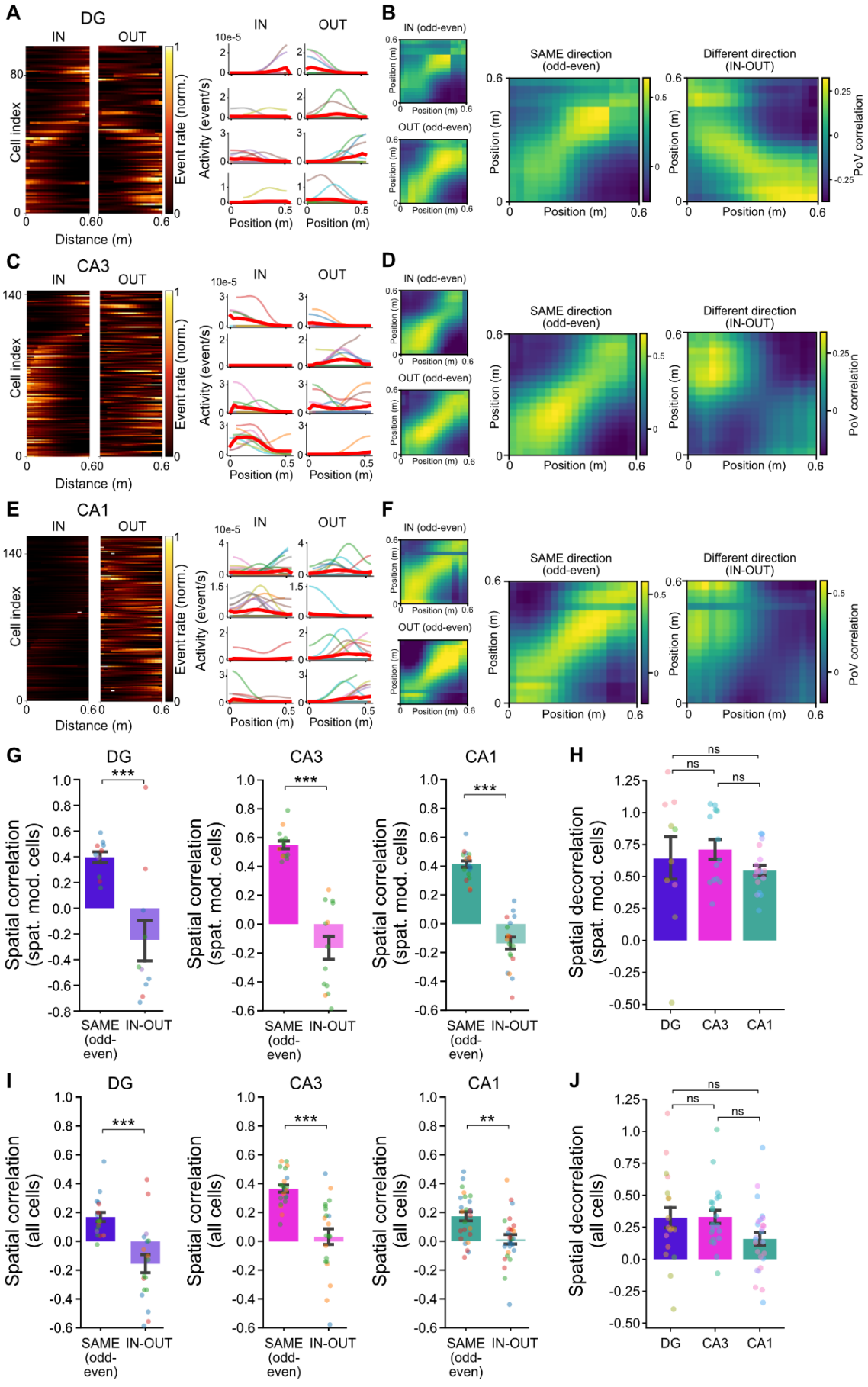
A
DG
IN
OUT
Cell index
Event rate (norm.)
Distance (m)
Activity (event/s)
Position (m)
B
IN (odd-even)
OUT (odd-even)
SAME direction (odd-even)
Different direction (IN-OUT)
PoV correlation
C
CA3
D
E
CA1
F
G
DG
CA3
CA1
Spatial correlation (spat. mod. cells)
SAME (odd-even)
IN-OUT
***
H
Spatial decorrelation (spat. mod. cells)
ns
I
Spatial correlation (all cells)
**
J
Spatial decorrelation (all cells)

Figure 3. Spatial representations are modulated by running direction in all hippocampal subregions.

(**A**) Left: pair of spatial activity maps of all spatially modulated neurons in DG sorted by the position of maximal activity in the left map (inbound direction). Right: spatial activity map of four example neurons. (**B**) Left: Spatial population vector (PoV) correlation matrices for inbound (top) and outbound (bottom) running directions in the DG. PoV correlations were computed for each spatial bin in the even lap crossings (x axis) with each bin in the odd lap crossings (y axis). Right: Spatial PoV correlation matrices for same (left, SAME odd-even) and different (right, IN-OUT) running directions in the DG. (**C, D**) Same as A-B but for CA3. (**E, F**) Same as A-B but for CA1. (**G**) Correlations between mean spatial activity maps across recording sessions within the same direction (SAME even-odd) and between different directions (IN-OUT) in the DG (left, spatial correlation: SAME even-odd, 0.39 ± 0.04; IN-OUT, -0.25 ± 0.17; Wilcoxon test, $p = 7 \times 10^{-7}$), CA3 (middle, spatial correlation: SAME even-odd, 0.549 ± 0.03. IN-OUT, -0.16 ± 0.08; Wilcoxon test, $p = 3 \times 10^{-6}$) and CA1 (right, spatial correlation: SAME even-odd, 0.41 ± 0.02; IN-OUT, -0.13 ± 0.04; Wilcoxon test, $p = 3 \times 10^{-6}$). PCs: spatially modulated cells. (**H**) Spatial decorrelation, quantified as the difference between spatial correlations within the same direction (even-odd) and between different directions (inbound and outbound) in spatially modulated neurons in the DG (0.64 ± 0.17), CA3 (0.71 ± 0.08) and CA1 (0.55 ± 0.04). No differences have been found between the three hippocampal subregions (DG vs CA3: ANOVA with Bonferroni correction, p = 0.99; DG vs CA1: ANOVA with Bonferroni correction, p = 0.99; CA3 vs CA1: ANOVA with Bonferroni correction, p = 0.16). (**I**) Same as G but including both spatially modulated and unmodulated cells in the DG (SAME even-odd, 0.17 ± 0.03; IN-OUT, -0.16 ± 0.06; Wilcoxon test, $p = 2 \times 10^{-6}$), CA3 (SAME even-odd, 0.36 ± 0.03; IN-OUT, 0.03 ± 0.06; Wilcoxon test, $p = 4 \times 10^{-6}$) and CA1 (SAME even-odd, 0.17 ± 0.03; IN-OUT, 0.01 ± 0.03; Wilcoxon test, p = 0.002). (**J**) Same as H but including both spatially modulated and unmodulated cells in the DG (0.35 ± 0.08), CA3 (0.33 ± 0.05) and CA1 (0.16 ± 0.05). No differences have been found between the three hippocampal subregions (DG vs CA3: ANOVA with Bonferroni correction, p = 0.99; DG vs CA1: ANOVA with Bonferroni correction, p = 0.25; CA3 vs CA1: ANOVA with Bonferroni correction, p = 0.08). Bars represent mean ± SEM. Circles represent recording sessions color-coded for each animal (DG, n = 10 sessions from 5 animals; CA3, n = 13 sessions from 3 animals; CA1, n = 18 sessions from 4 animals). ns, not significant; **, $p < 0.01$; ***, $p < 0.001$.

Selectivity for running direction is higher in DG and CA3 than in CA1

Activity in the dentate gyrus has been reported to be highly selective for the environmental context (Allegra et al., 2020; Neunuebel and Knierim, 2014). We wondered whether such selectivity would also be reflected by overall changes in firing rates across running directions. To assess whether distinct hippocampal subregions show selective activity for different running directions within the same environment, we quantified relative differences in event rates during runs in one vs the other direction, without accounting for the spatial modulation of individual neurons. We found that context (directional) selectivity was highest in the DG and CA3 (Fig 4A ; DG vs CA3, $p > 0.05$). Consistent with previous reports of CA1 showing low context selectivity (Allegra et al., 2020; Leutgeb et al., 2004; Neunuebel and Knierim, 2014), CA1 selectivity for running direction was lower than in the dentate gyrus ($p < 0.01$) and in CA3 ($p < 0.01$). Sparse firing in the dentate gyrus may contribute to its high selectivity, as we found lower activity in the dentate gyrus compared to CA3 and CA1 (Fig 4B; DG vs CA3, $p < 0.05$; DG vs CA1, $p > 0.05$; CA3 vs CA1, $p > 0.05$). In contrast, activity rates in CA3 and CA1 were similarly high. To verify whether the higher selectivity for running directions in the DG may arise from its sparse coding, we computed the expected selectivity from a shuffled version of the experimental dataset. We found that selectivity in the DG was comparable to the selectivity expected from the shuffled dataset ($p > 0.05$). By contrast, selectivity in

CA3 was higher than expected from the bootstrap dataset ($p < 0.001$). Together, these results reveal that selectivity for running directions is highest in the DG and CA3. Furthermore, sparse firing can explain the high selectivity in the DG but not in CA3, which may inherit selectivity from the upstream DG.

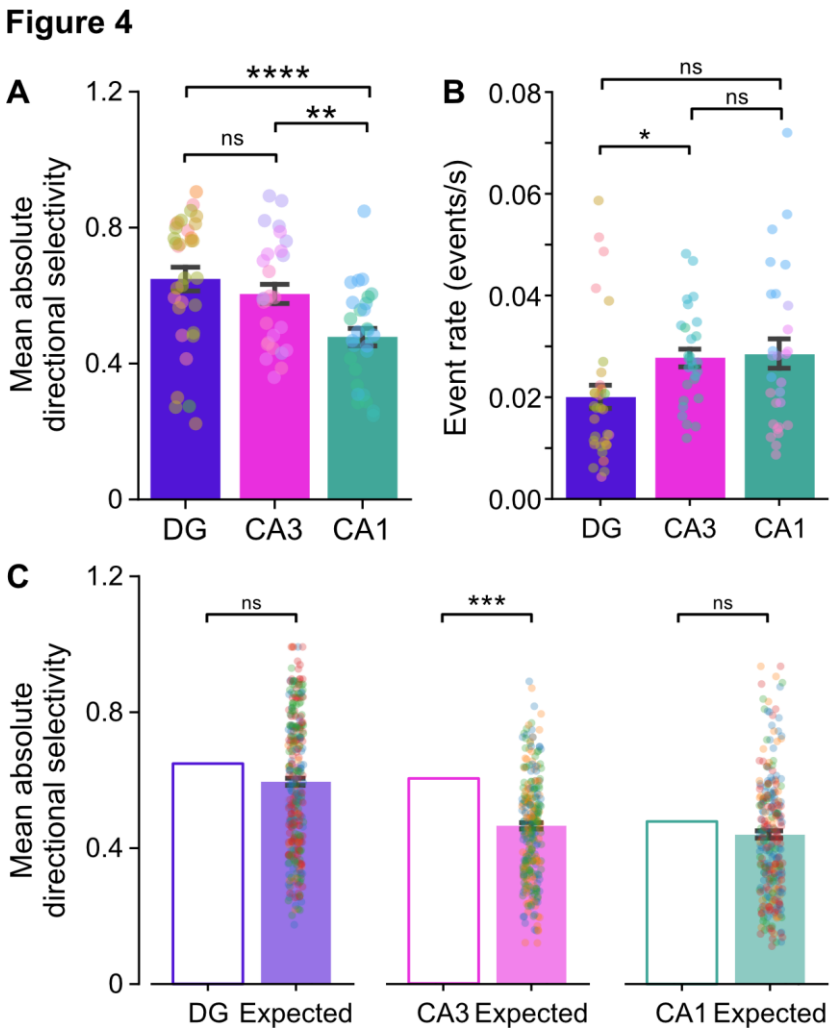

Figure 4. Selectivity for running direction is higher in DG and CA3 than CA1

(**A**) Absolute selectivity for running direction in DG (0.65 ± 0.03), CA3 (0.60 ± 0.03) and CA1 (0.48 ± 0.03). Absolute selectivity was higher in both DG and CA3 compared to CA1 (DG vs CA1: ANOVA with Bonferroni correction, p = 0.0008; CA3 vs CA1, ANOVA with Bonferroni correction, p = 0.008), whereas DG and CA3 showed comparable levels (DG vs CA3, ANOVA with Bonferroni correction, p = 0.99). (**B**) Event rate in the three hippocampal subregions (left; DG, 0.020 ± 0.002; CA3, 0.028 ± 0.002; CA1, 0.028 ± 0.003. DG vs CA3, ANOVA with Bonferroni correction, p = 0.04; DG vs CA1, ANOVA with Bonferroni correction, p = 0.08; CA3 vs CA1, ANOVA with Bonferroni correction, p = 0.99). (**C**) Absolute selectivity for running direction compared to a bootstrap dataset (expected selectivity) within each region (left: DG, same as A; expected, 0.59 ± 0.01, p = 0.14; middle: CA3, same as A; expected, 0.46 ± 0.01, p = 7 x 10^{-6}; right: CA1, same as A; expected, 0.44 ± 0.01, p = 0.26). Bars represent mean ± SEM. Circles represent recording sessions color-coded for each animal (DG, n = 33 sessions from 5 animals; CA3, n = 28 sessions from 3 animals; CA1, n = 28 sessions from 4 animals). ns, not significant; *, p < 0.05; **, p < 0.01; ***, p < 0.001.

The dentate gyrus uses distance coding to build spatial representations

While spatial representations in all regions were uncorrelated between different running directions, we noticed that population vector correlations in the dentate gyrus were correlated when one of the running directions was reversed (Fig. 3B). This observation suggests that representations at corresponding distances measured from the starting point of a track traversal are preserved, indicating that spatial firing is tuned to the distance covered by the animal rather than to allocentric positional coordinates. To quantify this observation, we measured correlations between spatial activity maps for traversals in opposite directions after reversing the order ("flipping") of the maps for the outbound direction (Fig 5). We found that the dentate gyrus showed substantial correlations between flipped maps that were on the order of the correlations observed between maps for the same running direction (Fig 5C,F; $p > 0.05$). The same result was obtained when including all cells, both spatially modulated and unmodulated (Fig 5H; correlation value: $p > 0.05$). This finding is consistent with the notion that neuronal activity in the dentate gyrus encodes covered distance along the track in either running direction. By contrast, no substantial correlations between flipped maps were observed in the downstream region CA3 (Fig 5D,F). In this region, the correlation of the flipped maps was lower than correlation in the same direction, independently of whether all cells or only spatially modulated cells were included in the analysis (Fig 5F and H; $p < 0.01$ in both cases). In CA1, a significant difference was observed between flipped maps and maps of the same direction when including spatially modulated cells only (Figs 5E,F; $p < 0.01$), but the correlation between flipped maps was not significant when including all cells (Fig 5H; $p > 0.05$). We defined a measure of distance coding by subtracting the correlation value of the maps in opposite directions from the correlation values of the flipped maps, and found that when selecting spatially modulated cells exclusively, the measure of distance coding was not significantly different between hippocampal subregions (Fig 5G; $p > 0.05$). However, when selecting all cells, the measure of distance coding was significantly more pronounced in the DG than in the other regions (Fig 5I; $p < 0.01$). Overall, these results indicate that at the single-cell level, during track crossings in different directions, spatial firing fields in the DG appear at equivalent locations in egocentric coordinates, suggesting that they represent the distance that the animal has covered from its starting point rather than position in allocentric coordinates of the external world.

Figure 5

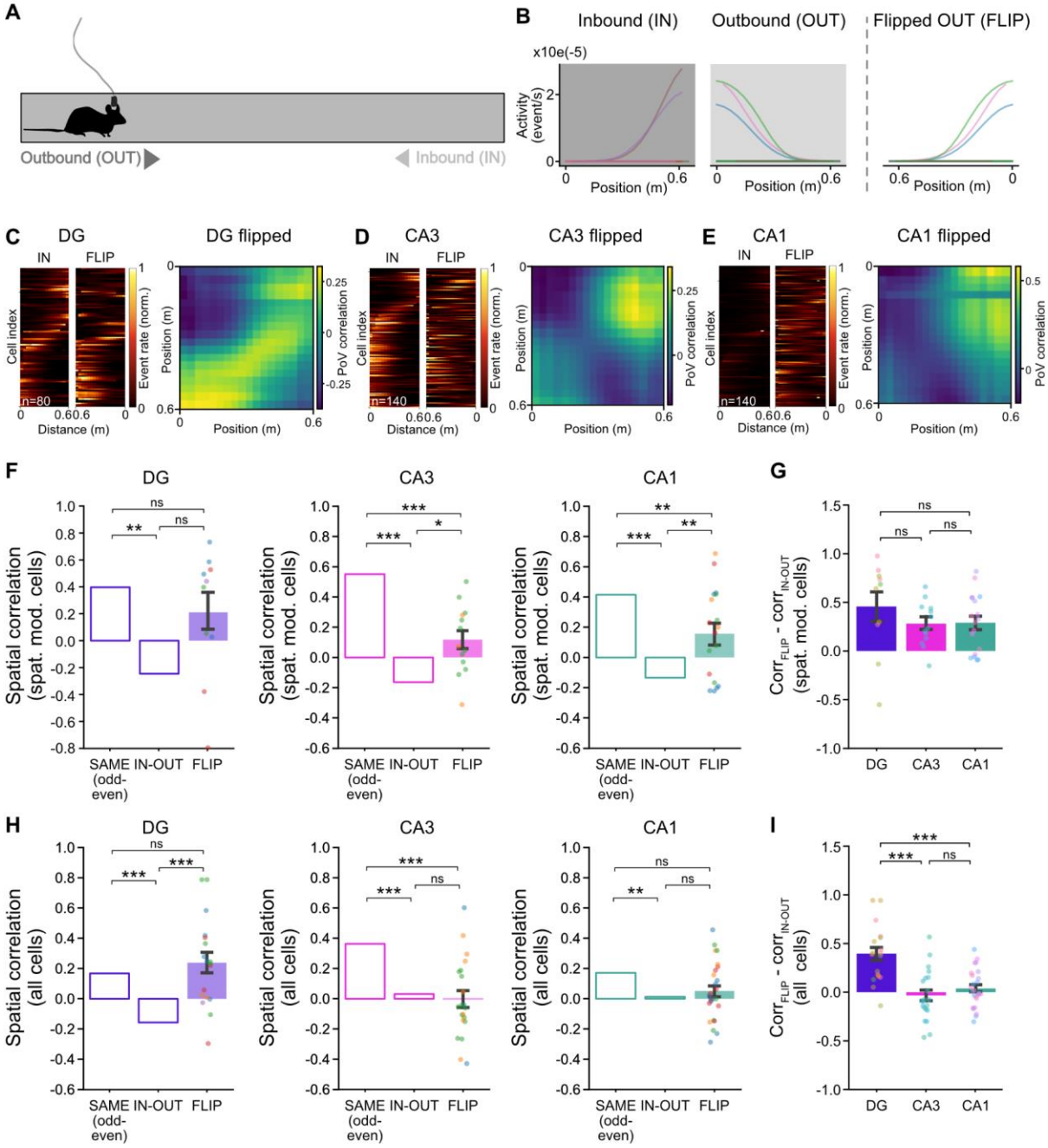

Figure 5. Spatial information in DG reflects distance coding in egocentric coordinates.

(**A**) Schematic of a mouse freely navigating along a linear corridor in outbound (OUT) and inbound (IN) running directions. (**B**) Spatial activity maps for an example cell in inbound (IN, left), outbound (OUT, middle) and flipped outbound running directions (FLIP, right). (**C**) Left: pair of spatial activity maps of all spatially modulated neurons in DG sorted by the position of maximal activity in the left map (inbound direction). Right: spatial population vector (PoV) correlation matrices for inbound and flipped outbound running direction in the DG. PoV correlations were computed for each spatial bin in the inbound lap crossings (x axis) with each bin in the flipped outbound lap crossings (y axis). (**D**) Same as C but for CA3. (**E**) Same as C but for CA1. (**F**) Correlations between mean spatial activity maps across recording sessions within the same direction (SAME even-odd), between different directions (IN-OUT) and between inbound and flipped outbound directions in the DG (left, spatial correlation: same dataset as Fig 3G left, FLIP, 0.21 ± 0.15; SAME odd-even vs IN-OUT, p = 0.005; IN-OUT vs FLIP, p = 0.17; SAME odd-even vs FLIP, p = 0.78), CA3 (middle, spatial correlation: same data as Fig 3G middle, FLIP, 0.12 ± 0.06; SAME odd-even vs IN-OUT, $p = 7 \times 10^{-8}$; IN-OUT vs FLIP, p = 0.04; SAME odd-even vs FLIP, $p = 5 \times 10^{-6}$) and CA1 (right, spatial correlation: same dataset as Fig 3G right, FLIP, 0.16 ± 0.07; SAME odd-even vs IN-OUT, $p = 1 \times 10^{-12}$; IN-OUT vs FLIP, p = 0.003; SAME odd-even vs FLIP, p = 0.004). Bars represent mean ± SEM. Circles represent recording sessions color-

coded for each animal. (**G**) Quantification of the difference between spatial correlations within the flipped (inbound-flipped outbound, FLIP) and different (inbound-outbound, IN-OUT) directions in the DG (0.46 ± 0.15), CA3 (0.28 ± 0.06) and CA1 (0.29 ± 0.07). No statistically significant differences were found between the three hippocampal subregions (DG vs CA3: p = 0.77; DG vs CA1, p = 0.80; CA3 vs CA1, p = 1.00). (**H**) Same as F but including both spatially modulated and unmodulated cells in the DG (same data as Fig 3I left, FLIP, 0.24 ± 0.07; SAME odd-even vs IN-OUT, p = 0.0003, IN-OUT vs FLIP, p = 0.0006; SAME odd-even vs FLIP, p = 0.99), CA3 (same data as Fig 3I middle, FLIP, -0.001 ± 0.06; SAME odd-even vs IN-OUT, $p = 1 \times 10^{-5}$; IN-OUT vs FLIP, p = 0.99; SAME odd-even vs FLIP, $p = 2 \times 10^{-6}$) and CA1 (same data as Fig 3I right, FLIP, 0.05 ± 0.04; SAME odd-even vs IN-OUT, p = 0.004; IN-OUT vs FLIP, p = 0.99; SAME odd-even vs FLIP, p = 0.99). (**I**) Same as G but including both spatially modulated and unmodulated cells in the DG (0.39 ± 0.07), CA3 (-0.03 ± 0.06) and CA1 (0.04 ± 0.04). The difference between the spatial correlations within flipped (FLIP) and opposite (IN-OUT) directions was significantly higher in DG than in CA3 and CA1 (CA3 vs DG, $p = 7 \times 10^{-5}$; DG vs CA1, $p = 4 \times 10^{-5}$), whereas no difference was found between CA3 and CA1 (p = 0.85). Bars represent mean ± SEM. Circles indicate single recorded sessions color-coded for each animal (DG, n = 10 sessions from 5 animals; CA3, n = 13 sessions from 3 animals; CA1, n = 18 sessions from 4 animals). ANOVA with Bonferroni correction: ns, not significant; *, $p < 0.05$; **, $p \leq 0.01$; ***, $p < 0.001$.

Transformation of population codes for position and distance along hippocampal circuits

Our analysis of spatial correlations of “flipped” maps indicates that in the dentate gyrus, but not in CA3 and CA1, individual neurons produce spatial representations consistent with an *egocentric* spatial representation, encoding the distance that the animal has travelled from its starting point rather than its allocentric position along the track. However, a low egocentric map correlation at the single-cell level does not imply that traveled distance is *not* represented in CA3 and CA1 activity, as these neural populations could employ different encoding schemes to jointly represent position and traveled distance. For example, separate coding schemes could be used to encode traveled distance at different running directions, resulting in low spatial “flip” correlations despite a high discriminability of different running distances.

To evaluate the extent to which egocentric and allocentric coordinates are represented in hippocampal populations, we isolated population activity vectors from the first and the last 20% of the track and labeled them according to both position and distance traveled. Then, we used a linear decoder to predict the value of these labels from population activity in a cross-validated decoding scheme (Stefanini et al., 2020) (Fig 6A). To ensure that the two variables were independently assessed, the decoder for one variable was performed on a balanced training set that did not favor any of the two values of the second variable. To do so, the decoder for position (divided into two conditions labeled as 0 and 1) was trained on a balanced mix of distance conditions (labeled as *start* and *end*) for each of the two position values: (0-*start* + 0-*end*) vs (1-*start* + 1-*end*) - and vice versa for the distance decoding analysis. Consistent with the findings on single-cell spatial remapping (Fig 5), our decoding analysis revealed that information on egocentric distance is more decodable than

allocentric position in the dentate gyrus ($p < 0.001$), whereas the opposite is true for CA1 activity ($p < 0.001$). Interestingly, despite the low flipped spatial correlation, we found that neuronal activity in CA3 represents both variables similarly well ($p > 0.5$), suggesting that CA3 employs different coding strategies for egocentric and allocentric position in different running directions, while DG and CA1 primarily encode egocentric and allocentric position, respectively.

Figure 6

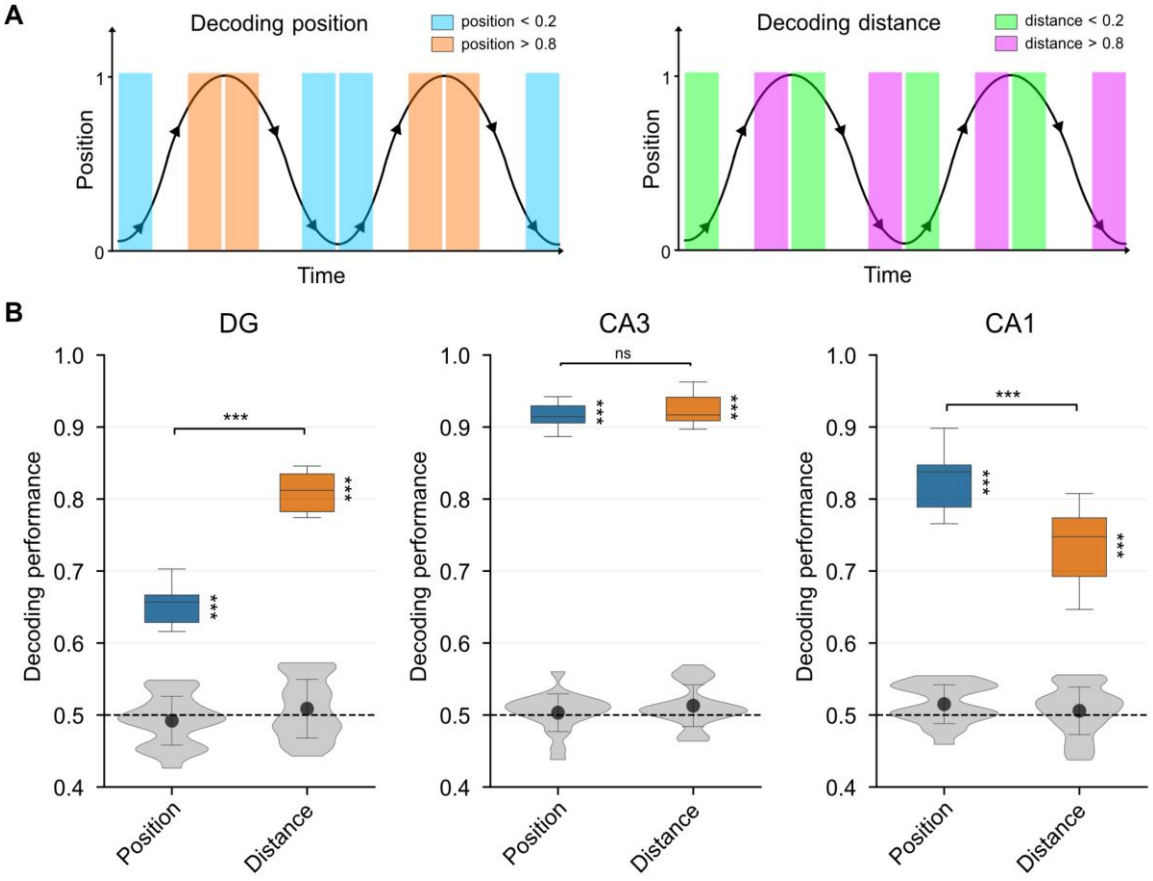

Figure 6. Transformation of population codes for egocentric position and allocentric distance along hippocampal circuits

(**A**) Schematic of the different labeling of the neural data used for the decoding analysis of allocentric position (left) and egocentric traveled distance (right). In the two cases, neural data is the same but the label is changed according to different behavioral correlates. (**B**) Decoding performance obtained by the analysis in A for activity in the three recorded regions (mean decoding performance: DG, position, 0.65; distance, 0.81; $p < 0.001$; CA3, position, 0.91; distance, 0.92; $p > 0.05$; CA1, position, 0.83; distance, 0.73; $p < 0.001$). Box plots show the distribution for n=25 cross-validation folds using pseudo-simultaneous activity built from all animals combined. Grey violin plots show decoding results for a shuffled dataset (see Methods). Significance levels are computed by a Mann-Whitney U test (ns, not significant; ***, $p < 0.001$).

DISCUSSION

In this study, we explore how representations of spatial position, running direction, and distance evolve along the hippocampal circuit. By performing single-photon calcium imaging from the dentate gyrus, CA3, and CA1, we provide one of the first descriptions of these representations in all major hippocampal subregions under the same task conditions in freely moving animals. We find that in mice spontaneously running back and forth along a linear track, all regions display directionality in their spatial firing patterns, with spatial activity maps for the two opposing running directions being almost completely uncorrelated. However, when spatial modulation is not taken into account, neuronal activity in the dentate gyrus and in CA3 is more selective for the direction of running than activity in CA1. Furthermore, activity in the dentate gyrus shows pronounced correlations of spatial activity maps after aligning them to the running direction, indicating that it encodes covered distance in egocentric coordinates. Consistently, decoding of population responses suggests that hippocampal representations evolve from primarily egocentric representations in the dentate gyrus to allocentric representations in CA1.

Directional modulation of spatial activity and selectivity in hippocampal subregions

Hippocampal neurons are known to change the location of their spatial firing fields to represent a novel environment or contextual changes within a given environment (Anderson and Jeffery, 2003; McNaughton et al., 1983; Muller and Kubie, 1987; Navratilova et al., 2012). Here, we measured the ability of neuronal populations to discriminate distinct environments by quantifying the correlations of spatial activity maps across running directions. To promote directional representations, we make use of a narrow linear track, where directional modulation is known to be particularly pronounced (McNaughton et al., 1983; Navratilova et al., 2012). We find that in the DG, CA3 and CA1, spatial activity maps are modulated by the direction of running of the animal (outbound and inbound), consistent with previous reports (Jung and McNaughton, 1993; Navratilova et al., 2012; Schwindel et al., 2016). Our data indicate that the directional spatial modulation is implemented through changes in the location of firing fields in an allocentric coordinate system, in a process called ‘global remapping’. The hippocampus might therefore construct, at least partially, a spatial representation of the inbound and outbound trajectories as two distinct contexts.

To assess directional discrimination independently of the spatial modulation of

individual neurons, we quantified “directional selectivity” as the relative difference in firing rates between the two running directions. Our findings show that this directional selectivity varies along the hippocampal circuit and is more pronounced in the dentate gyrus and CA3 than in CA1 (Fig. 3). This observation is consistent with previous reports of high context selectivity in the dentate gyrus (Allegra et al., 2020; Neunuebel and Knierim, 2012) and selectivity for running direction in both the dentate gyrus and CA3 (Jung and McNaughton, 1993; Schwindel et al., 2016). We show that in the dentate gyrus, selectivity is not significantly different from that expected from a bootstrap dataset. This result agrees with previous experimental evidence that selectivity in the dentate gyrus is implemented by sparse coding (GoodSmith et al., 2017; Jung and McNaughton, 1993; Neunuebel and Knierim, 2012). Sparse coding allows the dentate gyrus to orthogonalise ambiguous spatial inputs by mapping spatial environments onto non-overlapping pools of active cells. Conversely, selectivity in CA3 differs significantly from the bootstrap, suggesting that another neural mechanism is at play in CA3 to generate high selectivity for running direction. For example, the high selectivity for running direction observed in CA3 could be inherited from the DG.

Our data show that CA1 is less selective for running direction than the DG and CA3, but do not rule out that CA1 might represent changes in contextual information by more subtle changes in its firing rates (McNaughton et al., 1983; Navratilova et al., 2012). However, these firing rate changes might be less pronounced than firing rate changes in CA3 and in the dentate gyrus, where they can reach up to an order of magnitude (Leutgeb et al., 2007, 2005), possibly to limit interference between resembling environments and events (Colgin et al., 2008). It is important to note that fine-grained rate changes are difficult to assess with single-photon *in* vivo calcium imaging, as individual spikes cannot easily be resolved, and therefore smaller changes in firing rates might be missed.

Lower selectivity for running direction in CA1 than in CA3 and DG is consistent with recent work showing that CA1 is less selective for context than the dentate gyrus and responds to environmental features common to both environments (Allegra et al., 2020; Leutgeb et al., 2007, 2004, 2005; Schwindel et al., 2016). Low selectivity for running direction might therefore indicate that CA1 constructs a global representation of the environment, consistent with reports that CA1 represents abstract information relative to the environment and shows activity that is correlated with the animal’s behaviour (Allegra et al., 2020; Plitt and Giocomo, 2021). These findings offer a possible interpretation of our results of low selectivity for running direction, whereby

CA1 might construct a representation of the environment that is relevant to the animal's behaviour, such as the entirety of the linear track, rather than one-way trajectories. CA1 could for example encode temporal parameters such as sequences and task phases (Dragoi and Buzsáki, 2006; Griffin et al., 2007), memories of recent experiences (Keinath et al., 2020) or future paths of the animal (Keinath et al., 2020; Leutgeb and Leutgeb, 2007; Miao et al., 2015; Stachenfeld et al., 2017). Such a coding scheme would result in relatively low selectivity for directions, yet strong directional modulation of the spatial activity maps, as similar aspects of the task would be encountered in both directions of the track, but at different allocentric positions.

The notion that CA1 produces allocentric maps of the environment that are segmented by running direction, but bound together by task, experience, and predictions, can be related to previous work showing that CA1 switches between different stable spatial maps of the same environment (Sheintuch et al., 2020). These findings offer a possible interpretation of our results, whereby directionally selective spatial maps in CA1 correspond to fragmented spatial maps of the global environment. In this scenario, CA1 would be switching between stable spatial maps for each running direction in order to construct a global representation of the environment.

Origin of directional signals

One possible source of directionally tuned inputs to the hippocampus might be head-direction cells that are located in the MEC (Sargolini et al., 2006). Alternatively, directionally tuned inputs to the hippocampus might be provided by grid cells. Even though grid cells are not tuned to a single direction, they show modulation by head direction in a location-dependent manner (Gerlei et al., 2019). Grid cells are most abundant in layer II of the MEC and while they only represent a minority of MEC neurons (10/20%) that project to the hippocampus (Diehl et al., 2017; Kitamura et al., 2015; Sargolini et al., 2006; Zhang et al., 2013), the MECII projects heavily to the dentate gyrus and provides the main source of EC inputs to CA3 (Kerr et al., 2007; Witter and Amaral, 1991; Witter et al., 2000). A second type of grid cells might also provide directionally tuned inputs to the hippocampus: a majority of grid cells located in MEC III and V show conjunctive coding of position and direction (Sargolini et al., 2006). The MEC III projects to CA1 (Li et al., 2017) and might provide CA1 with a source of directionally tuned inputs. By contrast to the DG and CA1, the source of

directionally tuned inputs remains to be elucidated, since the connectivity patterns between the EC and CA3 vary across species: the rat CA3 receives inputs from ECII (Dolorfo and Amaral, 1998; Kerr et al., 2007; Steward, 1976), while the mouse CA3 receives inputs from ECIII (van Groen et al., 2003). It is possible that hippocampal neurons receive multiple sources of inputs such that the dentate gyrus and CA3 receive directionally tuned inputs from grid cells in MEC II while CA1 receives directionally tuned inputs from conjunctive coding grid cells in MEC III. Such a dual nature of directionally tuned inputs to the hippocampus might explain why the dentate gyrus and CA3 are selective for running direction based on firing rates but not CA1.

By contrast to head-direction cells in other brain regions, it is thought that directional tuning is not a fundamental firing property of hippocampal neurons, and may instead arise from experience-dependent learning. This notion is based on the variability of directional firing in hippocampal neurons (McNaughton et al., 1983; Muller et al., 1994; Navratilova et al., 2012; Schwindel et al., 2016) and the modulation of directional firing by different factors such as experience (McNaughton et al., 1983; Navratilova et al., 2012; Schwindel et al., 2016) and the availability of local cues (Battaglia et al., 2004). Directional tuning of hippocampal neurons may therefore arise from non-homogeneous distributions of head direction signals caused by differences in the positions visited at different head directions, which may then lead to preferred firing in the running directions that have been encountered most (Muller et al., 1994). Related theoretical work has proposed that directional firing can be interpreted as a predictive code that emerges from repeated visits of the same running direction (Stachenfeld et al., 2017). Thus, directionality might also arise in hippocampal neurons *de novo* during experience, without necessarily requiring a precomputed directional signal as input.

Distance coding in the dentate gyrus

Our finding that spatial activity maps are decorrelated for different running directions in all three hippocampal subregions indicates that the environment is not represented in a single, allocentric reference frame when it is encountered in different running directions. However, we find that spatial activity maps for the dentate gyrus show substantial correlations after aligning them to the direction of running, which are on the order of the correlations observed between maps for the same running direction. This finding indicates that rather than encoding position of the animal in allocentric

coordinates, the dentate gyrus encodes distance run along the linear track. Such egocentric distance coding was not observed in other hippocampal regions. Notably, this observation is made when including all recorded cells, but not when selecting only spatially modulated cells, indicating that neurons that are not apparently spatially modulated play an important role in encoding distance run along the track to construct spatial representations. These results are consistent with previous reports of mixed selectivity and multiplexed coding in the dentate gyrus (Morris et al., 2013a, 2013b; Murano et al., 2020; Stefanini et al., 2020).

At first sight, high directional selectivity and distance coding appear contradictory, as distance coding requires neuronal activity at equivalent distances in both directions of running, and would therefore counteract directionally selective firing. We hypothesize that the two observations can be reconciled by rate changes of the distance-coding, “flipped” firing fields - i.e. the firing fields appear at equivalent distances, but with different rates. In addition, a separate population of dentate gyrus neurons shows complete selectivity (selectivity = 1) by only firing during runs in one direction, but not in the other, as has been described by previous reports about context selectivity in dentate gyrus neurons (Allegra et al., 2020; Cholvin et al., 2021). Thus, a combination of “flipped” rate change signals along with a population of purely directional neurons allows the dentate gyrus to reconcile high directional selectivity with distance coding.

What is the source of distance information?

While directional signals to the dentate gyrus might be provided by the MEC, where does information about distance arise? MEC neurons generate a dynamic representation of the animal’s position during navigation by integrating information about self motion (Campbell et al., 2018; Savelli et al., 2008; Solstad et al., 2008). Specifically, some MEC neurons are tuned to distance travelled and integrate self-motion information to modulate estimates of position (Campbell et al., 2021). MEC neurons are also sensitive to the distance that separates an animal from an object, which led to categorising a subpopulation of MEC neurons as ‘object-vector cells’ (Høydal et al., 2019). Integration of self-motion information was also reported in grid cells, which constitute a subpopulation of MEC neurons (Jacob et al., 2019; Kraus et al., 2015). Grid cells exhibit spatial representations that are highly dynamic and display mixed selectivity (Hardcastle et al., 2017) and it is thought that conjunctive coding of position, direction and distance updates grid coordinates during self-

motion-based navigation (Sargolini et al., 2006). The MEC projects to the dentate gyrus via the medial perforant path that contacts granule cell dendrites (Dolorfo and Amaral, 1998; van Groen et al., 2003; Kerr et al., 2007; Steward, 1976). The conversion of inputs from the entorhinal cortex to dentate gyrus is thought to enable fast encoding and efficient recall of spatio-temporal information (Cholvin et al., 2021). Consistent with the notion that distance signals are conveyed to the DG by the MEC, the MECII-DG pathway was shown to create a persistent representation of the behavioural task performed by the animal, based on learned visual cues and integration of positional and spatial information, suggesting that the MECII-DG pathway plays a crucial role in the representation of non-allocentric information (Cholvin et al., 2021; Qin et al., 2018).

Bearing versus sketch maps: the parallel maps theory

Our decoding of population activity confirms that the DG primarily produces egocentric representations, whereas CA1 mainly builds an allocentric map of the environment. Notably, we found that neuronal activity in CA3 similarly represents both ego- and allocentric variables at the population level, but not at the level of spatial activity maps in individual neurons. These results indicate that CA3 differentially encodes ego- and allocentric information as a function of running directions, and then binds these two streams of information together before transmitting them to CA1.

Our findings provide direct experimental evidence for several theories of how the hippocampus constructs the cognitive map along its circuits. First, our finding that the dentate gyrus encodes distance supports the view that it is required for aligning internally generated spatial representations to external landmarks, as has been suggested based on lesion experiments (Lee et al., 2012). Second, our finding that CA3 uses separate and parallel coding strategies to represent position and traveled distance is compatible with theoretical models where the place cell population creates a cognitive map by parallel integration of two different input streams of allocentric and egocentric information (Laptev and Burgess, 2019; Posani et al., 2018)**.** Finally, our results are consistent with the parallel maps theory, which predicts that the dentate gyrus constructs primarily a “bearing map” from self-movement and directional cues, whereas CA1 constructs a “sketch map” from positional cues (Jacobs and Schenk, 2003). In addition, our results are also compatible with the two-stream hypothesis, which describes a separation between the processing of

information relative to the content (‘what’) and the location (‘where’) of an event within hippocampal subregions (Hoang et al., 2018). Our results provide direct evidence for these predictions for the differential roles of hippocampal subregions in representing space, where the dentate gyrus provides egocentric navigational signals, CA3 binds ego- and allocentric streams of information and then transmits them to CA1, where a global segmented allocentric map of space is produced.

METHODS

Mice

All procedures were performed in accordance with European and French guidelines on the ethical use of animals for experimentation (EU Directive 2010/63/EU) after approval by the Institut Pasteur Ethics Committee (CETEA protocol number 160066). Wild-type male C57BL/6J mice from Janvier labs aged 6 to 39 weeks were used for all experiments. They were housed collectively or individually in a room maintained at 21C with a 12 h inverted light/dark cycle, in polycarbonate individually ventilated cages, enriched with running wheels, and *ad libitum* access to food and water. A total of 12 mice were used in this study.

Surgical procedures

The surgical procedures were performed at least 7 days after the arrival of the mice in the animal facility, and were carried out using a stereotaxic apparatus (Kopf instruments). Mice were anesthetized with isoflurane throughout the surgery (3/4% during induction and 1/2 % to during the remainder of the surgery**;** 2 l/minO2 and 0.2-0.5 l/minO2 respectively). An analgesic solution (buprenorphine, 0.05mg/kg i.p., Vetergesic) was administered at least 30 minutes prior to the surgical intervention. Incision sites were infiltrated with lidocaine at the start of the procedure. A second analgesic solution consisting of meloxicam (10 mg/kg s.c., Metacam) was administered prior to the end of the surgery. The body temperature of the mice was maintained at 36C using a heating pad, and their eyes were protected using a hydrating eye gel (Ocrygel). A postoperative analgesic solution (meloxicam 5mg/kg) was administered orally in combination with surgical recovery Dietgel (ClearH2O) for 2 days. The recovery of the mice was monitored for 72h.

Stereotaxic injections of viral vectors

The skin was first covered with Providone-iodine (Betadine) and then cut using a scalpel blade. A small craniotomy was then carried out above the right dorsal hippocampus (1.5mm lateral and 1.9mm posterior to Bregma). An injection of AAV1.Syn.GCaMP6f.WPRE.SV4 (500 nL; $3.4x10^{12}$ TU/mL, Addgene) was made in n=5 animals with DG implants, n=1 animal with a CA3 implant and n=2 animals with CA1 implants and an injection of AAV-CamKII-GCaMP6f-WRPE-SV40 (500 nL; ≥ $1×10^{12}$ vg/mL, Addgene) was made in n=2 animals with CA3 implants and n=2 animals with CA1 implants. The injection was carried out using an oil injection pump

and a glass micropipette at the injection site defined by the following stereotaxic coordinates: DG: 1.9 mm posterior from Bregma, 1.5 mm lateral from the midline and at 1.7 mm depth from the dural surface; CA3: 1.9 mm posterior from Bregma, 2.0 mm lateral from the midline and at 2.1 mm depth from the dural surface; CA3**:** 1.9 mm posterior from Bregma, 1.5 mm lateral from the midline and at 1.25 mm depth from the dural surface. Viral vector injection and GRIN lens implantation were either carried out simultaneously or separately to allow expression of the genetically-encoded calcium indicator and implantation under visual control. In instances where the injection and implant were carried out separately, mice recovered from the injection for at least 1 day before undergoing subsequent procedures.

Chronic GRIN lens implantation

To perform *in vivo* calcium imaging from the dentate gyrus, a Gradient Refractive Index Lens (GRIN lens) was implanted above the granule cell layer of the dentate gyrus, the pyramidal cell layer of CA3 or CA1 (Fig 1A-1C). GRIN lens implants were performed two to three weeks after viral injection. Mice were anesthetized (see surgical procedure), and the head position and angle was closely monitored to target the region of interest. Following application of Betadine on the skin surface and local analgesic, the skin covering the skull was cut using scissors and removed. Following cleaning of the exposed skull with saline solution, all overlying connective tissue was then cleared out by applying a green and a red activator (Super-bond C&B, Sun Medical) onto the exposed skull for one minute and thirty seconds, respectively**.** A craniotomy was performed (600-900 µm diameter) and the dura mater was removed. First, a stainless steel needle (500 µm diameter, custom-made, Phymep) was lowered down to 1.9 mm for DG, 2.15 mm for CA3 and 1.35 mm for CA1, at a rate of 400 µm/minute. Second, the imaging cannula was slowly lowered at a rate of 100 µm/minute into the implant site at the following target coordinates: DG: 1.9 mm posterior from Bregma, 1.5 mm lateral from the midline and at 1.9 mm depth from the dural surface; CA3: 1.9 mm posterior from Bregma, 2.0 mm lateral from the midline and at 2.15 mm depth from the dural surface; CA1: 1.9 mm posterior from Bregma, 1.5 mm lateral from the midline and at 1.35 mm depth from the dural surface. The procedure was performed blindly in n=1 animal with a DG implant and n=1 animal with a CA1 implant (using 0.5 mm diameter SICL_D_500_80 Snap-in Imaging Cannula, Model L-D Depth range: 0mm – 3.46 mm from Doric lenses) or under visual control of the microendoscope to increase the success rate of the implant in n=4 animals with DG implants, and n=3 animals with CA3 implants and n=3 animals with CA1 implants (using eSICL_D_500_80 Snap-in Imaging Cannula, eFocus, Model L-

D Depth range: 0 mm – 3.46 mm from Doric lenses; Fig 1D-1F). A focussing ring was screwed around the metallic headpost attached to the lens to calibrate the implant depth and increase adhesion to the skull in n=2 animals with DG implants, n=2 animals with CA3 implants and n=4 animals with CA1 implants. Metallic screws were used to stabilize the position of the GRIN lens in n=2 animals with CA3 implants. The lens and protruding metal headpost were then stabilized in all animals using opaque dental cement (Super-bond C&B, Sun Medical).

Behavioural Paradigm

Single-photon microendoscope widefield calcium imaging in mice freely navigating in a linear track.

During the imaging sessions, the microscope head was clipped to the metallic ring protruding from the imaging cannula (Snap-in Surface Fluorescence Microscope Body-L, SFMB_L_458, Doric Lenses in n=1 animal with DG implants and n=1 animal with a CA1 implant or eFocus Snap-In Fluorescence Microscope Body-L, eSFMB_L_458, Doric lenses in n=4 animals with DG implants, n=3 animals with CA3 implants and n=3 animals with CA1 implants). A fiberoptic patchcord transmitting LED light and an HDMI cable collecting the digital signal connected the mouse to the microscope (Fluorescence microscope driver, FMD_L, Doric Lenses). Cable lengths were optimised to allow unrestricted movement of the mouse. In order to obtain high spatial sampling of the physical environment, we chose to expose the animals to a linear track similarly to previous studies (Ziv et al., 2013). The mice were freely navigating in a 60 cm-long, 6 cm-wide and 31 cm-high linear track made of PVC and enriched with visual cues: 3 playing cards placed on one wall and a sheet of paper placed onto the opposing wall, a piece of lego positioned at each end of the linear track and a drawing positioned on each extremity of the linear track made up the visual cues. A plexiglass lid with a linear opening allowing the passage of the microscope cables was placed on top of the linear track. The imaging recordings were carried out using Doric Neuroscience studio software and the behaviour of the animal was recorded using a camera (Doric, Sony IMX290 sensor) to allow tracking of the animal's trajectory. Doric Neuroscience studio software triggered the behavioural camera by sending a TTL signal for each frame to synchronize the 2 recordings. The exposure used was 50 ms (20Hz) and the illumination power setting was optimised for each animal and imaging region, and maintained throughout the experiments.

The imaging field of view (FOV) was first inspected 2-3 weeks following the implant

to check for the presence of fluorescent neurons. If fluorescence signals were observed in the FOV, the mice were handled daily the week prior to the start of recordings in order to reduce the animals' stress during the experiments (Fig 2D-2F).

Navigation in the linear track

The activity of hippocampal neurons was recorded while the mouse navigated back and forth in opposite directions along a linear track (length: 60 cm). Mice were exposed to the linear track for 4 consecutive days: the first session was considered to be novel, subsequent exposures were considered to be familiar. On the first day of recording, mice were exposed to the linear track and recorded for 10 minutes. The mice were spontaneously exploring the environment without being given any reward. During imaging sessions, mice completed 17.0 ± 2.5 (n = 33 sessions from DG implants), 20.3 ± 2.1 (n = 28 sessions from CA3 implants), or 23.8 ± 4.0 (n = 28 sessions from CA1 implants) continuous runs ("laps" according to the definition given below) across the linear track. Imaging sessions lasted 734 ± 77 s (DG implants), 801 ± 73 s (CA3 implants), or 1034 ± 103 s (CA1 implants).

Post-hoc analysis

Upon completion of the experiments, the animals were perfused with 4% formaldehyde (Sigma) after lethal injection with pentobarbital (150 mg/kg). The brain tissue was collected and sliced into 60-µm thick sections using a vibratome (Leica). The cell bodies were stained using Hoechst 33342, Trihydrochloride, Trihydrate - FluoroPure Grade. Images of the lens position in the tissue and viral injection sites were obtained with confocal microscopy (Bruker, Zeiss; Fig 1D-1F).

Data analysis

Behavioural analysis (Fig 2G-2I)

Analysis of behavioural and imaging data was performed using established procedures in the laboratory (Allegra et al., 2020; Zhang et al., 2021), with some adaptations to account for the specific properties of single-photon widefield imaging.

To track the position of the animal, we filmed the linear track using a camera (Doric, Sony IMX 290 sensor) operating at the same frame rate as the microscope sensor (typically 20Hz). For every frame captured by the microscope sensor, the acquisition software emitted a TTL pulse to trigger a corresponding frame capture with the behavior camera. Animal motion was analyzed with the markerless pose estimation software DeepLabCut (Mathis et al., 2018). 4 labels (snout tip, left and right ear, tail

base) were identified across all captured frames. The position of the animal was computed as the mean of the coordinates of the 4 labels. “Laps”, i.e. continuous runs at a speed of >0.5 cm/s in a single direction along the linear track, were identified after low-pass filtering positional data at f_c=0.5Hz. We were stringent with the lap definition and only included periods of active running to discard large synchronous patterns of population activity observed prior to movement onset in the dentate gyrus, consistent with previous findings (Pofahl et al., 2021). Only continuous runs in one direction that covered at least 70% of the full length of the track were considered a lap. Neuronal activity data were assigned one of two directions (“IN” or “OUT”). Neuronal activity data outside of any laps, including resting periods, were not used for analysis.

Imaging data processing (Fig 2G-2I)

Recordings of neural activity were first motion corrected in the xy plane to account for artefacts induced by the movement of the animal using an algorithm built into the Doric Neuroscience Studio software. Segmentation into regions of interest (ROIs) was carried out using a singular value decomposition algorithm built into the suite2p software (Pachitariu_Harris16). In order to select DG granule cells, we only selected ROIs corresponding to small and densely packed cell bodies to discard inhibitory interneurons and mossy cells. The fluorescent signal from the neuropil was subtracted from the extracted fluorescence using the suite2p software. The quantification of neuronal activity was consistent with previously reported methods (Dombeck et al., 2010). ‘Events’ were defined as regions in the normalized fluorescence changes (dF/F) exceeding a threshold of mean +1.0 standard deviations of the overall dF/F signal, a minimum duration above threshold of 300 ms (which corresponds approximately to the GCaMP6f half decay time (Dana et al., 2019)), and exceeding an integral of 50 dF/F x 1s. Visual inspection of the event detection result confirmed these parameters (Allegra et al., 2020).

During some recordings of populations of CA1 neurons, we rarely observed large generalised fluorescence transients which saturated the whole field of view, likely caused by motion artefacts as they were typically related to certain movement patterns of the animal, such as exploring the side walls on their hind paws. We chose to discard these periods manually from further analysis.

Identification of spatially modulated cells

Spatial activity maps were computed based on data from continuous running periods.

The linear track was split into 20 spatial bins (3 cm bin width). The sum of events in each spatial bin was divided by the occupancy of the animal in that bin; spatial maps were smoothed with a Gaussian filter (sigma = 4 bins).

Spatially modulated neurons were defined as cells firing consistently at the same location of the linear track across lap crossings in the same running direction. We identified spatially modulated cells by computing the mean pairwise Pearson's R correlation between spatial maps across lap crossings. Outbound and inbound lap crossings were analysed separately. To obtain a null model for the mean correlation and selectivity, we dissociated firing activity for each neuron and spatial position by shuffling the recorded position in chunks of 300 ms and repeated this bootstrap procedure 10 times. The neurons whose mean correlation value exceeded the bootstrap with a Z-score higher than 1.0 in at least one direction of running were identified as spatially modulated cells. This approach accounts for both coherence and stability of spatially modulated cells, since it will not identify as spatially modulated a cell that fires in a single lap (low stability), or if it fires in different locations across laps (low coherence), or if it fires sparsely yielding a high mean pairwise correlation by chance (low stability, giving low Z score from the bootstrap procedure).

Spatial correlations and decorrelations

To quantify session-wise correlations between spatial activity maps in the running direction (In/In or Out/Out), we split even and odd laps crossings in the same direction of motion. We calculated mean spatial activity maps for each cell for even and odd laps and computed correlations (Pearson's R) between mean spatial activity maps for either all or only neurons that were spatially modulated (see above). We then computed the mean correlation values for each session. To quantify session-wise correlations between spatial activity maps in Inbound and Outbound directions, we computed correlations between spatial activity maps for the Inbound and Outbound directions as described above. To quantify distance-coding, we measured correlations between spatial activity maps for lap crossings in the opposite directions after inverting the order ("flipping") of the maps for the outbound direction.

Population vector (PoV) analysis

Population vectors (PoV) were defined as the collection of event rates of the population of all spatially modulated neurons measured in a spatial bin. PoV correlations were obtained by computing Pearson's R between corresponding PoVs

of different running directions (OUT vs IN) or of the same running direction split into even and odd lap crossings. PoV correlation matrices depict color-coded PoV correlations between all spatial bins in one condition versus all spatial bins in the other condition.

Rate vector and selectivity

In order to compute contextual selectivity, the event rate for the i-th cell ri was defined as the number of neural events of a cell divided by the amount of running time in a given direction. For each recording session, selectivity of the *i*-th neuron was defined as the normalized difference of event rates *r* of that neuron computed during inbound and outbound running: $|r_i^I - r_i^O| / (r_i^I + r_i^O)$. The rate vector was defined as the entirety of event rates of a population of neurons during a lap crossing or a session.

Decoding of position and distance from population responses

For the decoding analysis, we used custom-written Python scripts and the scikit-learn SVC implementation (Pedregosa et al., 2011). The neural decoder algorithm was based on linear classifiers trained on pseudo-simultaneous population activity created by combining 100 ms-binned neural patterns recorded from different animals performing the same behavioral task. The decoding algorithm was cross-validated and tested against a null model with shuffled trial condition labels.

Data labeling: for each session, we labeled the recorded neural data according to the position of the animal along the track (denoted as *position*) and according to the ego-centric distance traveled in the run event (denoted as *distance*). For each variable, we defined two classes which were used to train and test the decoding algorithm. Being *L* the length of the track, we labeled the data as follows:

Position:

- (0) := position < 0.2 L
- (1) := position > 0.8 L

Distance:

- (start) := distance < 0.2 L
- (end) := distance > 0.8 L

To avoid that the two variables act as a confound to each other, we balanced the data so that the four combined classes (0-start, 0-end, 1-start, 1-end) contained the

same amount of data. *Position* decoding was therefore performed by training and testing a decoder to discriminate a balanced mix of *distance* values in the two *position* classes: (0-start, 0-end) vs. (1-start, 1 end). Similarly, *distance* decoding was performed on a balanced mix of *positional* values: (0-start, 1-start) vs. (0-end + 1-end). Only data where at least n=1 neurons showed activity were considered for the decoding analysis.

Cross-validation: All performance assessments were performed using n=10 cross validation (CV) folds. For each CV fold, we randomly selected 80% of the time bins of each condition and used them to build pseudo-simultaneous (PS) activity (see below) which was used to train a Support Vector Machine (SVM) with a linear kernel to classify PS patterns into one of the two conditions. Similarly, the remaining 20% of the trials were used to build PS activity that was used to test the trained SVM. When showing a single value, the decoding performance was then assessed as the mean accuracy on the test set over the CV folds.

Pseudo-population: To build pseudo-populations, we randomly selected 100 ms binned neural patterns from training and testing trials of all animals and concatenated them to form a larger pseudo-simultaneous neural pattern. To obtain the training and testing data sets used in the cross-validation scheme, this procedure was repeated 2N times per condition, where N is the total number of neurons. To increase the signal to noise ratio of the decoder, we used a procedure where the decoder is trained to classify groups of *n=3* time bins (n = 1 corresponds to standard single time-bin decoding). In practice, this was done at the moment of creating pseudo-population activity by sampling and concatenating 3 random time bins for each individual animal, effectively creating pseudo-population vectors of 3N neurons, with N being the total number of recorded neurons across animals.

Null model and p-value: All decoding performance values were tested against a null model created by shuffling the condition labels of individual trials. After each shuffle of the labels, the exact same 10-fold cross-validated decoding procedure described above was repeated on the shuffled data. The p-value of the decoding performance was computing the z-score of the performance of the data compared to the distribution of performances obtained by 20 repetitions of the shuffling procedure.

Statistics

Data are presented as mean ± SEM across sessions, unless stated otherwise.

Statistical significance was assessed using Wilcoxon signed-rank tests for paired data and Mann-Whitney U tests for unpaired data. When comparing more than two groups, we first performed an analysis of variance (ANOVA) followed by Bonferroni *post-hoc* correction of the test results.

References

Allegra, M., Posani, L., Gómez-Ocádiz, R., and Schmidt-Hieber, C. (2020). Differential Relation between Neuronal and Behavioral Discrimination during Hippocampal Memory Encoding. Neuron *108*, 1103–1112.

Amaral, D.G., and Witter, M.P. (1989). The three-dimensional organization of the hippocampal formation: a review of anatomical data. Neuroscience *31*, 571–591.

Anderson, M.I., and Jeffery, K.J. (2003). Heterogeneous modulation of place cell firing by changes in context. J. Neurosci. *23*, 8827–8835.

Battaglia, F.P., Sutherland, G.R., and McNaughton, B.L. (2004). Local sensory cues and place cell directionality: additional evidence of prospective coding in the hippocampus. J. Neurosci. *24*, 4541–4550.

Burke, S.N., Maurer, A.P., Nematollahi, S., Uprety, A.R., Wallace, J.L., and Barnes, C.A. (2011). The influence of objects on place field expression and size in distal hippocampal CA1. Hippocampus *21*, 783–801.

Campbell, M.G., Ocko, S.A., Mallory, C.S., Low, I.I.C., Ganguli, S., and Giocomo, L.M. (2018). Principles governing the integration of landmark and self-motion cues in entorhinal cortical codes for navigation. Nat. Neurosci. *21*, 1096–1106.

Campbell, M.G., Attinger, A., Ocko, S.A., Ganguli, S., and Giocomo, L.M. (2021). Distance-tuned neurons drive specialized path integration calculations in medial entorhinal cortex. Cell Rep. *36*, 109669.

Chawla, M.K., Guzowski, J.F., Ramirez-Amaya, V., Lipa, P., Hoffman, K.L., Marriott, L.K., Worley, P.F., McNaughton, B.L., and Barnes, C.A. (2005). Sparse, environmentally selective expression of Arc RNA in the upper blade of the rodent fascia dentata by brief spatial experience. Hippocampus *15*, 579–586.

Cholvin, T., Hainmueller, T., and Bartos, M. (2021). The hippocampus converts volatile entorhinal inputs into stable spatial maps. SSRN Electron. J.

Colgin, L.L., Moser, E.I., and Moser, M.-B. (2008). Understanding memory through hippocampal remapping. Trends Neurosci. *31*, 469–477.

Dana, H., Sun, Y., Mohar, B., Hulse, B.K., Kerlin, A.M., Hasseman, J.P., Tsegaye, G., Tsang, A., Wong, A., Patel, R., et al. (2019). High-performance calcium sensors for imaging activity in neuronal populations and microcompartments. Nat. Methods *16*, 649–657.

Diehl, G.W., Hon, O.J., Leutgeb, S., and Leutgeb, J.K. (2017). Grid and Nongrid Cells in Medial Entorhinal Cortex Represent Spatial Location and Environmental Features with Complementary Coding Schemes. Neuron *94*, 83–92.e6.

Dolorfo, C.L., and Amaral, D.G. (1998). Entorhinal cortex of the rat: topographic organization of the cells of origin of the perforant path projection to the dentate gyrus. J. Comp. Neurol. *398*, 25–48.

Dombeck, D.A., Harvey, C.D., Tian, L., Looger, L.L., and Tank, D.W. (2010). Functional imaging of hippocampal place cells at cellular resolution during virtual navigation. Nat. Neurosci. *13*, 1433–1440.

Dragoi, G., and Buzsáki, G. (2006). Temporal encoding of place sequences by hippocampal cell assemblies. Neuron *50*, 145–157.

Felleman, D.J., and Van Essen, D.C. (1991). Distributed hierarchical processing in the primate cerebral cortex. Cereb. Cortex *1*, 1–47.

Gerlei, K., Passlack, J., Hawes, I., Vandrey, B., Stevens, H., Papastathopoulos, I., and Nolan, M.F. (2019). Grid cells encode local head direction (bioRxiv).

GoodSmith, D., Chen, X., Wang, C., Kim, S.H., Song, H., Burgalossi, A., Christian, K.M., and Knierim, J.J. (2017). Spatial Representations of Granule Cells and Mossy Cells of the Dentate Gyrus. Neuron *93*, 677–690.e5.

Griffin, A.L., Eichenbaum, H., and Hasselmo, M.E. (2007). Spatial representations of hippocampal CA1 neurons are modulated by behavioral context in a hippocampus-dependent memory task. J. Neurosci. *27*, 2416–2423.

van Groen, T., Miettinen, P., and Kadish, I. (2003). The entorhinal cortex of the mouse: organization of the projection to the hippocampal formation. Hippocampus *13*, 133–149.

Hafting, T., Fyhn, M., Molden, S., Moser, M.-B., and Moser, E.I. (2005). Microstructure of a spatial map in the entorhinal cortex. Nature *436*, 801–806.

Hainmueller, T., and Bartos, M. (2018). Parallel emergence of stable and dynamic memory engrams in the hippocampus. Nature *558*, 292–296.

Hardcastle, K., Ganguli, S., and Giocomo, L.M. (2017). Cell types for our sense of location: where we are and where we are going. Nat. Neurosci. *20*, 1474–1482.

Henriksen, E.J., Colgin, L.L., Barnes, C.A., Witter, M.P., Moser, M.-B., and Moser, E.I. (2010). Spatial representation along the proximodistal axis of CA1. Neuron *68*, 127–137.

Hoang, T.-H., Aliane, V., and Manahan-Vaughan, D. (2018). Novel encoding and updating of positional, or directional, spatial cues are processed by distinct hippocampal subfields: Evidence for parallel information processing and the “what” stream. Hippocampus *28*, 315–326.

Høydal, Ø.A., Skytøen, E.R., Andersson, S.O., Moser, M.-B., and Moser, E.I. (2019). Object-vector coding in the medial entorhinal cortex. Nature *568*, 400–404.

Jacob, P.-Y., Capitano, F., Poucet, B., Save, E., and Sargolini, F. (2019). Path integration maintains spatial periodicity of grid cell firing in a 1D circular track. Nat. Commun. *10*, 840.

Jacobs, L.F., and Schenk, F. (2003). Unpacking the cognitive map: the parallel map theory of hippocampal function. Psychol. Rev. *110*, 285–315.

Jung, M.W., and McNaughton, B.L. (1993). Spatial selectivity of unit activity in the hippocampal granular layer. Hippocampus *3*, 165–182.

Keinath, A.T., Nieto-Posadas, A., Robinson, J.C., and Brandon, M.P. (2020). DG-CA3 circuitry mediates hippocampal representations of latent information. Nat. Commun. *11*, 3026.

Kerr, K.M., Agster, K.L., Furtak, S.C., and Burwell, R.D. (2007). Functional

neuroanatomy of the parahippocampal region: the lateral and medial entorhinal areas. Hippocampus *17*, 697–708.

Kitamura, T., Sun, C., Martin, J., Kitch, L.J., Schnitzer, M.J., and Tonegawa, S. (2015). Entorhinal Cortical Ocean Cells Encode Specific Contexts and Drive Context-Specific Fear Memory. Neuron *87*, 1317–1331.

Kraus, B.J., Brandon, M.P., Robinson, R.J., 2nd, Connerney, M.A., Hasselmo, M.E., and Eichenbaum, H. (2015). During Running in Place, Grid Cells Integrate Elapsed Time and Distance Run. Neuron *88*, 578–589.

Laptev, D., and Burgess, N. (2019). Neural Dynamics Indicate Parallel Integration of Environmental and Self-Motion Information by Place and Grid Cells. Front. Neural Circuits *0*.

Lee, J.W., Kim, W.R., Sun, W., and Jung, M.W. (2012). Disruption of Dentate Gyrus Blocks Effect of Visual Input on Spatial Firing of CA1 Neurons. Journal of Neuroscience *32*, 12999–13003.

Leutgeb, S., and Leutgeb, J.K. (2007). Pattern separation, pattern completion, and new neuronal codes within a continuous CA3 map. Learn. Mem. *14*, 745–757.

Leutgeb, J.K., Leutgeb, S., Moser, M.-B., and Moser, E.I. (2007). Pattern separation in the dentate gyrus and CA3 of the hippocampus. Science *315*, 961–966.

Leutgeb, S., Leutgeb, J.K., Treves, A., Moser, M.-B., and Moser, E.I. (2004). Distinct ensemble codes in hippocampal areas CA3 and CA1. Science *305*, 1295–1298.

Leutgeb, S., Leutgeb, J.K., Barnes, C.A., Moser, E.I., McNaughton, B.L., and Moser, M.-B. (2005). Independent codes for spatial and episodic memory in hippocampal neuronal ensembles. Science *309*, 619–623.

Li, Y., Xu, J., Liu, Y., Zhu, J., Liu, N., Zeng, W., Huang, N., Rasch, M.J., Jiang, H., Gu, X., et al. (2017). A distinct entorhinal cortex to hippocampal CA1 direct circuit for olfactory associative learning. Nat. Neurosci. *20*, 559–570.

Lisman, J.E. (2007). Role of the dual entorhinal inputs to hippocampus: a hypothesis based on cue/action (non-self/self) couplets. Prog. Brain Res. *163*, 615–625.

McNaughton, B.L., Barnes, C.A., and O'Keefe, J. (1983). The contributions of position, direction, and velocity to single unit activity in the hippocampus of freely-moving rats. Exp. Brain Res. *52*, 41–49.

Miao, C., Cao, Q., Ito, H.T., Yamahachi, H., Witter, M.P., Moser, M.-B., and Moser, E.I. (2015). Hippocampal Remapping after Partial Inactivation of the Medial Entorhinal Cortex. Neuron *88*, 590–603.

Morris, A.M., Weeden, C.S., Churchwell, J.C., and Kesner, R.P. (2013a). The role of the dentate gyrus in the formation of contextual representations. Hippocampus *23*, 162–168.

Morris, A.M., Curtis, B.J., Churchwell, J.C., Maasberg, D.W., and Kesner, R.P. (2013b). Temporal associations for spatial events: the role of the dentate gyrus. Behav. Brain Res. *256*, 250–256.

Muller, R.U., and Kubie, J.L. (1987). The effects of changes in the environment on the spatial firing of hippocampal complex-spike cells. J. Neurosci. *7*, 1951–1968.

Muller, R.U., Bostock, E., Taube, J.S., and Kubie, J.L. (1994). On the directional firing properties of hippocampal place cells. J. Neurosci. *14*, 7235–7251.

Murano, T., Nakajima, R., Nakao, A., Hirata, N., Amemori, S., Murakami, A., Kamitani, Y., Yamamoto, J., and Miyakawa, T. (2020). Multiple types of navigational information are independently encoded in the population activities of the dentate gyrus neurons.

Navratilova, Z., Hoang, L.T., Schwindel, C.D., Tatsuno, M., and McNaughton, B.L. (2012). Experience-dependent firing rate remapping generates directional selectivity in hippocampal place cells. Front. Neural Circuits *6*, 6.

Neunuebel, J.P., and Knierim, J.J. (2012). Spatial firing correlates of physiologically distinct cell types of the rat dentate gyrus. J. Neurosci. *32*, 3848–3858.

Neunuebel, J.P., and Knierim, J.J. (2014). CA3 retrieves coherent representations from degraded input: direct evidence for CA3 pattern completion and dentate gyrus pattern separation. Neuron *81*, 416–427.

O'Keefe, J., and Dostrovsky, J. (1971). The hippocampus as a spatial map. Preliminary evidence from unit activity in the freely-moving rat. Brain Res. *34*, 171–175.

Pedregosa, F., Varoquaux, G., Gramfort, A., Michel, V., Thirion, B., Grisel, O., Blondel, M., Prettenhofer, P., Weiss, R., Dubourg, V., et al. (2011). Scikit-learn: Machine Learning in Python. J. Mach. Learn. Res. *12*, 2825–2830.

Plitt, M.H., and Giocomo, L.M. (2021). Experience-dependent contextual codes in the hippocampus. Nat. Neurosci. *24*, 705–714.

Pofahl, M., Nikbakht, N., Haubrich, A.N., Nguyen, T., Masala, N., Distler, F., Braganza, O., Macke, J.H., Ewell, L.A., Golcuk, K., et al. (2021). Synchronous activity patterns in the dentate gyrus during immobility. Elife *10*.

Posani, L., Cocco, S., and Monasson, R. (2018). Integration and multiplexing of positional and contextual information by the hippocampal network. PLoS Comput. Biol. *14*, e1006320.

Qin, H., Fu, L., Hu, B., Liao, X., Lu, J., He, W., Liang, S., Zhang, K., Li, R., Yao, J., et al. (2018). A Visual-Cue-Dependent Memory Circuit for Place Navigation. Neuron *99*, 47–55.e4.

Sargolini, F., Fyhn, M., Hafting, T., McNaughton, B.L., Witter, M.P., Moser, M.-B., and Moser, E.I. (2006). Conjunctive representation of position, direction, and velocity in entorhinal cortex. Science *312*, 758–762.

Savelli, F., Yoganarasimha, D., and Knierim, J.J. (2008). Influence of boundary removal on the spatial representations of the medial entorhinal cortex. Hippocampus *18*, 1270–1282.

Schwindel, C.D., Navratilova, Z., Ali, K., Tatsuno, M., and McNaughton, B.L. (2016). Reactivation of Rate Remapping in CA3. J. Neurosci. *36*, 9342–9350.

Sheintuch, L., Geva, N., Baumer, H., Rechavi, Y., Rubin, A., and Ziv, Y. (2020). Multiple Maps of the Same Spatial Context Can Stably Coexist in the Mouse Hippocampus. Curr. Biol. *30*, 1467–1476.e6.

Solstad, T., Boccara, C.N., Kropff, E., Moser, M.-B., and Moser, E.I. (2008). Representation of geometric borders in the entorhinal cortex. Science *322*, 1865–1868.

Stachenfeld, K.L., Botvinick, M.M., and Gershman, S.J. (2017). The hippocampus as a predictive map. Nat. Neurosci. *20*, 1643–1653.

Stefanini, F., Kushnir, L., Jimenez, J.C., Jennings, J.H., Woods, N.I., Stuber, G.D., Kheirbek, M.A., Hen, R., and Fusi, S. (2020). A Distributed Neural Code in the Dentate Gyrus and in CA1. Neuron *107*, 703–716.e4.

Steward, O. (1976). Topographic organization of the projections from the entorhinal area to the hippocampal formation of the rat. J. Comp. Neurol. *167*, 285–314.

Wang, C., Chen, X., Lee, H., Deshmukh, S.S., Yoganarasimha, D., Savelli, F., and Knierim, J.J. (2018). Egocentric coding of external items in the lateral entorhinal cortex. Science *362*, 945–949.

Witter, M.P., and Amaral, D.G. (1991). Entorhinal cortex of the monkey: V. Projections to the dentate gyrus, hippocampus, and subicular complex. J. Comp. Neurol. *307*, 437–459.

Witter, M.P., Naber, P.A., van Haeften, T., Machielsen, W.C., Rombouts, S.A., Barkhof, F., Scheltens, P., and Lopes da Silva, F.H. (2000). Cortico-hippocampal communication by way of parallel parahippocampal-subicular pathways. Hippocampus *10*, 398–410.

Zhang, S.-J., Ye, J., Miao, C., Tsao, A., Cerniauskas, I., Ledergerber, D., Moser, M.-B., and Moser, E.I. (2013). Optogenetic dissection of entorhinal-hippocampal functional connectivity. Science *340*, 1232627.

Ziv, Y., Burns, L.D., Cocker, E.D., Hamel, E.O., Ghosh, K.K., Kitch, L.J., El Gamal, A., and Schnitzer, M.J. (2013). Long-term dynamics of CA1 hippocampal place codes. Nat. Neurosci. *16*, 264–266.